MOSCOW CENTER
FOR DIAGNOSTICS & TELEMEDICINE

ISSN 2712–8490 (Print)
ISSN 2712-8962 (Online)

DIGITAL DIAGNOSTICS

A peer-reviewed scientific medical journal

2 Volume 3 Issue

ECO • VECTOR

2021

https://journals.eco-vector.com/DD

УЧРЕДИТЕЛИ

- ГБУЗ «Научно-практический клинический центр диагностики и телемедицинских технологий ДЗМ»
- ООО «Эко-Вектор»

ИЗДАТЕЛЬ

ООО «Эко-Вектор»
Адрес: 191186, г. Санкт-Петербург, Аптекарский переулок, д. 3, литера А, помещение 1Н
E-mail: info@eco-vector.com
WEB: https://eco-vector.com

РЕКЛАМА

Отдел рекламы
Тел.: +7 495 308 83 89

РЕДАКЦИЯ

Зав. редакцией
Елена Андреевна Филиппова
Email: ddjournal@eco-vector.com
Тел: +7 (965) 012 70 72

ПОДПИСКА

Подписка на печатную версию через интернет:
www.journals.eco-vector.com/
www.akc.ru
www.pressa-rf.ru

OPEN ACCESS

В электронном виде журнал распространяется бесплатно — в режиме немедленного открытого доступа

ИНДЕКСАЦИЯ

- РИНЦ
- Google Scholar
- Ulrich's International Periodicals Directory
- WorldCat

Оригинал-макет

подготовлен в издательстве «Эко-Вектор».
Литературный редактор: *М.Н. Шошина*
Корректор: *М.Н. Шошина*
Вёрстка: *Ф.А. Игнащенко*
Обложка: *И.С. Феофанова*

Сдано в набор 06.10.2021.
Подписано в печать 05.10.2021.
Формат 60 × 88⅛. Печать офсетная.
Печ. л. 24. Усл. печ. л. 22,32.
Уч.-изд. л. 13,09. Тираж 5000 экз. Заказ № 210070

Отпечатано в ООО «Полиграфист и издатель»
г. Москва, ул. Веерная, д. 22, корп. 3, кв. 48

ISSN 2712-8490 (Print)
ISSN 2712-8962 (Online)

Digital Diagnostics

Том 2 | Выпуск 3 | 2021

ЕЖЕКВАРТАЛЬНЫЙ РЕЦЕНЗИРУЕМЫЙ НАУЧНЫЙ МЕДИЦИНСКИЙ ЖУРНАЛ

ЭКО • ВЕКТОР

FOUNDERS
- Moscow Center for Diagnostics and Telemedicine
- Eco-Vector

PUBLISHER
Eco-Vector
Address: 3 liter A, 1H, Aptekarsky pereulok, 191186, Saint Petersburg Russian Federation
E-mail: info@eco-vector.com
WEB: https://eco-vector.com

ADVERTISE
Adv. department
Phone: +7 (495) 308 83 89

EDITORIAL
Executive editor
Elena A. Philippova
Email: ddjournal@eco-vector.com
Phone: +7(965)0127072

SUBSCRIPTION
For print version:
www.journals.eco-vector.com/

PUBLICATION ETHICS
Journal's ethic policies are based on:
- ICMJE
- COPE
- ORE
- CSE
- EASE

OPEN ACCESS
Immediate Open Access is mandatory for all published articles

INDEXATION
- Russian Science Citation Index
- Google Scholar
- Ulrich's International Periodicals Directory
- WorldCat

TYPESET
compleate in Eco-Vector
Copyeditor: *M.N. Shoshina*
Proofreader: *M.N. Shoshina*
Layout editor: *Ph. Ignashchenko*
Cover: *I. Feofanova*

ISSN 2712-8490 (Print)
ISSN 2712-8962 (Online)

Digital Diagnostics

Volume 2 | Issue 3 | 2021

QUARTERLY PEER-REVIEW MEDICAL JOURNAL

ECO • VECTOR

CONTENTS

ORIGINAL STUDY ARTICLES

TECHNICAL REPORTS

SYSTEMATIC REVIEWS

REVIEWS

EDITORIALS

СОДЕРЖАНИЕ

DOI: https://doi.org/10.17816/DD71885

Электрокардиографические феномены при COVID-19: анализ теле-ЭКГ-исследований IT-центра ЭКГ г. Москвы

В.Ю. Таскина[1], А.Е. Демкина[1], Т.М. Газашвили[2], А.С. Шкода[2], А.В. Владзимирский[1, 3], С.П. Морозов[1]

[1] Научно-практический клинический центр диагностики и телемедицинских технологий Департамента здравоохранения г. Москвы, Москва, Российская Федерация
[2] Городская клиническая больница № 67 имени Л.А. Ворохобова Департамента здравоохранения города Москвы, Москва, Российская Федерация
[3] Первый Московский государственный медицинский университет имени И.М. Сеченова (Сеченовский Университет), Москва, Российская Федерация

АННОТАЦИЯ

Обоснование. При новой коронавирусной инфекции (COVID-19) наряду с доминирующим поражением органов дыхания в патологический процесс вовлекается сердечно-сосудистая система. Однако в доступной литературе аналитические оценки электрокардиографических (ЭКГ) феноменов опираются лишь на результаты исследований небольших выборок и описания единичных клинических случаев, что определяет актуальность проведения более масштабных исследований для уточнения характера и распространённости ЭКГ-изменений у лиц с подтверждённой коронавирусной инфекцией.

Цель — структуризация изменений ЭКГ у пациентов с COVID-19, представляющих неселективную популяцию жителей г. Москвы.

Материалы и методы. Проведён ретроспективный анализ электрокардиографических исследований, выполненных у 42 799 пациентов с верифицированным диагнозом COVID-19 в период с 10.03.2020 по 10.03.2021. Все включённые в исследование лица проходили стационарное лечение в клинических больницах г. Москвы, подключённых к IT-центру ЭКГ. Регистрация ЭКГ производилась в 12 стандартных отведениях, после чего путём интернет-соединения информация передавалась на сервер IT-центра ЭКГ с целью формулировки соответствующих заключений.

Результаты. Изменения ЭКГ обнаружены у 54% пациентов. Наиболее частыми аритмиями были наджелудочковая экстрасистолия и фибрилляция предсердий — у 12,6 и 12,0% пациентов соответственно. Признаки перегрузки правых отделов сердца выявлены у 12,5% больных, из них в 1,13% случаев — ЭКГ-паттерн тромбоэмболии лёгочной артерии. Инфарктоподобные изменения на ЭКГ имели место у 4,5% субъектов, в том числе 3 случая паттерна Бругада. Частота встречаемости изменений ST-T составила 2,2% от числа всех исследований. ЭКГ с удлинённым интервалом QT и QTc зарегистрирована у 540 (1,26%) пациентов. Отмечены единичные случаи фибрилляции желудочков, синдрома Фредерика и АВ-блокады различной степени.

Заключение. На основе проведённого анализа получено представление о частоте встречаемости электрокардиографических феноменов у больных COVID-19. Подтверждена высокая инцидентность фибрилляции предсердий — фактора риска тромбоэмболических осложнений. Одновременно установлена значительная распространённость ЭКГ-паттернов перегрузки правых отделов сердца, часть из которых ассоциирована с тромбоэмболией лёгочной артерии. Другие наблюдаемые изменения ЭКГ характеризовались значительно меньшей распространённостью, что, однако, не снижает их клинического значения. Собранный материал в перспективе может служить оптимизации тактики ведения пациентов при коронавирусной инфекции.

Ключевые слова: электрокардиография; COVID-19; сердечно-сосудистые заболевания; аритмии; миокардит; тромбоэмболия лёгочной артерии; ТЭЛА; теле-ЭКГ.

Как цитировать

Таскина В.Ю., Демкина А.Е., Газашвили Т.М., Шкода А.С., Владзимирский А.В., Морозов С.П. Электрокардиографические феномены при COVID-19: анализ теле-ЭКГ-исследований IT-центра ЭКГ г. Москвы // *Digital Diagnostics.* 2021. Т. 2, № 3. С. 235–248. DOI: https://doi.org/10.17816/DD71885

Рукопись получена: 21.06.2021 **Рукопись одобрена:** 21.09.2021 **Опубликована:** 27.09.2021

ЭКО•ВЕКТОР

DOI: https://doi.org/10.17816/DD71885

Electrocardiographic findings in COVID-19: analysis of tele-ECGs in Moscow ECG IT Center

Varvara Y. Taskina[1], Alexandra E. Demkina[1], Tamara M. Gazashvili[2], Andrey S. Shkoda[2], Anton V. Vladzymyrskyy[1, 3], Sergey P. Morozov[1]

[1] Moscow Center for Diagnostics and Telemedicine, Moscow, Russian Federation
[2] L.A. Vorokhobov Municipal Clinical Hospital No 67 of the Moscow Health Department, Moscow, Russian Federation
[3] The First Sechenov Moscow State Medical University (Sechenov University), Moscow, Russian Federation

ABSTRACT

BACKGROUND: Coronavirus disease (COVID-19) affects the cardiovascular system and the primary damage to the respiratory system involved in the pathological process. However, in the available literature, the electrocardiography (ECG) analyses are based only on small-sample studies and case reports, which determine the relevance of larger-scale studies to clarify the nature and prevalence of ECG abnormalities in subjects with confirmed coronavirus infection.

AIM: To determine the distribution of ECG changes in COVID-19 patients representing a non-selective population of Moscow residents.

MATERIALS AND METHODS: We performed a retrospective analysis of ECGs from 42,799 patients from March 10, 2020 to March 10, 2021 with a verified diagnosis of COVID-19. The study included patients admitted to Moscow clinical hospitals connected to the ECG IT Center. A standard 12-lead ECG was obtained and transmitted via an Internet connection to the server of the ECG IT Center, where the ECG interpretation was performed.

RESULTS: ECG changes were detected in 54% of patients. The most common cardiac arrhythmias were supraventricular extrasystole (12.6%) and atrial fibrillation (12.0%) reported in patients. Signs of the overloaded right heart were detected in 12.5% of cases, of which the ECG pattern of pulmonary embolism was confirmed in 485 patients (1.13%). Infarction ECG pattern was observed in 4.5% of patients, among which 3 cases of Brugada ECG pattern were reported. The incidence of ST-T changes was 2.2% of all studies. Prolonged QT and QTc intervals were recorded in 540 patients (1.26%). In addition, individual cases of ventricular fibrillation, Frederick syndrome, and atrioventricular block of various degrees were reported.

CONCLUSION: The distribution of incidence of ECG changes in COVID-19 was shown based on the data obtained. The high incidence of atrial fibrillation, which is a risk factor for thromboembolic complications, was confirmed. Moreover, a significant prevalence of ECG patterns of overloaded right heart was shown, some are associated with pulmonary embolism. Other reported ECG changes were characterized by a significantly lower prevalence, which does not reduce their clinical significance. The data obtained may be used to improve COVID-19 patient management strategy in the future.

Keywords: electrocardiography, COVID-19; cardiovascular diseases; arrhythmias; myocarditis; pulmonary embolism; tele-ECG.

To cite this article

Taskina VY, Demkina AE, Gazashvili TM, Shkoda AS, Vladzymyrskyy AV, Morozov SP. Electrocardiographic findings in COVID-19: analysis of tele-ECGs in Moscow ECG IT Center. *Digital Diagnostics.* 2021;2(3):235–248. DOI: https://doi.org/10.17816/DD71885

Received: 21.06.2021 **Accepted:** 21.09.2021 **Published:** 27.09.2021

ECO•VECTOR

DOI: https://doi.org/10.17816/DD71885

Covid-19的心电图现象：莫斯科IT中心电视心电图研究的分析

Varvara Y. Taskina[1], Alexandra E. Demkina[1], Tamara M. Gazashvili[2], Andrey S. Shkoda[2], Anton V. Vladzymyrskyy[1, 3], Sergey P. Morozov[1]

[1] Moscow Center for Diagnostics and Telemedicine, Moscow, Russian Federation
[2] L.A. Vorokhobov Municipal Clinical Hospital No 67 of the Moscow Health Department, Moscow, Russian Federation
[3] The First Sechenov Moscow State Medical University (Sechenov University), Moscow, Russian Federation

简评

论证通过新的冠状病毒感染（Covid-19），随着病理过程中呼吸器官的主要损伤，涉及一种心血管系统。然而，在可用文献中，心电图（ECG）现象的分析估计是基于对小样本的研究结果和单一临床病例的描述，这决定了开展更多大规模研究以澄清性质和患病率的相关性ECG改变冠状病毒感染的人。

目标是构建Covid-19患者ECG的变化，代表莫斯科居民的非选择性人口。

材料与方法心电图研究的回顾性分析，42,799名患者在10.03.2020至10.03.2021期间验证了Covid-19验证诊断。 所有包括在研究人员中的所有人都在莫斯科的临床医院通过住院治疗，连接到ECG IT中心。 12根标准导联上进行ECG登记， 然后，通过互联网连接，将信息传输到ECG IT中心服务器，以形成相关结论。

结果。54％的患者中检测到ECG变化。最常见的心律失常是心室外收缩和心房颤动，分别占12.6%和12.0%。12.5%的患者表现出右心室过载的迹象，其中1.13%的患者表现出肺动脉血栓栓塞的心电图模式。 心电图梗死样改变发生在4.5%的受试者中，包括3例Brugada型。ST-T发生变化的发生频率为所有研究的数量的2.2％。 带有细长QT和QTC间隔的ECG在540（1.26％）患者中注册。 报告了不同程度的心室颤动，弗雷德里克综合征和AB阻滞的单位病例.

结论。基于分析，获得了Covid-19患者心电图现象的发生频率的思路。 确认心房颤动的高发病率 - 血栓栓塞并发症的危险因素。 与此同时，建立了右侧心脏部门过载的ECG模式的显着普遍性，其中一些与光动脉的血栓栓塞相关。 其他观察到的ECG变化的特征在于显着较差的患病率，然而，这不会降低其临床意义。 未来的收集材料可以是冠状病毒感染的患者管理策略的优化。

关键词：心电图；新冠肺炎；心血管疾病；心律失常；心肌炎；肺栓塞；tele- 远程心电图。

引用本文

Taskina VY, Demkina AE, Gazashvili TM, Shkoda AS, Vladzymyrskyy AV, Morozov SP. Covid-19的心电图现象：莫斯科IT中心电视心电图研究的分析. *Digital Diagnostics.* 2021;2(3):235–248. DOI: https://doi.org/10.17816/DD71885

收到： 21.06.2021 **接受：** 21.09.2021 **发布日期：**27.09.2021

BACKGROUND

In December 2019, the first case of a new coronavirus disease (COVID-19) caused by SARS-CoV-2 was reported in Wuhan (Hubei Province, China). The spread of the virus accelerated, and as early as March 2020, the World Health Organization declared an outbreak of the COVID-19 pandemic.

Thus, Wu and McGoogan reported an overall mortality rate of 2.3% from confirmed COVID-19, with a significant increase (by 5.6%–10.5%) among those with comorbidities, reaching 49% in critically ill patients [1]. The clinical signs of the disease range from asymptomatic infection to multiple organ failure leading to death. The upper respiratory tract is the entry point for infection, and involvement of the lungs is the dominant clinical sign of COVID-19, including acute respiratory distress syndrome, according to most reports. However, patients with the new coronavirus infection develop cardiovascular complications [2, 3], which are caused by three factors:

- A history of cardiovascular diseases
- Myocardial damage by an infectious agent
- The cardiotoxic effect of drugs for COVID-19 treatment, which may concomitantly affect the cardiac conduction system

Cardiovascular complications on electrocardiographic examination (ECG) include signs of ischemia, myocarditis, Brugada pattern, various types of arrhythmias (including fatal), thromboembolic complications, and QT and QTc (corrected interval) prolongation and its proarrhythmogenic value [3–5]. Such myocardial damage is associated with negative disease outcomes, prolongation of the recovery period, and aggravation of the prognosis [2, 6–9]. Therefore, clinical specialists must pay close attention and recognize ECG changes that are characteristic of COVID-19.

Due to published results of clinical studies in small samples and analyses of single clinical cases, data on various types of ECG phenomena in coronavirus infection have already been accumulated in the international and domestic literature [2, 4, 7, 8]. However, no systematization of ECG frequency changes based on larger observations has yet been presented, which is important for determining the tactics of patient management and prognosis.

The goal of the study was to structure ECG changes in COVID-19 patients, who were drawn from a nonselective population of Moscow residents.

MATERIALS AND METHODS

Study design

From March 10, 2020, to March 10, 2021, 42,799 patients were treated for the new coronavirus infection in Moscow medical institutions as part of an observational retrospective study. The ECG findings were obtained from the telemedical system of ECG registration and remote analysis (tele-ECG system) of ATES MEDICA Company (Russia). In addition, the ECG findings received from the tele-ECG system were registered in the Moscow Unified Medical Information and Analysis System.

Eligibility criteria

Inclusion criteria: Persons over the age of 18 with a clinical and laboratory-verified diagnosis of the new coronavirus infection determined in accordance with the Interim Guidelines of the Ministry of Health of the Russian Federation on the COVID-19 Prevention, Diagnosis, and Treatment (based on a positive polymerase chain reaction test and/or the presence of viral pneumonia according to computed tomography)

Exclusion criteria: Patients under the age of 18 and the absence of ECG findings in the tele-EKG system and/or electronic patient records

Setting

Patients were admitted to the Moscow City Health Department's Municipal Clinical Hospital No. 40, as well as clinical departments, a pulmonology center, and a reserve hospital at the Vorokhobov Municipal Clinical Hospital No. 67.

A remote electrocardiography center (ECG IT Center) was established at the Vorokhobov City Clinical Hospital No. 67 of the Moscow City Health Department. In accordance with the guidelines on centralization of ECG descriptions, all ECGs recorded in the abovementioned medical institutions were accumulated in the tele-ECG system of the ECG IT Center to further describe and transfer the findings to the electronic patient records [10]. Morozov et al. reported that such an approach to the centralization of analytical processing of registered ECGs is adequate and allows for the optimization of materials and time costs, which is especially important given the increased load on the public health system during the COVID-19 pandemic [11].

Study duration

This retrospective study was conducted between April and June 2021, based on the ECG findings of coronavirus-infected patients who received inpatient treatment within a year (from March 10, 2020, to March 10, 2021).

Medical intervention

ECGs were recorded in all patients upon admission to the hospital and then every 3 days depending on the clinical situation and baseline ECG changes.

Main study outcome

The main outcome was the ECG recorded in patients with a confirmed COVID-19 diagnosis who received inpatient treatment in clinical departments and structural units of medical organizations that collaborated with the ECG IT Center. The ECG parameters listed below were assessed:

- *Rhythm and conduction disorders:* The grading of supraventricular and ventricular rhythm disorders was performed using the conventional criteria. The QT interval duration was calculated automatically using the ATES MEDICA software, taking into account the variance in

12 leads. When calculating these intervals, the averaged QRST complex of each lead was superimposed on each subsequent lead. The QT interval was calculated by measuring the time between the first point of ventricular depolarization and the last point of T-wave termination. In addition, using Bazett's formula, heart rate data were corrected to obtain the QTc interval value. Thus, the cut-off values for the QTc interval for men and women were 450 and 460 ms, respectively.

- *Morphological abnormalities (ST-T changes):* At 60–80 ms intervals, the ST segment was measured from point J. ST-T abnormality was defined as downsloping and/or horizontal ST segment depression of ≥0.05 mV and/or ST segment elevation of ≥0.10 mV in limb and $V_{5–6}$ leads and/or >0.25 mV in $V_{1–3}$, with a maximum in V_2 leads. Abnormalities of the T-wave were defined as changes in shape and polarity according to the generally accepted criteria, whereas secondary ST-T changes caused by ventricular premature excitation, intraventricular conduction block, and ventricular stimulation rhythm were not considered.
- *Right heart overload and enlargement:* Standard criteria were used to assess right atrial and right ventricular enlargement as well as the presence of acute pulmonary heart marker and pulmonary embolism, as reflected on ECG by $S_IQ_{III}T_{III}$ pattern and its combination with T-wave inversion in right chest leads, transient right bundle branch block, P-pulmonale, and depressed ST segment in left chest leads.

Subgroup analyses

The sample for this study was a nonselective population of Moscow residents who received hospital treatment for COVID-19. The sample was formed regardless of age, concomitant pathologies, severity of clinical condition, laboratory data, and duration of hospital stay. Retrospectively, patients were divided into two subgroups based on the presence or absence of ECG syndromes.

Any additional subgrouping was not anticipated by the aim and objectives of the study.

Outcome recording methods

The ECG was recorded in 12 standard leads using EASY ECG digital electrocardiographs (ATES MEDICA), which were equipped with modules for remote data transmission and an automatic ECG interpretation function with measurements of the main ECG parameters, such as duration of waves and intervals, voltaic characteristics, and subsequent formation of the preliminary report. When the electrocardiograph was connected to a laptop or tablet, the registered ECG records were visualized with the display of automatic analysis. Then, via Internet connection, the registered ECG was transmitted to the ECG IT Center's server, where functional diagnosticians reviewed the automatic ECG analysis and formulated a final conclusion. Subsequently, the ECG report was transferred to the electronic patient records.

Ethical review

The study was approved by the Independent Ethics Committee of the Moscow Regional Branch of the Russian Society of Roentgenologists and Radiologists, No. 5/2021, on May 20, 2021.

Statistical analysis

The statistical analysis included data from all subjects, which were divided into two subgroups based on the presence or absence of the ECG pathological phenomenon. For each subgroup, descriptive statistics of baseline characteristics were provided, with the following parameters: number of missing values (N), minimum value (Min), maximum value (Max), arithmetic mean (M), standard deviation (SD), 95% confidence interval (CI) for the mean, and median (Me).

A t-test was used to compare data between subgroups. For intergroup comparison of categorical baseline characteristics, the chi-square test or Fisher's exact test (if the expected frequency in any of the cells was >5) was used. The level of statistical significance (p) was set at 0.05 (two-sided). All statistical parameters were calculated using Stata 14 software.

RESULTS

Study subjects/participants

The current study included 42,799 patients who had clinical and laboratory-verified COVID-19 infection.

In the primary analysis of ECG findings, 47,292 recordings with or without diagnosed ECG phenomenon were selected. In the subsequent assessment, ECG recordings with no change in previous ECG diagnosis (n = 3927), duplicated patient records (n = 563), and records with incomplete data (n = 3) were excluded from the data analysis. Thus, the exclusion of 4,493 ECG recordings due to baseline material analysis allowed achieving quantitative matching of ECG findings with patients, i.e., one of the findings with a leading ECG diagnosis was considered for each study subject. The total number of registered primary and repeated ECG findings was 34,510 and 8,289, respectively.

Participants in the study ranged in age from 23 to 98 years. The mean age of patients with no pathologic ECG changes was 52.0 ± 14.5 years, whereas that of patients with various pathologic ECG syndromes was 69.6 ± 15.7 years ([p < 0.0001], Table 1).

Female patients (52%) outnumbered male patients in the study, but statistically significant differences between the subgroups for this parameter were not found (Table 2).

Main study results

Pathological ECG phenomena were recorded in 54% (n=23,113) of the study participants, with the percentage calculated based on the total number of patients.

Table 1. Descriptive statistics of the sample age structure

Parameters	Normal ECG	Abnormal ECG	Total
N	19 686	23 113	42 799
Mean	52,0	69,6	61,7
SD	14,5	15,7	17,5
95% ДИ	(47,7; 56,4)	(65,4; 73,9)	(58,2; 65,2)
Min	23	30	23
Max	77	98	98
Med	55	71	62
P (t-test)	<0,0001		-

Table 2. Distribution of examined subjects by gender

Gender	Normal ECG	Abnormal ECG	Total	*p*-value
Female	9626 (48,9%)	12 629 (54,6%)	22 255 (52,0%)	0,299
Male	10 060 (51,1%)	10 484 (45,4%)	20 544 (48,0%)	

The most common cardiac rhythm and conduction disorders were supraventricular arrhythmia and atrial fibrillation, found in 12.6% and 12.0% of the patients examined, respectively. Moreover, sinus tachycardia was found in 7.13% of the patients.

Signs of right heart overload were registered in 12.5% of patients. This was demonstrated by ECG signs of right atrial and ventricular enlargement, diastolic and systolic tension in the right ventricular myocardium, pulmonary hypertension, and $S_IQ_{III}T_{III}$ patterns, which indicated the development of pulmonary embolism. In this study, the ECG pattern of pulmonary embolism was discovered in 485 patients. Figure 1 depicts an example of the $S_IQ_{III}T_{III}$ ECG pattern.

Infarct-like changes were found in 4.5% of the patients, including three cases of the Brugada pattern (Fig. 2).

Signs of acute myocardial ischemia were observed in 0.5% of cases. Further, acute tissue abnormalities manifested by ECG ST-T changes were found in 2.2% of patients. Figure 3 shows a case of ST segment and T-wave changes.

ECGs with prolonged QT and QTc intervals were recorded in 540 patients, accounting for 1.26% of all subjects examined. Notably, all these subjects were treated with azithromycin and hydroxychloroquine.

During the specified time period, single cases of ventricular fibrillation, Frederick's syndrome, and AV blocks of various degrees were recorded (Table 3).

Fig. 1. $S_IQ_{III}T_{III}$ ECG pattern. Male patient, 81 years old. Diagnosis: COVID-19, negative polymerase chain reaction test. Out-of-hospital bilateral polysegmental pneumonia. Computed tomography findings: Pulmonary tissue involvement of approximately 80%. ECG findings of 02/02/2021: First-degree AV block and second-degree AV block type 2 (2:1; 3:1), 61 bpm. Left axis deviation. $S_IQ_{III}T_{III}$ type, ST elevation, and negative T-wave in II, III, AVF, and V_1–V_5 leads

DISCUSSION

Main study result summary

Cardiovascular complications are common in COVID-19 patients and are reflected in altered ECGs. Thus, ECG phenomena were found in 54% of patients. The most common disorders were supraventricular arrhythmia and atrial

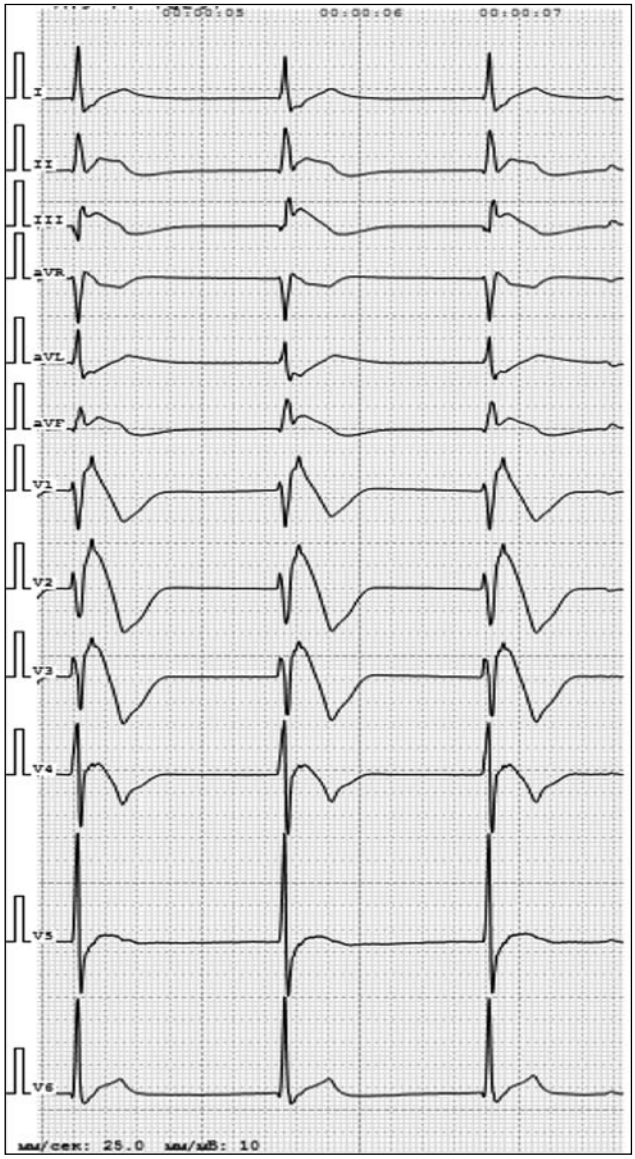

Fig. 2. ECG pattern of Brugada syndrome. Male patient, 67 years old. Diagnosis: COVID-19, positive polymerase chain reaction tests. Out-of-hospital bilateral polysegmental pneumonia. Computed tomography findings: Pulmonary tissue involvement of approximately 75%. ECG findings of 05/22/2020: Wandering of atrial pacemaker. Single supraventricular arrhythmia, 51 bpm. Normal axis. Right bundle branch block. Left ventricular hypertrophy. ST elevation in II, III, AVF, and V_1–V_5 leads

fibrillation, found in 12.6% and 12.0% of patients, respectively. Signs of right heart overload were seen in 12.5% of patients, including 1.13% (485 patients) with ECG pattern of pulmonary embolism. Infarct-like ECG changes occurred in 4.5% of cases, with three patients exhibiting the Brugada pattern. Moreover, ST-T changes were observed in 2.2% of all patients. In 540 patients, ECGs with prolonged QT and QTc intervals were recorded (1.26%).

In addition, single cases of ventricular fibrillation, Frederick's syndrome, and AV blocks of various degrees were observed.

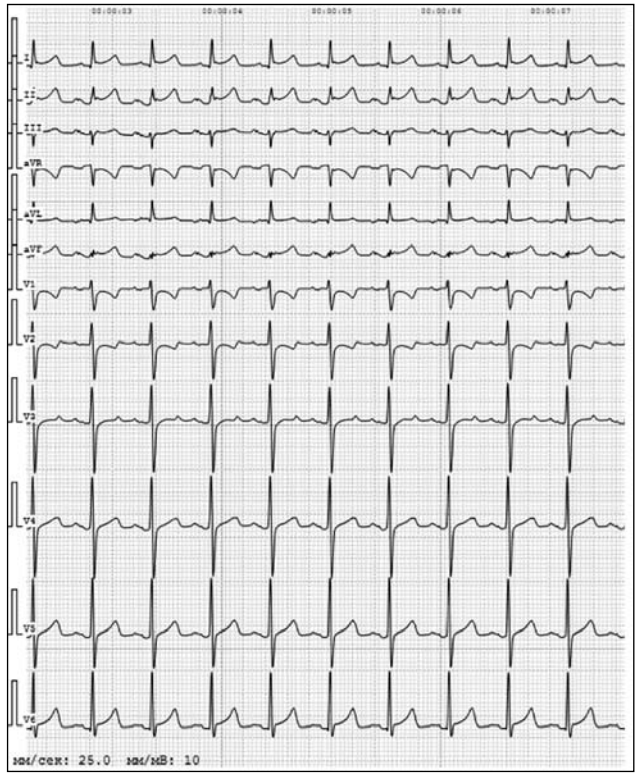

Fig. 3. ST segment and T-wave changes. Female patient, 74 years old. Diagnosis: COVID-19, positive polymerase chain reaction tests. Out-of-hospital bilateral polysegmental pneumonia. Computed tomography findings: Pulmonary tissue involvement of approximately 25% and 50% on the left and right, respectively. ECG findings of 02/25/2021: Sinus tachycardia, 111 bpm. Left axis deviation. ST elevation in I, II, AVL, and AVF leads and ST depression in AVR and V_1 leads

Main study result discussion

The analysis of ECG studies showed that ECG changes are common and occur in more than half (54%) of hospitalized patients with confirmed COVID-19. The obtained data are consistent with global statistics on the prevalence of cardiovascular complications in coronavirus infection and have been confirmed in a number of papers [9, 12–14]. One of the reasons for the high prevalence of cardiovascular complications in COVID-19 is the disease pathogenesis. The binding of the viral surface protein to the angiotensin-converting enzyme 2 (ACE2) receptor is necessary for the infectious process to progress. Moreover, ACE2 receptors located on the membranes of type II pneumocytes are found in high concentrations in the heart and vascular endothelium, including the coronary artery. Thus, the virus causes direct myocardial damage. Cardiovascular complications may develop as a result of molecular mimicry, with immune reactions being activated by a type of "cytokine storm," which is exacerbated by hypoxia due to respiratory failure [6]. In patients with preexisting cardiovascular diseases, SARS-CoV-2 infection aggravates the underlying disease (even if it was previously well controlled by drug therapy) due to pulmonary hypertension, impaired immune regulation, and the direct

Table 3. Structure of ECG phenomena in COVID-19

ECG phenomena	Patients (*n* = 42799)	
	n	%
Supraventricular arrhythmia	5401	12,6
Tachyarrhythmias:		
• Atrial fibrillation	5142	12,0
• Sinus tachycardia	3050	7,13
• Ventricular tachycardia	3	0,007
Bradyarrhythmias:		
• Atrioventricular block (varying degrees)	19	0,04
• Sinus bradycardia	7	0,016
ST-T changes	924	2,2
Brugada-like changes	3	0,007
$S_IQ_{III}T_{III}$ pattern	485	1,13
Infarct-like changes	1941	4,5
Acute myocardial ischemia	214	0,5
Right heart overload	5338	12,5
QT-QTc prolongation	540	1,26
Other ECG changes (ventricular fibrillation, Frederick's syndrome, etc.)	46	0,11

effect of the viral agent, resulting in a more severe course of COVID-19, including prolonged hospitalization, increased risk of death, and transfer to the intensive care unit [2, 6, 12, 15]. Thus, the link between COVID-19 and cardiovascular disease becomes evident, with preexisting pathologies exacerbating the course of the infectious disease and SARS-CoV-2 contributing to or resulting in acute cardiovascular events [6].

Systematization of ECG phenomena in COVID-19 patients using a large dataset allowed for the identification and categorization of various electrocardiographic changes by prevalence, which is characteristic of rhythm and conduction disorders, myocarditis, ischemia, right heart overload, pulmonary embolism, and cardiotoxic effect of drugs in the 4-aminoquinoline derivatives group.

Supraventricular arrhythmia was the most common ECG phenomenon in COVID-19 patients. In clinical practice, it is one of the most common arrhythmias, regardless of gender or age, and develops in the presence of cardiovascular, endocrine, and bronchopulmonary diseases, as well as other disorders, leading to the involvement of the cardiovascular system in the pathological process. Remarkably, supraventricular arrhythmia may occur in a relatively healthy patient when exposed to a stressor or physical activity, or due to the use of drugs, caffeine, and smoking. Direct or mediated exposure of the SARS-CoV-2 viral agent to the myocardium and metabolic disorders caused by the coronavirus infection contribute to the development of supraventricular arrhythmia. In addition, other authors state that it is the most common arrhythmia in COVID-19 patients [2, 6, 9, 12].

In the structure of ECG phenomena, atrial fibrillation took the lead among tachyarrhythmias and was recorded in 12% of patients with confirmed COVID-19. In the general population, the prevalence of atrial fibrillation ranges between 1% and 2% [16]. Its occurrence in a viral process is linked to the pathophysiological mechanisms of arrhythmia, which requires a trigger and a substrate for its maintenance [16]. In the context of coronavirus infection, systemic inflammatory response, fever, and COVID-induced hypoxemia may be triggers for arrhythmia [12, 14, 17]. According to our findings, the mean age of patients with abnormal ECG changes was 69.6 ± 15.7 years, which is a risk factor for atrial fibrillation because the probability of developing atrial fibrillation increases in persons over the age of 40, according to numerous clinical studies. Moreover, age is 1 of the 15 key factors in determining the risk of thromboembolic complications [16]. The prevalence of concomitant cardiovascular and endocrine pathologies, which also contribute to the development of atrial fibrillation, increases with age. The authors of several studies concluded that the presence of atrial fibrillation in patients with coronavirus pneumonia significantly worsens the prognosis of the disease [9, 13, 17, 18]. Thus, Wang et al. analyzed clinical features in 319 patients with severe and extremely severe course of COVID-19 [18]. Male patients predominated among the extremely severe group, whereas females prevailed among the subjects with a severe course of the disease ($p < 0.05$). The proportion of stroke patients in the group of critically ill patients was significantly higher than in the group with a severe course of

the disease ($p < 0.05$). The frequency of increased levels of cardiac-specific troponin I, natriuretic peptide (NT-proBNP), D-dimer, C-reactive protein, and hypocalcemia was higher in critically ill patients than in those with a severe disease ($p < 0.001$). Multivariate logistic regression analysis showed that increased NT-proBNP levels and age were independent predictors of atrial fibrillation, which was then an independent risk factor for hospital mortality (OR = 3.857, 95% CI 1.506–9.879) and artificial respiration (OR = 4.701, 95% CI 1.864–11.856) [18]. Based on the results of studies indicating an increased risk of thromboembolic complications and death in the severe course of coronavirus infection, careful selection of anticoagulant therapy in patients with COVID-19 and concomitant atrial fibrillation is necessary to balance the risk of thromboembolism and possible bleeding.

Furthermore, sinus tachycardia is a common ECG syndrome in coronavirus infection. Thus, the overall prevalence of sinus tachycardia in COVID-19 patients was 7.13%. In a study by D. Wang et al., which included 138 patients hospitalized for COVID-19, tachycardia was found in 17% of cases, and the frequency of arrhythmia reached 44.4% in severely ill patients and those in the intensive care unit, but did not exceed 6.9% in other hospitalized patients [19]. Sinus tachycardia has a negative impact on the clinical course and prognosis of the disease. Y. Wang et al. reported that sinus tachycardia was found to be an independent risk factor for hospital mortality (OR = 6.545, 95% CI 3.166–13.531, and $p < 0.001$) and artificial respiration (OR = 4.804, 95% CI 2.322–9.941, and $p < 0.001$) [18]. In addition, the functional reserve of the left ventricle in long-term tachycardia may decrease due to a weakening of its pumping function, increasing the risk of tachycardia-induced cardiomyopathy.

Bradyarrhythmias were much less common. Thus, out of 23,113 subjects with coronavirus infection and registered ECG abnormalities, sinus bradycardia and atrioventricular blocks of varying degrees were found in 7 and 19 cases, respectively.

In the conducted study, right heart overload was confirmed by signs of right atrial and ventricular hypertrophy, diastolic and systolic tension of the right ventricular myocardium, pulmonary hypertension, and patterns of pulmonary embolism. Signs of right ventricular overload were recorded in 12.5% of COVID-19 patients. The most common manifestation of right heart overload was diastolic overload in the form of right bundle branch block, most of which was incomplete. Thus, Ryabykina investigated the signs of electrocardiographic right ventricular stress in COVID-19 patients and, when analyzing 150 ECGs, discovered that the most common signs of right ventricular dysfunction were incomplete right bundle branch block (42.6%), right atrial phase of P-wave (41.3%), $S_IQ_{III}T_{III}$ ECG type (33.3%), and right ventricular hypertrophy, mostly represented by increasing of $S_{V5–6}$ waves (14.7%) [7]. The registration of the $S_IQ_{III}T_{III}$ pattern as a marker of acute cor pulmonale and pulmonary embolism required special attention due to the right atrial changes. According to the literature, registration of $S_IQ_{III}T_{III}$, complete right bundle branch block, and ST elevation in $V_{1–4}$ chest leads is associated with a high risk of death [20]. This ECG pattern was observed in 485 patients who were later diagnosed with pulmonary embolism. Thus, given the acute damage to the pulmonary tissue and the preexisting hypercoagulable syndrome associated with COVID-19, acute pulmonary thromboembolism should be ruled out first when recording ECG patterns of right heart involvement in the pathological process.

Moreover, markers of acute myocardial damage and infarct-like changes revealed on ECG are noteworthy. Myocarditis caused by the coronavirus infection is a common phenomenon, and its pathogenesis is associated with an active immune response to the myocardium affected by the virus [2, 3, 6, 8, 19, 20]. Acute myocardial damage correlates with an increased risk of hospital mortality. Thus, Shi et al., as a result of the analysis of clinical, laboratory, and instrumental data of 416 hospitalized patients with confirmed coronavirus infection, revealed that those with signs of myocardial damage had a higher in-hospital mortality rate when compared to patients without such signs (51.2% vs. 4.5% [$p < 0.001$]) [2]. Patients with myocardial damage had a higher risk of death compared to those without such a complication, both from the onset of symptoms (OR = 4.26, 95% CI 1.92–9.49) and from admission to the endpoint (OR = 3.41, 95% CI 1.62–7.16) [2].

ECG signs of myocarditis include reduced wave amplitude in limb leads, ST segment elevation predominant in the lower and lateral leads, and ST segment depression with T-wave inversion in V_1 and aVR leads [20]. In our study, such ST-T patterns were observed in 2.2% of patients. Notably, myocarditis can cause life-threatening arrhythmias, bundle branch blocks, QT interval prolongation, and infarct-like changes [3, 6, 20].

Special attention should be given to Brugada-like ECG changes, which include pseudoblocks of the right bundle branch and persistent ST segment elevation in $V_{1–2}$ leads [7]. In the analyzed material, three such cases were found. True Brugada syndrome is a genetic disorder that increases the risk of fatal arrhythmias and sudden death. In COVID-19 patients, existing long-term fever, metabolic disorders, and viral myocardial damage may result in ECG patterns similar to Brugada syndrome; however, unlike true Brugada syndrome, these disorders are transient and disappear when the overall disease pattern improves. Nevertheless, Brugada-like ECG changes significantly complicate diagnostic and clinical strategies, because they are frequently associated with chest pain, mimicking acute myocardial infarction [4, 20]. Coronary artery thrombosis and hyperactivation of coagulation cascade are the primary causes of acute myocardial ischemia in coronavirus infection [6, 7]. Therefore, the patient's history and the data of coronary angiography and laboratory markers of myocardial damage are important for differential diagnosis. In this study, ECG patterns of acute ischemia were detected in 0.5% of patients.

QT and QTc interval prolongation was reported as one of the possible causes of life-threatening arrhythmias in 1.26% of patients who were hospitalized for COVID-19. Remarkably, off-label patients were given antimalarials such as chloroquine and hydroxychloroquine, as well as azithromycin (a macrolide antibiotic). These drugs have a pro-arrhythmogenic effect because of their direct influence on cellular transmembrane potential, which is expressed by QT and QTc interval prolongation, potentially leading to the development of pirouette-type tachycardia [5, 7, 20]. In addition, macrolide use is associated with QT interval prolongation and may lead to pirouette-type tachycardia, especially when combined with concomitant bradycardia, hypokalemia, and hypomagnesemia [20]. Given these peculiarities of pharmacological effects of the aforementioned drugs, continuous monitoring of the QT interval for timely correction of drug therapy and prevention of life-threatening arrhythmias may be recommended for all patients who receive such therapy.

Study limitations

There were some limitations to the study.

The current study used a nonselective sample of patients with confirmed COVID-19 infection, regardless of concomitant pathology, severity of clinical condition, data of laboratory and other instrumental examinations, and duration of hospital stay. This approach to sampling is relevant in the context of the present study's aim because it allows for the primary structuring of ECG changes in the population of Moscow residents. However, stratification of the risk of death, time to complete recovery, and the risk of transferring patients to the intensive care unit are of broad practical interest. Therefore, a future study with subgrouping of patients for the aforementioned analysis is planned.

Importantly, when ranking ECG phenomena among tachyarrhythmias, atrial fibrillation was considered as a single nosology, without differentiating its forms. The revealed ECG changes peculiar to right heart overload, myocarditis, and coronary heart disease are often insufficiently specific, necessitating verification with laboratory tests and instrumental diagnostic methods.

CONCLUSIONS

Based on the analysis, the frequency of ECG phenomena in COVID-19 patients was determined. In addition, a high incidence of atrial fibrillation, which is a risk factor for thromboembolic complications, especially in the elderly, was associated with activation of the hemostasis system due to the coronavirus infection. Simultaneously, a significant prevalence of ECG patterns of right heart overload, including some associated with pulmonary thromboembolism, was established and may be associated with COVID-induced pulmonary tissue lesions. The remaining ECG changes were characterized by a much lower prevalence. However, this does not reduce their clinical significance given the risk to the patients' health and quality of life.

ECG remains the most convenient and accessible method for assessing the pathology of the cardiovascular system in COVID-19 patients, which is explained by the ECG technical simplicity and low cost, as well as the ability to remotely evaluate the obtained results.

The information gathered may serve to optimize the management tactics of patients with coronavirus infection in the long-term.

ADDITIONAL INFORMATION

Funding source. This article was prepared with support of Moscow Healthcare Department as a part of Program "Scientific Support of the Capital's Healthcare" for 2020–2022 (Unified State Information System for Accounting of Research, Development, and Technological Works No: EGISU: AAAA-A20-120071090050-1.

Competing interests. The authors declare no obvious and potential conflicts of interest related to the publication of this article.

Authors' contributions. A.E. Demkina, V.Y. Taskina, T.M. Gazashvili, A.V. Vladzymyrskyy, S.P. Morozov — study concept and design; V.Y. Taskina — literature search, manuscript writing; T.M. Gazashvili — collection and processing of material; A.E. Demkina, T.M. Gazashvili, A.V. Vladzymyrskyy, S.P. Morozov, A.S. Shkoda — manuscript review. All authors made a substantial contribution to the conception of the work, acquisition, analysis, interpretation of data for the work, drafting and revising the work, final approval of the version to be published and agree to be accountable for all aspects of the work.

REFERENCES

1. Wu Z, McGoogan JM. Characteristics of and important lessons from the Coronavirus Disease 2019 (COVID-19) outbreak in China: summary of a report of 72314 cases from the Chinese Center for Disease Control and Prevention. *JAMA*. 2020;323(13):1239–1242. doi:10.1001/jama.2020.2648

2. Shi S, Qin M, Shen B, et al. Association of cardiac injury with mortality in hospitalized patients with COVID-19 in Wuhan, China. *JAMA Cardiol*. 2020;5(7):802–810. doi: 10.1001/jamacardio.2020.0950

3. Madjid M, Safavi-Naeini P, Solomon SD, Vardeny O. Potential effects of coronaviruses on the cardiovascular system: a review. *JAMA Cardiol*. 2020;5(7):831–840. doi: 10.1001/jamacardio.2020.1286

4. Vidovich MI. Transient Brugada-like electrocardiographic pattern in a patient with COVID-19. *JACC Case Rep*. 2020;2(9):1245–1249. doi: 10.1016/j.jaccas.2020.04.007

5. Gérard A, Romani S, Fresse A, et al. "Off-label" use of hydroxychloroquine, azithromycin, lopinavir-ritonavir and chloroquine in COVID-19: A survey of cardiac adverse drug reactions by the French Network of Pharmacovigilance Centers. *Therapie*. 2020;75(4):371–379. doi:10.1016/j.therap.2020.05.002

6. Mai F, Del Pinto R, Ferri C. COVID-19 and cardiovascular diseases. *J Cardiol*. 2020;76(5):453–458. doi: 10.1016/j.jjcc.2020.07.013

7. Ryabykina GV. ECG changes in COVID-19. *Kardiologiia*. 2020; 60(8):16–22. (In Russ). doi: 10.18087/cardio.2020.8.n1192
8. Poteshkina NG, Lysenko MA, Kovalevskaya EA, et al. Cardiac damage in patients with COVID-19 coronavirus infection. *Arterial Hypertension*. 2020;26(3):277–287. (In Russ). doi: 10.18705/1607-419X-2020-26-3-277-287
9. Lanza GA, De Vita A, Ravenna SE, et al. Electrocardiographic findings at presentation and clinical outcome in patients with SARS-CoV-2 infection. *Europace*. 2021;23(1):123–129. doi: 10.1093/europace/euaa245
10. Morozov SP, Vladzimirskyy AV, Demkina AE, et al. Centralization of descriptions of electrocardiographic studies in primary health care: guidelines. The series "Best practices of radiation and instrumental diagnostics". Issue 62. Moscow: Scientific and Practical Clinical Center for Diagnostics and Telemedicine Technologies of the Department of Healthcare of the City of Moscow; 2020. 24 p. (In Russ).
11. Morozov SP, Vladzimirskyy AV, Simenyura SS, et al. Digitalization of primary functional diagnostics data (example of electrocardiographic studies). *Creative Cardiology*. 2020;14(1):16–23. doi: 10.24022/1997-3187-2020-14-1-16-23
12. Li Y, Liu T, Tse G, et al. Electrocardiograhic characteristics in patients with coronavirus infection: A single-center observational study. *Ann Noninvasive Electrocardiol*. 2020;25:e12805. doi: 10.1111/anec.12805
13. Bertini M, Ferrari R, Guardigli G, et al. Electrocardiographic features of 431 consecutive, critically ill COVID-19 patients: An insight into the mechanisms of cardiac involvement. *Europace*. 2020;22(12):1848–1854. doi: 10.1093/europace/euaa258
14. Angeli F, Spanevello A, De Ponti R, et al. Electrocardiographic features of patients with COVID-19 pneumonia. *Eur J Intern Med*. 2020;78:101–106. doi: 10.1016/j.ejim.2020.06.015
15. Demkina AE, Morozov SP, Vladzymyrskyy AV, et al. Risk factors for outcomes of COVID-19 patients: an observational study of 795572 patients in Russia. *medRxiv*. 2020;11.02.20224253. doi: 10.1101/2020.11.02.20224253
16. Atrial fibrillation and flutter. Clinical guidelines (approved by the Ministry of Health of the Russian Federation). 2020. Available from: https://scardio.ru/content/Guidelines/2020/Clinic_rekom_FP_TP.pdf. Accessed: 21.05.2021.
17. Hu YF, Cheng WH, Hung Y, et al. Management of atrial fibrillation in COVID-19 pandemic. *Circ J*. 2020;84(10):1679–1685. doi: 10.1253/circj.CJ-20-0566
18. Wang Y, Chen L, Wang J, et al. Electrocardiogram analysis of patients with different types of COVID-19. *Ann Noninvasive Electrocardiol*. 2020;25(6):e12806. doi: 10.1111/anec.12806
19. Wang D, Hu B, Hu C, et al. Clinical characteristics of 138 hospitalized patients with 2019 novel coronavirus-infected pneumonia in Wuhan, China [published correction appears in JAMA. 2021 Mar 16;325(11):1113]. *JAMA*. 2020;323(11):1061–1069. doi: 10.1001/jama.2020.1585
20. Shlyakhto EV, Parmon EV, Berngardt ER, Zhabina ES. Features of electrocardiographic changes in non-coronarogenic syndromes in patients with COVID-19. *Russian Journal of Cardiology*. 2020; 25(7):4019. (In Russ). doi: 10.15829/1560-4071-2020-4019

СПИСОК ЛИТЕРАТУРЫ

1. Wu Z., McGoogan J.M. Characteristics of and important lessons from the Coronavirus Disease 2019 (COVID-19) outbreak in China: Summary of a Report of 72314 cases from the Chinese Center for Disease Control and Prevention // JAMA. 2020. Vol. 323, N 13. P. 1239–1242. doi: 10.1001/jama.2020.2648
2. Shi S., Qin M., Shen B., et al. Association of cardiac injury with mortality in hospitalized patients with COVID-19 in Wuhan, China // JAMA Cardiol. 2020. Vol. 5, N 7. P. 802–810. doi: 10.1001/jamacardio.2020.0950
3. Madjid M., Safavi-Naeini P., Solomon S.D., Vardeny O. Potential effects of coronaviruses on the cardiovascular system: a review // JAMA Cardiol. 2020. Vol. 5, N 7. P. 831–840. doi: 10.1001/jamacardio.2020.1286
4. Vidovich M.I. Transient Brugada-like ECG pattern in a patient with coronavirus disease 2019 (COVID-19) // JACC Case Rep. 2020. Vol. 2, N 9. P. 1245–1249. doi: 10.1016/j.jaccas.2020.04.007
5. Gérard A., Romani S., Fresse A., et al. "Off-label" use of hydroxychloroquine, azithromycin, lopinavir-ritonavir and chloroquine in COVID-19: A survey of cardiac adverse drug reactions by the French Network of Pharmacovigilance Centers // Therapie. 2020. Vol. 75, N 4. P. 371–379. doi: 10.1016/j.therap.2020.05.002
6. Mai F., Del Pinto R., Ferri C. COVID-19 and cardiovascular diseases // J Cardiol. 2020. Vol. 76, N 5. P. 453–458. doi: 10.1016/j.jjcc.2020.07.013
7. Рябыкина Г.В. Изменения электрокардиограммы при инфекции COVID-19 // Кардиология. 2020. Т. 60, № 8. С. 16–22. doi: 10.18087/cardio.2020.8.n1192
8. Потешкина Н.Г., Лысенко М.А., Ковалевская Е.А., и др. Кардиальное повреждение у пациентов с коронавирусной инфекцией COVID-19 // Артериальная гипертензия. 2020. Т. 26, № 3. С. 277–287. doi: 10.18705/1607-419X-2020-26-3-277-287
9. Lanza G.A., De Vita A., Ravenna S.E., et al. Electrocardiographic findings at presentation and clinical outcome in patients with SARS-CoV-2 infection // Europace. 2021. Vol. 23, N 1. P. 123–129. doi: 10.1093/europace/euaa245
10. Морозов С.П., Владзимирский А.В., Демкина А.Е., и др. Централизация описаний электрокардиографических исследований в первичном звене здравоохранения: методические рекомендации. Серия «Лучшие практики лучевой и инструментальной диагностики». Вып. 62. Москва: ГБУЗ «НПКЦ ДиТ ДЗМ», 2020. 24 с.
11. Морозов С.П., Владзимирский А.В., Сименюра С.С., и др. Эффективность централизации электрокардиографических исследований в первичном звене здравоохранения // Креативная кардиология. 2020. Т. 14, № 1. С. 16–23. doi: 10.24022/1997-3187-2020-14-1-16-23
12. Li Y., Liu T., Tse G., et al. Electrocardiograhic characteristics in patients with coronavirus infection: A single-center observational study // Ann Noninvasive Electrocardiol. 2020. Vol. 25, N 6. P. e12805. doi: 10.1111/anec.12805
13. Bertini M., Ferrari R., Guardigli G., et al. Electrocardiographic features of 431 consecutive, critically ill COVID-19 patients: an insight into the mechanisms of cardiac involvement // EP Europace. 2020. Vol. 22, N 12. P. 1848–1854. doi: 10.1093/europace/euaa258

14. Angeli F., Spanevello A., De Ponti R., et al. Electrocardiographic features of patients with COVID-19 pneumonia // Eur J Intern Med. 2020. Vol. 78. P. 101–106. doi: 10.1016/j.ejim.2020.06.015
15. Demkina A.E., Morozov S.P., Vladzymyrskyy A.V., et al. Risk factors for outcomes of COVID-19 patients: an observational study of 795 572 patients in Russia // medRxiv. 2020. P. 2020.11.02.20224253. doi: 10.1101/2020.11.02.20224253
16. Фибрилляция и трепетание предсердий. Клинические рекомендации (утв. Министерством здравоохранения Российской Федерации). 2020. Режим доступа: https://scardio.ru/content/Guidelines/2020/Clinic_rekom_FP_TP.pdf. Дата обращения: 21.05.2021.
17. Hu Y.F, Cheng W.H., Hung Y., et al. Management of atrial fibrillation in COVID-19 Pandemic // Circ J. 2020. Vol. 84, N 10. P. 1679–1685. doi: 10.1253/circj.CJ-20-0566
18. Wang Y., Chen L., Wang J., et al. Electrocardiogram analysis of patients with different types of COVID-19 // Ann Noninvasive Electrocardiol. 2020. Vol. 25, N 6. P. e12806. doi: 10.1111/anec.12806
19. Wang D., Hu B., Hu C., et al. Clinical characteristics of 138 hospitalized patients with 2019 novel coronavirus-infected pneumonia in Wuhan, China // JAMA. 2020. Vol. 323, N 11. P. 1061–1069. doi: 10.1001/jama.2020.1585 [published correction appears in JAMA. 2021. Vol. 325, N 11. P. 1113. doi: 10.1001/jama.2021.2336]
20. Шляхто Е.В., Пармон Е.В., Бернгардт Э.Р., Жабина Е.С. Особенности электрокардиографических изменений при некоронарогенных синдромах у пациентов с COVID-19 // Российский кардиологический журнал. 2020. Т. 25, № 7. С. 194–200. doi: 10.15829/1560-4071-2020-4019

AUTHORS' INFO

*** Varvara Y. Taskina**, MD, Cand. Sci. (Med.);
address: 24 bld.1, Petrovka street, Moscow, 127051, Russia;
ORCID: https://orcid.org/0000-0003-4452-7667;
eLibrary SPIN: 6314-8190; e-mail: varvara.taskina@gmail.com

Alexandra E. Demkina, MD, Cand. Sci. (Med.);
ORCID: https://orcid.org/0000-0001-8004-9725;
eLibrary SPIN: 4657-5501; e-mail: a.demkina@npcmr.ru

Tamara M. Gazashvili, MD;
ORCID: https://orcid.org/0000-0002-5875-9699;
eLibrary SPIN: 4208-2303; e-mail: tamaradoc24@gmail.com

Andrey S. Shkoda, MD, Dr. Sci. (Med.), Professor;
ORCID: https://orcid.org/0000-0002-9783-1796;
eLibrary SPIN: 4520-2141; e-mail: a.shkoda@67gkb.ru.

Anton V. Vladzymyrskyy, MD, Dr. Sci. (Med.);
ORCID: https://orcid.org/0000-0002-2990-7736;
eLibrary SPIN: 3602-7120; e-mail: a.vladzimirsky@npcmr.ru

Sergey P. Morozov, MD, Dr. Sci. (Med.), Professor;
ORCID: http://orcid.org/0000-0001-6545-6170;
eLibrary SPIN: 8542-1720; e-mail: morozov@npcmr.ru

ОБ АВТОРАХ

*** Таскина Варвара Юрьевна**, к.м.н.;
Россия, 127051, Москва, ул. Петровка, д.24, стр.1;
ORCID: https://orcid.org/0000-0003-4452-7667;
eLibrary SPIN: 6314-8190; e-mail: varvara.taskina@gmail.com

Демкина Александра Евгеньевна, к.м.н.;
ORCID: https://orcid.org/0000-0001-8004-9725;
eLibrary SPIN: 4657-5501; e-mail: a.demkina@npcmr.ru

Газашвили Тамара Михайловна;
ORCID: https://orcid.org/0000-0002-5875-9699;
eLibrary SPIN: 4208-2303; e-mail: tamaradoc24@gmail.com

Шкода Андрей Сергеевич, д.м.н., профессор;
ORCID: https://orcid.org/0000-0002-9783-1796;
eLibrary SPIN: 4520-2141; e-mail: a.shkoda@67gkb.ru

Владзимирский Антон Вячеславович, д.м.н.;
ORCID: https://orcid.org/0000-0002-2990-7736;
eLibrary SPIN: 3602-7120; e-mail: a.vladzimirsky@npcmr.ru

Морозов Сергей Павлович, д.м.н., профессор;
ORCID: http://orcid.org/0000-0001-6545-6170;
eLibrary SPIN: 8542-1720; e-mail: morozov@npcmr.ru

* Corresponding author / Автор, ответственный за переписку

DOI: https://doi.org/10.17816/DD76726

Оценка диаметра лёгочной артерии при различной степени тяжести течения COVID-19 (по данным бесконтрастной компьютерной томографии лёгких)

А.Ф. Алиев[1, 3], Н.Д. Кудрявцев[1, 2], А.В. Петряйкин[2], З.Р. Артюкова[2], А.С. Шкода[1], С.П. Морозов[2]

[1] Городская клиническая больница № 67 имени Л.А. Ворохобова Департамента здравоохранения города Москвы, Москва, Российская Федерация
[2] Научно-практический клинический центр диагностики и телемедицинских технологий Департамента здравоохранения г. Москвы, Москва, Российская Федерация
[3] Московский городской научно-практический центр борьбы с туберкулезом Департамента здравоохранения г. Москвы, Москва, Российская Федерация

АННОТАЦИЯ

Обоснование. Компьютерная томография является методом выбора при оценке объёма поражения лёгких при вирусных пневмониях, в том числе ассоциированных с COVID-19. Помимо оценки объёма поражения лёгких, компьютерная томография позволяет определить размеры магистральных сосудов грудной клетки. Это позволило проанализировать связь между тяжестью течения COVID-19 и наличием изменения диаметров лёгочной артерии и восходящей аорты. Расширение лёгочной артерии является признаком лёгочной гипертензии. Изучение данных закономерностей может иметь клиническое значение в отношении определения тактики лечения и прогноза течения заболевания COVID-19.

Цель — оценить зависимость между диаметром лёгочной артерии и степенью тяжести течения COVID-19 у пациентов различного возраста.

Материалы и методы. Одноцентровое одномоментное сплошное неконтролируемое исследование выполнено в группе пациентов (n=511, 267 мужчин, медиана 59 лет, IQR 49,0–65,0, размах от 31 до 84 лет), проходивших лечение во временном госпитале для лечения пациентов с COVID-19. При госпитализации все пациенты прошли компьютерное томографическое исследование органов грудной клетки с помощью мобильной системы Airo TruCT (Stryker, США). Степень поражения лёгочной ткани оценивалась по шкале КТ 1–4. Измерение диаметра лёгочной артерии и восходящей аорты проводилось стандартными инструментами рабочей станции врача-рентгенолога перпендикулярно длинной оси сосуда.

Результаты. Получены следующие статистически значимые закономерности: расширение лёгочной артерии и увеличение отношения лёгочной артерии/восходящей аорты было связано с увеличением степени поражения лёгких при COVID-19 (критерий Краскела–Уоллиса, p <0,001; медианный тест, p <0,001); диаметр восходящего отдела аорты достоверно увеличивается с возрастом пациента (критерий Краскела–Уоллиса, p <0,001; медианный тест, p <0,001). Показаны недостоверная связь между увеличением диаметра лёгочной артерии и возрастом пациента (критерий Краскела–Уоллиса, p=0,094; медианный тест, p=0,311) и недостоверная связь между изменением диаметра восходящей аорты и степенью поражения лёгких (критерий Краскела–Уоллиса, p=0,061; медианный тест, p=0,165). Во всех возрастных группах с тяжёлым течением заболевания и большим объёмом поражения лёгких (КТ-3 и КТ-4) показано достоверно большее количество пациентов с признаками лёгочной гипертензии (расширенная от 29 мм и более лёгочная артерия).

Заключение. Дилатация лёгочной артерии и увеличение отношения диаметров лёгочной артерии/восходящей аорты достоверно связано с увеличением объёма поражения лёгких при COVID-19 во всех возрастных группах.

Ключевые слова: COVID-19; лёгочная артерия; лёгочная гипертензия; аорта; компьютерная томография.

Как цитировать

Алиев А.Ф., Кудрявцев Н.Д., Петряйкин А.В., Артюкова З.Р., Шкода А.С., Морозов С.П. Оценка диаметра лёгочной артерии при различной степени тяжести течения COVID-19 (по данным бесконтрастной компьютерной томографии лёгких) // *Digital Diagnostics.* 2021. Т. 2, № 3. С. 249–260. DOI: https://doi.org/10.17816/DD76726

Рукопись получена: 26.07.2021 **Рукопись одобрена:** 07.09.2021 **Опубликована:** 29.09.2021

DOI: https://doi.org/10.17816/DD76726

Changing of pulmonary artery diameter in accordance with severity of COVID-19 (assessment based on non-contrast computer tomography)

Alexander F. Aliev[1, 3], Nikita D. Kudryavtsev[1, 2], Alexey V. Petraikin[2], Zlata R. Artyukova[2], Andrey S. Shkoda[1], Sergey P. Morozov[2]

[1] L.A. Vorokhobov Municipal Clinical Hospital No 67 of the Moscow Health Department, Moscow, Russian Federation
[2] Moscow Center for Diagnostics and Telemedicine, Moscow, Russian Federation, Moscow, Russian Federation
[3] The Moscow Research and Clinical Center for Tuberculosis Control of the Moscow Health Department, Moscow, Russian Federation

ABSTRACT

BACKGROUND: Computed tomography is the method of choice for assessing the volume of lung damage in viral pneumonia, including those associated with COVID-19. In addition, computed tomography can determine the main vessels size of the thorax. This allowed us to analyze the relationship between the severity of COVID-19 and the changes in the diameters of the pulmonary artery (PA) and ascending aorta (Ao). Dilation of the PA is a sign of pulmonary hypertension. The study of these patterns may be of clinical significance in determining the treatment tactics and prognosis of the course of COVID-19 disease.

AIM: To evaluate the relationship between PA diameter and the severity of the COVID-19 course in patients of different ages.

MATERIALS AND METHODS: This study is a single-centered, cross-section, continuous, uncontrolled study performed on a group of patients (*n*=511, 267 men, median 59 years, IQR 49.0–65.0, ages 31–84 years) who were treated in a temporary hospital to treat patient with COVID-19. During hospitalization all patients were examined by CT scan of the chest. All studies were carried out using a mobile CT scan system Airo TruCT (Stryker, USA). The degree of damage to the lung tissue was assessed using the CT volume scale 1–4. Measurement of the LA and Ao diameters was carried out using standard instruments of the radiologist's CT workstation perpendicular to the long axis of the vessel.

RESULTS: The following statistically significant regularities were obtained: the detection of a dilated pulmonary artery (PA) and an increased PA/Ao ratio correlated to an increase in the degree of lung damage in COVID-19 (Kruskal-Wallis test, K-W p <0.001; median test, MT p <0.001), the diameter of the ascending aorta (Ao) significantly increases with the patient's age (K-W p <0.001; MT p <0.001). An insignificant correlation between an increase in the diameter of the pulmonary artery (PA) and the patient's age (K-W p=0.094; MT p=0.311) and an insignificant correlation between detection of a change in aortic (Ao) diameter and the degree of lung damage (K-W p=0.061; MT p=0.165) were shown. In groups with a severe course of the disease and a large volume of lung lesions (CT-3 and CT-4), a significantly greater number of patients with signs of pulmonary hypertension (detection of the dilated pulmonary artery: 29 mm and more) was shown for all age groups.

CONCLUSION: The study showed that PA dilatation and increased PA/Ao diameter ratio were significantly associated with increased pulmonary lesion volume in COVID-19 in all age groups.

Keywords: COVID-19; pulmonary artery; pulmonary hypertension; thoracic aorta; X-ray computed tomography.

To cite this article
Aliev AF, Kudryavtsev ND, Petraikin AV, Artyukova ZR, Shkoda AS, Morozov SP. Changing of pulmonary artery diameter in accordance with severity of COVID-19 (assessment based on non-contrast computer tomography). *Digital Diagnostics.* 2021;2(3):249–260. DOI: https://doi.org/10.17816/DD76726

Received: 26.07.2021 **Accepted:** 07.09.2021 **Published:** 29.09.2021

DOI: https://doi.org/10.17816/DD76726

评价当前COVID-19不同严重程度的光动脉直径(根据肺的非敏感性计算机断层扫描)

Alexander F. Aliev[1, 3], Nikita D. Kudryavtsev[1, 2], Alexey V. Petraikin[2], Zlata R. Artyukova[2], Andrey S. Shkoda[1], Sergey P. Morozov[2]

[1] L.A. Vorokhobov Municipal Clinical Hospital No 67 of the Moscow Health Department, Moscow, Russian Federation
[2] Moscow Center for Diagnostics and Telemedicine, Moscow, Russian Federation, Moscow, Russian Federation
[3] The Moscow Research and Clinical Center for Tuberculosis Control of the Moscow Health Department, Moscow, Russian Federation

简评

论证。计算机断层扫描是评估病毒性肺炎（包括COVID-19相关肺炎）肺部损伤的一种选择方法。除了评估肺损伤外，计算机断层扫描还可以确定胸腔主要血管的大小。分析了COVID-19流动的严重程度与肺动脉和上主动脉直径变化的存在之间的关系。肺动脉扩张是肺高压的标志. 研究这些模式可能对确定治疗策略和预测COVID-19疾病的趋势具有临床意义。

目标是估计不同年龄患者的光动脉直径和COVID-19流量的严重程度

材料与方法患者组中进行单核单级固体不受控制的研究 （n=511,267男性，中美洲59岁，IQR 49.0-65.0，范围从31至84岁），在临时医院治疗COVID-19患者。 随着住院治疗，所有患者都通过了使用IISRO Truct Mobile System（Stryker，美国）的胸部器官的计算机断层研究。 CT 1-4规模上估计了轻微组织的病变程度。 通过垂直于容器的长轴的放射科医生的工作站的标准工具来进行光动脉直径和上升主动脉的测量。

结果。获得以下统计学显着的模式：光动脉的膨胀和光动脉/升序姿势的升高与COVID-19肺部病变程度的增加有关（克拉克尔-沃利斯准则，p<0.001;中值测试，p<0.001）； 升高主动脉的直径随着患者的年龄而显着增加（克拉克尔-沃利斯准则，p <0.001;中值测试，p<0.001）。 显示了光动脉直径和患者年龄的直径之间的不准确的关系（克拉克尔-沃利斯准则，p=0.094;嗜源性测试，p=0.311）和腹腔直径的变化和肺部的病变程度之间的不准确的联系（克拉克尔-沃利斯准则，p=0,061;中值测试，p=0.165）。 所有年龄段的疾病方面和大量的肺病灶（KT-3和KT-4）中，可靠地增加了患有轻质高血压症状的患者（从29毫米和更多的光动脉膨胀）是显示。

结论。光动脉的扩张和光动脉/升序的直径比率的增加与在所有年龄组中COVID-19的肺病变的体积增加是可靠的。

关键词：COVID-19； 易动脉； 轻盈高血压； 主动脉； CT扫描。

引用本文

Aliev AF, Kudryavtsev ND, Petraikin AV, Artyukova ZR, Shkoda AS, Morozov SP. 评价当前COVID-19不同严重程度的光动脉直径（根据肺的非敏感性计算机断层扫描）. *Digital Diagnostics.* 2021;2(3):249–260. DOI: https://doi.org/10.17816/DD76726

收到： 26.07.2021 **接受：** 07.09.2021 **发布日期：**29.09.2021

BACKGROUND

In the context of the coronavirus disease-2019 (COVID-19) pandemic, pulmonary computed tomography (CT) became one of the leading methods for COVID-19 severity diagnosis and assessment [1–3].

The federal clinical guidelines for the prevention, diagnosis, and treatment defined four degrees of COVID-19 severity [2]. This division is based on several clinical and laboratory parameters, including the volume of pulmonary tissue lesions according to grades 1–4 of the CT classification [1, 3]. Patients with a mild degree of disease severity had no lung lesions (CT–0); moderate disease severity had up to 25% (CT–1) and 50%–75% (CT–2) lung involvement degree; 50%–75% (CT–3) in severe disease course; and over 70% (CT–4) in extremely severe disease. In addition, the degree of pneumonia severity according to the CT classification has prognostic value. Thus, a significantly increased proportion of patients who died depending on the volume of the affected pulmonary parenchyma according to the CT scale was shown, including a jump in the risk of lethality when transitioning from mild and moderate to severe and extremely severe disease course (from CT 1–2 to CT 3–4) [4].

The radiological sign analyses, which are typical for COVID-19-associated pneumonia, paid considerable attention to the pulmonary parenchyma, pleura, and bronchial tree assessment, and to a lesser extent, to the great vessel changes [5, 6]. The most characteristic and stable signs of COVID-19-associated pneumonia are segmental pulmonary artery (PA) dilation [7] and high risks of pulmonary embolism and acute respiratory distress syndrome, which is accompanied by gas exchange worsening, hypoxemia, and multiple organ failure [4, 7, 8].

A significantly increased PA diameter and PA and ascending aorta (Asc Ao) diameter ratio is shown in patients with lethal outcomes compared to those who recovered [9].

Thus, the lung lesion volume and the state of the pulmonary vessels (both segmental PAs, [10–12] and the pulmonary trunk [main PA]) are considered to assess the course of COVID-19, current therapy effectiveness, and prognosis using CT [9]. Increased pressure in the arterial vascular bed of the pulmonary circulation indicates the difficulty of blood transit through the lungs, which reduces the patient's compensatory abilities, leading to heart failure.

AIM: This study is aimed to determine the relationship between the COVID-19 severity and the PA and Asc Ao diameters in patients of different ages.

METHODS

Study design

A single-center, cross-sectional, continuous, and non-controlled study based on chest CT was conducted (Fig. 1).

Eligibility criteria

Inclusion criteria are COVID-19 diagnosis that is confirmed by polymerase chain reaction, signs of viral pneumonia on CT scan, and voluntary informed consent for

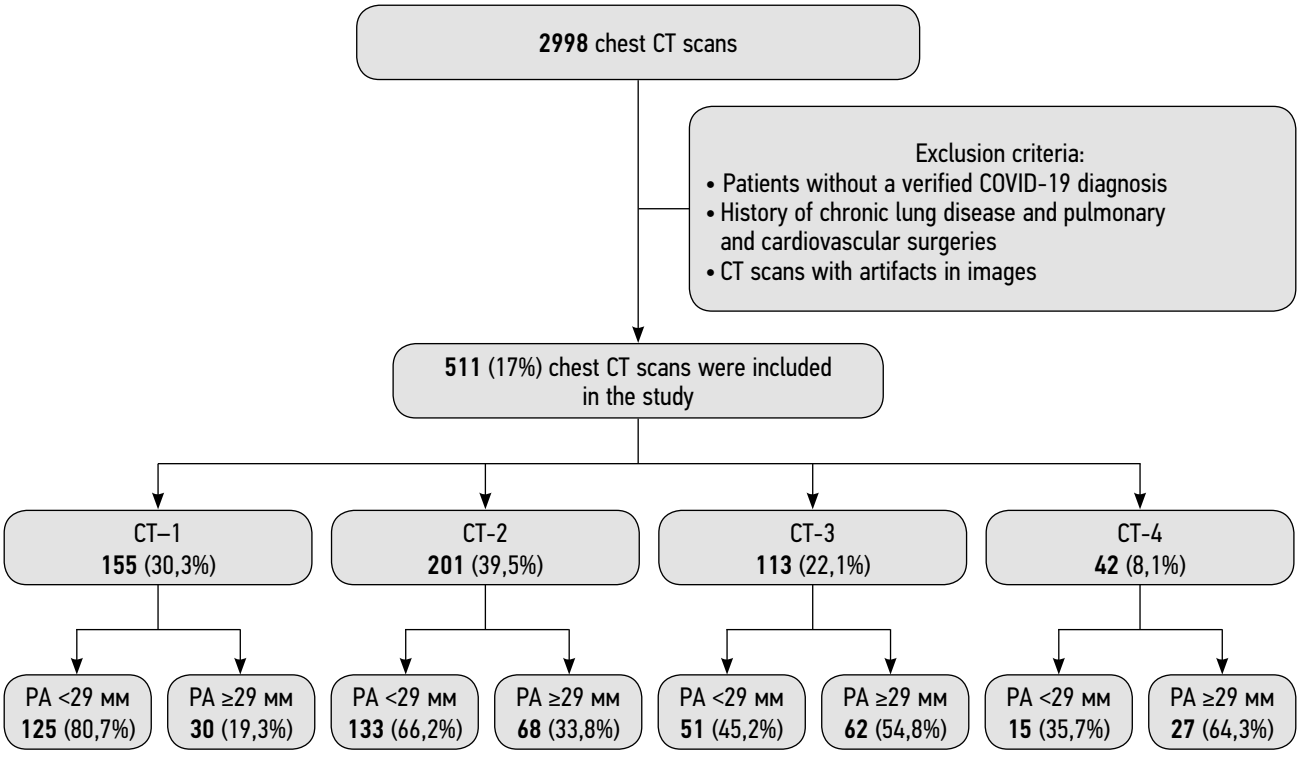

Fig. 1. Study design
CT: computed tomography; CT 1–4: adapted scale for visual assessment of the relationship between the severity of the patient's general condition and the nature and intensity of radiological signs of pulmonary changes in COVID-19; PA: pulmonary artery.

medical intervention. Chest CT scans were performed for the first time in a reserve hospital during admission or within 4 days after admission, provided that chest CT scans were performed in another medical institution at the prehospital stage [3].

Exclusion criteria are the history of chronic lung disease diagnosis, surgical interventions on the chest organs, and pronounced artifacts on CT scans that prevent an adequate lung lesion assessment and measurement of the great vessel diameters.

The non-inclusion criterion is the absence of viral pneumonia signs on CT scans (CT–0) due to a limited number of such admissions.

Setting

The study was conducted with a group of patients who were treated at the temporary reserve hospital in Krylatskoye Ice Palace (Vorokhobov City Clinical Hospital No. 67) from October 08, 2020, to December 05, 2020.

Medical intervention

in a specific period, 2998 non-contrast chest CT scans were performed in the hospital for diagnosis or follow-up of patients with COVID-19 viral pneumonia.

CT scans were performed on an Airo TruCT mobile CT scanner (Stryker, USA), which was installed at the reserve hospital for the treatment of patients with COVID-19 (Fig. 2). The mobile CT scanner has an extended aperture diameter of 105 cm and 32 detector rows. This CT system was designed for neurosurgical operating rooms. However, its compact size and low power requirements (possibility of connection to the 1.5 kW power grids) allows an effective usage of the device in a temporary hospital setting. In addition, the power supply unit of the tomograph allows short-term scanning with a power of up to 30 kV. Given the necessity of providing around-the-clock operation mode, the following scanning parameters were chosen: X-ray tube voltage: 120 kV, current: 38 mA, slice thickness:1 mm, matrix: 512×512, pitch: 1.415, rotation time: 1.92 sec, average scanning length: 30 cm (12 sec), and effective dose: 3.9 mSv. Maximum flow is up to 6 patients per hour.

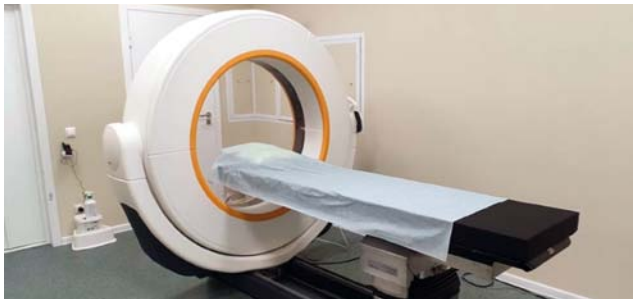

Fig. 2. Airo TruCT mobile CT scanner was installed in the admission department of the temporary reserve hospital for the treatment of patients with COVID-19, which was organized in the Krylatskoe Ice Palace.

The anonymized CT scans were independently assessed by two radiologists with 3 and 9 years of experience, respectively. The software of the Unified Radiological Information Service of the Unified Medical Information and Analytical System of Moscow City was used on the Agfa Enterprise Imaging platform (Agfa HealthCare, Belgium) to view CT scans and perform measurements. Axial CT 1 mm slices with pulmonary and soft-tissue viewing window parameters, (window width and level of 1500 HU, -500 HU, 350 HU, and 50 HU, respectively) were used for lung lesion degree assessment and great vessel measurement.

With a large patient flow, an empirical visual scale was used to assess the lung lesions based on the visual assessment of the thickened lung tissue volume according to axial and reconstructed chest coronal and sagittal images. Computer-assisted methods of assessing the affected parenchyma were not used.

The lung lesions, according to grades 1–4 of the CT classification, were assessed according to the approved guidelines [1, 2] and the scheme for describing pathological changes, which was proposed by domestic authors, based on the indication of the pulmonary parenchymal lesion volume. Pulmonary tissue changes (frosted glass, reticular thickening, consolidation, "cobblestone" appearance, "air bronchogram," and inverse "halo") were determined with the assessment of the lesion volume and localization of changes by the lung lobes and segments.

The PA size was measured on axial sections at the widest point, perpendicular to the long axis of the vessel (Fig. 3, *a*, *c*, *e*, *g*). The Asc Ao size was measured at the level of the maximum diameter of the right PA [13]. The accuracy of measurements was limited by the absence of contrast enhancement, cardiac gating, and reduced signal-to-noise ratio. Results were obtained by averaging independent measurements taken by two radiologists. A significant difference in the results of parenchymal lesion assessment or great vessel measurement (>2 mm) considers the opinion of a third radiologist with 15 years of work experience.

Main study outcome

The main study outcome is an assessment of the correlation between various measured PA and Asc Ao parameters and their derivative value with pulmonary parenchymal lesions and age dependence.

Additional study outcomes

An additional study outcome is an assessment of the relationship between the Asc Ao diameter and the patient's age, which confirm the previously established patterns.

Subgroup analyses

In the course of the study, patients of both genders were divided into four groups depending on the lung lesion volume (CT 1–4) and three age ranges (up to 50, 51–69, and over 70 years).

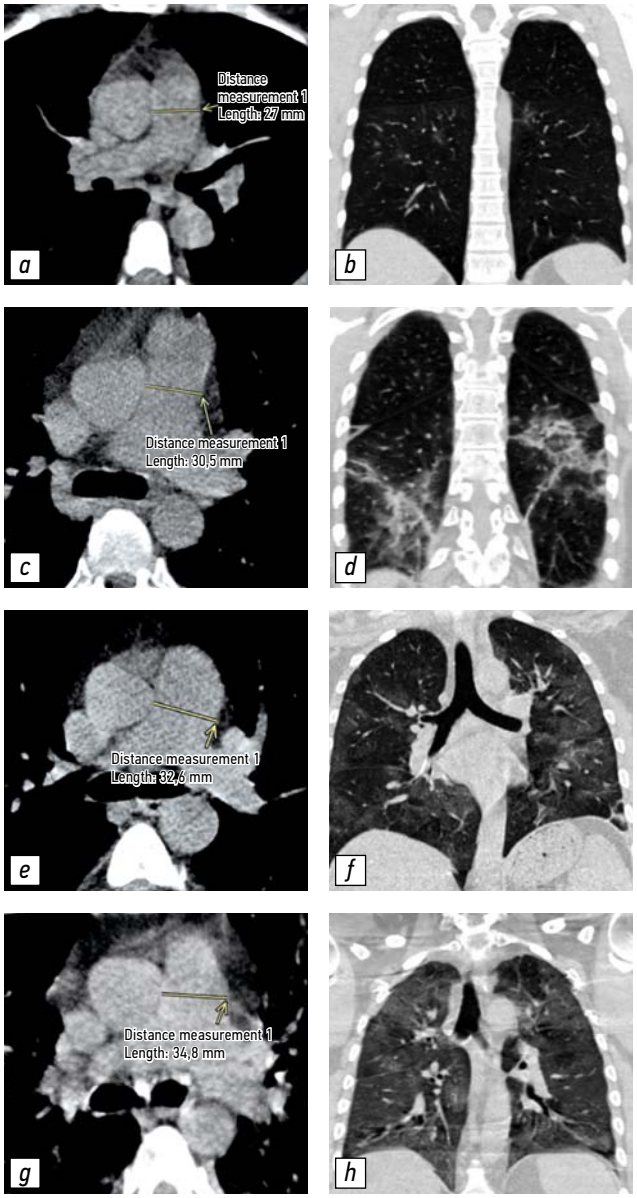

Fig. 3. Examples of CT scans with different PA diameters and lung lesion degrees: a, b, non-dilated PA (27.0 mm) with CT-1 lung lesion (<25%); c, d, dilated PA (30.5 mm) with CT-2 lung lesion (25%–50%); e, f, dilated PA (32.6 mm) with CT-3 lung lesion (50%–75%); g, h, dilated PA (34.8 mm) with CT-4 lung lesion (over 75%). CT: computed tomography; CT 1–4: adapted scale for visual assessment of the relationship between the patient's general condition severity and the nature and intensity of radiological signs of pulmonary changes in COVID-19; PA: pulmonary artery.

Ethical review

The study was conducted under the Declaration of Helsinki, which was developed by the World Medical Association.

The study was approved by the Independent Ethics Committee of the Moscow Regional Branch of the Russian Society of Roentgenologists and Radiologists, No. 2/2021, dated February 18, 2021.

Informed consent for medical intervention (CT examination) and the use of their medical data for scientific purposes was obtained from all participants.

Statistical analysis

Statistical data processing was conducted using StatSoft Statistica 12.0 software. The required sample size was determined using Altman's nomogram (with a power of 0.8 and a significance level of 0.05). Examination of over 500 patients obtained the minimum sufficient sample size and statistically significant results. The quantitative data distribution normality was checked using the Kolmogorov–Smirnov criterion and adjusted for Lilliefors and Shapiro–Wilk tests. Given the non-normal distribution of PA and Asc Ao parameters in several studied groups and different numbers of patients divided into groups, the reliability of differences was assessed using the nonparametric Kruskal–Wallis (K-W) test, nonparametric ANOVA analog, and median test (MT). The nonparametric Spearman's correlation coefficient (ρ) was used to further assess the relationship of several studied parameters of great vessel sizes, whereas 2 × 2 tables and nonparametric Fisher F-criterion were used to analyze differences between the groups. The significance level (p) in all tests was <0.05.

RESULTS

Study subjects/participants

CT scans of 511 patients both male (52.2%) and female (47.8%), with a mean age of 57 ± 12 years, the median age of 59 years, IQR of 49.0–65.0 years, min. of 31 years, and max. of 84 years, were analyzed. The distribution of patients by gender, lung lesion degree, and age intervals is shown in Table 1. Patient CT scans with different pulmonary parenchymal lesions and corresponding PA measurements are presented in Fig. 3.

Main study results

The following significant patterns were obtained: an increased PA diameter with lung lesion severity (K-W, $p < 0.001$; MT, $p < 0.001$), increasd Asc Ao diameter with the patient's age (K-W, $p < 0.001$; MT, $p < 0.001$), increased PA/Asc Ao ratio with lung lesion severity (K-W, $p < 0.001$; MT, $p = 0.008$), and decreased parameter with age (K-W, $p < 0.001$; MT, $p < 0.001$). Both the correlation of a small increase in the pulmonary trunk diameter with age (K-W, $p = 0.094$; MT, $p = 0.311$) and a small increase in the aortic diameter depending on lung lesion degree (K-W, $p = 0.061$; MT, $p = 0.165$) were not significant.

Results presented in Fig. 4 determined the following Spearman's correlation coefficients (between the PA diameter and lesion severity): for the entire sample, $\rho = 0.268$, $p < 0.005$; up to 50 years, $\rho = 0.245$, $p < 0.005$; 50–70 years, $\rho = 0.229$, $p < 0.005$; and over 70 years, $\rho = 0.374$, $p < 0.005$, thus a weak positive relationship was noted. The analysis of differences by Fisher's one-sided F-criterion showed reliable PA dilation (>29 mm) in patients with severe pneumonia (CT 3–4) (Table 2).

Table 1. Distribution of patients in groups by gender (M: males), age, and severity of pneumonia according to the CT 1-4 scale

Parameters	CT-1	CT-2	CT-3	CT-4	Total, *n*
Group I (up to 50 years old)	47 (34 M)	56 (38 M)	19 (14 M)	9 (9 M)	131 (95 M)
Group II (50–69 years old)	84 (36 M)	127 (56 M)	78 (39 M)	24 (19 M)	313 (150 M)
Group III (over 70 years old)	24 (8 M)	18 (4 M)	16 (4 M)	9 (6 M)	67 (22 M)
Total, *n*	155 (78 M)	201 (98 M)	113 (57 M)	42 (34 M)	511 (267 M)

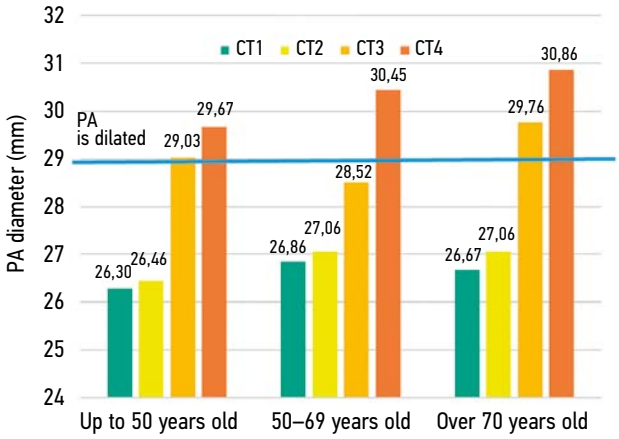

Fig. 4. Dependence of the PA diameter on age and lung lesion severity in COVID-19.
CT 1–4: adapted scale for visual assessment of the relationship between the patient's general condition severity and the nature and intensity of radiological signs of pulmonary changes in COVID-19; PA: pulmonary artery.

Additional study results

The following additional study results were obtained: a more frequently (37%) observed severe COVID-19 (CT 3–4) in the older patient group (>70 years); less frequently (21%) observed in the second age group (<50 years); and intermediately (32%) observed in the middle age group (50–69 years old).

In addition, an increased PA diameter from CT–1 to CT–4 was 12.9% (calculated as the ratio of the difference in values to half of the sum), whereas the ratio of the standard deviation to the mean PA values was 13.5%. The relative increase of the PA/Asc Ao ratio was 8.3% and the ratio of the standard deviation to the mean was 11.9%. Therefore, an increased PA diameter was more pronouncedly associated with an increased CT degree compared to the PA/Asc Ao ratio with a smaller difference in the coefficient of variation. In addition, a separate PA changes assessment by this parameter in contrast to the PA/Asc Ao ratio is more preferable.

Adverse events

No adverse events were observed in patients when performing the non-contrast chest CT. Scans were obtained according to the standard non-contrast protocol for chest disease diagnoses.

No adverse events associated with the use of the Airo TruCT mobile CT scanner were registered. The radiation exposure did not exceed the typical values for stationary computed tomographs.

DISCUSSION

Main study result summary

The relationships of PA and Asc Ao diameters and their ratios in patients with different COVID-19-associated pneumonia severity depending on age were studied. A significant positive correlation between the pulmonary trunk diameter and the pulmonary parenchymal lesion in COVID-19 was revealed. A non-significant increased pulmonary trunk diameter with age was shown. A significant aortic dilatation was observed in older age groups, without relation to the increasing disease severity.

Table 2. Distribution of examined patients by age interval, pneumonia severity, and pulmonary artery dilation

Age interval, years	Parameters			
	CT severity	PA < 29 mm	PA ≥ 29 mm	PA ≥ 29 mm, %
Up to 50*	CT 3–4	10	18	64,3
	CT 1–2	80	23	22,3
50–69**	CT 3–4	47	51	52,0
	CT 1–2	145	62	29,9
Over 70***	CT 3–4	10	19	65,5
	CT 1–2	30	16	34,8

Note. The differences are significant: *p < 0.0001, **p = 0.0001, and ***p = 0.0089 (Fisher's F-criterion). CT: computed tomography; CT 1–4: adapted scale for visual assessment of the relationship between the patient's general condition severity and the nature and intensity of radiological signs of pulmonary changes in COVID-19; PA: pulmonary artery.

Main study result discussion

An equal but not significant increased pulmonary trunk diameter with age (see Fig. 4) was shown. Values for age intervals up to 50, 50–69, and over 70 years amounted for 27.0 ± 3.6, 27.6 ± 3.8, and 28.2 ± 4.1 mm (mean ± standard deviation), respectively. However, a significantly increased PA diameter was shown about pulmonary parenchymal lesion severity in COVID-19-associated viral pneumonia (see Fig. 4). CT grades 1–4 determined the following mean PA values: 26.7 ± 3.4, 26.9 ± 3.4, 28.8 ± 4.1, and 30.4 ± 4.4 mm, respectively. Reverse patterns were shown for the aortic diameter. In addition, a significant change (increase) in the aortic diameter with age (31.2 ± 3.7, 34.6 ± 3.9, and 34.8 ± 5.6 mm) for age intervals defined above was observed. No significant change (increase) was noted in the aortic diameter with increasing lung lesion severity (CT 1–4), that is, 33.3 ± 4.9, 33.7 ± 4.2, 34.2 ± 3.9, and 34.6 ± 4.3 mm, respectively. The derived parameter (PA/Asc Ao ratio) showed a significant change (decrease) with age (0.87 ± 0.11, 0.80 ± 0.12, and 0.82 ± 0.15 RU, respectively) due to a pronounced increased Asc Ao diameter with age and a slight increased PA diameter. A significant change (increase) in the PA/Asc Ao ratio with increasing degree of the pulmonary tissue lesion (CT 1–4) was shown, that is 0.81 ± 0.13, 0.81 ± 0.11, 0.85 ± 0.14, and 0.88 ± 0.12 RU, respectively.

The obtained mean PA diameter and PA/Asc Ao ratio in the CT–1 group with the smallest lesion volume (26.7 ± 3.4 and 0.81 ± 0.13) were slightly higher compared with the mean values defined as normal in the Framingham Heart Study [14], where the mean PA size was 25.1 ± 2.8 mm and the mean PA/Asc Ao ratio was 0.77 ± 0.09. This is due to the methodological peculiarities, as measurements were performed without cardiac gating, which resulted in increased measured vessel diameters and disproportionate division of the studied groups by gender. The mean measured aortic diameter in the group of patients up to 50 years old (31.2 ± 3.7 mm) was well comparable with the review results [15], which is devoted to age-related aortic measurements (31.1 ± 4 mm). In addition, this review noted an increased aortic diameter with age due to decreased vessel wall elasticity.

The groups with severe COVID-2019 (CT 3–4) (see Fig. 2, *b, d, f, h*) demonstrated a statistically significant increased proportion of patients with PA diameter dilation of >29 mm for all ages (Table 2). On average, this group of patients was 60.6%, which was twice the average number of patients with PA dilation of >29 mm in the groups with mild COVID-19 (CT 1–2).

Our data agree well with the previously obtained results [9], where PA dilation in patients with COVID-19-associated pneumonia compared to the data before the disease showed a significantly increased PA/Asc Ao ratio. However, the relationship of these parameters with the pneumonia severity was not pronounced.

The threshold PA diameter values, above which the pulmonary hypertension is reliably stated, were different. For example, the upper limits of the PA diameter, above which patients had dyspnea, were 29 mm in males and 27 mm in females, whereas the critical PA/Asc Ao ratio was 0.9 [13, 16]. Another study proposed PA values of 29 mm and PA/Asc Ao ratio as criteria above which pulmonary hypertension is diagnosed. However, these values showed high sensitivity and insufficient specificity [14]. Alternatively, another proposed threshold of 31.5 mm, above which pulmonary hypertension is registered, showed low specificity [14]. The guidelines for pulmonary hypertension diagnosis and treatment noted a threshold of 29 mm [17].

Thus, the chosen threshold of 29 mm is reasonable. However, this value will probably be adjusted for the additional PA pressure assessment data, which is obtained by ultrasound measurements [18]. The statistical data on a significantly higher number of patients with a PA diameter of >29 mm in groups with a severe course (see Table 2) indicate a possible contribution of pulmonary hypertension to a more severe disease course.

The PA/Asc Ao ratio did not demonstrate threshold values exceeding 0.9 and 1 [9] and reached maximum values of 0.88 ± 0.12 in the group with a CT-4 degree of lung lesions. A significant increase of this index corresponds to the results reported by P. Spagnolo et al. [9]. While emphasizing the clinical significance of PA dilation, the authors provided reliable data on increased PA diameter and PA diameter/Asc Ao ratio in patients with lethal outcomes compared to those who recovered. This study revealed a weak positive correlation between the lung lesion degree (also divided into severity grades 1–4) and an increased PA diameter. A significant PA diameter dilation was shown in the examined patients compared to the state before the development of pneumonia; however, the sample size was small (45 patients). The necessity of PA dilation correction with PA/Asc Ao ratio determination is confirmed by a reliably smaller, but rather high number of patients with PA dilation in the cohort with small lesion volume (up to 50%) (Table 2). The use of this criterion is reasonable for constitutionally excluding conditioned wide PA. However, this auxiliary comparative criterion is inefficient in patients over 50 years old with hypertension since the aorta also expands due to the vessel wall connective tissue damage [15].

The effectiveness of the PA measurement as a prognostic sign of pulmonary hypertension and an additional severity marker is confirmed by the preferential bilateral process of pulmonary tissue lesions [9]. The PA accumulates increasing hemodynamic distress in the small circle as an additional predictor of COVID-19-associated viral pneumonia severity. PA dilation, which was a reliable relationship with parenchymal lesions, resulted from increasing pulmonary hypertension.

Pulmonary autoimmune diseases show signs of interstitial pneumonia, and pulmonary hypertension develops,

for example, with progressing idiopathic pulmonary fibrosis due to massive interstitial lung lesions [19]. The normal architectonics of the pulmonary vessels is deformed due to the massive pulmonary interstitium inflammation. Capillary constriction and endothelium integrity failure lead to small vessel microthrombosis and sclerosis and, consequently, to an increased hydraulic resistance, which results in pulmonary hypertension [20]. The development of COVID-19-associated viral pneumonia is due to high levels of expression of angiotensin-converting enzyme type 2 (ACE2) in type II alveolar pulmonary cells, which are targets of the spike antigen of severe acute respiratory syndrome coronavirus 2 virus that leads to interstitial lung lesions [11, 12]. The affecting factor that leads to microthrombosis is both a direct vascular endothelium lesion due to ACE2 receptor expression [15, 20, 21] and a possible secondary vascular bed immune lesion and the development of edema and exudation. This is facilitated by the extensive accumulation of complement components in the alveolar walls, which results in endothelial cell damage to the pulmonary capillaries and subsequent coagulation activation [20]. ACE2 receptor system depletion in the pulmonary vascular bed contributes to endothelial dysfunction and inflammation and aggravates the course of atherosclerosis and diabetic angiopathy [15, 20]. In COVID-19, this process leads to delayed adverse reactions in the form of progressing atherosclerotic vascular lesions.

Moreover, the phenomenon of vascular enlargement sign that is a sign of dilated vessels in COVID-19 pneumonia was reported. However, this phenomenon was not deeply studied, and several available studies showed its inconsistent prevalence. This sign occurs in 76.9% of patients with viral pneumonia [7, 10].

Pulmonary hypertension, regardless of its causes, has a secondary negative effect on the course of viral pneumonia, especially with massive lung lesions.

The pulmonary trunk dilation, depending on the severity of pulmonary parenchymal lesions, allows pulmonary hypertension consideration as one of the important signs of COVID-19-associated pneumonia severity. The established pattern allows a more differentiated approach in predicting outcomes of this infectious disease, developing effective therapy methods, and identifying population risk groups for a severe disease course that require increased attention from clinicians.

Study limitations

The study does not answer the question of whether pulmonary hypertension, which is noted as PA dilation, is an initial condition or whether it develops within the course of coronavirus infection. This study did not measure the PA diameter in patients of different ages without signs of viral pneumonia to assess the population prevalence of pulmonary hypertension (PA dilation). Data on the population prevalence of pulmonary hypertension and PA dilation are presented in the mentioned study [20].

CONCLUSIONS

The study showed a statistically significant positive relationship between PA dilation and lung lesion severity in COVID-19-associated pneumonia in all age groups. A higher number of patients with PA dilation of ≥29 mm (signs of pulmonary hypertension) and a severe degree of pulmonary parenchymal lesions (CT 3–4) is statistically significant. The obtained patterns require further study, which allows a more differentiated approach in predicting outcomes of this infectious disease, developing effective therapy methods, and identifying population risk groups for a severe disease course that require increased clinician attention.

ADDITIONAL INFORMATION

Funding source. This study was not supported by any external sources of funding.

Competing interests. The authors declare that they have no competing interests.

Authors' contribution. A.F. Aliyev — research idea and design, data collection, processing and analysis; N.D. Kudryavtsev — research design, data collection, processing and analysis; A.V. Petryaykin — research design, data processing and analysis; Z.R. Artyukova — data processing; A.S. Skoda, S.P. Morozov — research design, data analysis. All authors made a substantial contribution to the conception of the work, acquisition, analysis, interpretation of data for the work, drafting and revising the work, final approval of the version to be published and agree to be accountable for all aspects of the work.

Acknowledgments. We express our gratitude to Fuzuli K. Aliyev, Doctor of Physical and Mathematical Sciences and Tatiana I. Aliyeva, Candidate of Pedagogical Sciences for help in statistical data processing, primary focus of patients' groups and advice on study design.

REFERENCES

1. Morozov SP, Protsenko DN, Smetanina SV, et al. Radiation diagnostics of coronavirus disease (COVID-19): organization, methodology, interpretation of results: preprint No. CDT-2020-II. Version 2 from 17.04.2020. The series "Best practices of radiation and instrumental diagnostics". Issue 65. Moscow: Scientific and Practical Clinical Center for Diagnostics and Telemedicine Technologies of the Department of Healthcare of the City of Moscow; 2020. 78 p. (In Russ).

2. Prevention, diagnosis and treatment of a new coronavirus infection (COVID-19): Temporary methodological recommendations. Version 10 (08.02.2020). 2020. 261 p. (In Russ).

3. Fomin VV, Ternovoy SK, Serova NS. Radiological guidelines in patients with COVID-19 (Sechenov University experience). *REJR*. 2020;10(2):8–13. (In Russ). doi: 21569/2222-7415-2020-10-2-8-13

4. Henkel M, Weikert T, Marston K, et al. Lethal COVID-19: radiological-pathological correlation of the lungs. *Radiol Cardiothorac Imaging*. 2020;2(6):e200406. doi: 10.1148/ryct.2020200406
5. Sun Z, Zhang N, Li Y, et al. A systematic review of chest imaging findings in COVID-19. *Quant Imaging Med Surg*. 2020;10(5): 1058–1079. doi: 10.21037/qims-20-564
6. Salehi S, Abedi A, Balakrishnan S, et al. Coronavirus disease 2019 (COVID-19): A systematic review of imaging findings in 919 patients. *AJR Am J Roentgenol*. 2020;215(1):87–93. doi: 10.2214/AJR.20.23034
7. Qanadli SD, Beigelman-Aubry C, Rotzinger DC. Vascular changes detected with thoracic CT in coronavirus disease (COVID-19) might be significant determinants for accurate diagnosis and optimal patient management. *AJR Am J Roentgenol*. 2020;215(1):15. doi: 10.2214/AJR.20.23185
8. Li X, Ma X. Acute respiratory failure in COVID-19: Is it "typical" ARDS? *Crit Care*. 2020;24(1):198. doi: 10.1186/s13054-020-02911-9
9. Spagnolo P, Cozzi A, Foà RA, et al. CT-derived pulmonary vascular metrics and clinical outcome in COVID-19 patients. *Quant Imaging Med Surg*. 2020;10(6):1325–1333. doi: 10.21037/qims-20-546
10. Lv H, Chen T, Pan Y, et al. Pulmonary vascular enlargement on thoracic CT for diagnosis and differential diagnosis of COVID-19: a systematic review and meta-analysis. *Ann Transl Med*. 2020; 8(14):878–878. doi: 10.21037/atm-20-4955
11. Chang YC, Yu CJ, Chang SC, et al. Pulmonary sequelae in convalescent patients after severe acute respiratory syndrome: Evaluation with thin-section CT. *Radiology*. 2005;236(3):1067–1075. doi: 10.1148/radiol.2363040958
12. Prokop M, van Everdingen W, van Rees Vellinga T, et al. CO-RADS: A categorical CT assessment scheme for patients suspected of having COVID-19-definition and evaluation. *Radiology*. 2020;296(2):E97–E104. doi: 10.1148/radiol.2020201473
13. Corson N, Armato SG, Labby ZE, et al. CT-based pulmonary artery measurements for the assessment of pulmonary hypertension. *Acad Radiol*. 2014;21(4):523–530. doi: 10.1016/j.acra.2013.12.015
14. Truong QA, Massaro JM, Rogers IS, et al. Reference values for normal pulmonary artery dimensions by noncontrast cardiac computed tomography the framingham heart study. *Circ Cardiovasc Imaging*. 2012;5(1):147–154. doi: 10.1161/CIRCIMAGING.111.968610
15. Collins JA, Munoz JV, Patel TR, et al. The anatomy of the aging aorta. *Clin Anat*. 2014;27(3):463–466. doi: 10.1002/ca.22384
16. Compton GL, Florence J, MacDonald C, et al. Main pulmonary artery-to-ascending aorta diameter ratio in healthy children on MDCT. *AJR Am J Roentgenol*. 2015;205(6):1322–1325. doi: 10.2214/AJR.15.14301
17. Galiè N, Humbert M, Vachiery JL, et al. 2015 ESC/ERS guidelines for the diagnosis and treatment of pulmonary hypertension: the joint task force for the diagnosis and treatment of pulmonary hypertension of the European society of cardiology (ESC) and the European Respiratory Society (ERS): Endorsed by: Association for European Paediatric and Congenital Cardiology (AEPC), International Society for Heart and Lung Transplantation (ISHLT). *European Heart Journal*. 2016;37(1):67–119. doi: 10.1093/eurheartj/ehv317
18. Parasuraman S, Walker S, Loudon BL, et al. Assessment of pulmonary artery pressure by echocardiography — A comprehensive review. *Int J Cardiol Heart Vasc*. 2016;12:45–51. doi: 10.1016/j.ijcha.2016.05.011
19. Chuchalin AG, Avdeev SN, Aysanov ZR, et al. Diagnosis and treatment of idiopathic pulmonary fibrosis federal clinical guidelines. *Pulmonology*. 2016;26(4):399–419. (In Russ). doi: 10.18093/0869-0189-2016-26-4-399-419
20. Chernyaev AL, Samsonova MV. Pathological anatomy of the lungs. Atlas. 2nd ed., revised and updated. A series of monographs of the Russian Respiratory Society. Ed. by A.G. Chuchalin. Moscow: Atmosfera; 2011. 111 p. (In Russ).
21. Dolhnikoff M, Duarte-Neto AN, de Almeida Monteiro RA, et al. Pathological evidence of pulmonary thrombotic phenomena in severe COVID-19. *J Thromb Haemost*. 2020;18(6):1517–1519. doi: 10.1111/jth.14844

СПИСОК ЛИТЕРАТУРЫ

1. Морозов С.П., Проценко Д.Н., Сметанина С.В., и др. Лучевая диагностика коронавирусной болезни (COVID-19): организация, методология, интерпретация результатов: препринт № ЦДТ-2020-II. Версия 2 от 17.04.2020. Серия «Лучшие практики лучевой и инструментальной диагностики». Вып. 65. Москва: ГБУЗ «НПКЦ ДиТ ДЗМ», 2020. 78 с.
2. Профилактика, диагностика и лечение новой коронавирусной инфекции (COVID-19): Временные методические рекомендации. Версия 10 (08.02.2020). 2020. 261 с.
3. Фомин В.В., Терновой С.К., Серова Н.С. Рекомендации по лучевой диагностике у пациентов с COVID-19 (опыт Сеченовского Университета) // REJR. 2020. Т. 10, № 2. С. 8–13. doi: 10.21569/2222-7415-2020-10-2-8-13
4. Henkel M., Weikert T., Marston K., et al. Lethal COVID-19: radiological-pathological correlation of the lungs // Radiol Cardiothorac Imaging. 2020. Vol. 2, N 6. P. e200406. doi: 10.1148/ryct.2020200406
5. Sun Z., Zhang N., Li Y., et al. A systematic review of chest imaging findings in COVID-19 // Quant Imaging Med Surg. 2020. Vol. 10, N 5. P. 1058–1079. doi: 10.21037/qims-20-564
6. Salehi S., Abedi A., Balakrishnan S., et al. Coronavirus disease 2019 (COVID-19): A systematic review of imaging findings in 919 patients // AJR Am J Roentgenol. 2020. Vol. 215, N 1. P. 87–93. doi: 10.2214/AJR.20.23034
7. Qanadli S.D., Beigelman-Aubry C., Rotzinger D.C. Vascular changes detected with thoracic CT in coronavirus disease (COVID-19) might be significant determinants for accurate diagnosis and optimal patient management // AJR Am J Roentgenol. 2020. Vol. 215, N 1. P. 15. doi: 10.2214/AJR.20.23185
8. Li X., Ma X. Acute respiratory failure in COVID-19: Is it "typical" ARDS? // Crit Care. 2020. Vol. 24, N 1. P. 198. doi: 10.1186/s13054-020-02911-9
9. Spagnolo P., Cozzi A., Foà R.A., et al. CT-derived pulmonary vascular metrics and clinical outcome in COVID-19 patients // Quant Imaging Med Surg. 2020. Vol. 10, N 6. P. 1325–1333. doi: 10.21037/qims-20-546
10. Lv H., Chen T., Pan Y., et al. Pulmonary vascular enlargement on thoracic CT for diagnosis and differential diagnosis of COVID-19: a systematic review and meta-analysis // Ann Transl Med. 2020. Vol. 8, N 14. P. 878–878. doi: 10.21037/atm-20-4955

11. Chang Y.C., Yu C.J., Chang S.C., et al. Pulmonary sequelae in convalescent patients after severe acute respiratory syndrome: Evaluation with thin-section CT // Radiology. 2005. Vol. 236, N 3. P. 1067–1075. doi: 10.1148/radiol.2363040958
12. Prokop M., van Everdingen W., van Rees Vellinga T., et al. CO-RADS: A categorical CT assessment scheme for patients suspected of having COVID-19-definition and evaluation // Radiology. 2020. Vol. 296, N 2. P. E97–E104. doi: 10.1148/radiol.2020201473
13. Corson N., Armato S.G., Labby Z.E., et al. CT-based pulmonary artery measurements for the assessment of pulmonary hypertension // Acad Radiol. 2014. Vol. 21, N 4. P. 523–530. doi: 10.1016/j.acra.2013.12.015
14. Truong Q.A., Massaro J.M., Rogers I.S., et al. Reference values for normal pulmonary artery dimensions by noncontrast cardiac computed tomography the Framingham heart study // Circ Cardiovasc Imaging. 2012. Vol. 5, N 1. P. 147–154. doi: 10.1161/CIRCIMAGING.111.968610
15. Collins J.A., Munoz J.V., Patel T.R., et al. The anatomy of the aging aorta // Clin Anat. 2014. Vol. 27, N 3. P. 463–466. doi: 10.1002/ca.22384
16. Compton G.L., Florence J., MacDonald C., et al. Main pulmonary artery-to-ascending aorta diameter ratio in healthy children on MDCT // AJR Am J Roentgenol. 2015. Vol. 205, N 6. P. 1322–1325. doi: 10.2214/AJR.15.14301
17. Galiè N., Humbert M., Vachiery J.L., et al. 2015 ESC/ERS guidelines for the diagnosis and treatment of pulmonary hypertension: the joint task force for the diagnosis and treatment of pulmonary hypertension of the European society of cardiology (ESC) and the European Respiratory Society (ERS): Endorsed by: Association for European Paediatric and Congenital Cardiology (AEPC), International Society for Heart and Lung Transplantation (ISHLT) // European Heart Journal. 2016. Vol. 37, N 1. P. 67–119. doi: 10.1093/eurheartj/ehv317
18. Parasuraman S., Walker S., Loudon B.L., et al. Assessment of pulmonary artery pressure by echocardiography — A comprehensive review // Int J Cardiol Heart Vasc. 2016. Vol. 12. P. 45–51. doi: 10.1016/j.ijcha.2016.05.011
19. Чучалин А.Г., Авдеев С.Н., Айсанов З.Р., и др. Диагностика и лечение идиопатического легочного фиброза. Федеральные клинические рекомендации // Пульмонология. 2016. Т. 26, № 4. С. 399–419. doi: 10.18093/0869-0189-2016-26-4-399-419
20. Черняев А.Л., Самсонова М.В. Патологическая анатомия лёгких. Атлас. 2-е изд., испр. и доп. Серия монографий Российского респираторного общества / под ред. А.Г. Чучалина. Москва: Атмосфера, 2011. 111 с.
21. Dolhnikoff M., Duarte-Neto A.N., de Almeida Monteiro R.A., et al. Pathological evidence of pulmonary thrombotic phenomena in severe COVID-19 // J Thromb Haemost. 2020. Vol. 18, N 6. P. 1517–1519. doi: 10.1111/jth.14844

AUTHORS' INFO

*** Alexander F. Alie**v, MD, Cand. Sci. (Med.);
address: 10 Stromynka str., Moscow, 107076, Russia;
ORCID: https://orcid.org/0000-0003-3282-0567;
eLibrary SPIN: 7891-9314; e-mail: alijealex83@gmail.com

Nikita D. Kudryavtsev, MD;
ORCID: https://orcid.org/0000-0003-4203-0630;
eLibrary SPIN: 1125-8637; e-mail: n.kudryavtsev@npcmr.ru

Alexey V. Petraikin, MD, Cand. Sci. (Med.), Associate Professor;
ORCID: http://orcid.org/0000-0003-1694-4682;
eLibrary SPIN: 6193-1656; e-mail: alexeypetraikin@gmail.com

Zlata R. Artyukova, MD;
ORCID: http://orcid.org/0000-0003-2960-9787;
eLibrary SPIN: 5873-2280; e-mail: zl.artyukova@gmail.com

Andrey S. Shkoda, MD, Dr. Sci. (Med.), Professor;
ORCID: https://orcid.org/0000-0002-9783-1796

Sergey P. Morozov, MD, Dr. Sci. (Med.), Professor;
ORCID: http://orcid.org/0000-0001-6545-6170;
eLibrary SPIN: 8542-1720; e-mail: morozov@npcmr.ru

ОБ АВТОРАХ

*** Алиев Александр Физулиевич**, к.м.н.;
адрес: Россия, 107076, Москва, ул. Стромынка, д. 10;
ORCID: https://orcid.org/0000-0003-3282-0567;
eLibrary SPIN: 7891-9314; e-mail: alijealex83@gmail.com

Кудрявцев Никита Дмитриевич;
ORCID: https://orcid.org/0000-0003-4203-0630;
eLibrary SPIN: 1125-8637; e-mail: n.kudryavtsev@npcmr.ru

Петряйкин Алексей Владимирович, к.м.н., доцент;
ORCID: http://orcid.org/0000-0003-1694-4682;
eLibrary SPIN: 6193-1656; e-mail: alexeypetraikin@gmail.com

Артюкова Злата Романовна;
ORCID: http://orcid.org/0000-0003-2960-9787;
eLibrary SPIN: 5873-2280; e-mail: zl.artyukova@gmail.com

Шкода Андрей Сергеевич, д.м.н., профессор;
ORCID: https://orcid.org/0000-0002-9783-1796

Морозов Сергей Павлович, д.м.н., профессор;
ORCID: http://orcid.org/0000-0001-6545-6170;
eLibrary SPIN: 8542-1720; e-mail: morozov@npcmr.ru

* Corresponding author / Автор, ответственный за переписку

DOI: https://doi.org/10.17816/DD76511

Наблюдения доплеровского мерцающего артефакта: база данных радиочастотных ультразвуковых сигналов

Д.В. Леонов[1, 2], Р.В. Решетников[1, 3], Н.С. Кульберг[1, 4], А.А. Насибуллина[2], А.И. Громов[5]

[1] Научно-практический клинический центр диагностики и телемедицинских технологий Департамента здравоохранения г. Москвы, Москва, Российская Федерация
[2] Национальный исследовательский университет МЭИ, Москва, Российская Федерация
[3] Первый Московский государственный медицинский университет имени И.М. Сеченова (Сеченовский Университет), Москва, Российская Федерация
[4] Федеральный исследовательский центр «Информатика и управление» Российской академии наук, Москва, Российская Федерация
[5] Московский государственный медико-стоматологический университет имени А.И. Евдокимова, Москва, Российская Федерация

АННОТАЦИЯ

Обоснование. Мерцающий артефакт в доплеровских режимах ультразвукового исследования проявляется быстрой хаотической сменой окрашенных пикселей на экране прибора. Явление, которое можно использовать в качестве полезного диагностического признака, исследовано недостаточно. Большинство предположений о причинах артефакта сделаны на основании изображений с экрана ультразвукового прибора без глубокого изучения свойств принимаемых сигналов.

Материалы и методы. Радиочастотные ультразвуковые сигналы были записаны при исследовании фантомов. Исследовались как объекты, приводящие к появлению мерцающего артефакта на экране прибора, так и имитации сосудов и мягких тканей. Сбор данных проводился с июля 2016 по март 2021 г. Данные получены при помощи исследовательского ультразвукового прибора «Сономед-500» с датчиками 7,5 L38 и 3,4 C60.

Содержимое базы данных. Представлена база данных, содержащая радиочастотные сигналы, полученные с выхода формирователя луча из приёмного тракта ультразвукового медицинского диагностического прибора в режиме цветового доплеровского картирования и B-режиме. Представленные в базе данных сигналы содержат признаки мерцающего артефакта. База состоит из исследований пяти различных фантомов общим объёмом 10,5 ГБ. Радиочастотные данные сохранены в бинарном виде. Настройки сканирования, необходимые для анализа радиочастотных данных, содержатся в текстовых файлах. Каждое исследование сопровождается примером характерной сонограммы в графическом формате. База данных доступна по адресу: https://mosmed.ai/datasets/ultrasound_doppler_twinkling_artifact.

Доступность кода. Для просмотра и анализа базы данных к архиву прилагаем разработанную нами программу TwinklingDatasetDisplay. Доступен исходный код программы: https://github.com/Center-of-Diagnostics-and-Telemedicine/TwinklingDatasetDisplay.git.

Условия использования. База данных может быть использована для разработки и тестирования алгоритмов обработки ультразвуковых сигналов. Доступ к базе данных и коду для её просмотра открыт для всех желающих.

Ключевые слова: цветовая ультразвуковая доплерография; мерцающий артефакт; база данных; «сырые» радиочастотные данные; ультразвуковые фантомы.

Как цитировать

Леонов Д.В., Решетников Р.В., Кульберг Н.С., Насибуллина А.А., Громов А.И. Наблюдения доплеровского мерцающего артефакта: база данных радиочастотных ультразвуковых сигналов // *Digital Diagnostics.* 2021. Т. 2, № 3. С. 261–276. DOI: https://doi.org/10.17816/DD76511

Рукопись получена: 24.07.2021 **Рукопись одобрена:** 24.08.2021 **Опубликована:** 27.09.2021

ЭКО•ВЕКТОР

DOI: https://doi.org/10.17816/DD76511

Doppler twinkling artifact observations: an open-access database of raw ultrasonic signals

Denis V. Leonov[1, 2], Roman V. Reshetnikov[1, 3], Nikolay S. Kulberg[1, 4], Anastasia A. Nasibullina[2], Alexandr I. Gromov[5]

[1] Moscow Center for Diagnostics and Telemedicine, Moscow, Russian Federation
[2] National Research University Moscow Power Engineering Institute, Moscow, Russian Federation
[3] The First Sechenov Moscow State Medical University (Sechenov University), Moscow, Russian Federation
[4] Federal Research Center Computer Science and Control of the Russian Academy of Sciences, Moscow, Russian Federation
[5] Moscow State University of Medicine and Dentistry named after A.I. Evdokimov, Moscow, Russian Federation

ABSTRACT

BACKGROUND: Doppler twinkling artifact is a rapid change of colors seen in CFI-mode in the presence of kidney stones and calculi. Therefore, numerous researchers use the twinkling artifact as a diagnostic sign. However, this phenomenon is under-researched, because most assumptions concerning its causes are made based on pure visual observations of the scanner's screen leaving the important steps of signal transformation hidden behind the "black box" curtains of ultrasound machines.

MATERIALS AND METHODS: Raw radiofrequency ultrasound signals were recorded in the phantom studies. The recorded echoes were received from objects that create the Doppler twinkling artifact and artificial blood vessels and soft tissues imitators. The data were collected between June 2016 and March 2021. Sonomed-500 with the 7.5 L38 and 3.4 C60 probes served as the research machine for the signal capture.

Data records: We present the database containing raw radiofrequency ultrasound signals from the beam former output of the research ultrasound machine. The dataset consists of CFI and B-mode echoes recorded from twinkling objects. Therefore, this database can be useful for those who test, develop and study ultrasound signal processing algorithms. Furthermore, the database is freely available online. The 10.5 GB database consists of echoes received from five phantoms. Raw radiofrequency signals were stored in the binary files; scanning parameters were stored in text files. The database is available at: https://mosmed.ai/datasets/ultrasound_doppler_twinkling_artifact.

Code availability: The public can visualize the database content with the specially written program TwinklingDatasetDisplay available at: https://github.com/Center-of-Diagnostics-and-Telemedicine/TwinklingDatasetDisplay.git.

Usage notes: The database can be used to test and develop signal-processing algorithms, such as wall filtration, velocity estimation, feature extraction, speckle reduction, etc. Furthermore, the public is free to share (copy, distribute, and transmit) and remix (adapt and do derivative works) the dataset considering appropriate credit is given.

Keywords: ultrasonography; color flow imaging; Doppler twinkling artifact; dataset; raw radiofrequency signals; ultrasound phantoms.

To cite this article

Leonov DV, Reshetnikov RV, Kulberg NS, Nasibullina AA, Gromov AI. Doppler twinkling artifact observations: an open-access database of raw ultrasonic signals. *Digital Diagnostics.* 2021;2(3):261–276. DOI: https://doi.org/10.17816/DD76511

Received: 24.07.2021 **Accepted:** 24.08.2021 **Published:** 27.09.2021

DOI: https://doi.org/10.17816/DD76511

多普勒观测闪烁神器：射频超声信号数据库

Denis V. Leonov[1, 2], Roman V. Reshetnikov[1, 3], Nikolay S. Kulberg[1, 4], Anastasia A. Nasibullina[2], Alexandr I. Gromov[5]

[1] Moscow Center for Diagnostics and Telemedicine, Moscow, Russian Federation
[2] National Research University Moscow Power Engineering Institute, Moscow, Russian Federation
[3] The First Sechenov Moscow State Medical University (Sechenov University), Moscow, Russian Federation
[4] Federal Research Center Computer Science and Control of the Russian Academy of Sciences, Moscow, Russian Federation
[5] Moscow State University of Medicine and Dentistry named after A.I. Evdokimov, Moscow, Russian Federation

简评

论证。通过仪器筛网上涂漆像素的快速混乱变化，表现出多普勒模式中的闪烁伪影。 不能足够地研究可用作有用的诊断特征的现象。 关于工件的原因的大多数假设是基于来自超声波装置屏幕的图像而没有深入研究接收信号的性质的深度研究。

材料与方法射频超声信号记录在幽灵的研究中。 这些物体导致器件屏幕上的闪烁伪像以及血管和软组织的模仿。 从2016年7月到3月2021年进行数据收集使用Sonad-500研究超声仪器获得数据，具有7,5 L38和3,4 C60传感器。

内容数据库 提供了一个包含射频信号的数据库，彩色多普勒成像模式下超声医学诊断仪接收通路波束形成器输出的结果和B-式。数据库中呈现的信号包含闪烁的伪影的符号。 基础包括研究五种不同幽灵的研究，总体积为10.5 GB。 射频数据以二进制形式存储。 分析射频数据所需的扫描设置包含在文本文件中。 每项研究伴随着以图形格式的特征超声图的示例。 数据库可在以下网址查阅：Https://mosmed.ai/datasets/ultrasound_doppler_twinkling_artifact.

代码可用性。为了查看和分析数据库，请将我们开发的TwinklingDataSetDisplay软件添加到存档中。程序源代码可用：https://github.com/Center-of-Diagnostics-and-Telemedicine/TwinklingDatasetDisplay.git.

使用条款。数据库可用于开发和测试用于处理超声信号的算法。 访问数据库和用于查看它的代码为每个人都打开。

关键词：彩色超声波多普拉洛林；闪烁的神器；数据库；“原始”射频数据；超声波幻影。.

引用本文

Leonov DV, Reshetnikov RV, Kulberg NS, Nasibullina AA, Gromov AI. 多普勒观测闪烁神器：射频超声信号数据库. *Digital Diagnostics.* 2021;2(3):261–276. DOI: https://doi.org/10.17816/DD76511

收到： 24.07.2021 **接受：** 24.08.2021 **发布日期：**27.09.2021

BACKGROUND

A twinkling artifact in the color flow mapping (CFM) mode appears as a fast chaotic change of colored pixels on the screen of ultrasonic medical devices. This artifact is observed in the modes that were originally designed to assess blood flow, with marking of areas where blood motion is excluded. The clinical significance of the problem is related to the potential use of a twinkling artifact as an additional diagnostic sign when searching for stones in the kidney, ureter and bladder, and gallbladder and bile duct. Moreover, this artifact may be useful for detecting micro calcifications in breast neoplasms [1–8]. The high prevalence and social significance of these diseases and possible difficulties in their detection using traditional ultrasonic imaging require additional diagnostic options, such as the skillful use of the twinkling artifact. The detectability and intensity of the twinkling artifact varied and depend on the scanning equipment and its settings.

Several competing and weakly related hypotheses have tried to explain the cause of the twinkling artifact [9–16]. To prove their hypotheses, most authors have cited images from the screen of the ultrasonic device. The ultrasonic device was a "black box" for the authors of these hypotheses. Assumptions about the causes of the twinkling artifact were made without studying all signal processing steps. Thus, most hypotheses cannot be substantiated.

Unfortunately, the majority of available studies on the twinkling artifact did not analyze radiofrequency (RF) data, which carry more information compared with sonograms. Thus, hard-to-reach research instruments that provide access to raw RF signals are needed to obtain such data. Currently, no datasets exist in the public domain that contains ultrasonic Doppler signals with signs of the twinkling artifact.

This article presents an open-access database of RF signals, which were obtained from the beamformer output of the preprocessing path of a research ultrasonic device, and a tool for its viewing and analysis.

METHODS

Eligibility criteria

The database contains RF signals of observations of artificial objects (phantoms) that contain signs of the twinkling artifact. Only after the appearance of the stable twinkling artifact on two ultrasound machines was achieved, the corresponding signals were included in the database. The database also includes records of a blood mimicking fluid from a Doppler flow phantom, which imitates the normal blood flow in the vessel.

Data collection

The study was conducted between July 2016 and July 2021.

Ultrasonic equipment

Data were obtained from the CFI- and B-mode channels of the Sonomed-500 ultrasonic device (Spectromed, Moscow) by using linear (7.5 L38) and convex (3.4 C60) transducers.

RF signals from which the database was formed are shown in Fig. 1. The 64 elements of the phased array transducer were used to form a beam for each scanning direction. At the transmission stage, all selscted elements emit pulses with specific delays to focus ultrasound at a predetermined depth. Pulses of approximately 1 μs and 4 μs duration for the B-mode and Doppler mode, respectively, were emitted. Echoes were received separately by each array element, further amplified in an analog receiver module, and digitized at a frequency of 50 MHz. Digital signals of individual channels were coherently summarized in the beamformer with delays that provide dynamic focusing. Each signal or the formed beam was subjected to decimation, that is, the frequency of digitization was reduced to 10 MHz. The scanning direction was selected by reconnecting the active elements of the transducer.

An auxiliary ultrasound scanner Medison SA-8000 EX (South Korea), which does not provide access to raw data, was used to control the reliability of observations. This scanner was with used a linear L5-9EC transducer and a convex C3-7ED transducer. The use of the control machine ensured that the artifact appeared as a result of objective physical processes occurring in the examined objects. This reduces the probability of situations in which the twinkling artifact results not from the properties of the object under investigation but from some unknown features of one of the devices.

Principles of CFM Data Acquisition

The size of the CFM area was determined interactively by the examiner. Each direction (beam) in the selected area was sonified *N* times. A group of *N* signals obtained by sonifying the same area of tissue is called a Doppler pulse train. The time within the pulse train is called "slow" time, it is measured for a single spatial position, as opposed to the "fast" time, which is directly proportional to the depth. Blood flow and other processes are tracked by changes in "slow" time signals within a single pulse train. If there are no changes in the examined object, these signals are

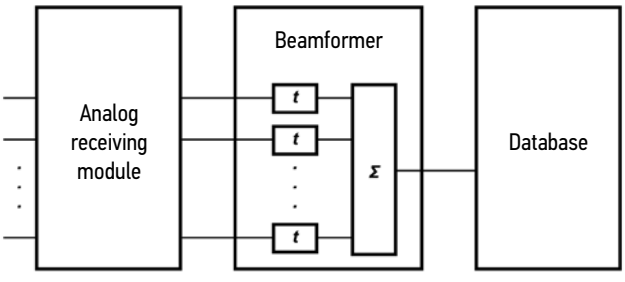

Fig. 1. Data capture scheme.

almost identical, the slight difference is the contribution of the noise.

If the same direction is sonified sequentially to obtain a pulse train, a pulse repetition rate of approximately 5 kHz may be obtained, which is not appropriate for most medical applications. To reduce the pulse repetition rate, the examined area was divided into S scanning subareas (*sweeps*), each of which consisted of *M* beams (Fig. 2). When obtaining a pulse train, the beams of one subarea were sequentially irradiated from the 1st to the *M*-th beam. Thus, Doppler pulse trains were formed in parallel for *M* beams of one subarea. Subsequently, the process was repeated for other subareas, whereas the pulse repetition rate was decreased by *M* times.

The total size of the range of interest determined the number of beams (*S*×*M*). One beam consisted of *P* complex samples. The *Q* beam density was sometimes changed to increase the frame rate. Thus, if *Q* = 2, the CFM window was updated twice as fast; however, the information about every second beam was lost.

All these steps were repeated *F* times; thus, a cine loop was formed, which consisted of *F* frames. The received signals were recorded in a binary file, and the scanning parameters were placed in a text file of the same name (Table).

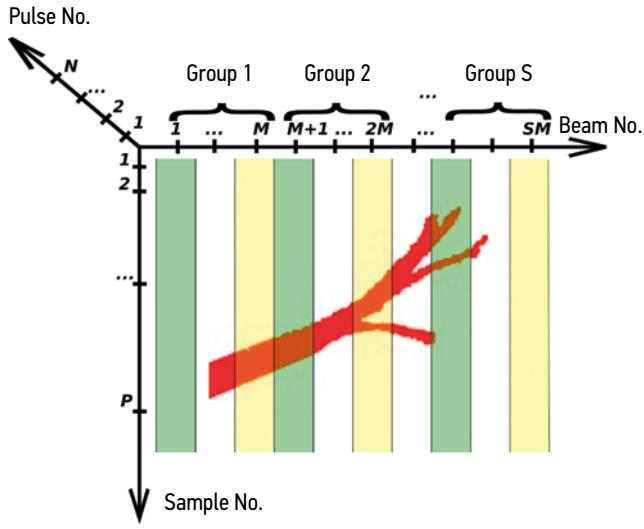

Fig. 2. Explanation of the scanning scheme in the color flow mapping mode. The color coding of the vertical bars corresponds to the number of the beam in the sweep. Red color shows the examined vessel.

Examined objects and observations

Most of the items in the database contain signals that were reflected from objects on which a twinkling artifact is observed in Doppler modes. Artificial objects included rough and smooth wire made of low carbon raw steel, and rods made of plastic (ABS), aluminum, and wood. The objects were placed in fixed positions in the body of a specially designed phantom. The body was filled with agar-agar, water, and ethyl alcohol. A Doppler phantom Gammex 1430 LE Mini-Doppler Flow System (USA) was used to record signals from the flowing fluid.

Table. Main scanning parameters displayed in the .par file

Parameters	Description	Symbols
Number of frames	Number of frames	*F*
Raw frame size	Memory size in bytes occupied by the RF data that is required to build one frame in the duplex B+CFM mode	-
Header size	Memory size in bytes that is reserved in front of each beam	-
Number of B-beams	Number of beams that are used to obtain a gray-scale image	*B*
Size of B-beam in samples	Number of samples that are used when obtaining a gray-scale image, which depends on the scanning depth	*G*
Number of CF shots	Number of pulses in a Doppler pulse train	*N*
Number of sweeps	Number of beam groups in the CFM mode. A group of beams is called a *sweep*. The CFM-frame consists of several sweeps	*S*
Beams in sweep	Number of beams in each sweep	*M*
Size of CFM beam in samples	Number of samples in the CFM mode	*P*
First scan CFM beam	CFM window position by B-image width	-
CFM density	Beam density in the CFM mode is determined by the formula (*b*-*a*)/*c*, where *a* and *b* are the numbers of B-beams, which define the left and right borders of the CFM window, and c is the number of CFM beams	*Q*
Number of CFM beams	Number of beams in the CFM mode	*S*×*M*
Number of first CFM sample	Depth position of the CFM window relative to the B-image	-

Note. CFM, color flow mapping.

The Doppler pulse train consisted of 5, 9, or 17 pulses. Examinations with a linear transducer were conducted at a carrier frequency of 7.5 MHz and a power of 74% for B-mode. For the CFM mode, the carrier frequency, power, and pulse repetition rate were 6.3 MHz, 97%, and 750 Hz, respectively. Examinations with a convex transducer were conducted at a carrier frequency and power of 3.3 MHz and 95% in B-mode and 3.3 MHz and 98%, respectively, with a pulse repetition rate of 1 kHz, in the CFM mode. The sampling rate in all cases was 10 MHz. Other settings, such as interframe averaging and wall filter settings, did not affect the data, since the data were obtained from the preprocessing path.

Database contents

Summary of database contents

Records of digital RF signals with twinkling artifact features were collected and placed in the public domain (https://mosmed.ai/datasets/ultrasonic_doppler_twinkling_artifact). The database also contains signals from areas with vessels in the Gammex phantom, specialized phantoms of proprietary design, and reflections from tissue-imitating materials. This database will be useful to researchers who study algorithms for B-mode and CFM signal processing.

The database includes five sets of examinations, which differ in the object of study (Fig. 3). Each examination is a pair of files with the same name and.dat and.par extensions. "Raw" data records are accompanied by images and videos that illustrate the appearance of the twinkling artifact. The examined objects and environments are specified in the directory names of the database. In the directory name, the word "linear" indicates the use of the 7.5 L38 linear transducers, while "convex" indicates the use of the 3.4 C60 convex transducers.

Database file format

RF signals were recorded in binary form in a file with .dat extension (Fig. 4). This file contained complex data for building a frame in the B-mode (*B-frame*) and CFM mode (*CFM-frame*). The real and imaginary parts of each dataset were written in a "32-bit little-endian (LE) signed integer" format. Initially, a 20-bit header was recorded, which is denoted in Fig. 4 as *H* symbol. Afterward, the samples of the first beam of the B-image, which are denoted as *B-sample 1 to B*, the header, and the samples of the second and subsequent beams of the B-image were recorded.

Then, the samples for constructing the CFM, which are denoted as a *CFM-sample*, were recorded. In this case, the *H* header was recorded first, followed by recording all depth samples, which are obtained for the first pulse in the pulse train and the first beam from the first group (*sweep*). Thus, we obtained the first line of the CFM data; each subsequent line was also separated by a header.

The second and subsequent frames were recorded in the same way. Each.dat file corresponded to a text file of the same name with the.par extension, which contained information on scanning parameters (Table) and specific *F, G, B, F, S, N, M, P*, and *Q* values.

Database viewer

The TwinklingDatasetDisplay program is developed to view and analyze the proposed database. The program

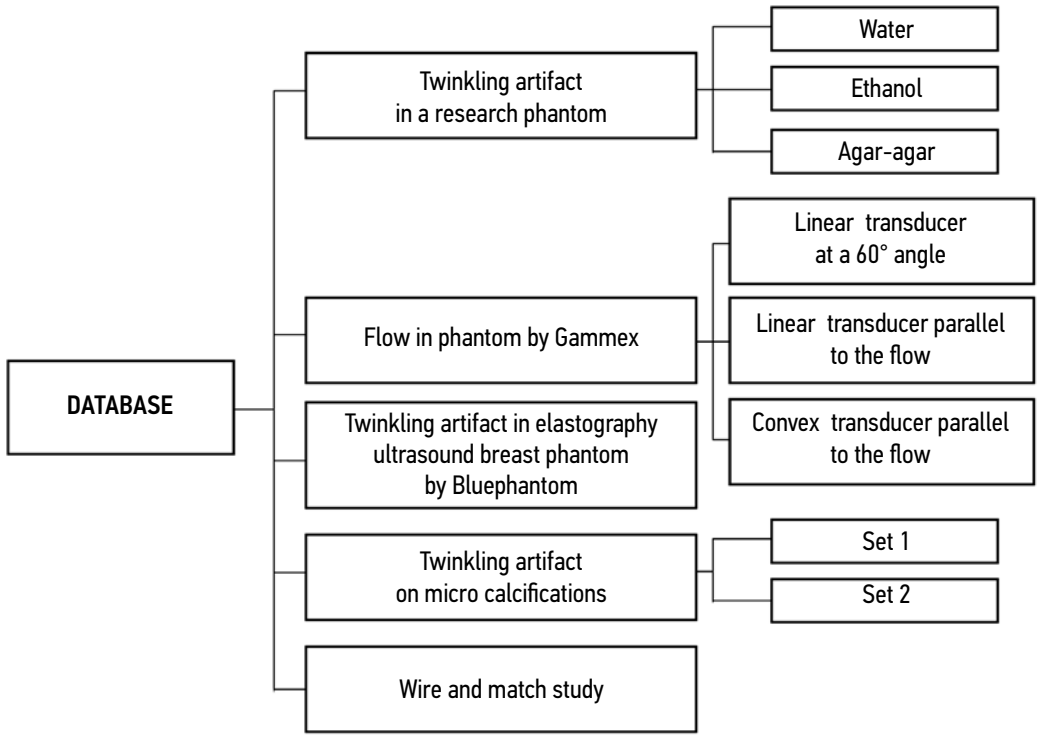

Fig. 3. Composition of the database.

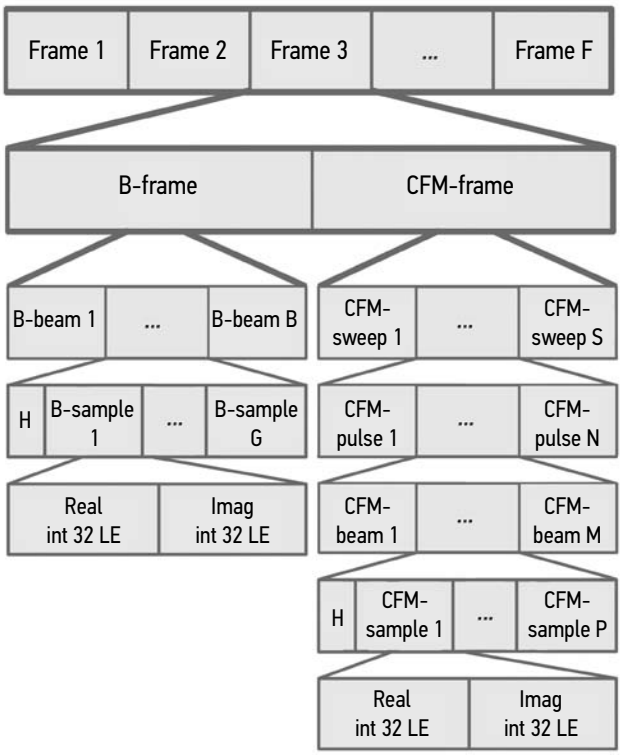

Fig. 4. Scheme for storing "raw" radio frequency data in a *.dat file.

is intended only for viewing RF signals and does not include any signal processing algorithms for CFM [17–30]. All software modules are written in C++ using the XRAD library [31]. The program is in the public domain (https://github.com/Center-of-Diagnostics-and-Telemedicine/TwinklingDatasetDisplay.git). The database also included Windows executable files.

The TwinklingDatasetDisplay program allows the following:

- Opening .dat files using information from the .par files.
- Forming a conventional B-mode image from the data.
- Displaying complex signals in the form of graphs depending on both "fast" and "slow" time of the CFM mode.
- Applying elements of spectral analysis thereto.

Examples of "slow" time signals, which determine the Doppler pattern, are shown in Fig. 5. Typical graphs of signals from different areas are shown here:

- The area of the blood-mimicking fluid flow in the Doppler phantom channel of the Gammex 1430 LE Mini-Doppler Flow System (real and imaginary parts of the signal change in quadrature, which is typical for moving objects; Fig. 5*a*).
- The area of soft tissues in the absence of motion (after filtering the signal from the tissues, only the noise remains; Fig. 5*b*).
- The observation area of the twinkling artifact on a steel wire (a random signal is observed, which differs from the noise in Fig. 5*b* by greater dispersion; Fig. 5*c)*.
- The observation area of the twinkling artifact on a smooth object (the signal shows a periodicity resulted from micro-oscillations of the observed object; Fig. 5*d*).

Database composition

1. A set of examinations of the Gammex 1430 LE Mini-Doppler Flow System.

Fig. 6 shows the external view and scheme of the phantom, and Fig. 7 shows examples of sonograms. In transverse scanning, the linear transducer was positioned at an angle of 60° to the vessel, the flow rate was 30 cm/s, data were obtained at 5, 9, and 17 pulses in train, and the pulse repetition frequency was 2.5 kHz. Concurrently, an observed sonogram in the phantom was very much alike that of the *in vivo* carotid artery.

In the course of longitudinal scanning with a linear transducer, the flow velocity was set to 50 cm/s, and the study was conducted with 17 probing pulses and a frequency of 1 kHz. The velocity projection, which was displayed in the Doppler mode, was close to zero. Such a study may be useful for debugging mapping algorithms.

Longitudinal scanning with a convex transducer was also performed, while three examinations were conducted at different flow rates (i.e., 30 cm/s, 65 cm/s, and 100 cm/s) at a pulse repetition frequency of 2 kHz. For these examinations, a convex transducer was used. The estimated value of the flow velocity projection along a horizontal vessel varied from a negative value, passing through zero, to a positive value; the vessel was colored in the whole palette of the CFM mode.

In Fig. 7 and all subsequent sonograms, both the B-image with the superimposed CFM imaging and the B-image without CFM are placed side by side. Subsequent examinations were conducted using a linear transducer, since it is commonly used in small depth examinations. Preference was given to small values of the pulse repetition frequency since both types of twinkling artifact signals be registered in this case [32].

2. A set of examinations of the custom phantom (Fig. 8; a detailed description of the phantom is available in [32]).

In the phantom study, the linear transducer was applied in fixed numbered positions. Cylinders, with a diameter of 1.75 mm, made of metal (positions 1, 4, and 8), plastic (positions 2, 5, and 7), and wooden rods (positions 3 and 6) in various media (water, alcohol, and agar-agar) were assessed. The set contains examinations that were conducted using a linear transducer at nine probing pulses and a pulse repetition rate of 1 kHz. Typical sonograms are shown in Fig. 9. If the phantom was filled with ethanol, the twinkling artifact was manifested much less frequently in contrast to other media used. In water, the artifact was also noticeable on the air bubbles that rose from the wooden rod. In addition, the twinkling intensity on aluminum rods was noticeably greater than that on plastic and wooden rods.

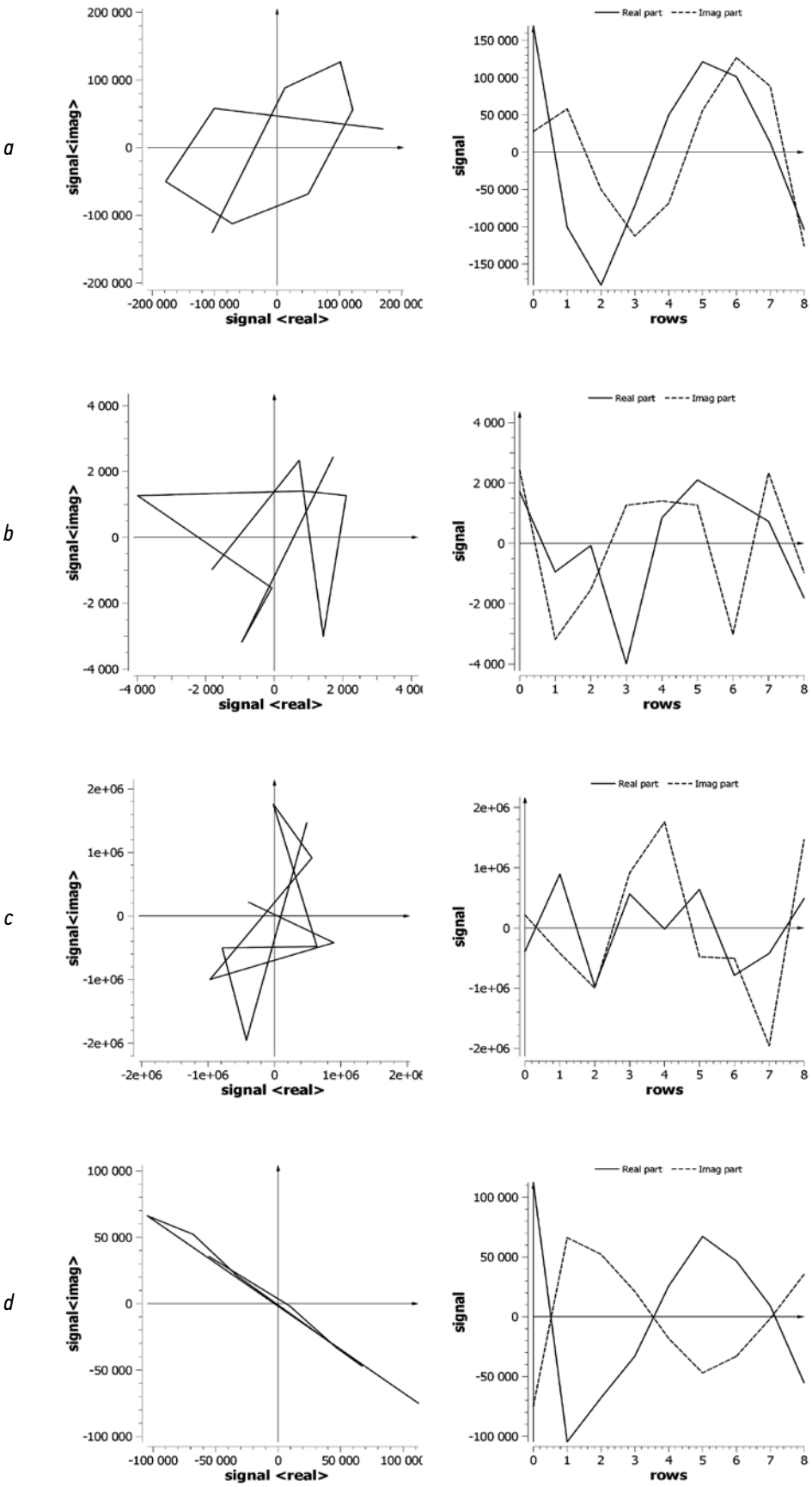

Fig. 5. Examples of visualization of radiofrequency signals using the TwinklingDatasetDisplay program: *a*, fluid flow in the Gammex phantom; *b*, soft tissue area in the absence of motion; *c*, twinkling artifact signal on a rough object; *d*, twinkling artifact signal on a smooth object. In the left column, the complex signals are represented as a parametric line in polar coordinates (the real and imaginary parts are shown on the abscissa and ordinate axes, respectively). The right column shows the dependence on the "slow" time within a pulse train.

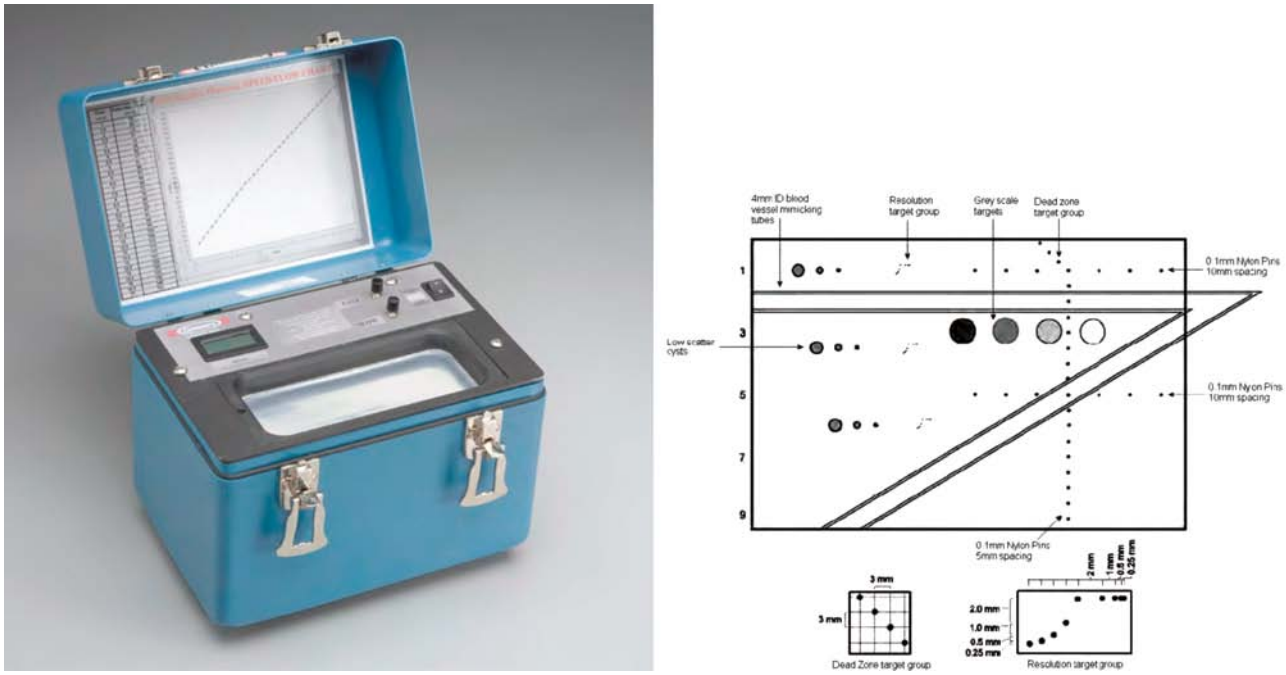

Fig. 6. External view and scheme of the Gammex 1430 LE Mini-Doppler phantom.

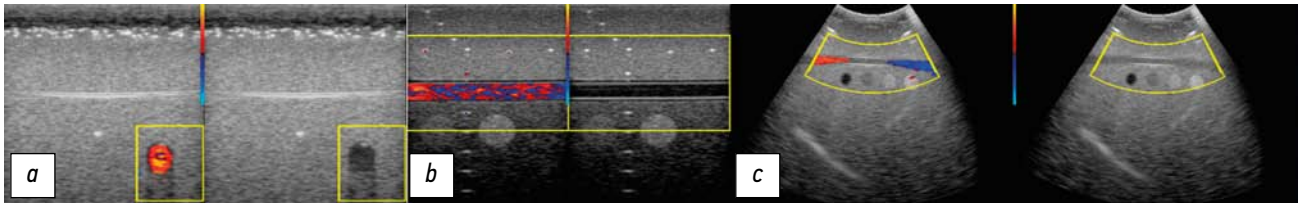

Fig. 7. Sonograms of the Gammex phantom: *a*, examination with a linear sensor at a 60° angle to the flow; *b*, parallel to the flow; *c*, examination with a convex sensor.

3. A set of examinations of elastographic breast Blue Phantom with the data that have been taken with a linear transducer at 5, 9, and 17 pulses in sequence for a pulse repetition frequency of 150 Hz and at 17 pulses and repetition frequencies of 300 Hz, 500 Hz, 750 Hz, and 1 kHz.

The phantom (photo and scheme shown in Fig. 10 *a, b*) contains inclusions that simulate micro calcifications, which are indicated by an arrow in a slice of the computer tomogram in Fig. 10*c*. On these inclusions, a twinkling artifact was observed at a low pulse repetition frequency in the CFM mode (Fig. 10*d*). With increasing frequency, the intensity of the artifact decreased until it completely disappeared at frequencies above 1 kHz.

4. A set of approximately 200-μm micro calcifications that were artificially grown in agar-agar jelly.

Two samples were examined with a linear sensor at a repetition rate of 500 Hz with nine pulses per pulse train. Typical sonograms are shown in Fig. 11.

5. A study of a steel rough wire and a wooden rod in agar-agar jelly.

The study was conducted with a linear transducer at nine pulses. In contrast to the experiment presented in Fig. 9, the wood was subjected to prolonged pre-wetting and degassing. Both objects produced an acoustic shadow and had the same echogenicity in the B-image (Fig. 12). However, the twinkling artifact appeared on the metal, but not on the wood. The difference in observations allows associating one of the twinkling types with air microbubbles in the wood structure.

Notes on the database use

In most studies [1–8, 10–13], which were devoted to the twinkling artifact, examinations were conducted using commonly available ultrasonic diagnostic devices with no access to the signal processing path. The ultrasonic device can be considered a "black box" in such examinations, and the analysis based only on sonograms on the device screen was not informative enough and created problems with reproducibility, since the algorithms of processing devices of different manufacturers are unique.

Collection of raw data is a prerequisite for developing new ultrasonic imaging tools. However, RF signals from the processing path are commonly not available because of the closed architecture of commercial

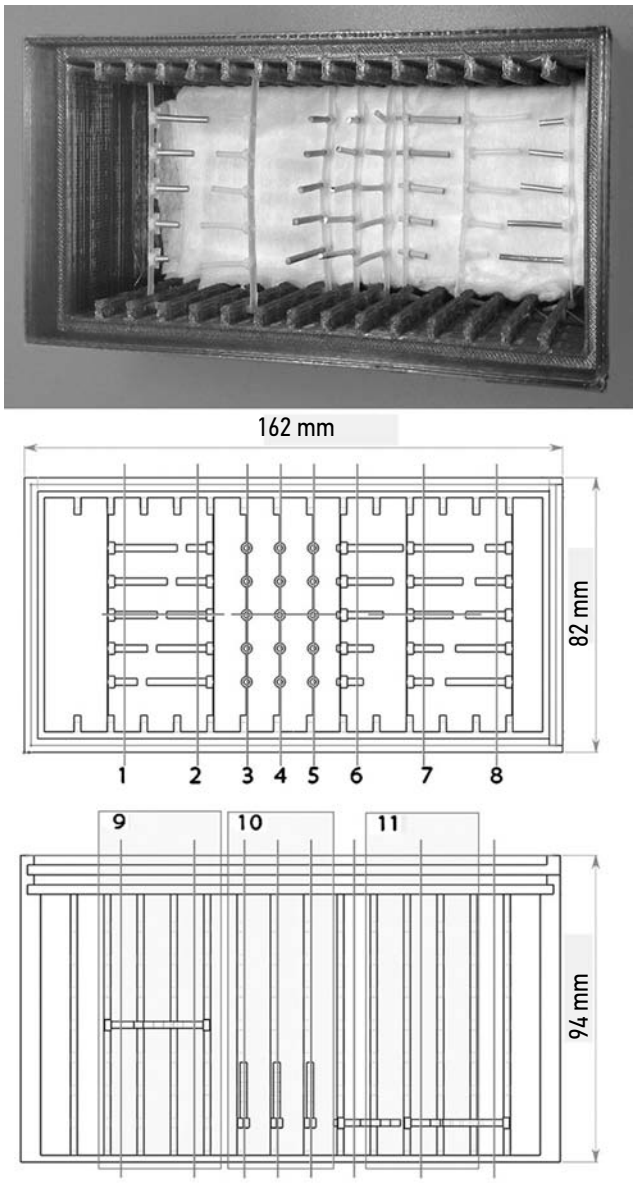

Fig. 8. Photo and drawings of the specialized phantom with dimensions in millimeters and measurement positions.

instruments. A previous study [33] demonstrated a possible solution to this problem, which required a manual modification of the equipment. The proposed database provides all information on signals without the need for self-modification of the commercial equipment with the inevitable loss of warranty and other undesirable consequences.

The proposed database may have great practical value, since it allows the creation of new tools [17] for the detection of kidney stones and other objects, which are associated with a twinkling artifact.

Using the database, we conducted several examinations, as shown below:

1) The signals of the twinkling artifact and blood flow were differentiated and two physical causes of the twinkling artifact were investigated. The image on the device screen looks the same; however, different physical processes are involved therein, which are visible at the signal level [32].
2) A special mode was developed, which allowed displaying twinkling not as a Doppler error, which happens to be useful, but as a special diagnostic option [17, 34]. Using this mode, the twinkling may be "pulled out" where a conventional device will not show this artifact. Twinkling and blood flow may be displayed separately or together using different color scales.
3) A comparative analysis of filtration algorithms for vessel wall motion (*wall filters*) was conducted [35, 36]. New filtering algorithms appeared in the literature [37–40], their fresh review and comparative analysis are in demand and can be done using our database.

In the future, we would like to complement the database with in vivo signals as well as signals that were obtained in other modes (e.g., spectral Doppler mode and vector flow).

Although the programm that we designed for opening the database has a minimal set of options, its open-source C++ code allows plentiful modifications. Moreover, the given in this article description gives sufficient information for opening of the database in any programming environment.

Disadvantages of the database

Among the disadvantages of the proposed database, the most significant is the incompleteness of the following information:

- On the examined objects (e.g., only the approximate size of calcinates that were grown in agar jelly was known, the geometrical parameters of the rough wire surface were not investigated).
- On the experimental conditions (in some examinations, the exact position of the transducer, focal distance, and emittion power were not recorded; the information on the pulse repetition frequency is not always available).

Code availability

The source code of the program (https://github.com/Center-of-Diagnostics-and-Telemedicine/TwinklingDataset-Display.git) is available.

Terms of use

The article presents a database, which contains digital records of raw RF signals from the preprocessing path of the Sonomed-500 ultrasonic device. The database with a total volume of 10.5 Gb contains mostly examinations of objects with a twinkling artifact in the CFM mode. The most obvious application of the database is the development and testing of algorithms for signal processing. The database is publicly available on the Internet under the Creative Commons Attribution – Noncommercial – Share Alike (CC BY-NC-SA) license (https://mosmed.ai/datasets/ultrasonic_doppler_twinkling_artifact).

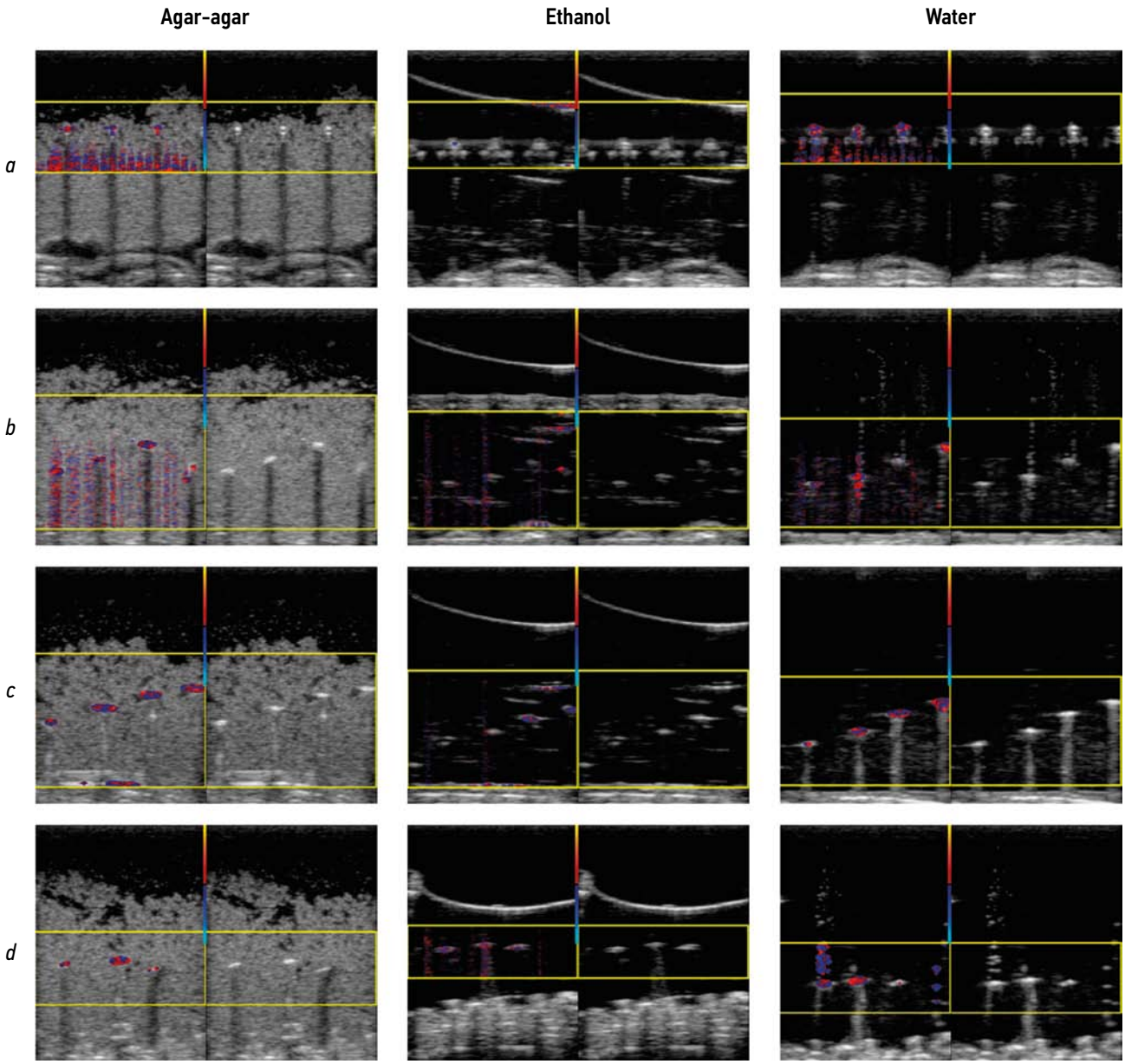

Fig. 9. Examples of sonograms of a specialized phantom with positions and a filling medium: *a*, position 2 (four plastic rods, which are located parallel to the sensor plane); *b*, position 3 (four wooden rods with their sides facing the sensor); *c*, position 4 (four aluminum rods with their sides facing the sensor); *d*, position 10 (wood, aluminum, and plastic rods with their sides facing the sensor).

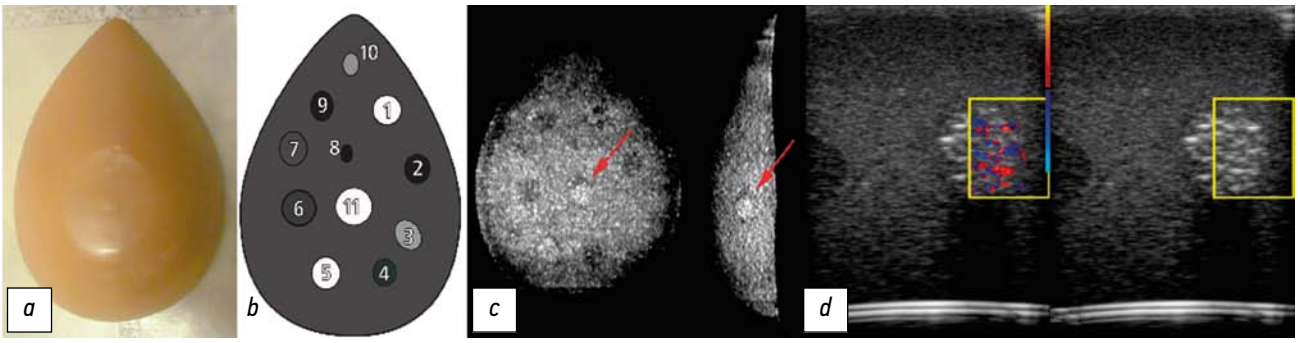

Fig. 10. Blue phantom mammary gland: *a*, external view; *b*, connection scheme; *c*, slices of computed tomogram (the arrow indicates the examined area); *d*, sonogram.

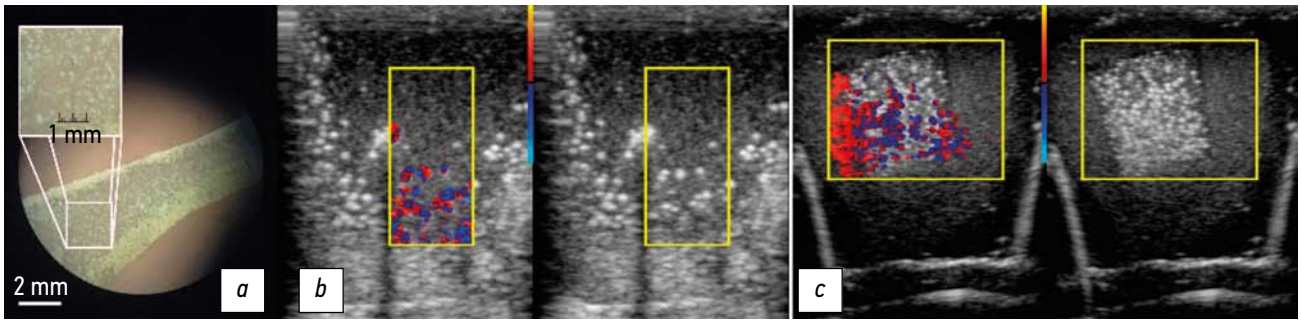

Fig. 11. Sonograms of phantoms with microcrystals that were grown in agar-agar jelly: *a*, sample slice under a microscope; *b*, microcrystals in the growth process; *c*, insertion with microcrystals in the agar-agar phantom.

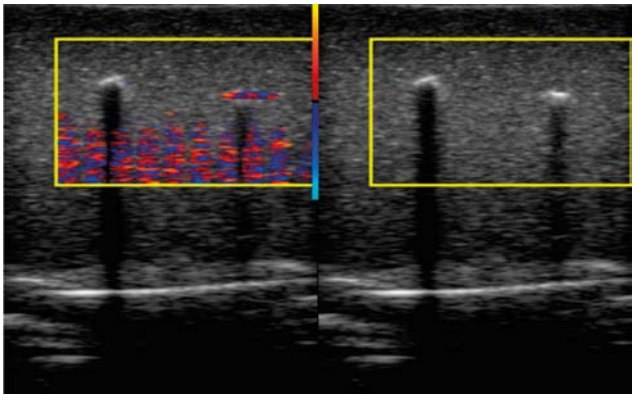

Fig. 12. Sonogram of a phantom with a wooden rod (left) and a steel wire (right).

ADDITIONAL INFORMATION

Funding source. This article was prepared with the support of Moscow Healthcare Department as a part of Program "Scientific Support of the Capital's Healthcare" for 2020–2022 (Unified State Information System for Accounting of Research, Development, and Technological Works No. AAAA-A20-120071090054-9).

Competing interests. The authors declare that they have no competing interests.

Authors' contribution. Kulberg N.S. and Leonov D.V. — research concept and design, data collection and processing, preparation of illustrations, and writing the text of the manuscript.

Reshetnikov R.V. and Nasibullina A.A. — participation in the formation of the research plan and discussion each chapter of the manuscript, checking the database, and preparing illustrations.

Gromov A.I. — research concept and design, and manuscript editing. All authors confirm the compliance of the authors with the international ICMJE criteria. All authors made a significant contribution to the development of the concept, research, and preparation of the article, read and approved the final version before publication.

REFERENCES

1. Masch WR, Cohan RH, Ellis JH, et al. Clinical effectiveness of prospectively reported sonographic twinkling artifact for the diagnosis of renal calculus in patients without known urolithiasis. *Am J Roentgenol*. 2016;206:326–331. doi: 10.2214/ajr.15.14998

2. Fujimoto Y, Shimono C, Shimoyama N, Osaki M. Twinkling artifact of microcalcifications in breast ultrasound. *Ultrasound Med Biol*. 2017;43(Suppl. 1):S21. doi: 10.1016/j.ultrasmedbio.2017.08.1010

3. Bennett J.M., Estrada J.C., Shoemaker M.B., Pretorius M. Twinkling Artifact Associated with Guidewire Placement. *Anesth Analg*. 2015;121(1):69–71. doi: 10.1213/ane.0000000000000683

4. Sen V, Imamoglu C, Kucukturkmen I, et al. Can Doppler ultrasonography Twinkling artifact be used as an alternative imaging modality to non-contrast-enhanced computed tomography in patients with ureteral stones? A prospective clinical study. *Urolithiasis*. 2017;45(2):215–219. doi: 10.1007/s00240-016-0891-8

5. Winkel RR, Kalhauge A, Fredfeldt KE. The usefulness of ultrasound colour-Doppler twinkling artefact for detecting urolithiasis compared with low dose nonenhanced computerized tomography. *Ultrasound Med Biol*. 2012;38(7):1180–1187. doi: 10.1016/j.ultrasmedbio.2012.03.003

6. Yavuz A, Ceken K, Alimoglu E, Kabaalioglu A. The reliability of color Doppler "twinkling" artifact for diagnosing millimetrical nephrolithiasis: comparison with B-Mode US and CT scanning results. *J Med Ultrasonics*. 2015;42(2):215–222. doi: 10.1007/s10396-014-0599-8

7. Tian J, Xu L. Color Doppler Twinkling artifact in diagnosis of tuberculous pleuritis: A comparison with gray-scale ultrasonography and computed tomography. *Ultrasound Med Biol*. 2018;44(6):1291–1295. doi: 10.1016/j.ultrasmedbio.2018.01.003

8. Relea A, Alonso JA, González M, et al. Usefulness of the twinkling artifact on Doppler ultrasound for the detection of breast microcalcifications. *Radiología*. 2018;60(5):413–423. doi: 10.1016/j.rx.2018.04.004

9. Lu W, Sapozhnikov OA, Bailey MR, et al. Evidence for trapped surface bubbles as the cause for the twinkling artifact in ultrasound imaging. *Ultrasound Med*. 2013;39(6):1026–1038. doi: 10.1016/j.ultrasmedbio.2013.01.011

10. Aytac SK, Ozcan H. Effect of color Doppler system on the «twinkling» sign associated with urinary

tract calculi. *J Clin Ultrasound*. 1999;27(8):433–439. doi: 10.1002/(sici)1097-0096(199910)27:8<433::aid-jcu4>3.0.co;2-1

11. Rahmouni A, Bargoin R, Herment A, et al. Color Doppler Twinkling artifactin hyperechoic regions. *Radiology*. 1996;199(1):269–271. doi: 10.1148/radiology.199.1.8633158

12. Kamaya A, Tuthill T, Rubin JM. Twinkling artifact on color Doppler sonography: dependence on machine parameters and underlying cause. *Am J Roentgenol*. 2003;180(1):215–222. doi: 10.2214/ajr.180.1.1800215

13. Weinstein SP, Seghal C, Conant EF, Patton JA. Microcalcifications in breast tissue phantoms visualized with acoustic resonance coupled with power doppler US: initial observations. *Radiology*. 2002:224(1):265–269. doi: 10.1148/radiol.2241010511

14. Seghal C. Apparatus for imaging an element within a tissue and method therefor. *United States Patent*. 1999;477(5):997.

15. Li T, Khokhlova TD, Sapozhnikov OA, et al. A new active cavitation mapping technique for pulsed HIFU applications–bubble Doppler. *IEEE Trans Ultrason Ferroelectr Freq Control*. 2014;61(10): 1698–1708. doi: 10.1109/TUFFC.2014.006502

16. Simon JC, Sapozhnikov OA, Kreider W, et al. The role of trapped bubbles in kidney stone detection with the color Doppler ultrasound twinkling artifact. *Phys Med Biol*. 2018;63(2):025011. doi: 10.1088/1361-6560/aa9a2f

17. Leonov DV, Kulberg NS, Gromov AI, et al. Diagnostic mode detecting solid mineral inclusions in medical ultrasound imaging. *Acoust Phys*. 2018;64(5):624–636. doi: 10.1134/S1063771018050068

18. Yu AC, Johnston KW, Cobbold RS. Frequency-based signal processing for ultrasound color flow imaging. *Canadian Acoustics*. 2007;35(2):11–23.

19. Yu AC, Løvstakken L. Eigen-based clutter filter design for ultrasound color flow imaging: a review. *IEEE Trans Ultrason Ferroelectr Freq Control*. 2010;57(5):1096–1111. doi: 10.1109/TUFFC.2010.1521

20. Yu AC, Cobbold RS. Single-ensemble-based eigen-processing methods for color flow imaging — Part I. The Hankel-SVD filter. *IEEE Trans Ultrason Ferroelectr Freq Control*. 2008;55(3):559–572. doi: 10.1109/TUFFC.2008.682

21. Shen Z, Feng N, Shen Y, Lee CH. An improved parametric relaxation approach to blood flow signal estimation with single-ensemble in color flow imaging. *J Med Biomed Engineering*. 2013;33(3):309–318. doi: 10.5405/jmbe.1368

22. Yoo YM, Managuli R, Kim Y. Adaptive clutter filtering for ultrasound color flow imaging. *Ultrasound Med Biol*. 2003;29(9): 1311–1320. doi: 10.1016/S0301-5629(03)01014-7

23. Torp H. Clutter rejection filters in color flow imaging: a theoretical approach. *IEEE Trans Ultrason Ferroelectr Freq Control*. 1997;44(2):417–424. doi: 10.1109/58.585126

24. Wang PD, Shen Y, Feng NZ. A novel clutter rejection scheme in color flow imaging. *Ultrasonics*. 2006;44(Suppl 1):e303–305. doi: 10.1016/j.ultras.2006.06.017

25. Bjærum S, Torp H. Statistical evaluation of clutter filters in color flow imaging. *Ultrasonics*. 2000;38(1-8):376–380. doi: 10.1016/s0041-624x(99)00153-5

26. Kargel C, Hoebenreich G, Plevnik G, et al. Velocity estimation and adaptive clutter filtering for color flow imaging. *WSEAS*. 2002. P. 1711–1716.

27. Kargel C, Höbenreich G, Trummer B, Insana MF. Adaptive clutter rejection filtering in ultrasonic strain-flow imaging. *IEEE Trans Ultrason Ferroelectr Freq Control*. 2003;50(7):824–835. doi: 10.1109/tuffc.2003.1214502

28. Lo MT, Hu K, Peng CK, Novak V. Multimodal pressure flow analysis: application of hilbert huang transform in carabral blood flow regulation. *EURASIP J Adv Signal Process*. 2008;2008:785243. doi: 10.1155/2008/785243

29. Gerbands JJ. On the relationships between SVD, KLT and PCA. *Pattern Recognition*. 1981;14:375–381. doi: 10.1016/0031-3203(81)90082-0

30. Løvstakken L. Signal processing in diagnostic ultrasound: algorithms for real-time estimation and visualization of blood flow velocity. Doctoral thesis, norwegian university of science and technology. Trondheim; 2007. Available from: https://pdfslide.net/documents/signal-processing-in-diagnostic-ultrasound-algorithms-for-real-time-.html. Accessed: 14.08.2021.

31. XRAD C++ software library. Available from: https://github.com/Center-of-Diagnostics-and-Telemedicine/xrad.git. Accessed: 14.08.2021.

32. Leonov DV, Kulberg NS, Gromov AI., et al. Causes of ultrasound doppler twinkling artifact. *Acoust Phys*. 2018;64(1):105–114. doi: 10.1134/S1063771018010128

33. Mari JM, Cachard C. Acquire real-time RF digital ultrasound data from a commercial scanner. *Electronic J Technical Acoustics*. 2007;3:28–43.

34. Leonov DV, Kulberg NS, Gromov AI, Morozov SP. Detection of microcalcifications using the ultrasound Doppler twinkling artifact. *Biomedical Engineering*. 2020;54(3):174–178. doi: 10.1007/s10527-020-09998-y

35. Leonov DV, Kulberg NS, Fin VA, et al. Clutter filtering for diagnostic ultrasound color flow imaging. *Biomedical Engineering*. 2019;53(3):217–221. doi: 10.1007/s10527-019-09912-1

36. Leonov DV, Kulberg NS, Fin VA, et al. Comparison of filtering techniques in ultrasound color flow imaging. *Biomedical Engineering*. 2019;53(2):97–101. doi: 10.1007/s10527-019-09885-1

37. Song P, Manduca A, Trzasko JD, Chen S. Ultrasound small vessel imaging with block-wise adaptive local clutter filtering. *IEEE Trans Med Imaging*. 2017;36(1):251–262. doi: 10.1109/TMI.2016.2605819

38. Li YL, Hyun D, Abou-Elkacem L, et al. Visualization of small-diameter vessels by reduction of incoherent reverberation with coherent flow power doppler. *IEEE Trans Ultrason Ferroelectr Freq Control*. 2016;63(11):1878–1889. doi: 10.1109/TUFFC.2016.2616112

39. Chee AJ, Alfred CH. Receiver operating characteristic analysis of eigen-based clutter filters for ultrasound color flow imaging. *IEEE Trans Ultrason Ferroelectr Freq Control*. 2017;65(3):390–399. doi: 10.1109/TUFFC.2017.2784183

40. Chee AJ, Yiu BY, Alfred CH. A GPU-Parallelized eigen-based clutter filter framework for ultrasound color flow imaging. *IEEE Trans Ultrason Ferroelectr Freq Control*. 2017;64(1):150–163. doi: 10.1109/TUFFC.2016.2606598

СПИСОК ЛИТЕРАТУРЫ

1. Masch W.R., Cohan R.H., Ellis J.H., et al. Clinical effectiveness of prospectively reported sonographic twinkling artifact for the diagnosis of renal calculus in patients without known urolithiasis // Am J Roentgenol. 2016. Vol. 206. P. 326–331. doi: 10.2214/ajr.15.14998

2. Fujimoto Y., Shimono C., Shimoyama N., Osaki M. Twinkling artifact of microcalcifications in breast ultrasound // Ultrasound Med Biol. 2017. Vol. 43, Suppl. 1. P. S21. doi: 10.1016/j.ultrasmedbio.2017.08.1010

3. Bennett J.M., Estrada J.C., Shoemaker M.B., Pretorius M. Twinkling artifact associated with guidewire placement // Anesth Analg. 2015. Vol. 121, N 1. P. 69–71. doi: 10.1213/ane.0000000000000683

4. Sen V., Imamoglu C., Kucukturkmen I., et al. Can Doppler ultrasonography Twinkling artifact be used as an alternative imaging modality to non-contrast-enhanced computed tomography in patients with ureteral stones? A prospective clinical study // Urolithiasis. 2017. Vol. 45, N 2. P. 215–219. doi: 10.1007/s00240-016-0891-8

5. Winkel R.R., Kalhauge A., Fredfeldt K.E. The usefulness of ultrasound colour-Doppler twinkling artefact for detecting urolithiasis compared with low dose nonenhanced computerized tomography // Ultrasound Med Biol. 2012. Vol. 38, N 7. P. 1180–1187. doi: 10.1016/j.ultrasmedbio.2012.03.003

6. Yavuz A., Ceken K., Alimoglu E., Kabaalioglu A. The reliability of color Doppler "twinkling" artifact for diagnosing millimetrical nephrolithiasis: comparison with B-Mode US and CT scanning results // J Med Ultrasonics. 2015. Vol. 42, N 2. P. 215–222. doi: 10.1007/s10396-014-0599-8

7. Tian J., Xu L. Color Doppler Twinkling artifact in diagnosis of tuberculous pleuritis: A comparison with gray-scale ultrasonography and computed tomography // Ultrasound Med Biol. 2018. Vol. 44, N 6. P. 1291–1295. doi: 10.1016/j.ultrasmedbio.2018.01.003

8. Relea A., Alonso J.A., González M., et al. Usefulness of the twinkling artifact on Doppler ultrasound for the detection of breast microcalcifications // Radiología. 2018. Vol. 60, N 5. P. 413–423. doi: 10.1016/j.rx.2018.04.004

9. Lu W., Sapozhnikov O.A., Bailey M.R., et al. Evidence for trapped surface bubbles as the cause for the twinkling artifact in ultrasound imaging // Ultrasound Med. 2013. Vol. 39, N 6. P. 1026–1038. doi: 10.1016/j.ultrasmedbio.2013.01.011

10. Aytac S.K., Ozcan H. Effect of color Doppler system on the «twinkling» sign associated with urinary tract calculi // J Clin Ultrasound. 1999. Vol. 27, N 8. P. 433–439. doi: 10.1002/(sici)1097-0096(199910)27:8<433::aid-jcu4>3.0.co;2-1

11. Rahmouni A., Bargoin R., Herment A., et al. Color doppler twinkling artifactin hyperechoic regions // Radiology. 1996. Vol. 199, N 1. P. 269–271. doi: 10.1148/radiology.199.1.8633158

12. Kamaya A., Tuthill T., Rubin J.M. Twinkling artifact on color Doppler sonography: dependence on machine parameters and underlying cause // Am J Roentgenol. 2003. Vol. 180, N 1. P. 215–222. doi: 10.2214/ajr.180.1.1800215

13. Weinstein S.P., Seghal C., Conant E.F., Patton J.A. Microcalcifications in breast tissue phantoms visualized with acoustic resonance coupled with power doppler US: initial observations // Radiology. 2002: Vol. 4, N 1. P. 265–269. doi: 10.1148/radiol.2241010511

14. Seghal C. Apparatus for imaging an element within a tissue and method therefor // United States Patent. 1999. Vol. 477, N 5. P. 997.

15. Li T., Khokhlova T.D., Sapozhnikov O.A., et al. A new active cavitation mapping technique for pulsed HIFU applications–bubble Doppler // IEEE Trans Ultrason Ferroelectr Freq Control. 2014. Vol. 61, N 10. P. 1698–708. doi: 10.1109/TUFFC.2014.006502

16. Simon J.C., Sapozhnikov O.A., Kreider W., et al. The role of trapped bubbles in kidney stone detection with the color Doppler ultrasound twinkling artifact // Phys Med Biol. 2018. Vol. 63, N 2. P. 025011. doi: 10.1088/1361-6560/aa9a2f

17. Leonov D.V., Kulberg N.S., Gromov A.I., et al. Diagnostic mode detecting solid mineral inclusions in medical ultrasound imaging // Acoust Phys. 2018. Vol. 64, N 5. P. 624–636. doi: 10.1134/S1063771018050068

18. Yu A.C., Johnston K.W., Cobbold R.S. Frequency-based signal processing for ultrasound color flow imaging // Canadian Acoustics. 2007. Vol. 35, N 2. P. 11–23.

19. Yu A.C., Løvstakken L. Eigen-based clutter filter design for ultrasound color flow imaging: a review // IEEE Trans Ultrason Ferroelectr Freq Control. 2010. Vol. 57, N 5. P. 1096–1111. doi: 10.1109/TUFFC.2010.1521

20. Yu A.C., Cobbold R.S. Single-Ensemble-based eigen-processing methods for color flow imaging — Part I. The Hankel-SVD filter // IEEE Trans Ultrason Ferroelectr Freq Control. 2008. Vol. 55, N 3. P. 559–572. doi: 10.1109/TUFFC.2008.682

21. Shen Z., Feng N., Shen Y., Lee C.H. An improved parametric relaxation approach to blood flow signal estimation with single-ensemble in color flow imaging // J Med Biomed Engineering. 2013. Vol. 33, N 3. P. 309–318. doi: 10.5405/jmbe.1368

22. Yoo Y.M., Managuli R., Kim Y. Adaptive clutter filtering for ultrasound color flow imaging // Ultrasound Med Biol. 2003. Vol. 29, N 9. P. 1311–1320. doi: 10.1016/S0301-5629(03)01014-7

23. Torp H. Clutter rejection filters in color flow imaging: a theoretical approach // IEEE Trans Ultrason Ferroelectr Freq Control. 1997. Vol. 44, N 2. P. 417–424. doi: 10.1109/58.585126

24. Wang P.D., Shen Y., Feng N.Z. A novel clutter rejection scheme in color flow imaging // Ultrasonics. 2006. Vol. 44, Suppl 1. P. e303–305. doi: 10.1016/j.ultras.2006.06.017

25. Bjærum S., Torp H. Statistical evaluation of clutter filters in color flow imaging // Ultrasonics. 2000. Vol. 38, N 1-8. P. 376–380. doi: 10.1016/s0041-624x(99)00153-5

26. Kargel C., Hoebenreich G., Plevnik G., et al. Velocity estimation and adaptive clutter filtering for color flow imaging // WSEAS. 2002. P. 1711–1716.

27. Kargel C., Höbenreich G., Trummer B., Insana M.F. Adaptive clutter rejection filtering in ultrasonic strain-flow imaging // IEEE Trans Ultrason Ferroelectr Freq Control. 2003. Vol. 50, N 7. P. 824–835. doi: 10.1109/tuffc.2003.1214502

28. Lo M.T., Hu K., Peng C.K., Novak V. Multimodal pressure flow analysis: application of hilbert huang transform in carabral blood flow regulation // EURASIP J Adv Signal Process. 2008. Vol. 2008. P. 785243. doi: 10.1155/2008/785243

29. Gerbands J.J. On the relationships between SVD, KLT and PCA // Pattern Recognition. 1981. Vol. 14. P. 375–381. doi: 10.1016/0031-3203(81)90082-0

30. Løvstakken L. Signal processing in diagnostic ultrasound: algorithms for real-time estimation and visualization of blood flow velocity. Doctoral thesis, norwegian university of science and technology. Trondheim; 2007. Режим доступа: https://pdfslide.net/documents/signal-processing-in-diagnostic-ultrasound-algorithms-for-real-time-.html. Дата обращения: 14.08.2021.
31. XRAD C++ software library. Режим доступа: https://github.com/Center-of-Diagnostics-and-Telemedicine/xrad.git. Дата обращения: 14.08.2021.
32. Leonov D.V., Kulberg N.S., Gromov A.I., et al. Causes of ultrasound doppler twinkling artifact // Acoust Phys. 2018. Vol. 64, N 1. P. 105–114. doi: 10.1134/S1063771018010128
33. Mari J.M., Cachard C. Acquire real-time RF digital ultrasound data from a commercial scanner // Electronic J Technical Acoustics. 2007. Vol. 3. P. 28–43.
34. Leonov D.V., Kulberg N.S., Gromov A.I., Morozov S.P. Detection of microcalcifications using the ultrasound Doppler twinkling artifact // Biomedical Engineering. 2020. Vol. 54, N 3. P. 174–178. doi: 10.1007/s10527-020-09998-y
35. Leonov D.V., Kulberg N.S., Fin V.A., et al. Clutter filtering for diagnostic ultrasound color flow imaging // Biomedical Engineering. 2019. Vol. 53, N 3. P. 217–221. doi: 10.1007/s10527-019-09912-1
36. Leonov D.V., Kulberg N.S., Fin V.A., et al. Comparison of filtering techniques in ultrasound color flow imaging // Biomedical Engineering. 2019. Vol. 53, N 2. P. 97–101. doi: 10.1007/s10527-019-09885-1
37. Song P., Manduca A., Trzasko J.D., Chen S. Ultrasound small vessel imaging with block-wise adaptive local clutter filtering // IEEE Trans Med Imaging. 2017. Vol. 36, N 1. P. 251–262. doi: 10.1109/TMI.2016.2605819
38. Li Y.L., Hyun D., Abou-Elkacem L., et al. Visualization of small-diameter vessels by reduction of incoherent reverberation with coherent flow power doppler // IEEE Trans Ultrason Ferroelectr Freq Control. 2016. Vol. 63, N 11. P. 1878–1889. doi: 10.1109/TUFFC.2016.2616112
39. Chee A.J., Alfred C.H. Receiver operating characteristic analysis of eigen-based clutter filters for ultrasound color flow imaging // IEEE Trans Ultrason Ferroelectr Freq Control. 2017. Vol. 65, N 3. P. 390–399. doi: 10.1109/TUFFC.2017.2784183
40. Chee A.J., Yiu B.Y., Alfred C.H. A GPU-Parallelized eigen-based clutter filter framework for ultrasound color flow imaging // IEEE Trans Ultrason Ferroelectr Freq Control. 2017. Vol. 64, N 1. P. 150–163. doi: 10.1109/TUFFC.2016.2606598

AUTHORS' INFO

*** Denis V. Leonov**, Cand. Sci. (Tech);
address: 28-1, Srednyaya Kalitnikovskaya street, Moscow, 109029, Russia;
ORCID: http://orcid.org/0000-0003-0916-6552;
eLibrary SPIN: 5510-4075; e-mail: strat89@mail.ru

Roman V. Reshetnikov, Cand. Sci. (Phys.-Math.);
ORCID: http://orcid.org/0000-0002-9661-0254;
eLibrary SPIN: 8592-0558; e-mail: reshetnikov@fbb.msu.ru

Nikolay S. Kulberg, Cand. Sci. (Phys.-Math.);
ORCID: http://orcid.org/0000-0001-7046-7157;
eLibrary SPIN: 2135-9543; e-mail: kulberg@npcmr.ru

Anastasia A. Nasibullina;
ORCID: http://orcid.org/0000-0003-1695-7731;
eLibrary SPIN: 2482-3372; e-mail: nastya.nasibullina@yandex.ru

Alexandr I. Gromov, MD, Dr. Sci. (Med.), Professor;
ORCID: http://orcid.org/0000-0002-9014-9022;
eLibrary SPIN: 6842-8684; e-mail: gromov.ai@medsigroup.ru

ОБ АВТОРАХ

*** Леонов Денис Владимирович**, к.т.н.;
адрес: Россия, 109029, Москва, ул. Средняя Калитниковская, д. 28, стр. 1;
ORCID: http://orcid.org/0000-0003-0916-6552;
eLibrary SPIN: 5510-4075; e-mail: strat89@mail.ru

Решетников Роман Владимирович, к.ф.-м.н.;
ORCID: http://orcid.org/0000-0002-9661-0254;
eLibrary SPIN: 8592-0558; e-mail: reshetnikov@fbb.msu.ru

Кульберг Николай Сергеевич, к.ф.-м.н.;
ORCID: http://orcid.org/0000-0001-7046-7157;
eLibrary SPIN: 2135-9543; e-mail: kulberg@npcmr.ru

Насибуллина Анастасия Александровна;
ORCID: http://orcid.org/0000-0003-1695-7731;
eLibrary SPIN: 2482-3372; e-mail: nastya.nasibullina@yandex.ru

Громов Александр Игоревич, д.м.н., профессор;
ORCID: http://orcid.org/0000-0002-9014-9022;
eLibrary SPIN: 6842-8684; e-mail: gromov.ai@medsigroup.ru

* Corresponding author / Автор, ответственный за переписку

DOI: https://doi.org/10.17816/DD63680

Оценка геометрических отклонений, возникающих при воспроизведении трёхмерных моделей средствами аддитивного производства, по данным компьютерной томографии

А.В. Ширшин[1, 2], И.С. Железняк[1], В.Н. Малаховский[1], С.В. Кушнарев[1], Н.С. Горина[1]

[1] Военно-медицинская академия имени С.М. Кирова, Санкт-Петербург, Российская Федерация
[2] Национальный исследовательский университет ИТМО, Санкт-Петербург, Российская Федерация

АННОТАЦИЯ

Обоснование. Технологии трёхмерного моделирования и трёхмерной печати к настоящему времени нашли применение в различных областях клинической и фундаментальной медицины, преимущественно хирургической направленности. Говоря о предоперационной подготовке хирургов, соответствие напечатанных изделий анатомии пациента может играть важную роль в оценке патологических изменений и способах их коррекции. Определение отклонений размеров получаемых моделей сопряжено с этическими и техническими трудностями, связанными с необходимостью определения эталона и проведения большого количества измерений соответственно. В настоящей работе предлагаются использование в качестве эталона геометрической фигуры с заранее известными размерами и оценка линейных отклонений при помощи итеративного алгоритма ближайших точек для каждой из вершин полученной средствами прототипирования полигональной сетки.

Цель — оценить геометрические отклонения, возникающие при воспроизведении объектов, имитирующих костную ткань, средствами трёхмерного моделирования (на основе данных компьютерной томографии) и аддитивного производства.

Материалы и методы. Для создания исходного объекта использовали программу FreeCAD, редактирование полигональных сеток проводили в программах Blender и Meshmixer. 3D-печать моделей выполняли на принтере Ender-3 из содержащего частицы меди PLA-пластика BFCopper. Сканирование производили 128-срезовым компьютерным томографом Philips Ingenuity CT. Серии томографических изображений загружали в программу 3D Slicer, где на их основе создавали виртуальные модели методами автоматической (с пороговыми значениями 500 HU, 0 HU, -500 HU, -750 HU) и ручной сегментации. Сравнение исходных и воспроизведённых моделей производили на основе итеративного алгоритма ближайших точек в программе CloudCompare.

Результаты. В зависимости от метода сегментации объём воспроизведённых моделей превышал объём соответствующих исходных моделей на 1–27%. Средние значения линейных отклонений полигональных сеток воспроизведённых моделей от исходных составили 0,03–0,41 мм. Сравнение значений интегральных сумм линейных отклонений и изменений объёма моделей с использованием коэффициента ранговой корреляции Спирмена показало между ними значимую корреляционную связь (ρ=0,83; $t_{эмп}$=5,27, p=0,05).

Заключение. Геометрические параметры воспроизводимого объекта неизбежно изменяются, при этом искажение больше зависит от выбранного способа сегментации, чем от общих масштабов модели или её частей. Использование ручного способа сегментации может привести к большему искажению линейных размеров (по сравнению с автоматическим), но позволяет сохранить все необходимые анатомические структуры.

Ключевые слова: компьютерная томография; 3D-моделирование; 3D-печать; предоперационный период; точность воспроизведения; итеративный алгоритм ближайших точек.

Как цитировать

Ширшин А.В., Железняк И.С., Малаховский В.Н., Кушнарев С.В., Горина Н.С. Оценка геометрических отклонений, возникающих при воспроизведении трёхмерных моделей средствами аддитивного производства, по данным компьютерной томографии // *Digital Diagnostics.* 2021. Т. 2, № 3. С. 277–288. DOI: https://doi.org/10.17816/DD63680

Рукопись получена: 19.03.2021 **Рукопись одобрена:** 04.08.2021 **Опубликована:** 16.08.2021

DOI: https://doi.org/10.17816/DD63680

Evaluation of geometric deviations in rapid prototyped three-dimensional models created from computed tomography data

Aleksandr V. Shirshin[1, 2], Igor S. Zheleznyak[1], Vladimir N. Malakhovsky[1], Sergey V. Kushnarev[1], Nataliya S. Gorina[1]

[1] Kirov Military Medical Academy, Saint-Petersburg, Russian Federation

[2] ITMO University, Saint-Petersburg, Russian Federation

ABSTRACT

BACKGROUND: Computer-aided design and three-dimensional printing have been used in various clinical and fundamental medicine fields, especially in surgery. For example, in the preoperative period, the correspondence of printed products to the anatomy can play an important role in evaluating pathological changes and correction methods. However, determining dimensional deviations of printed models involves ethical and technical difficulties associated with defining a reference and taking many measurements, respectively. Therefore, we propose to use a geometric object with known dimensions as a reference and estimate linear deviations using the Iterative Closest Point algorithm for each of the vertices of the prototyped polygonal mesh.

AIMS: To evaluate the geometric deviations associated with creation of bone-like physical objects from computed tomography data using computer-aided design and additive manufacturing.

MATERIALS AND METHODS: The source object was created using the FreeCAD application; Blender and Meshmixer software was used for polygon meshes correction and transformation. The 3D printing was carried out on an Ender-3 printer with copper-impregnated polylactide plastic BFCopper. Scanning was performed using a 128-slice tomograph Philips Ingenuity CT. A series of tomographic images were processed in 3DSlicer software to create virtual models by semiautomatic segmentation with threshold values of 500 HU, 0 HU, –500 HU, –750 HU, and manual segmentation. Reproduced and reference polygon meshes were compared using the Iterative Closest Point algorithm in CloudCompare software.

RESULTS: The volume of reproduced models exceeded the volume of respective reference models by 1%–27%. The average point cloud linear deviation values of reproduced models from the reference ones were 0.03–0.41 mm. A significant correlation between integral sums of linear deviations and changes in the volume of reproduced models was shown using Spearman's rank correlation coefficient ($\rho = 0.83$; $t_{emp} = 5.27$, $p=0.05$).

CONCLUSION: The geometry of the reproduced object changes inevitably, while the linear deviations depend more on the chosen segmentation method than on the overall size of the model or its structures. The manual segmentation method can lead to greater linear deviations, though it saves all the necessary anatomical structures.

Keywords: computed tomography; computer aided design; 3D printing; preoperative period; dimensional measurement accuracy; Iterative Closest Point algorithm.

To cite this article

Shirshin AV, Zheleznyak IS, Malakhovsky VN, Kushnarev SV, Gorina NS. Evaluation of geometric deviations in rapid prototyped three-dimensional models created from computed tomography data. *Digital Diagnostics.* 2021;2(3):277–288. DOI: https://doi.org/10.17816/DD63680

Received: 19.03.2021 **Accepted:** 04.08.2021 **Published:** 16.08.2021

DOI: https://doi.org/10.17816/DD63680

根据计算机断层扫描数据评估通过增材制造复制三维模型引起的几何偏差

Aleksandr V. Shirshin[1, 2], Igor S. Zheleznyak[1], Vladimir N. Malakhovsky[1], Sergey V. Kushnarev[1], Nataliya S. Gorina[1]

[1] Kirov Military Medical Academy, Saint-Petersburg, Russian Federation

[2] ITMO University, Saint-Petersburg, Russian Federation

简评

论证。三维建模和三维打印技术现已在临床和基础医学的各个领域得到应用，主要是在外科领域。谈到外科医生的术前准备，印刷品与患者解剖结构的一致性可以在评估病变和纠正病变的方法方面发挥重要作用。确定所得模型大小的偏差与伦理和技术困难有关，这些困难分别与确定标准和进行大量测量的需要相关。 本文中我们建议使用具有预定尺寸的几何图形作为参考，并使用通过原型制作获得的多边形网格的每个顶点的最近点的迭代算法来估计线性偏差。

目标是通过三维建模（基于计算机断层扫描数据）和增材制造来评估模拟骨组织的物体复制时出现的几何偏差。

材料与方法为了创建初始对象，使用了 FreeCAD 程序，在 Blender 和 Meshmixer 程序中编辑多边形网格。 这些模型是在含有铜颗粒的 BFCopper PLA 的 Ender-3 打印机上进行 3D 打印的。 使用飞利浦 Ingenuity CT 128 层 CT 扫描仪进行扫描。 将一系列断层图像加载到 3D Slicer 程序中，使用自动（阈值为 500 HU、0 HU、-500 HU、-750 HU）和手动分割的方法创建虚拟模型. 原始模型和复制模型的比较是基于 CloudCompare 程序中最近点的迭代算法进行的。

结果。根据分割方法的不同，复制模型的体积超过相应原始模型的体积 1-27%。 复制模型的多边形网格与原始模型的线性偏差平均值为 0.03-0.41 毫米。 使用斯皮尔曼等级相关系数比较线性偏差和模型体积变化的积分和的值显示它们之间存在显着相关性（ $\rho = 0.83$; $t_{emp}=5.27$, $p=0.05$）。

结论。再现对象的几何参数不可避免地会发生变化，失真更多地取决于所选的分割方法，而不是模型或其零件的总体比例。 使用手动分割方法会导致线性尺寸的更大失真（与自动分割方法相比），但它允许您保留所有必要的解剖结构。

关键词：计算机断层扫描； 3D建模； 3D打印； 术前期； 保真度； 迭代最近点算法。

引用本文

Shirshin AV, Zheleznyak IS, Malakhovsky VN, Kushnarev SV, Gorina NS. 根据计算机断层扫描数据评估通过增材制造复制三维模型引起的几何偏差. *Digital Diagnostics*. 2021;2(3):277–288. DOI: https://doi.org/10.17816/DD63680

收到： 19.03.2021 **接受：** 04.08.2021 **发布日期：** 16.08.2021

BACKGROUND

Medical prototyping technologies, which combine computer-aided design (CAD) and three-dimensional (3D) printing methods, have been increasingly used in various fields of clinical and basic medicine in recent decades [1–4]. Particularly, this was facilitated by the widespread use of additive manufacturing facilities since the 2000s, following the launch of the replicating rapid prototypes and the patent expiration for the fused deposition modeling technology.

The medical prototyping success in the clinical practice depends on the maximum compliance of the resulting products with the patient's anatomy [5]. Thus, in some cases (printing personalized implants and creating guiding resection templates), the degree of congruence between the printed medical product and the bone surface may directly influence the surgical treatment outcome [6]. In other situations (preoperative assessment and creating training phantoms), accurate reproduction of geometric relations between the normal and abnormal tissues predicts possible complications during surgery [7].

Obtaining the reference values for the dimensions of the studied anatomical structures is difficult due to the barrier in the accuracy assessment of the resulting models *in vivo*. Direct measurement of the object of interest is not always possible even during the surgical intervention (due to organ deformations), and obtaining 3D models and assessing their inaccuracies are based on the medical imaging methods used for the noninvasive collection of morphological characteristics of organs. Alternatively, a comparison of models derived from *ex vivo* scans of bone structures may be used; however, this approach uses a relatively small number of checkpoints, and the complexity of their interpretation by different specialists may lead to errors [8]. Tests on 3D models of large mammals (e.g., pigs) give good results with their subsequent introduction into the clinical practice [9].

Physical models were selected as objects of study in earlier works devoted to the accuracy assessment of model reproduction by additive manufacturing tools. These models were measured by several checkpoints using direct means: ruler, caliper, and coordinate measuring machine [10–12]. The present study proposes to use a fundamentally different approach to assess geometric deviations, which consists of all polygonal mesh points comparison obtained using additive technologies with a reference representing the original 3D model. Therefore, a model of complex shape and predetermined dimensions designed using parametric modeling was used as a reference. Conversely, the compared object was a virtual model of a reference passed three main stages of medical prototyping (3D printing, scanning, and modeling). This approach simultaneously assessed the deviations over the entire surface of the product, without the need for numerous linear measurements, while reducing the human factor influence on the measurement process.

This study aimed to assess the geometric deviations that occurred when reproducing objects imitating bone tissues using 3D modeling (based on computed tomography [CT] data) and additive manufacturing.

MATERIALS AND METHODS

The study design is shown in Fig. 1.

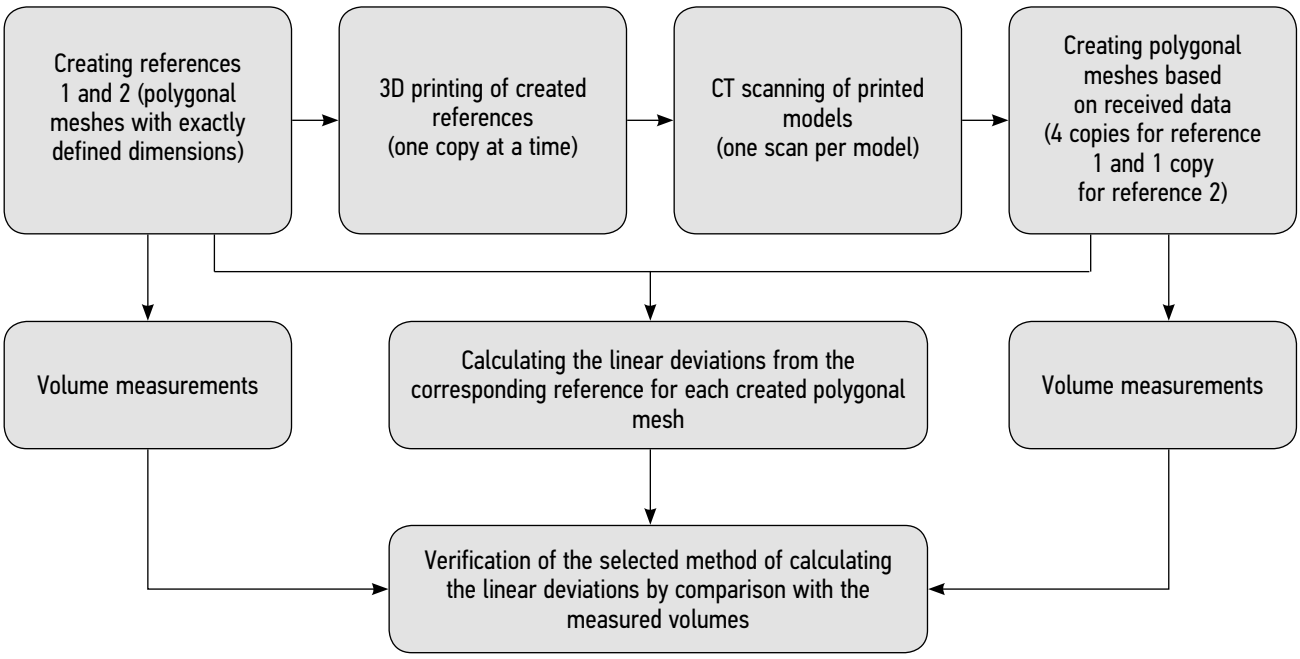

Fig. 1. Study design.
CT: computed tomography.

In the FreeCAD[1] parametric modeling program (FreeCAD Community, Germany), a solid model based on a cuboid with dimensions of 20 × 20 × 12 mm (l × w × h) was designed, which contained five end-to-end parallel channels with diameters of 1, 2, 3, 4, and 10 mm. Two recesses and two eminences in the form of a hemisphere and a cone (imitating rounded and sharpened notches and protrusions on the bone surface) at 4 mm in height were created on the upper edge of the model (hereinafter—reference 1). The diameter of the channels was selected to simulate the different foramina of the human skull on one product, which are visualized by modern CT methods. A 1-mm step for smaller diameter channels and irregularities of a given shape on the product surface was applied to manually assess the quality during model printing. Using the Blender[2] software package (Blender Foundation, the Netherlands), volumes were calculated and a copy of this reference, doubled in length, width, and height (hereinafter—reference 2), was created to check the effect of size increase on linear deviations.

Parametric models saved in Standard Triangle Language (STL) format were uploaded to the Repetier Host[3] program (Hot-World GmbH & Co. KG, Germany), where the G-code file for the 3D printer was generated using the CuraEngine[4] slicer (Ultimaker, Netherlands) with the following printing parameters: 0.2 mm layer height, 0.8 mm wall thickness, 33% filling (selected empirically), 50 mm/s speed, 210°C nozzle temperature, 50°C platform temperature, forced model blowing, 5 mm retract, and 100% filament flow. The printing was performed on an Ender-3 3D printer (Creality3D, China) with 0.4 mm nozzle diameter using the BFCopper PLA plastic (Best Filament, Russia) containing copper particles to simulate the X-ray density of bone tissue (average X-ray density of plastic at 100% filling was +1762 HU, σ = 172 HU).

The resulting products were scanned using a 128-slice Ingenuity CT scanner (Philips, the Netherlands) in the air with channels oriented perpendicular to the gentry plane. The X-ray tube voltage, current, slice thickness, and pixel size of the reconstructed slices were 120 kV, 117 mA, 0.625 mm, and 0.43 × 0.43 mm, respectively.

Series of tomographic images in Digital Imaging and Communication in Medicine (DICOM) format were loaded into 3D Slicer[5] software (3D Slicer Community, US). The images were used to create STL models of reference 1: four by automatic voxel selection with the threshold values of +500 HU, 0 HU, –500 HU, and –750 HU, respectively (Threshold Paint tool), and one by manual slice voxel tracing (Paint tool). In addition, one model of reference 2 was created by automatic selection of voxels with values > –500 HU. The threshold values for reference 1 were selected empirically based on the X-ray density values in the outer layer of the model (approximately 0.9 mm thick) as –1000...+500 HU (–1000 HU was replaced with –750 HU to exclude the ambient air from the model). Low parameters (–500 HU and –750 HU) were deliberately chosen due to the pronounced defects when using positive values of the segmentation threshold. The density threshold for reference 2 was randomly selected from the thresholds used for reference 1.

The resulting models were loaded into the Meshmixer[6] program (Autodesk, USA), where polygonization errors were analyzed and corrected, structures not in contact with the outer shell of the models were removed, and the model mesh was rebuilt with a fixed polygon edge length (Remesh-Target Edge Length tool) equal to 0.25 mm. The appearance of the model at each of the listed stages is shown in Fig. 2.

At the final stage, the models obtained from CT data, together with their references, were loaded in pairs into

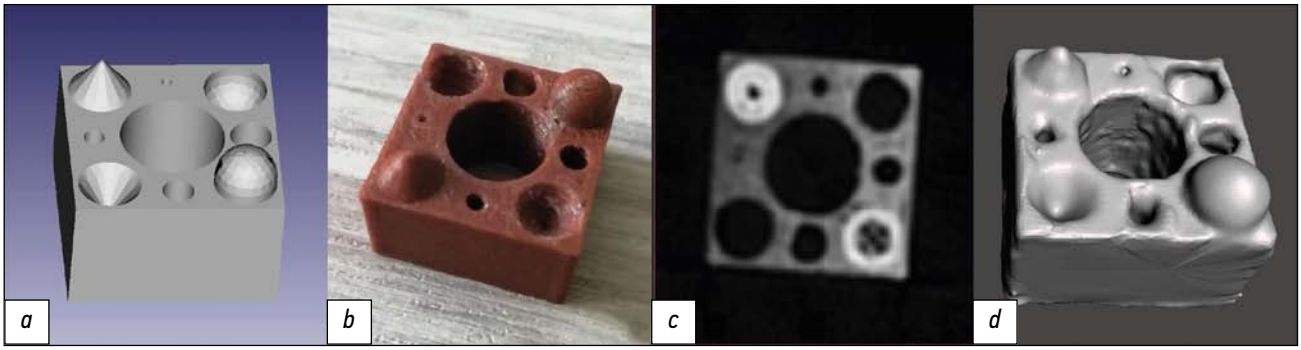

Fig. 2. The appearance of the reference model 1 after the following stages: *a*, parametric modeling; *b*, 3D-printing; *c*, CT scanning (axial slice, +805 HU window level, and 3718 HU window width; greater density of protrusions due to closer filament stacking in the horizontal plane), and *d*, creating a polygonal mesh based on CT data.
CT: computed tomography.

[1] FreeCAD Your own 3D parametric modeler. Available at https://www.freecadweb.org/. Accessed on 05/15/2021.
[2] Blender 2.93.2 LTS. Available at https://www.blender.org/. Accessed on 05/15/2021.
[3] Repetier. Available at https://www.repetier.com/. Accessed on 05/15/2021.
[4] Ultimaker Cura. Available at https://ultimaker.com/software/ultimaker-cura/. Accessed on 05/15/2021.
[5] 3D Slicer image computing platform. Available at https://www.slicer.org/. Accessed on 05/15/2021.
[6] Autodesk Meshmixer free software for making awesome stuff. Available at https://www.meshmixer.com/. Accessed on 05/15/2021.

CloudCompare[7] software (CloudCompare Project, France), where linear deviations of the final CAD model were calculated based on the iterative closest point (ICP) algorithm. The calculation was performed from each vertex of the obtained polygonal mesh along the normal to the nearest surface of the reference. Statistical analysis was performed using the GNU PSPP[8] program (Free Software Foundation, US).

RESULTS

Model volumes were determined for a preliminary assessment of their shape distortion. Particularly, if the volume of the rebuilt polygonal mesh was less/more compared to that of the reference CAD model, the linear dimensions of the analyzed model were expected to decrease/increase. In the case of equal volumes, either a size match or a compensated distortion was expected. The volumes of references and models obtained by different methods of segmentation are shown in Table 1.

Polygonal meshes processed with the Remesh tool have an approximately equal density of polygonal vertices distribution per surface unit. When comparing the models (combining cuboidal vertices) with the references, the resulting data set was the number of polygonal mesh nodes removed from the surface of the CAD model at a certain distance (mm) in the outer (positive values) or inner (negative values) directions. An example of aligning the model and the resulting histogram of surface point deviation is shown in Fig. 3. The additional peak in the region of positive values is due to the anisotropy of the voxels along the Z-axis, as well as a slightly excessive material application on the side faces of the cuboid.

Obtained values of distorted geometric dimensions for each model are summarized in Table 2.

Table 1. Volumes of virtual models

Model name, cuboid dimensions, mm (segmentation type and threshold)	Volume, mm^3	Differences with the reference, mm^3
Reference 1	3576	-
20×20×12 (auto +500)	3607	31 (0,9%)
20×20×12 (auto 0)	3901	325 (9,1%)
20×20×12 (auto -500)	4255	679 (19%)
20×20×12 (auto -750)	4480	904 (25,3%)
20×20×12 (manual)	4538	962 (26,9%)
Reference 2	28 608	-
40×40×24 (auto -500)	31 140	2532 (8,9%)

The number of measurements performed by the program corresponded to the number of vertices of the polygonal mesh (approximately 100 thousand), and the distribution of deviations of linear dimensions were close to normal. Based on obtained values, the program built a Gaussian (real Gaussian function), with the argument of maximization, which was used as the average deviation of linear dimensions of this model. All linear deviations calculated by the program were divided by their values into intervals of equal width (classes) to build a histogram. For each model, the value of the integral sum (hereinafter—Sum) of linear model deviations was calculated as follows:

$$\text{Sum} = \sum_{i=1}^{n} (d_i \times q_i), \quad (1)$$

Where d_i is the minimum value of the linear deviation in the i-th class; q_i is the number of representatives in the i-th class; and n is the total number of classes.

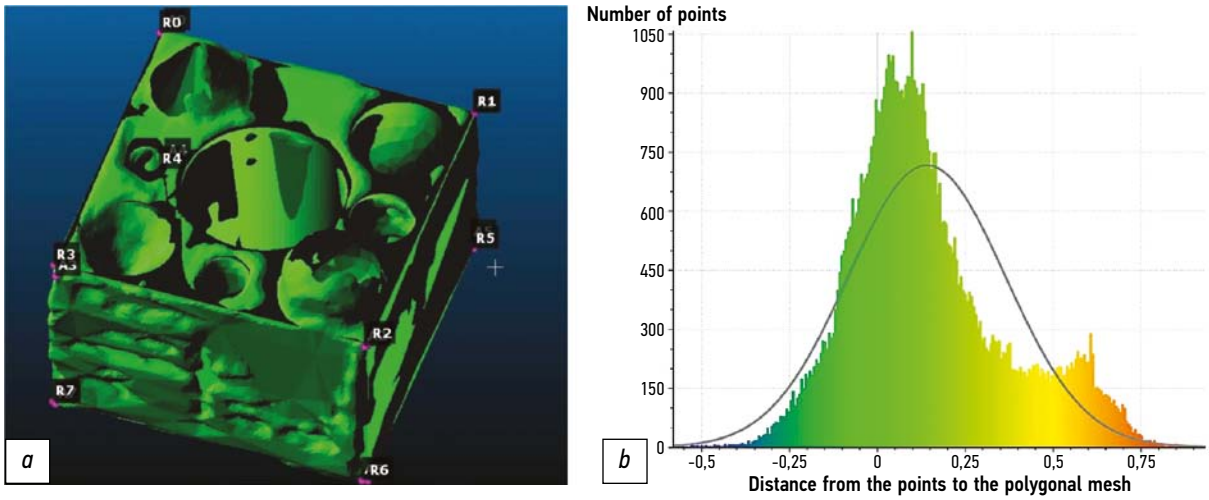

Fig. 3. Alignment of polygonal meshes of models (*a*) and a histogram of the calculated deviations of linear dimensions (*b*).

[7] CloudCompare: 3D point cloud and mesh processing software. Open Source Project. Available at http://www.cloudcompare.org/. Accessed on 05/15/2021.

[8] GNU PSPP. Available at https://www.gnu.org/software/pspp/. Accessed on 05/15/2021.

Table 2. Linear deviations of model dimensions

Model name	Minimum value, mm	Maximum value, mm	Average value, mm	Standard deviation, mm	Integral sum, mm
20×20×12 (auto +500)	-0,58	1,146	0,026	0,214	1904
20×20×12 (auto 0)	-0,533	1,019	0,141	0,223	9532
20×20×12 (auto -500)	-0,421	1,129	0,296	0,211	20 756
20×20×12 (auto -750)	-0,675	1,107	0,373	0,197	27 179
20×20×12 (manual)	-0,809	1,068	0,411	0,253	18 190
40×40×24 (auto -500)	-0,862	1,353	0,37	0,275	50 213

Linear normalization by formula (2) was applied to each of the values (sum and volume change) for their bringing to a dimensionless form.

$$\tilde{x}_i = \frac{x_i - x_{i,\,min}}{x_{i,\,max} - x_{i,\,min}}. \quad (2)$$

The linearly normalized sum values were compared with the volume change indices of the corresponding models to check the shape distortion direction (Fig. 4).

A comparison of the sums of linear deviations and relative changes in the model volumes using Spearman's rank correlation coefficient showed a high level of correlation (ρ = 0.83, t_{emp} = 5.27, and p = 0.05). Therefore, the change in the reproduced model volume corresponds to the linear deviations measured by the used software tools.

DISCUSSION

The process of creating a medical prototype includes three main stages: data aquisition (scanning), data processing (creating a virtual model), and 3D printing [13].

The first stage is a radiological examination, which obtains data on the 3D structure of the region of interest with a high spatial resolution (CT or magnetic resonance imaging or 3D ultrasound scanning), results of which are saved as discretized images in DICOM format. The change in geometry at this stage may be due to the specifics of obtaining and processing diagnostic information by the selected imaging method.

The second stage involves segmentation (selecting voxels of medical images related to the created model), voxel mesh into a polygonal mesh conversion, and resulting 3D model editing. Segmentation may be of three types: manual (fully performed by the operator), semiautomatic (performed by the computer and corrected by the operator), and automatic (fully performed by the computer) [14]. Automated methods are more attractive due to lower labor costs; however, because of characteristics of used computer algorithms, the geometry of the final product may be severely distorted, and their accuracy requires a separate study [15]. At this stage,

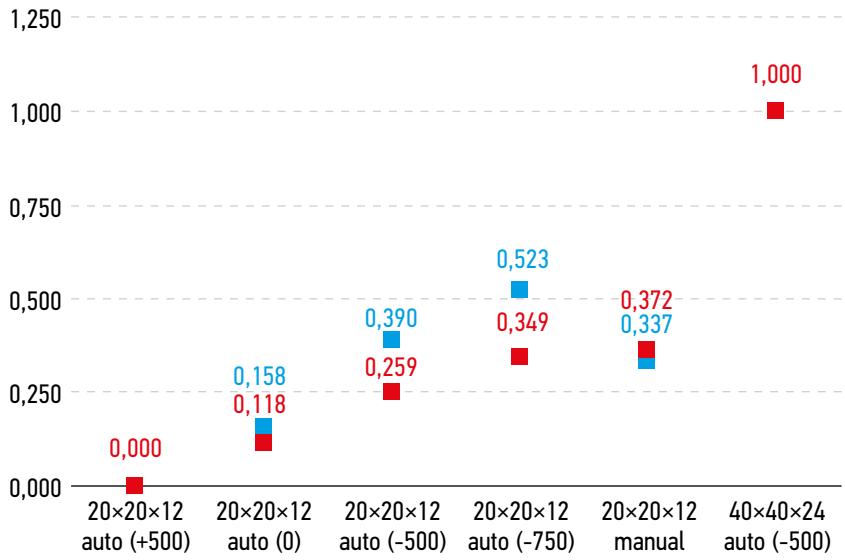

Fig. 4. Linear normalized values. Red color: differences in the volume of models with the reference; blue color: differences in the integral sum of linear deviations.

a specialist with knowledge in anatomy (particularly, radiological anatomy) should be involved to correctly select and edit the objects of interest. Thus, geometry distortion at this stage mainly results from the human factor.

The third stage is the 3D printing of the resulting virtual model. For its successful implementation, the model is pre-processed (slicing) and post-processed (removal of supports and surface handling) after printing (if necessary). The contribution of this stage to the distortion of the final product geometry primarily depends on the type of used additive equipment.

Therefore, to assess geometric distortions in the prototyping process, all three stages must be performed on some physical phantom with known linear dimensions and defined design elements. Scanning conditions and printing settings may affect the accuracy of the resulting product [10, 16]. Thus, the relevant parameters were kept at the same level for all produced models.

Many different software packages can be used to segment medical images. The use of 3D Slicer at the stage of virtual model creation from the DICOM data was due to its accessibility (distributed as open-source software) and a large number of additional modules and extensions that make it an ideal tool for preoperative planning [17].

The results confirm the "dumbbell" effect described earlier, according to which a decreased automatic segmentation threshold leads to an expansion of resulting model outlines [8]. Thus, when the threshold was decreased from +500 to –750 HU, the average value of the surface point displacement from the reference consistently increased from 0.026 to 0.373 mm, respectively. These distortions depend more on the segmentation method compared to the size of the scanned object, since the average linear deviations were 24% higher in all dimensions when the model was proportionally doubled compared to the original size models with the same threshold, and 10% lower as opposed to the original size of manually segmented models.

The relatively high values of geometric deviations in the manually segmented model (by 0.41 mm for a 20 × 20 mm sample) may result from the operator's aligning the side faces of the cuboid along the edges, which were somewhat displaced outward (during 3D printing). Moreover, similar deviations were observed during semiautomatic segmentation. Remarkably, these models reproduced the original shape better due to the preservation of all control elements and the absence of wall defects (Fig. 5).

The visual assessment of models that are automatically segmented with a threshold of 0 and +500 HU observed

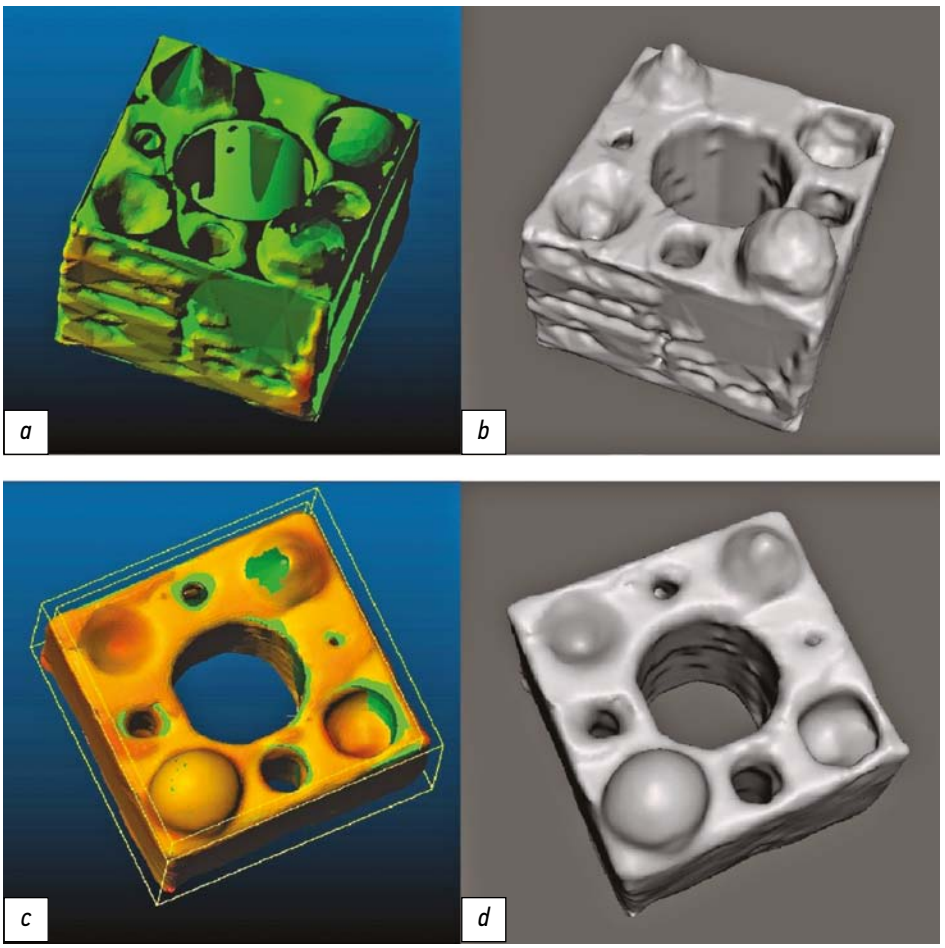

Fig. 5. The appearance of models segmented semi-automatically with a cutoff threshold of 0 HU (*a*, using a map of deviations from the reference; *b*, general view) and manually (*c*, using a map of deviations from the reference; *d*, general view).

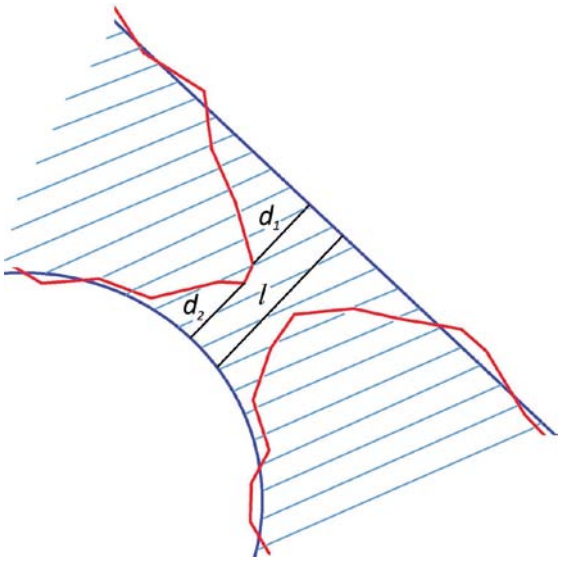

Fig. 6. Measurement of the linear deviations from the reference (blue lines) in the defect area of the compared model (red lines).

1.2 mm thick wall defects, whereas models with –750, –500, and 0 HU thresholds lacked created end-to-end holes with a diameter of 1 mm. The defects with a width exceeding the module of minimum geometry deviations are explained by the thickness measurements performed from two surfaces, each with appropriate deviations (Fig. 6). Thus, the linear displacement summation of the vertex relative to the outer surface (d_1 segment) with the nearby vertex displacement relative to the inner surface (d_2 segment) may correspond to a wall defect of l thickness exceeding the maximum linear deviation value. Similarly, the positive deviation summation leads to the "obliteration" of holes that exceed the maximum size deviation calculated from the ICP algorithm results. Thus, the linear dimensions of the reproduced models include two values of linear displacement.

In addition, channels with a diameter of 1 mm, which were not detected on the mentioned copies during the visual assessment, were not evaluated by the algorithm since the polygonal vertices corresponding to these channels were absent on the models.

Study limitations

The limitations of this study could be the relatively small sample size and the use of materials that did not correspond to the true bone tissue composition.

CONCLUSIONS

Distortion of the original shape inevitably occurs in the creation of a product using medical prototyping (CT scanning, 3D modeling, and 3D printing). The change in the model volumes and the average linear deviations of their surface points from the reference, determined using the ICP algorithm, have positive values. The distortion depends more on the selected segmentation method compared to the overall scale of the model or its parts. The use of the manual segmentation compared to the semiautomatic method leads to a slightly higher distortion of linear dimensions resulting from aligning the model to the unreliable landmarks; however, it reproduces all elements of the original sample. Thus, for necessary visualized anatomical structure preservation, the resulting virtual models should be corrected by a specialist. In this case, the use of different thresholds in areas with dense and sparse structures may be sufficient for segmentation. Using the semiautomatic segmentation is more preferable if several small structures can be neglected and the main task is to match the overall product dimensions to the simulated organ; however, the thresholds of this method should be selected experimentally depending on the tissue composition and scanning parameters.

ADDITIONAL INFORMATION

Funding source. The authors declare that there is no external funding for the exploration and analysis work.

Competing interests. The authors declare no obvious and potential conflicts of interest related to the publication of this article.

Authors' contribution. Aleksandr V. Shirshin — search for relevant publications, literature analysis, research design development, data processing, writing; Igor S. Zheleznyak — determination of the main focus of the review, expert evaluation of literature review, research design development; Vladimir N. Malakhovsky — expert evaluation of literature review, systematization and final editing of the review; Sergey V. Kushnarev — search for relevant publications, determination of research materials; Nataliya S. Gorina — literature analysis, determination of research methods. All authors made a substantial contribution to the conception of the work, acquisition, analysis, interpretation of data for the work, drafting and revising the work, final approval of the version to be published and agree to be accountable for all aspects of the work.

REFERENCES

1. Trauner KB. The emerging role of 3D printing in arthroplasty and orthopedics. *J Arthroplasty*. 2018;33(8):2352–2354. doi: 10.1016/j.arth.2018.02.033

2. Randazzo M, Pisapia JM, Singh N, Thawani JP. 3D printing in neurosurgery: a systematic review. *Surg Neurol Int.* 2016;7(Suppl 33):S801–S809. doi: 10.4103/2152-7806.194059

3. Meier LM, Meineri M, Qua Hiansen J, Horlick EM. Structural and congenital heart disease interventions: the role of three-dimensional printing. *Neth Heart J.* 2017;25(2):65–75. doi: 10.1007/s12471-016-0942-3

4. Ochoa S, Segal J, Garcia N, Fischer EA. Three-dimensional printed cardiac models for focused cardiac ultrasound instruction. *J Ultrasound Med*. 2019;38(6):1405–1409. doi: 10.1002/jum.14818

5. Takao H, Amemiya S, Shibata E, Ohtomo K. 3D printing of preoperative simulation models of a splenic artery aneurysm:

precision and accuracy. *Acad Radiol*. 2017;24(5):650–653. doi: 10.1016/j.acra.2016.12.015
6. Owen BD, Christensen GE, Reinhardt JM, Ryken TC. Rapid prototype patient-specific drill template for cervical pedicle screw placement. *Comput Aided Surg*. 2007;12(5):303–308. doi: 10.3109/10929080701662826
7. Sánchez-Sánchez Á, Girón-Vallejo Ó, Ruiz-Pruneda R, et al. Three-dimensional printed model and virtual reconstruction: an extra tool for pediatric solid tumors surgery. *European J Pediatr Surg Rep*. 2018;6(1):e70–e76. doi: 10.1055/s-0038-1672165
8. Choi JY, Choi JH, Kim NK, et al. Analysis of errors in medical rapid prototyping models. *Int J Oral Maxillofac Surg*. 2002;31(1): 23–32. doi: 10.1054/ijom.2000.0135
9. Kwun JD, Kim HJ, Park J, et al. Open wedge high tibial osteotomy using three-dimensional printed models: Experimental analysis using porcine bone. *Knee*. 2017;24(1):16–22. doi: 10.1016/j.knee.2016.09.026
10. Chung M, Radacsi N, Robert C, et al. On the optimization of low-cost FDM 3D printers for accurate replication of patient-specific abdominal aortic aneurysm geometry. Version 2. *3D Prin Med*. 2018;4(1):2. doi: 10.1186/s41205-017-0023-2
11. El-Katatny I, Masood SH, Morsi YS. Error analysis of FDM fabricated medical replicas. *Rapid Prototyp J*. 2010;16(1):36–43. doi: 10.1108/13552541011011695
12. Salmi M, Paloheimo KS, Tuomi J, et al. Accuracy of medical models made by additive manufacturing (rapid manufacturing). *J Craniomaxillofac Surg*. 2013;41(7):603–609. doi: 10.1016/j.jcms.2012.11.041
13. Mitsouras D, Liacouras P, Imanzadeh A, et al. Medical 3D printing for the radiologist. *Radiographics*. 2015;35(7):1965–1988. doi: 10.1148/rg.2015140320
14. Dionísio FC, Oliveira LS, Hernandes MA, et al. Manual and semiautomatic segmentation of bone sarcomas on MRI have high similarity. *Braz J Med Biol Res*. 2020;53(2):e8962. doi: 10.1590/1414-431x20198962
15. Parmar C, Rios Velazquez E, Leijenaar R, et al. Robust radiomics feature quantification using semiautomatic volumetric segmentation. *PLoS One*. 2014;9(7):e102107. doi: 10.1371/journal.pone.0102107
16. De Lima Moreno JJ, Liedke GS, Soler R, et al. Imaging factors impacting on accuracy and radiation dose in 3D printing. *J Maxillofac Oral Surg*. 2018;17(4):582–587. doi: 10.1007/s12663-018-1098-z
17. Narizzano M, Arnulfo G, Ricci S, et al. SEEG assistant: a 3DSlicer extension to support epilepsy surgery. *BMC Bioinformatics*. 2017;18(1):124. doi: 10.1186/s12859-017-1545-8

СПИСОК ЛИТЕРАТУРЫ

1. Trauner K.B. The emerging role of 3D printing in arthroplasty and orthopedics // Journal of Arthroplasty. 2018. Vol. 33, N 8. P. 2352–2354. doi: 10.1016/j.arth.2018.02.033
2. Randazzo M., Pisapia J.M., Singh N., Thawani J.P. 3D printing in neurosurgery: a systematic review // Surgical Neurology International. 2016. Vol. 7, Suppl. 33. P. S801–S809. doi: 10.4103/2152-7806.194059
3. Meier L.M., Meineri M., Qua Hiansen J., Horlick E.M. Structural and congenital heart disease interventions: the role of three-dimensional printing // Netherlands Heart Journal. 2017. Vol. 25, N 2. P. 65–75. doi: 10.1007/s12471-016-0942-3
4. Ochoa S., Segal J., Garcia N., Fischer E.A. Three-dimensional printed cardiac models for focused cardiac ultrasound instruction // Journal of Ultrasound in Medicine. 2019. Vol. 38, N 6. P. 1405–1409. doi: 10.1002/jum.14818
5. Takao H., Amemiya S., Shibata E., Ohtomo K. 3D printing of preoperative simulation models of a splenic artery aneurysm: precision and accuracy // Academic Radiology. 2017. Vol. 24, N 5. P. 650–653. doi: 10.1016/j.acra.2016.12.015
6. Owen B.D., Christensen G.E., Reinhardt J.M., Ryken T.C. Rapid prototype patient-specific drill template for cervical pedicle screw placement // Computer Aided Surgery. 2007. Vol. 12, N 5. P. 303–308. doi: 10.3109/10929080701662826
7. Sánchez-Sánchez Á., Girón-Vallejo Ó., Ruiz-Pruneda R., et al. Three-dimensional printed model and virtual reconstruction: an extra tool for pediatric solid tumors surgery // European Journal of Pediatric Surgery Reports. 2018. Vol. 6, N 1. P. e70–e76. doi: 10.1055/s-0038-1672165
8. Choi J.Y., Choi J.H., Kim N.K., et al. Analysis of errors in medical rapid prototyping models // International Journal of Oral and Maxillofacial Surgery. 2002. Vol. 31, N 1. P. 23–32. doi: 10.1054/ijom.2000.0135
9. Kwun J.D., Kim H.J., Park J., et al. Open wedge high tibial osteotomy using three-dimensional printed models: experimental analysis using porcine bone // Knee. 2017. Vol. 24, N 1. P. 16–22. doi: 10.1016/j.knee.2016.09.026
10. Chung M., Radacsi N., Robert C., et al. On the optimization of low-cost FDM 3D printers for accurate replication of patient-specific abdominal aortic aneurysm geometry. Version 2 // 3D Printing in Medicine. 2018. Vol. 4, N 1. P. 2. doi: 10.1186/s41205-017-0023-2
11. El-Katatny I., Masood S.H., Morsi Y.S. Error analysis of FDM fabricated medical replicas // Rapid Prototyping Journal. 2010. Vol. 16, N 1. P. 36–43. doi: 10.1108/13552541011011695
12. Salmi M., Paloheimo K.S., Tuomi J., et al. Accuracy of medical models made by additive manufacturing (rapid manufacturing) // Journal of Craniomaxillofacial Surgery. 2013. Vol. 41, N 7. P. 603–609. doi: 10.1016/j.jcms.2012.11.041
13. Mitsouras D., Liacouras P., Imanzadeh A., et al. Medical 3D printing for the radiologist // Radiographics. 2015. Vol. 35, N 7. P. 1965–1988. doi: 10.1148/rg.2015140320
14. Dionísio F.C., Oliveira L.S., Hernandes M.A., et al. Manual and semiautomatic segmentation of bone sarcomas on MRI have high similarity // Brazilian Journal of Medical and Biological Research. 2020. Vol. 53, N 2. P. e8962. doi: 10.1590/1414-431x20198962
15. Parmar C., Rios Velazquez E., Leijenaar R., et al. Robust radiomics feature quantification using semiautomatic volumetric segmentation // PLoS One. 2014. Vol. 9, N 7. P. e102107. doi: 10.1371/journal.pone.0102107
16. De Lima Moreno J.J., Liedke G.S., Soler R., et al. Imaging factors impacting on accuracy and radiation dose in 3D printing // Journal of Maxillofacial and Oral Surgery. 2018. Vol. 17, N 4. P. 582–587. doi: 10.1007/s12663-018-1098-z
17. Narizzano M., Arnulfo G., Ricci S., et al. SEEG assistant: a 3DSlicer extension to support epilepsy surgery // BMC Bioinformatics. 2017. Vol. 18, N 1. P. 124. doi: 10.1186/s12859-017-1545-8

AUTHORS' INFO

*** Aleksandr V. Shirshin**;
address: 6G, Akademika Lebedeva street, Saint-Petersburg, 194044, Russia; ORCID: https://orcid.org/0000-0002-1494-9626; eLibrary SPIN: 4412-0498; e-mail: asmdot@gmail.com

Igor S. Zheleznyak, MD, Dr. Sci. (Med.), Assistant Professor; ORCID: https://orcid.org/0000-0001-7383-512X; eLibrary SPIN: 1450-5053; e-mail: igzh@bk.ru

Vladimir N. Malakhovsky, MD, Dr. Sci. (Med.), Professor, Assistant Lecturer; ORCID: https://orcid.org/0000-0002-0663-9345; eLibrary SPIN: 2014-6335; e-mail: malakhovskyvova@gmail.com

Sergey V. Kushnarev, MD, Cand. Sci. (Med.); ORCID: https://orcid.org/0000-0003-2841-2990; eLibrary SPIN: 5859-0480; e-mail: s.v.kushnarev@yandex.ru

Nataliya S. Gorina; ORCID: https://orcid.org/0000-0002-6220-8195; eLibrary SPIN: 8175-6746; e-mail: natali_bgmu@mail.ru

ОБ АВТОРАХ

*** Ширшин Александр Вадимович**;
адрес: Россия, 194044, Санкт-Петербург, ул. Академика Лебедева, д. 6Ж; ORCID: https://orcid.org/0000-0002-1494-9626; eLibrary SPIN: 4412-0498; e-mail: asmdot@gmail.com

Железняк Игорь Сергеевич, д.м.н., доцент; ORCID: https://orcid.org/0000-0001-7383-512X; eLibrary SPIN: 1450-5053; e-mail: igzh@bk.ru

Малаховский Владимир Николаевич, д.м.н., профессор, ассистент кафедры; ORCID: https://orcid.org/0000-0002-0663-9345; eLibrary SPIN: 2014-6335; e-mail: malakhovskyvova@gmail.com

Кушнарев Сергей Владимирович, к.м.н.; ORCID: https://orcid.org/0000-0003-2841-2990; eLibrary SPIN: 5859-0480; e-mail: s.v.kushnarev@yandex.ru

Горина Наталья Сергеевна; ORCID: https://orcid.org/0000-0002-6220-8195; eLibrary SPIN: 8175-6746; e-mail: natali_bgmu@mail.ru

* Corresponding author / Автор, ответственный за переписку

DOI: https://doi.org/10.17816/DD77311

Объективные критерии МРТ-оценки эффективности лечения метастазов в кости у больных раком предстательной железы и раком молочной железы: систематический обзор и метаанализ

В.О. Рипп, Т.П. Березовская, С.А. Иванов

Медицинский радиологический научный центр имени А.Ф. Цыба — филиал федерального государственного бюджетного учреждения «Национальный медицинский исследовательский центр радиологии» Министерства здравоохранения Российской Федерации, Обнинск, Российская Федерация

АННОТАЦИЯ

Обоснование. Возможность персонифицированного подхода к лечению метастатического рака предстательной железы (РПЖ) и рака молочной железы (РМЖ) требует объективных методов оценки ответа на лечение очагов в скелете. Доказанная высокая эффективность МРТ в выявлении метастазов в кости в сочетании с отсутствием ионизирующего излучения создаёт предпосылки для использования метода в мониторировании хода лечения на основе объективных критериев оценки терапевтического эффекта.

Цель — оценить возможности объективных количественных и полуколичественных МРТ-критериев в определении эффективности лечения (радио-, химио-, гормоно- и таргетная терапия) метастазов в кости, применявшихся в клинических исследованиях у больных РПЖ и РМЖ.

Материалы и методы. Поиск в базах данных Embase, PubMed, Cochrane Central Register of Controlled trials (CENTRAL), eLibrary осуществлялся до 01.06.2021 по ключевым словам «magnetic resonance imaging», «MRI», «DWI», «treatment response», «prostate cancer», «breast cancer», «bone metastasis» на английском и русском языках. В обзор включали только исследования по объективной МРТ-оценке эффективности любого типа лечебного воздействия (за исключением хирургии) при метастатическом поражении скелета.

Результаты. На основании анализа 11 исследований, отобранных из 312 источников, выделены 4 группы объективных МРТ-критериев оценки терапевтического эффекта при метастатическом поражении костей у больных РПЖ и РМЖ, включающих динамику размеров, интенсивности сигнала на диффузионно-взвешенном изображении, числовых значений измеряемого коэффициента диффузии (ИКД), общей опухолевой нагрузки. Изменения этих количественных и полуколичественных показателей во всех работах, за единственным исключением, имели одинаковую направленность, хотя и различались числовыми значениями. Учитывая статистически значимую гетерогенность (p <0,1 для критерия x^2 и при I^2 >40%) для значений ИКД до и после лечения, для анализа использовалась модель случайных эффектов. Изменение ИКД в результате лечения в среднем составило +0,35 [+0,12; +0,49] $\times 10^{-3}$ мм^2/с со средними значениями ИКД до лечения 0,83 [0,71; 1,03] $\times 10^{-3}$ мм^2/с, после лечения — 1,18 [0,83; 1,49] $\times 10^{-3}$ мм^2/с.

Заключение. МРТ является информативной методикой для объективной оценки ответа костных метастазов на терапию у больных РПЖ и РМЖ на основе количественных и полуколичественных критериев и имеет значительный потенциал в качестве диагностического инструмента для мониторирования эффективности лечения метастатического поражения скелета.

Ключевые слова: магнитно-резонансная томография; метастазы в кости; ответ на лечение; метастатический рак молочной железы; метастатический рак предстательной железы.

Как цитировать

Рипп В.О., Березовская Т.П., Иванов С.А. Объективные критерии МРТ-оценки эффективности лечения метастазов в кости у больных раком предстательной железы и раком молочной железы: систематический обзор и метаанализ // *Digital Diagnostics.* 2021. Т. 2, № 3. С. 289–300. DOI: https://doi.org/10.17816/DD77311

Рукопись получена: 03.08.2021 **Рукопись одобрена:** 02.09.2021 **Опубликована:** 22.09.2021

ЭКО•ВЕКТОР

DOI: https://doi.org/10.17816/DD77311

Objective criteria for MRI evaluation of the effectiveness of treatment of bone metastases in patients with prostate cancer and breast cancer: systematic review and meta-analysis

Vladislav O. Ripp, Tatiana P. Berezovskaya, Sergey A. Ivanov

A. Tsyb Medical Radiological Research Center — branch of the National Medical Research Radiological Center of the Ministry of Health of the Russian Federation, Obninsk, Russian Federation

ABSTRACT

BACKGROUND: The possibility of a personalized approach to the treatment of metastatic prostate cancer and breast cancer requires objective methods for the evaluation of the response of foci treatment in the skeleton. The proven high efficiency of MRI in detecting bone metastases, in combination with the absence of ionizing radiation, has laid the groundwork for using this method in monitoring the treatment course based on objective criteria for evaluation of the therapeutic outcome.

AIM: To assess the possibilities of quantitative and semi-quantitative parameters of MRI-evaluation of treatment efficacy (radiation, chemotherapy, hormone therapy, and targeted therapy) of bone metastases that were used in prostate and breast cancer clinical trials.

MATERIALS AND METHODS: We searched the databases Embase, PubMed, Cochrane Central Register of Controlled Trials (CENTRAL), eLibrary until April 1, 2021, using the following keywords: magnetic resonance imaging, MRI, DWI, treatment response, prostate or breast cancer, and bone metastasis. We only included studies related to the MRI-evaluation of treatment efficacy of any type of therapeutic intervention (with the exception of surgery) for metastatic skeletal lesions in this review.

RESULTS: We selected and analyzed 11 out of 312 sources found as a result of the search. It allowed us to identify four groups of objective MRI criteria for evaluating the therapeutic effect in metastatic bone lesions in patients with prostate and breast cancer, including the dynamics of sizes, signal intensity on DWI, ADC, and tumor total diffusion volume (tDV). Changes in these quantitative and semi-quantitative indicators, with only one exception, had the same direction, although they differed in numerical values. A random-effects model was used for analysis considering the presence of statistically significant heterogeneity (p <0,1 for x^2 test; I^2 >40%),. The change in ADC as a result of treatment averaged +0.35 [+0.12; +0.49] $\times 10^{-3}$ mm^2/s, with average values of ADC before treatment — 0.83 [0.71; 1.03] $\times 10^{-3}$ mm^2/s, after treatment — 1.18 [0.83; 1.49] $\times 10^{-3}$ mm^2/s.

CONCLUSION: MRI is an informative technique for the objective evaluation of the response of bone metastases to therapy in patients with prostate cancer and breast cancer based on quantitative and semi-quantitative parameters. It has significant potential as a diagnostic test instrument for monitoring the effectiveness of treatment of metastatic skeletal lesions.

Keywords: magnetic resonance imaging; bone metastasis; treatment response; metastatic breast cancer; metastatic prostate cancer.

To cite this article

Ripp VO, Berezovskaya TP, Ivanov SA. Objective criteria for MRI evaluation of the effectiveness of treatment of bone metastases in patients with prostate cancer and breast cancer: systematic review and meta-analysis. *Digital Diagnostics.* 2021;2(3):289–300. DOI: https://doi.org/10.17816/DD77311

Received: 03.08.2021 **Accepted:** 02.09.2021 **Published:** 22.09.2021

DOI: https://doi.org/10.17816/DD77311

MRT评估前列腺癌和乳腺癌骨骨治疗骨转移有效性的客观标准：系统评论和核心分析

Vladislav O. Ripp, Tatiana P. Berezovskaya, Sergey A. Ivanov

A. Tsyb Medical Radiological Research Center — branch of the National Medical Research Radiological Center of the Ministry of Health of the Russian Federation, Obninsk, Russian Federation

简评

论证转移性前列腺癌（PC）和乳腺癌（BC）的个体化治疗需要客观的方法来评估对骨骼病灶治疗的反应。经过验证的高效MRT在骨骼中鉴定与没有电离辐射的组合的鉴定产生的前提是使用该方法在监测基于评估治疗效果的客观标准治疗治疗方法时的先决条件。

目标是估计客观定量和半定量MRT标准的可能性，用于确定患有PC和BC患者的临床研究中使用的骨骼中的治疗的有效性（无线电，化学 – 激素和靶向治疗）。

材料与方法Embase，PubMed数据库，Cochrane Central寄存器（中央），Elibrary通过关键词“磁共振成像”，“MRI”，“DWI”，“治疗反应”，“前列腺”癌症“，”乳腺癌“，英语和俄语”骨转移“。 概述仅包括在骨架的转移病变期间对任何类型治疗效果（外科除外）有效性的客观MRT评估的研究。

结果。根据分析选自312次来源的11项研究，4组客观MRI标准，用于估算PC和BC患者骨骼的转移损伤期间的治疗效果，包括尺寸的动态；扩散加权图像上的信号强度；测量扩散系数（MDC）的数值；总肿瘤载荷。 所有作品中，这些定量和半定量指标的变化在唯一的例外，虽然它们具有相同的焦点，但它们的数值不同。 鉴于治疗前后的ICD值的统计学上显着的异质性（p 〈0,1 对于 x 2标准和I2〉 40％）进行治疗前后的MDC值，用于分析随机效应的模型。 治疗导致的 CDI 变化平均为 +0.35 [+0.12; +0.49] × 10^{-3} 平方毫米/秒治疗前平均 ADC 值 0.83 [0.71; 1.03] × 10^{-3}平方毫米/秒，处理后 – 1.18 [0.83; 1.49] × 10^{-3} 平方毫米/秒。

结论MRI 是一种基于定量和半定量标准客观评估前列腺癌和乳腺癌患者骨转移对治疗反应的信息技术，具有作为监测转移性骨骼病变治疗效果的诊断工具的巨大潜力。

关键词：磁共振成像； 骨转移；对治疗的反应； 转移性乳腺癌；转移性前列腺癌。

引用本文

Ripp VO, Berezovskaya TP, Ivanov SA. MRT评估前列腺癌和乳腺癌骨骨治疗骨转移有效性的客观标准：系统评论和核心分析. *Digital Diagnostics*. 2021;2(3):289–300. DOI: https://doi.org/10.17816/DD77311

收到： 03.08.2021 **接受：** 02.09.2021 **发布日期：**22.09.2021

Abbreviations

HT — hormone therapy
DWI — diffusion-weighted imaging
ADC — apparent diffusion coefficient
SI — signal intensity
MRI — magnetic resonance imaging
PET-CT — positron emission tomography combined with computed tomography
BC — breast cancer
PC — prostate cancer
RT — radiotherapy
T1-WI — T1- weighted image
TT — targeted therapy
CT — chemotherapy
tDV — tumor total diffusion volume

INTRODUCTION

Metastatic skeletal lesions are common in disseminated prostate cancer (PC) and breast cancer (BC) and are found in 70%–80% of autopsies, sometimes the only localized distant metastases. In over 50% of patients, distant metastases begin with bone lesions [1–3].

Bone metastases lead to deterioration in the physical, functional, and emotional state of patients as well as a shortening in life expectancy. Although oligometastatic lesions can possibly be treated through radical therapy, the prognosis is much worse in disseminated lesions, with treatment becomes palliative (aimed at improving the overall quality of life of patients). Advancements in chemotherapy, hormone therapy and aggressive multimodal therapy allow for individualization and standardization on the assessment of the achieved therapeutic effect [4, 5].

Magnetic resonance imaging (MRI) is an effective method of detecting metastatic skeletal lesions with higher sensitivity and specificity rates (90.5% and 95%, respectively) compared with scintigraphy (72.9% and 93.9%), and comparable to combined choline positron emission tomography and computed tomography ([PET-CT] 89.7% and 96%) [6–8]. The MRI potential to assess the efficiency of bone metastasis treatment has been studied long enough by using the dynamics of the MR signal size and intensity on conventional images. The advent of diffusion-weighted imaging (DWI) and whole-body MRI has led to the generation of new criteria for assessing the response to the treatment of skeletal lesions. However, no unified approach has been developed for MRI assessment of the treatment efficiency of bone metastases based on objective criteria, and data on MRI findings of the responding lesions are contradictory [9–12].

The aim was to assess the possibilities of quantitative and semi-quantitative parameters of MRI-evaluation of treatment efficacy (radiation, chemotherapy, hormone therapy, and targeted therapy) of bone metastases that were used in PC and BC clinical trials.

METHODS

This paper is written according to the PRISMA criteria (Preferred Reporting Items for Systematic Reviews and Meta-Analyses) [13].

Eligibility criteria

inclusion criteria: Eligible papers were selected according to the Population, Intervention, Comparison, Outcomes and Study principle [14]. Patients: 18 years of age or older with histologically confirmed BC or PC and metastatic bone lesions. Intervention: MRI of both individual areas and the whole body. The MRI protocol included standard anatomical pulse sequences (T1- and T2-weighted images and STIR) and/or DWI with apparent diffusion coefficient (ADC) mapping. Comparison group: None. Outcome: Bone metastases were scanned at least one week before and 1–6 months after the start of anticancer treatment; reference assessment of the treatment response was performed by comparing MRI data using laboratory diagnostic methods (blood prostate-specific antigen level), results of instrumental studies (spiral CT, skeletal scintigraphy, and PET-CT), and histological examination with assessment of therapeutic tumor pathomorphosis. Studies: Studies in which MRI was performed before and after 1–6 months from the start of anticancer treatment. No restrictions on the type of received therapy (chemical, hormonal, targeted, and radiotherapy) were used.

Non-inclusion criteria: Patients who received surgical treatment for metastatic bone lesions.

With regard to the technical MRI developments, the following studies were selected, including: DWI and ADC assessments that were published after January 1, 2010; and standard anatomic sequences that were published after January 1, 1998.

Exclusion criteria: Papers not written in Russian or English, conference abstracts, descriptions of clinical cases, and animal studies.

Sources of information

Publications were searched and selected from Embase, PubMed, Cochrane Central Register of Controlled Trials (CENTRAL), and eLibrary electronic databases. Last search was on June 01, 2021.

Search: The search was conducted among prospective and retrospective clinical studies and randomized controlled studies using the following MeSH library terms and keywords: “Magnetic resonance imaging,” “DWI,” “treatment,” “response,” “prostate cancer,” “breast cancer,” and “bone metastasis.”

DOI: https://doi.org/10.17816/DD77311

Study selection: The search and subsequent selection were conducted by two independent reviewers. Any discrepancies were resolved by the principal investigator. At the first stage, titles/proceedings/abstracts were reviewed for relevance to the review topic and the presence of necessary data. The second stage involved a full analysis of publications according to the inclusion and exclusion criteria.

Data collection: A tabular form was developed for data collection. Data was extracted by two reviewers including: title of the article, year of publication, authors, DOI, primary lesion, population, treatment, study duration, pulse sequences, reference method, MR semiotics, and ADC and signal intensity values before and after treatment.

Risk of bias: The QUADAS-2 (Quality Assessment of Diagnostic Accuracy Studies) questionnaire was used to assess the risk of bias in individual studies [15]. The texts of articles were assessed according to the following criteria: patient enrollment, studied methods, reference methods, and time intervals between the study and reference methods. Certain questions from the QUADAS-2 checklist were not employed due to lack of necessity (for example, in the papers assessing the ADC, no question related to the study interpreter's blinding was used, since the ADC is an objective assessment). Finally, a histogram was generated after analyzing each study for the risk of bias.

Statistical analysis

The method for analyzing and grouping data (random-effects or fixed-effects model) was selected according to the results of heterogeneity assessment of studies that included ADC determination, which was performed using the x^2 criterion and I^2 heterogeneity index. Heterogeneity of studies was considered significant at $p < 0.1$ for the x^2 criterion and at $I^2 > 40\%$.

RESULTS

Study selection

The present study included 11 studies from 312 sources from Embase, PubMed, CENTRAL, and eLibrary databases (Fig. 1).

At the first stage, 273 sources were selected after sorting out duplicates (31) and animal studies (8). Next, 181 publications were sorted out after assessment of proceedings and abstracts at the screening stage. After checking full-text versions of the papers for inclusion criteria, 11 sources were remained and included in this review (Table).

We included 370 patients; among these, 147 patients responded to treatment. Three sources did not provide relevant information on the number of responders [5, 16, 17]. The sample size of each of the included studies ranged from 10 to 87 patients. Seven studies included only patients with a primary lesion in the prostate or mammary gland; four studies [5, 16, 20, 21] included these localizations in 85%–95% of the entire sample. The mean age of the patients was 47–73 years.

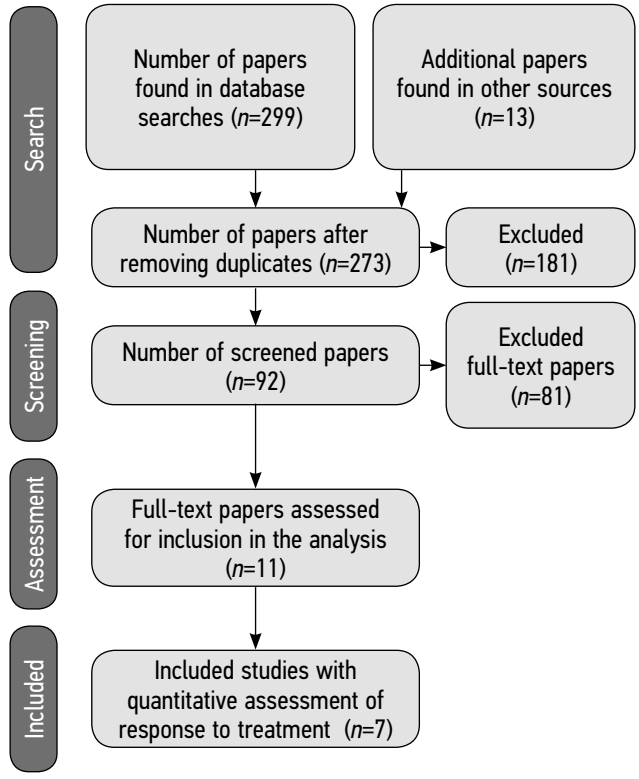

Fig. 1. PRISMA diagram of this study

The participants in the papers were divided into four groups according to the criteria which were used to assess the response to systemic therapy. These include size of metastatic lesions, DWI signal intensity, ADC, total tumor volume [5, 9–12, 16, 17, 20].

CT, skeletal scintigraphy, and prostate-specific antigen (in PC patients) were used as reference test [9–11, 16, 17, 20], whereas PET and biopsy were used in addition to these methods [5, 12]. Three papers did not contain data on the reference methods used [18, 19, 21].

Scanning parameters

The scanning parameters when using T1-SE-sequencing in different studies had slight differences in TR and TE values (400–600 ms and 5–16 ms, respectively). Only one paper had significantly different T1-WI parameters of 1000 ms and 3.7 ms. The number of b-factors was 2–3 with initial and highest values of 0–50 and 800–900, respectively [5, 10, 12, 13]. In one study [9], the number of b-factors was 4 (0, 50, 250, and 750), and in another study [20], it accounted for 6 (0, 50, 100, 250, 500, and 750), with obtaining higher ADC values compared with the other studies, which may result from changes in scanning parameters. The slice thickness in all studies was within 4–6 mm for both T1-WI and DWI images.

Classification of objective assessment criteria used in the literature

The first criterion for the therapeutic response of bone metastases was the change in the lesion size. Remarkably, bone lesions are recommended for measurements

Table. Characteristics of studies included in the systematic review and *meta-analysis*

No.	Authors	Year	Nosology	Treatment	Interval between studies	Magnetic field induction, T	MRI model and manufacturer	Objective criteria
1	Byun et al. [5]	2002	BC (90%)	RT	6 months	1.5	Not specified	ADC, SI (DWI)
2	Messiou et al. [9]	2011	PC	CT	3 months	1.5	Avanto, Siemens	ADC
3	Reischauer et al. [10]	2010	PC	HT	1–3 months	1.5	Achieva, Philips	ADC
4	Perez-Lopez et al. [11]	2016	PC	TT	3 months	1.5	Avanto, Siemens	ADC, tDV
5	Blackledge et al. [12]	2014	PC, BC	CT, HT, RT, TT	10–38 weeks	1.5	Avanto, Aera, Siemens	ADC, tDV
6	Sergeev et al. [16]	2016	BC, PC (90%)	CT, HT, RT	2–8 months	1.5	Excelart, Toshiba	ADC, SI (DWI)
7	Çiray et al. [17]	2001	BC	CT, HT	3–6 months	0.5	Gyroscan T5, Philips	Size
8	Brown et al. [18]	1998	BC	HT, CT, RT	6, 9 months	1.5	Vision, Siemens	Size
9	Tombal et al. [19]	2005	PC	CT	6 months	1.5	Intera, Philips	Size
10	Cappabianca et al. [20]	2014	PC, BC (90%)	RT	1, 2 months	1.5	Symphony, Siemens,	ADC, SI (DWI)
11	Kotlyarov et al. [21]	2006	BC, PC (75%)	CT, HT, RT	2–8 months	0.5	Proview Open, Philips	Size

Note. MRI, magnetic resonance imaging; BC, breast cancer; PC, prostate cancer; CT, chemotherapy; HT, hormone therapy; RT, radiotherapy; TT, targeted therapy; ADC, apparent diffusion coefficient; SI, signal intensity; DWI, diffusion-weighted images; tDV, tumor total diffusion volume.

on T1-WI due to higher contrast, clearer contours, and less pronounced perifocal edema [6, 22]. This criterion was used in 4 of 11 selected studies.

The second criterion for response assessment was semi-quantitative determination of DWI signal intensity, which was found in 3 of these papers. Since signal intensity is not a physical quantity, its numerical value may differ with different MRI scanners and at different scanning parameters. Therefore, the signal intensity ratio in metastases to the signal intensity in muscles was used.

The third criterion for assessing the response to treatment is the change in the numerical ADC value of the lesion. This criterion has been most widely used recently, including 7 of 11 selected papers; however, ADC values depend on imaging parameters.

The fourth and most novel criterion is the determination of the total diffusion volume (tDV), which is automatically calculated (in mL) using the maximum DWI intensity projection with a semi-automated and manually corrected 3D-mask by counting the number of voxels in a given range of signal intensities (Fig. 2). The distribution of the number of voxels over the ADC ranges, which correspond to responding, non-responding, and doubtful lesions, represented in a histogram [11, 12, 23].

Risk of bias

The risk of bias arises from differences in anticancer therapies and the time intervals between MRI before and after treatment. According to the QUADAS-2 criteria, the main point of the risk of bias was the selection of the

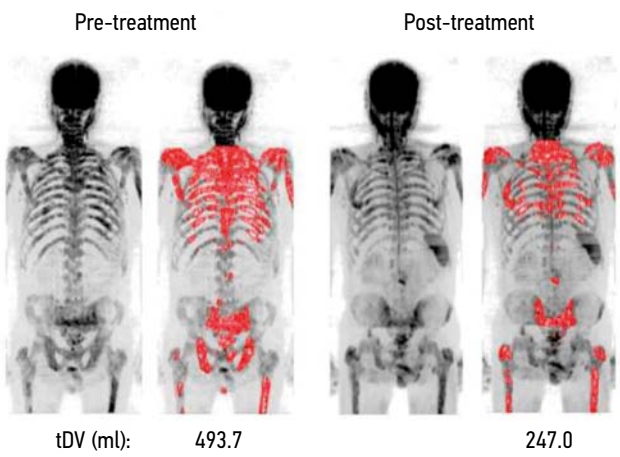

Fig. 2. Visualization and values of the total tumor volume before and after treatment in a patient with a significant response to systemic therapy

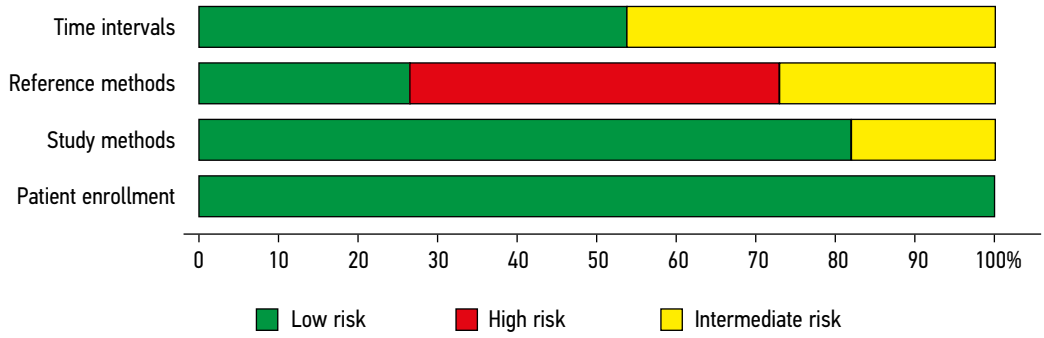

Fig. 3. Risk of bias according to QUADAS-2

reference methods (Fig. 3). Five papers used different imaging techniques for different patients as a reference [5, 12], or scintigraphy was used as a single method [16, 17, 20], which is inferior in diagnostic value to MRI and lacks the necessary values of sensitivity and specificity. The reference method was completely absent in three papers [18, 19, 21], and the assessment of the response to therapy was controlled by the level of prostate-specific antigen and clinical data. MR tomographs were used with a magnetic field intensity of 0.5 T, which might be an additional source of bias [17, 18].

Assessment results of bone lesion response to systemic therapy

Size: Changes in T1-WI size were assessed in four papers [17–19, 21]; among these, three showed a significant decrease in individual responding lesions and in tumor mass index, which was obtained as a result of sum of all metastatic lesion sizes in two dimensions. Moreover, B. Tombal et al. observed complete disappearance of metastatic lesions in two cases. However, the authors repeated the study after 6 months as opposed to a 2–3 -month follow-up in other publications. On the contrary, Brown et al. reported constant sizes in 77% as opposed to an increased size in 23% of patients with responding lesions.

DWI signal intensity: Three studies contain data on DWI signal intensity changes in bone metastases as a result of systemic therapy [5, 16, 20]. In all studies, the authors came to the unequivocal conclusion that the signal intensity decreased significantly in response to treatment. However, only one presented numerical values that indicated a 35% signal intensity reduction in lesions that responded to radiotherapy [20].

ADC: The assessment and analysis of quantitative ADC values were performed in seven papers [5, 9–12, 16, 20]. Sergeev et al. did not provide data for each patient or lesion; they demonstrated a 25% overall ADC increase in response to treatment of osteoblastic lesions and a 25% decrease in osteolytic lesions. Six papers presented accurate ADC values before and after treatment [5, 9–12, 20]. All authors noted increased ADC values in response to treatment of bone metastases, as reflected by the forest plot (Fig. 4) constructed using a random-effects model, given the presence of significant heterogeneity of the results ($p < 0.1$ for the x^2 test and $I^2 > 40\%$).

The ADC changes after treatment averaged + 0.35 [+ 0.12; + 0.49] × 10^{-3} mm^2/s. The range of baseline and post-therapy ADC values from all six papers is shown in Fig. 5 with mean ADC values before and after treatment, which accounted for 0.83 [0.71, 1.03] and 1.18 [0.83, 1.49] × 10^{-3} mm^2/s, respectively. Despite partially overlapping values, the ADC was generally higher in responding patients as compared to values before treatment.

tDV: In two studies, tDV was assessed by DWI using special software [11, 12]. Mean tDV values in responding patients decreased by 59% according to Perez-Lopez et al. [11] and by 42.3% according to Blackledge et al. [12].

DISCUSSION

This systematic review demonstrates the assessment potential in the evaluation of the response to therapy of

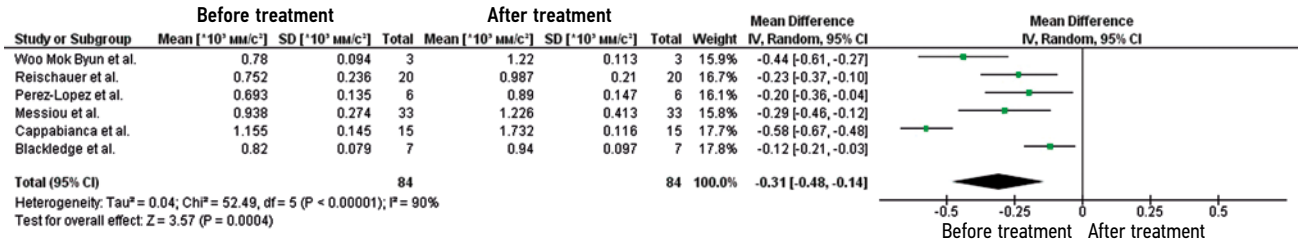

Fig. 4. Forest plot based on the results of studies that determined the changes in the apparent diffusion coefficient values in patients with bone metastases that responded to treatment

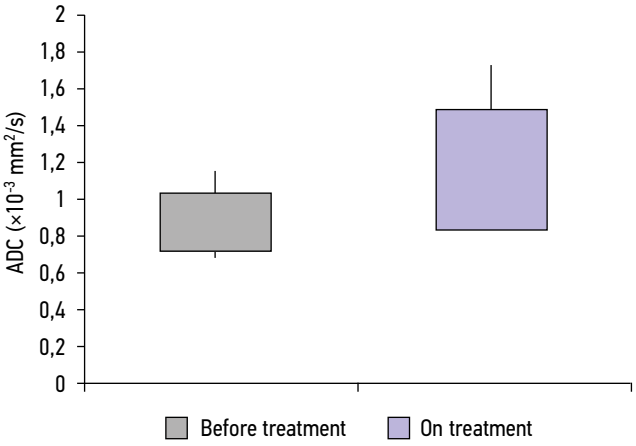

Fig. 5. Boxplot of the apparent diffusion coefficient values of bone metastases before treatment (gray) and after 1–6 months from the start of therapy (lilac), which was constructed according to the values of all included responding lesions (n = 156)

metastatic bone lesions based on the dynamics of objective criteria such as lesion size, relative DWI signal intensity, and ADC and tDV numerical values.

The relevance of this issue is due to the rapidly growing use of whole-body MRI for the primary diagnosis of bone metastases in patients with PC and BC [7, 8, 24, 25], who subsequently receive systemic therapy and radiotherapy and need to assess the treatment efficiency.

Assessment of the size of bone metastases as an objective indicator of the systemic therapy efficiency has long been used. RECIST 1.1 (Response Evaluation Criteria in Solid Tumors) criteria are most commonly used for this purpose, according to which only osteolytic and mixed lesions with a soft tissue component of at least 10 mm are considered measurable bone lesions, whereas diffuse and osteoblastic lesions are considered unmeasurable [26, 27]. Despite existing limitations, the RECIST 1.1 criteria for bone lesions are included in the MET-RADSP (METastasis Reporting and Data System for Prostate Cancer) recommendations for whole-body MRI and are used along with the ADC to assess response in metastatic PC [1, 6].

The MDA criteria were developed specifically for the bone metastasis assessment at the University of Texas MD Anderson Cancer Center to assess any type of lesions based on the dynamics of their number, size, and structural features [27]. These criteria are applicable to both radiography and computed tomography, and MRI; however, they are less common compared with RECIST 1.1.

Assessment of the dynamics of bone metastasis size on T1-WI showed a reduction in response to specific therapy [17–19, 21]. Only one study obtained data that contradicted the results of other works. Brown et al. noted an increase in responding lesions on T1-WI after 6–9 months from the start of systemic treatment [18]. In this study, all patients received systemic or local radiotherapy; of these, 17 patients received additional chemotherapy or hormone therapy. The response to therapy in these patients was assessed comprehensively using clinical, biochemical, radiological, and scintigraphic criteria. The findings might result from the treatment peculiarities that led to the formation of a pronounced and long-term persisting perifocal edema, which gives a hypointense signal on T1-WI leading to false-positive increased sizes of responding lesions according to the practical Met-RADS recommendations [6]. Thus, the dynamics of bone metastasis sizes in response to specific treatment has diagnostic value; however, the result may depend on the time of therapy, different therapeutic approaches and the nature of metastatic lesions. This indicates the necessity for supplementing this criterion with other objective data.

The dynamics of DWI signal intensity could be regarded as an objective criterion for response assessment [5, 16, 20]. The authors of all papers observed a decreased intensity of signal lesion in patients who responded to systemic therapy. However, given that numerical values are presented only in one work [20], and the nature of lesions and type of systemic therapy were not considered in all three papers, further study of the DWI signal intensity change dependence on the aforementioned conditions is necessary.

Determination of numerical ADC values has high potential as an objective assessment criterion and is one of the main ones in the Met-RADS recommendations for the whole-body MRI analysis. Data analysis from seven studies indicated a significant increase in ADC in responding patients [5, 9–12, 16, 20]. Concurrently, all the studies described single cases of ADC decrease with a good response to treatment. These cases were associated with the development of fibrosis or sclerosis in response to therapy. In addition, Messiou et al. demonstrated an increase in ADC in patients with progression; however, these values were less pronounced compared with those in responding patients. Among all seven publications, only one compared ADC values in responding patients with the lesion nature and obtained diverse changes: a 25% increase in ADC in osteoblastic lesions and a 25% decrease in osteolytic lesions [16]. Other studies did not divide lesions into osteolytic and osteoblastic types, thereby resulting in the discrepancy of ADC values in responding patients and clouding the interpretation of these results. These indicate the need for further studies with inclusion of homogeneous groups of lesions.

In studies that assessed tDV, similar results were obtained [11, 12]. They concluded that tDV decreased significantly in response to specific therapy. However, this approach has several limitations. First, these parameters were sensitive to the quality of the DWI, which may lead to tDV changes in the presence of artifacts or insufficient signal reduction by the surrounding tissues. Second, the signal above the 4^{th}–5^{th} cervical vertebrae was manually removed to eliminate a possibly false tDV increase from the brain, salivary glands, and large numbers of lymph nodes, leading to missed lesions in these areas. Third, this method is time-consuming due to a manual processing stage, thereby limiting its widespread use in clinical practice.

Thus, MRI offers a set of objective criteria allowing for the assessment of the efficiency of treating disseminated metastatic skeletal lesions in patients with PC and BC. However, additional studies are required to clarify the methodological aspects and quantitative values of the assessment criteria for different types of metastatic lesions in order to implement widely in clinical practice.

Study limitations

The results of this systematic review call for careful interpretation as we encountered some limitations, such as a small number of included studies, the retrospective nature of some studies, the lack of standardized reference methods, and different types of specific therapy, which may influence the microstructural changes and result in different MR characteristics of responding lesions.

In the reviewed studies and meta-analysis, scanning parameters slightly differ, in particular, different number and values of b-factors are used, which may affect the final ADC values.

CONCLUSIONS

MRI is an informative technique for objective assessment of the response to therapy of bone metastases in patients with PC and BC based on quantitative and semi-quantitative criteria. Currently, when assessing the treatment efficiency, the dynamics of lesion size in T1 mode and ADC values should be primarily analyzed as precise quantitative assessment criteria have not been developed yet. DWI-based parameters are the most promising; however, this does not exclude the use of traditional RECIST 1.1 and MDA criteria.

Thus, whole-body MRI is a potentially effective diagnostic tool for revealing and monitoring of metastatic skeletal lesions in patients with PC and BC.

ADDITIONAL INFORMATION

Funding source. This study was not supported by any external sources of funding.

Competing interests. The authors declare that they have no competing interests.

Authors' contribution. V.O. Ripp — search and analysis of literature, interpretation of literary data and writing of text, development of work design; T.P. Berezovskaya — development of the concept and design of the review, search and analysis of literature, text writing; S.A. Ivanov — expert assessment and final editing of the literature review. All authors made a substantial contribution to the conception of the work, acquisition, analysis, interpretation of data for the work, drafting and revising the work, final approval of the version to be published and agree to be accountable for all aspects of the work.

REFERENCES

1. Lecouvet FE, Larbi A, Pasoglou V, et al. MRI for response assessment in metastatic bone disease. *Eur Radiol*. 2013;23(7):1986–1997. doi: 10.1007/s00330-013-2792-3

2. Padhani AR, Makris A, Gall P, et al. Therapy monitoring of skeletal metastases with whole-body diffusion MRI. *J Magn Reson Imaging*. 2014;39(5):1049–1078. doi: 10.1002/jmri.24548

3. Woolf DK, Padhani AR, Makris A. Assessing response to treatment of bone metastases from breast cancer: what should be the standard of care? *Ann Oncol*. 2015;26(6):1048–1057. doi: 10.1093/annonc/mdu558

4. Padhani AR, Gogbashian A. Bony metastases: assessing response to therapy with whole-body diffusion MRI. *Cancer Imaging*. 2011;11(1A):S129–S145. doi: 10.1102/1470-7330.2011.9034

5. Byun WM, Shin SO, Chang Y, et al. Diffusion-weighted MR imaging of metastatic disease of the spine: assessment of response to therapy. *AJNR Am J Neuroradiol*. 2002;23(6):906–912.

6. Padhani AR, Lecouvet FE, Tunariu N, et al. METastasis reporting and data system for prostate cancer: practical guidelines for acquisition, interpretation, and reporting of whole-body magnetic resonance imaging-based evaluations of multiorgan involvement in advanced prostate cancer. *Eur Urol*. 2017;71(1):81–92. doi: 10.1016/j.eururo.2016.05.033

7. Zugni F, Ruju F, Pricolo P, et al. The added value of whole-body magnetic resonance imaging in the management of patients with advanced breast cancer. *PLoS One*. 2018;13(10):e0205251. doi: 10.1371/journal.pone.0205251

8. Yang HL, Liu T, Wang XM, et al. Diagnosis of bone metastases: a meta-analysis comparing ^{18}FDG PET, CT, MRI and bone scintigraphy. *Eur Radiol*. 2011;21(12):2604–2617. doi: 10.1007/s00330-011-2221-4

9. Messiou C, Collins DJ, Giles S, et al. Assessing response in bone metastases in prostate cancer with diffusion weighted MRI. *Eur Radiol*. 2011;21(10):2169–2177. doi: 10.1007/s00330-011-2173-8

10. Reischauer C, Froehlich JM, Koh DM, et al. Bone metastases from prostate cancer: assessing treatment response by using diffusion-weighted imaging and functional diffusion maps — initial observations. *Radiology*. 2010;257(2):523–531. doi: 10.1148/radiol.10092469

11. Perez-Lopez R, Mateo J, Mossop H, et al. Diffusion-weighted imaging as a treatment response biomarker for evaluating bone metastases in prostate cancer: a pilot study. *Radiology*. 2017;283(1):168–177. doi: 10.1148/radiol.2016160646

12. Blackledge MD, Collins DJ, Tunariu N, et al. Assessment of treatment response by total tumor volume and global apparent diffusion coefficient using diffusion-weighted MRI in patients with metastatic bone disease: a feasibility study. *PLoS One*. 2014;9(4):e91779. doi: 10.1371/journal.pone.0091779

13. Liberati A, Altman DG, Tetzlaff J, et al. The PRISMA statement for reporting systematic reviews and meta-analyses of studies that evaluate health care interventions: explanation and elaboration. *PLoS Med*. 2009;6(7):e1000100. doi: 10.1371/journal.pmed.1000100

14. Amir-Behghadami M, Janati A. Population, Intervention, Comparison, Outcomes and Study (PICOS) design as a framework to formulate eligibility criteria in systematic reviews. *Emerg Med J*. 2020;37(6):387. doi: 10.1136/emermed-2020-209567

15. Whiting PF. QUADAS-2: a revised tool for the quality assessment of diagnostic accuracy studies. *Ann Intern Med*. 2011;155(8): 529–536. doi: 10.7326/0003-4819-155-8-201110180-00009
16. Sergeev NI, Kotlyarov PM, Solodkii VA. Diffusion-weighted magnetic resonance imaging in the assessment of chemoradiation treatment of metastatic lesions of bone structures. *Bulletin of the Russian Scientific Center of Radiology of the Ministry of Health of the Russian Federation*. 2016;16(3):2. (In Russ).
17. Çiray I, Lindman H, Åström KGO, et al. Early response of breast cancer bone metastases to chemotherapy evaluated with mr imaging. *Acta Radiologica*. 2001;42(2):198–206. doi: 10.1080/028418501127346503
18. Brown AL, Middleton G, Macvicar AD, et al. T1-weighted magnetic resonance imaging in breast cancer vertebral metastases: Changes on treatment and correlation with response to therapy. *Clin Radiol*. 1998;53(7):493–501. doi: 10.1016/s0009-9260(98)80168-2
19. Tombal B, Rezazadeh A, Therasse P, et al. Magnetic resonance imaging of the axial skeleton enables objective measurement of tumor response on prostate cancer bone metastases. *Prostate*. 2005;65(2):178–187. doi: 10.1002/pros.20280
20. Cappabianca S, Capasso R, Urraro F, et al. Assessing response to radiation therapy treatment of bone metastases: short-term followup of radiation therapy treatment of bone metastases with diffusion-weighted magnetic resonance imaging. *J Radiotherapy*. 2014. doi: 10.1155/2014/698127
21. Kotlyarov PM, Sergeev NI, Fedina ON. MRI in the diagnosis of metastatic lesions of the skeleton and in assessing the effectiveness of treatment. *Radiology Practice*. 2006;6:10–15.
22. Lecouvet FE, Talbot JN, Messiou C, et al. Monitoring the response of bone metastases to treatment with Magnetic Resonance Imaging and nuclear medicine techniques: A review and position statement by the European Organisation for Research and Treatment of Cancer imaging group. *Eur J Cancer*. 2014;50(15):2519–2531. doi: 10.1016/j.ejca.2014.07.002
23. Grimm R, Padhani AR. Whole-body diffusion-weighted MR image analysis with syngo.via frontier MR total tumor. *Magn Flash*. 2017;68(2):73–75.
24. Jambor I, Kuisma A, Ramadan S, et al. Prospective evaluation of planar bone scintigraphy, SPECT, SPECT/CT, 18F-NaF PET/CT and whole body 1.5T MRI, including DWI, for the detection of bone metastases in high risk breast and prostate cancer patients: SKELETA clinical trial. *Acta Oncol*. 2016;55(1):59–67. doi: 10.3109/0284186X.2015.1027411
25. Heusner TA, Kuemmel S, Koeninger A, et al. Diagnostic value of diffusion-weighted magnetic resonance imaging (DWI) compared to FDG PET/CT for whole-body breast cancer staging. *Eur J Nucl Med Mol Imaging*. 2010;37(6):1077–1086. doi: 10.1007/s00259-010-1399-z
26. Eisenhauer EA, Therasse P, Bogaerts J, et al. New response evaluation criteria in solid tumours: revised RECIST guideline (version 1.1). *Eur J Cancer*. 2009;45(2):228–247. doi: 10.1016/j.ejca.2008.10.026
27. Costelloe CM, Chuang HH, Madewell JE, et al. Cancer response criteria and bone metastases: RECIST 1.1, MDA and PERCIST. *J Cancer*. 2010;1:80–92. doi: 10.7150/jca.1.80

СПИСОК ЛИТЕРАТУРЫ

1. Lecouvet F.E., Larbi A., Pasoglou V., et al. MRI for response assessment in metastatic bone disease // Eur Radiol. 2013. Vol. 23, N 7. P. 1986–1997. doi: 10.1007/s00330-013-2792-3
2. Padhani A.R., Makris A., Gall P., et al. Therapy monitoring of skeletal metastases with whole-body diffusion MRI // J Magn Reson Imaging. 2014. Vol. 39, N 5. P. 1049–1078. doi: 10.1002/jmri.24548
3. Woolf D.K., Padhani A.R., Makris A. Assessing response to treatment of bone metastases from breast cancer: what should be the standard of care? // Ann Oncol. 2015. Vol. 26, N 6. P. 1048–1057. doi: 10.1093/annonc/mdu558
4. Padhani A.R., Gogbashian A. Bony metastases: assessing response to therapy with whole-body diffusion MRI // Cancer Imaging. 2011. Vol. 11, N 1A. P. S129–S145. doi: 10.1102/1470-7330.2011.9034
5. Byun W.M., Shin S.O., Chang Y., et al. Diffusion-weighted MR imaging of metastatic disease of the spine: assessment of response to therapy // AJNR Am J Neuroradiol. 2002. Vol. 23, N 6. P. 906–912.
6. Padhani A.R., Lecouvet F.E., Tunariu N., et al. METastasis reporting and data system for prostate cancer: practical guidelines for acquisition, interpretation, and reporting of whole-body magnetic resonance imaging-based evaluations of multiorgan involvement in advanced prostate cancer // Eur Urol. 2017. Vol. 71, N 1. P. 81–92. doi: 10.1016/j.eururo.2016.05.033
7. Zugni F., Ruju F., Pricolo P., et al. The added value of whole-body magnetic resonance imaging in the management of patients with advanced breast cancer // PLoS One. 2018. Vol. 13, N 10. P. e0205251. doi: 10.1371/journal.pone.0205251
8. Yang H.L., Liu T., Wang X.M., et al. Diagnosis of bone metastases: a meta-analysis comparing ^{18}FDG PET, CT, MRI and bone scintigraphy // Eur Radiol. 2011. Vol. 21, N 12. P. 2604–2617. doi: 10.1007/s00330-011-2221-4
9. Messiou C., Collins D.J., Giles S., et al. Assessing response in bone metastases in prostate cancer with diffusion weighted MRI // Eur Radiol. 2011. Vol. 21, N 10. 2169–2177. doi: 10.1007/s00330-011-2173-8
10. Reischauer C., Froehlich J.M., Koh D.M., et al. Bone metastases from prostate cancer: assessing treatment response by using diffusion-weighted imaging and functional diffusion maps — initial observations // Radiology. 2010. Vol. 257, N 2. P. 523–531. doi: 10.1148/radiol.10092469
11. Perez-Lopez R., Mateo J., Mossop H., et al. Diffusion-weighted imaging as a treatment response biomarker for evaluating bone metastases in prostate cancer: a pilot study // Radiology. 2017. Vol. 283, N 1. P. 168–177. doi: 10.1148/radiol.2016160646
12. Blackledge M.D., Collins D.J., Tunariu N., et al. Assessment of treatment response by total tumor volume and global apparent diffusion coefficient using diffusion-weighted MRI in patients with metastatic bone disease: a feasibility study // PLoS One. 2014. Vol. 9, N 4. P. e91779. doi: 10.1371/journal.pone.0091779
13. Liberati A., Altman D.G., Tetzlaff J., et al. The PRISMA statement for reporting systematic reviews and meta-analyses of studies that evaluate health care interventions: explanation and elaboration // PLoS Med. 2009. Vol. 6, N 7. P. e1000100. doi: 10.1371/journal.pmed.1000100

14. Amir-Behghadami M., Janati A. Population, Intervention, Comparison, Outcomes and Study (PICOS) design as a framework to formulate eligibility criteria in systematic reviews // Emerg Med J. 2020. Vol. 37, N 6. P. 387. doi: 10.1136/emermed-2020-209567
15. Whiting P.F. QUADAS-2: a revised tool for the quality assessment of diagnostic accuracy studies // Ann Intern Med. 2011. Vol. 155, N 8. P. 529–536. doi: 10.7326/0003-4819-155-8-201110180-00009
16. Сергеев Н.И., Котляров П.М., Солодкий В.А. Диффузионно-взвешенная магнитно-резонансная томография в оценке химиолучевого лечения метастатического поражения костных структур // Вестник Российского научного центра рентгенорадиологии Минздрава России. 2016. Т. 16, № 3. С. 2.
17. Çiray I., Lindman H., Åström K.G., et al. early response of breast cancer bone metastases to chemotherapy evaluated with mr imaging // Acta Radiologica. 2001. Vol. 42, N 2. P. 198–206. doi: 10.1080/028418501127346503
18. Brown A.L., Middleton G., Macvicar A.D., et al. T1-weighted magnetic resonance imaging in breast cancer vertebral metastases: Changes on treatment and correlation with response to therapy // Clin Radiol. 1998. Vol. 53, N 7. P. 493–501. doi: 10.1016/s0009-9260(98)80168-2
19. Tombal B., Rezazadeh A., Therasse P., et al. Magnetic resonance imaging of the axial skeleton enables objective measurement of tumor response on prostate cancer bone metastases // Prostate. 2005. Vol. 65, N 2. P. 178–187. doi: 10.1002/pros.20280
20. Cappabianca S., Capasso R., Urraro F., et al. Assessing response to radiation therapy treatment of bone metastases: short-term followup of radiation therapy treatment of bone metastases with diffusion-weighted magnetic resonance imaging // J Radiotherapy. 2014. doi: 10.1155/2014/698127
21. Котляров П.М., Сергеев Н.И., Федина О.Н. МРТ в диагностике метастатического поражения скелета и в оценке эффективности лечения // Радиология практика. 2006. № 6. С. 10–15.
22. Lecouvet F.E., Talbot J.N., Messiou C., et al. Monitoring the response of bone metastases to treatment with Magnetic Resonance Imaging and nuclear medicine techniques: A review and position statement by the European Organisation for Research and Treatment of Cancer imaging group // Eur J Cancer. 2014. Vol. 50, N 15. P. 2519–2531. doi: 10.1016/j.ejca.2014.07.002
23. Grimm R., Padhani A.R. Whole-body diffusion-weighted MR image analysis with syngo.via frontier MR total tumor // Magn Flash. 2017. Vol. 68, N 2. P. 73–75.
24. Jambor I., Kuisma A., Ramadan S., et al. Prospective evaluation of planar bone scintigraphy, SPECT, SPECT/CT, 18F-NaF PET/CT and whole body 1.5T MRI, including DWI, for the detection of bone metastases in high risk breast and prostate cancer patients: SKELETA clinical trial // Acta Oncol. 2016. Vol. 55, N 1. P. 59–67. doi: 10.3109/0284186X.2015.1027411
25. Heusner T.A., Kuemmel S., Koeninger A., et al. Diagnostic value of diffusion-weighted magnetic resonance imaging (DWI) compared to FDG PET/CT for whole-body breast cancer staging // Eur J Nucl Med Mol Imaging. 2010. Vol. 37, N 6. P. 1077–1086. doi: 10.1007/s00259-010-1399-z
26. Eisenhauer E.A., Therasse P., Bogaerts J., et al. New response evaluation criteria in solid tumours: revised RECIST guideline (version 1.1) // Eur J Cancer. 2009. Vol. 45, N 2. P. 228–247. doi: 10.1016/j.ejca.2008.10.026
27. Costelloe C.M., Chuang H.H., Madewell J.E., et al. Cancer response criteria and bone metastases: RECIST 1.1, MDA and PERCIST // J Cancer. 2010. Vol. 1. P. 80–92. doi: 10.7150/jca.1.80

AUTHORS' INFO

*** Vladislav O. Ripp**, MD;
address: 4 Korolev street, Obninsk, 249036, Russia;
ORCID: https://orcid.org/0000-0001-8970-4212;
e-mail: rippnba@gmail.com

Tatiana P. Berezovskaya, MD, Senior Research Associate, Dr. Sci. (Med.), Professor;
ORCID: https://orcid.org/0000-0002-3549-4499

Sergey A. Ivanov, MD, Dr. Sci. (Med.), Professor;
ORCID: https://orcid.org/0000-0001-7689-6032;
eLibrary SPIN: 4264-5167

ОБ АВТОРАХ

*** Рипп Владислав Олегович**;
адрес: Россия, 249036, Обнинск, ул. Королева, д. 4;
ORCID: https://orcid.org/0000-0001-8970-4212;
e-mail: rippnba@gmail.com

Березовская Татьяна Павловна, гл.н.с., д.м.н., профессор;
ORCID: https://orcid.org/0000-0002-3549-4499

Иванов Сергей Анатольевич, д.м.н., профессор;
ORCID: https://orcid.org/0000-0001-7689-6032;
eLibrary SPIN: 4264-5167

* Corresponding author / Автор, ответственный за переписку

DOI: https://doi.org/10.17816/DD70306

Роль магнитно-резонансной томографии в выявлении злокачественных лёгочных узлов: систематический обзор и метаанализ

Ю.А. Васильев[1, 2], О.Ю. Панина[1, 2, 3], Е.А. Грик[3], Е.С. Ахмад[1], Ю.Н. Васильева[3]

[1] Научно-практический клинический центр диагностики и телемедицинских технологий, Москва, Российская Федерация
[2] Городская клиническая онкологическая больница № 1, Москва, Российская Федерация
[3] Московский государственный медико-стоматологический университет имени А.И. Евдокимова, Москва, Российская Федерация

АННОТАЦИЯ

Цель — оценка возможности метода магнитно-резонансной томографии (МРТ) органов грудной клетки для выявления лёгочных узлов, подозрительных в отношении злокачественности, в сравнении с компьютерной томографией (КТ).

Материалы и методы. Проведён поиск в базах данных PubMed и Google Scholar за период до 7 апреля 2021 г. включительно. В соответствии с критериями соответствия были отобраны исследования, в которых проводилась оценка способности МРТ и КТ к выявлению лёгочных узлов, подозрительных в отношении злокачественности. Выбор метода анализа и группировки данных о чувствительности и специфичности выполняли по результатам оценки гетерогенности исследований. Для оценки статистической гетерогенности исследований, включённых в метаанализ, применяли критерий согласия Пирсона x^2 и индекс гетерогенности I^2.

Результаты. По результатам поиска было отобрано 168 работ, в метаанализ вошло 21 исследование. Отобранные работы включали 1188 пациентов. По результатам метаанализа выявлено наличие статистически значимой гетерогенности p <0,00001 по критерию x^2 и индекс гетерогенности I^2=99% для чувствительности и специфичности. В связи с этим для анализа данных использовали метод случайных эффектов. Значения чувствительности для МРТ находились в диапазоне от 70,4 до 100%, специфичности — от 60,6 до 100%.

Заключение. МРТ обладает достаточной чувствительностью и специфичностью для определения злокачественности лёгочных узлов, обнаруженных при КТ-диагностике.

Ключевые слова: магнитно-резонансная томография; лёгочные узлы; рак лёгкого; чувствительность; специфичность.

Как цитировать
Васильев Ю.А., Панина О.Ю., Грик Е.А., Ахмад Е.С., Васильева Ю.Н. Роль магнитно-резонансной томографии в выявлении злокачественных лёгочных узлов: систематический обзор и метаанализ // *Digital Diagnostics*. 2021. Т. 2, № 3. С. 301–312. DOI: https://doi.org/10.17816/DD70306

Рукопись получена: 07.05.2021 **Рукопись одобрена:** 04.07.2021 **Опубликована:** 16.09.2021

ЭКО•ВЕКТОР

DOI: https://doi.org/10.17816/DD70306

Role of chest MRI for the diagnosis of malignant pulmonary nodules: a systematic review and a meta-analysis

Yuriy A. Vasilev[1, 2], Olga Yu. Panina[1, 2, 3], Evgeniia A. Grik[3], Kate A. Akhmad[1], Yulia N. Vasileva[3]

[1] Research and Practical Clinical Center for Diagnostics and Telemedicine Technologies of Moscow Health Care, Moscow, Russian Federation
[2] City Clinical Oncological Hospital No. 1, Moscow, Russian Federation
[3] Moscow State University of Medicine and Dentistry named after A.I. Evdokimov, Moscow, Russian Federation

ABSTRACT

AIM: To evaluate the ability of magnetic resonance imaging (MRI) of the chest to detect malignant pulmonary nodules compared to compute tomography (CT).

MATERIALS AND METHODS: We searched the following databases with the final date of search on April 7th, 2021: PubMed, Google Scholar. We selected studies according to the inclusion and exclusion criteria that assessed the detection of malignant lung nodules by MRI and CT and included information about sensitivity and specificity. Method of the analysis and data grouping was chosen with regard to statistical heterogeneity of the studies included in the analysis. We used the x^2 test and I^2 statistic to evaluate the heterogeneity.

RESULTS: We selected 168 articles for the systematic review from the PubMed and Google Scholar databases. We included 21 studies on 1,188 patients in the meta-analysis and revealed statistically significant heterogeneity (p<0,00001 for x^2 test; I^2=99%) for sensitivity and specificity. Hence, we used a random-effect model for further analysis. As a result, values of sensitivity for detection of pulmonary nodules with MRI of 70.4%–100%, specificity — from 60.6% to 100%.

CONCLUSIONS: Thus, MRI has sufficient sensitivity and specificity for detecting malignant pulmonary nodules primarily discovered with CT.

Keywords: MRI; solitary pulmonary nodule; lung cancer; benign; malignant.

To cite this article
Vasilev YuA, Panina OYu, Grik EA, Akhmad KA, Vasileva YuN. Role of chest MRI for the diagnosis of malignant pulmonary nodules: a systematic review and a meta-analysis. *Digital Diagnostics.* 2021;2(3):301–312. DOI: https://doi.org/10.17816/DD70306

Received: 07.05.2021 **Accepted:** 04.07.2021 **Published:** 16.09.2021

DOI: https://doi.org/10.17816/DD70306

磁共振成像在恶性肺结节检测中的作用 系统回顾和荟萃分析

Yuriy A. Vasilev[1, 2], Olga Yu. Panina[1, 2, 3], Evgeniia A. Grik[3], Kate A. Akhmad[1], Yulia N. Vasileva[3]

[1] Research and Practical Clinical Center for Diagnostics and Telemedicine Technologies of Moscow Health Care, Moscow, Russian Federation
[2] City Clinical Oncological Hospital No. 1, Moscow, Russian Federation
[3] Moscow State University of Medicine and Dentistry named after A.I. Evdokimov, Moscow, Russian Federation

简评

目的是评估胸部MRT与CT检测肺结节的可能性，怀疑有恶性肿瘤。

材料与方法。截至 2021 年 4 月 7 日（含） 进行了 PubMed 和 Google Scholar 数据库 根据资格标准，选择了评估 MRI 和 CT 识别可疑恶性肺淋巴结能力的研究。 分析方法的选择和敏感性和特异性数据的分组是根据评估研究异质性的结果进行的。 为了评估荟萃分析中包括的研究的统计异质性，使用了 Pearson $\chi 2$ 拟合检验和 I2 异质性指数。

结果。根据检索结果，筛选出 168 项研究，21 项研究纳入荟萃分析。 入选作品包括 1188 名患者。 根据 χ^2 标准和异质性指数 I^2 = 99% 的敏感性和特异性，荟萃分析显示存在统计学上显着的异质性 $p < 0.00001$。 对此，采用随机效应的方法对数据进行分析。 MRT 的灵敏度值范围从 70.4 到 100%，特异性 - 从 60.6 到 100%。

结论。因此，MRI 具有足够的敏感性和特异性来确定 CT 诊断中发现的肺淋巴结的恶性程度。

关键词：磁共振成像； 肺结节； 肺癌; 灵敏度; 特异性。

引用本文

Vasilev YuA, Panina OYu, Grik EA, Akhmad KA, Vasileva YuN. 磁共振成像在恶性肺结节检测中的作用：系统回顾和荟萃分析. *Digital Diagnostics*. 2021;2(3):301–312. DOI: https://doi.org/10.17816/DD70306

收到： 07.05.2021 **接受：** 04.07.2021 **发布日期：** 16.09.2021

BACKGROUND

The solitary pulmonary nodule (SPN) is a single, delimited, rounded lesion with a diameter of <3 cm [1, 2]. SPN is completely surrounded by unchanged pulmonary tissue and is unrelated to atelectasis, the root of the lung, or mediastinum. This mass could be caused by benign processes such as hamartoma, infectious lesions, granulomatous inflammation, or malignant processes (primary lung cancer, metastatic disease, or lymphoma). Malignancy of nodules is assumed until proven otherwise [2].

Currently, computed tomography (CT) is the gold standard for assessing SPN and monitoring patients who are at risk of cancer [3]. CT, despite its many advantages, has a major disadvantage: high radiation exposure, which certainly increases in dynamic monitoring. With the development and improvement of hardware and software, the search for new alternative visualization methods becomes evident. Over the last two decades, research into the potential use of magnetic resonance imaging (MRI) for the diagnosis of chest diseases has resulted in a separate research area devoted to SPN detection by MRI. The advantage of MRI is the lack of ionizing radiation exposure and the optional quantitative assessment of the revealed changes even without the use of contrast agents.

The aim of the study was to compare the capabilities of chest MRI to standard CT for detecting malignant SPN.

METHODS

This work was designed according to the PRISMA (Preferred Reporting Items for Systematic Reviews and Meta-Analyses) standard [4].

Study type

Inclusion criteria:

- (I) Prospective case-control studies, retrospective case-control studies, prospective cohort studies, and retrospective cohort studies;
- (II) Studies that included a description of the use of MRI to detect malignant SPN;
- (III) CT as the reference method; and
- (IV) Availability of sensitivity and specificity data.

Exclusion criteria:

- (I) The full text of the paper was not available.
- (II) The study did not involve humans.
- (III) The study involved children.
- (IV) Case reports, case series studies, systematic reviews, and meta-analyses.
- (V) Combination of positron emission tomography (PET) and CT (PET/CT) or PET and MRI (PET/MRI); contrast-enhanced studies.
- (VI) Involvement of patients with pulmonary tuberculosis and other inflammatory lung diseases.

Participants

Patients over 18 years of age.

The review excluded patients for whom diagnostic data could not be obtained using standard reference methods (standard chest CT).

Interventions

Studies that assessed the ability of MRI and standard CT to detect SPN suspicious for malignancy.

Results

Primary results: numerical values of lung MRI sensitivity and specificity to assess the detection of malignant SPN.

Secondary results: identification of the most optimal MR pulse sequences.

Sources of information

The databases PubMed and Google Scholar were searched until April 7, 2021.

Search

Since PubMed takes approximately a month to assign the term MeSH to a published paper, two types of queries were used in the PubMed database, that is, MeSH library terms and keywords to search among recent articles:

"Magnetic Resonance imaging" [Mesh] or "MRI" and "Computed tomography" or "CT" and "Lung neoplasms" [Mesh] or "Solitary Pulmonary Nodule" [Mesh] and "Sensitivity" and "Specificity";

"Lung MRI" or "chest MRI" and "Computed tomography" or "CT" and "lung cancer" or "Solitary Pulmonary Nodule".

The query "MRI, CT, lung cancer, specificity, sensitivity" was used to search in the Google Scholar database.

Data collection and data items

Using the Google Spreadsheet service, a data extraction table was created. The authors had simultaneous and unrestricted access to the document. The following data was extracted from the selected papers by two researchers (O.Yu. Panina and Ye.A. Grik): title of the article, journal (or service for posting preprints), publication date, DOI, MRI protocol, MRI magnetic induction value, types of lesions revealed, sensitivity, specificity, and standard deviation for MRI and CT. After calculating the sensitivity and specificity indicators for each pulse sequence (PS) separately, the most effective values were included in the meta-analysis.

Three other researchers (E.S. Akhmad, Yu.N. Vasilyeva, and Yu.A. Vasilyev) verified the extracted data. All disagreements were resolved through discussion among the authors.

Risk of bias in selected studies

The authors used the QUADAS-2 (Quality Assessment of Diagnostic Accuracy Studies) checklist [5], which is recommended by the Agency for Healthcare Research and Quality (Cochrane Collaboration, US) for systematic reviews. Each of

the selected papers was assessed based on four domains: patient selection, index test, reference test, and patient flow. For a detailed description of each domain and the judgment of the criteria used, see the *Cochrane Handbook for Systematic Reviews of Interventions* [6].

Statistical analysis

The selection of method for analyzing and grouping sensitivity and specificity data (random- or fixed-effects model) was performed according to the results of the study heterogeneity assessment. The x^2 criterion and I^2 heterogeneity index were used to assess the statistical heterogeneity of the studies included in the meta-analysis. In the studies, statistically significant heterogeneity corresponds to $p < 0.10$ in the x^2 criterion and $I > 40\%$. Moreover, meta-analysis was performed using the RevMan 5.4.1 software package.

RESULTS

Based on search results in the PubMed and Google Scholar databases, 168 selected papers were imported into the Mendeley Reference Manager software library. Following a second check for inclusion and exclusion criteria and text review, 33 papers remained (Fig. 1).

A text review of the remaining 33 papers [7–38] revealed that two studies performed contrast-enhanced CT [23, 24], which is not an appropriate type of intervention. Furthermore, the sensitivity and specificity data for CT were completely absent in ten papers [20–22, 25–29, 31, 32], so these studies were excluded. The meta-analysis included papers in which a low-dose CT was used as a control study [9, 10, 16] rather than an exclusion criterion. Thus, the meta-analysis included 21 studies (see Fig. 1).

The selected studies included 1188 patients and contained information on lung MRI and CT scans. Sensitivity data for MRI and CT were presented in all papers; however, specificity rates were not reported in three articles [8, 16, 30]. The majority of the studies were performed on tomographs with magnetic field induction of 1.5 T (Table. 1).

Risk of bias

Eleven studies adequately reported the index test and reference test data [7, 8, 10–13, 15–18, 33]. The primary sources of errors were the index test (MRI) and its interpretation (Fig. 2). Some studies lacked complete data to assess the risk of bias, for example, whether the index test results were interpreted without knowing the results of the reference test, or whether interpretation of the reference test was impossible without knowing the results of the index test. Moreover, the risk of bias was characteristic of studies that were more likely to be published if an effect was found as opposed to those that did not. However, participants in all studies met the protocol criteria for this review.

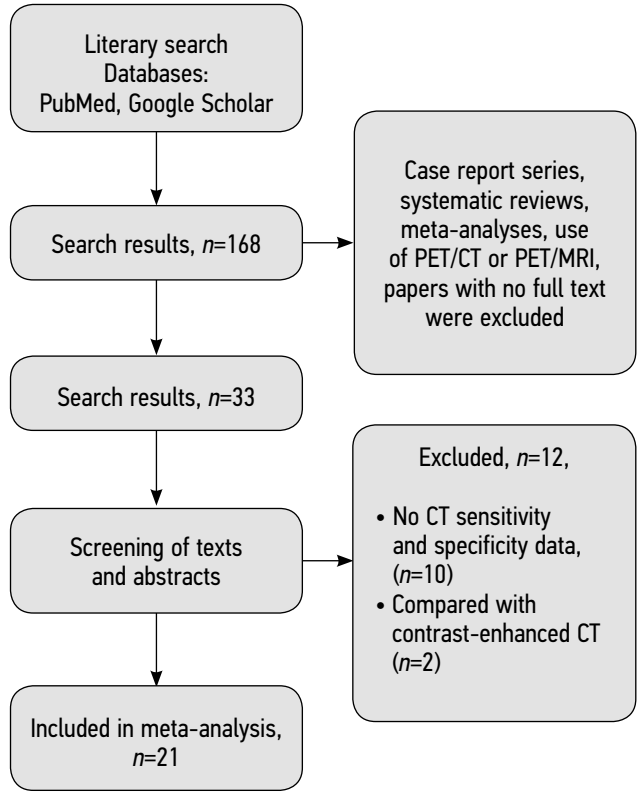

Fig. 1. Flow diagram

The meta-analysis revealed statistically significant heterogeneity ($p < 0.00001$) using the x^2 criterion and the heterogeneity index ($I^2=99\%$) for sensitivity and specificity. In this case, the random-effects method was used to analyze the data.

Diagnostic accuracy of chest MRI

In each of the 21 studies, MRI was compared to the reference method. Sensitivity for MRI ranged from 70.4% to 100%, while the specificity ranged from 60.6% to 100% (Fig. 3). The mean MRI sensitivity was 88.3%, while the mean MRI specificity was 71.3%. In studies where the standard deviation parameters for sensitivity and specificity were not specified, the calculation was performed by estimating the values of the indicators [40].

Table 2 shows the characteristics that were included in the meta-analysis of studies with the highest sensitivity and specificity values for MRI, which are comparable to CT.

DISCUSSION

The results of this meta-analysis show that MRI has lower mean specificity and sensitivity when compared to CT. In the majority of studies included in the meta-analysis, the sensitivity and specificity of chest CT for detecting SPN was 100%. Since CT was used as a reference test, only three studies had lower rates. For chest MRI, 5 of the 21 studies had 100% sensitivity, and only 2 studies had 100% sensitivity and specificity.

Table 1. Characteristics of studies included in the meta-analysis

No.	Studies	Year	Magnetic field induction, T	MRI model and manufacturer	MRI PS
1	Both [7]	2005	1,5	Magnetom Vision, Siemens	VIBE, HASTE, T2TSE
2	Bruegel [8]	2007	1,5	Magnetom Sonata, Siemens	STIR
3	Chang [19]	2015	1,5	Intera Achieva, Philips	SS-TSE-HF
4	Cieszanowski [30]	2016	1,5	Magnetom Avanto, Siemens	T2TSE, T2-STIR, T2-HASTE
5	Dewes [33]	2016	3,0	Magnetom Prisma, Siemens	CAIPIRINHA-VIBE
6	Fatihoğlu [34]	2019	1,5	Magnetom Aera, Siemens	DWI (ADC)
7	Heye [35]	2012	1,5	Avanto, Siemens	VIBE, HASTE
8	Huang [39]	2020	1,5	Magnetom Aera, Siemens	UTE free-breathing
9	Koo [36]	2019	3,0	Magnetom Skyra, Siemens	T2FSE
10	Koyama [37]	2008	1,5	Intera, Philips	STIR
11	Koyama [38]	2015	1,5	Achieva, Philips	DWI (ADC)
12	Meier-Schroers [9]	2016	1,5	Ingenia, Philips	T2FSE
13	Meier-Schroers [10]	2019	1,5	Ingenia, Philips	T2STIR
14	Ohno [11]	2017	3,0	Vantage Titan, Canon Medical Systme	UTE
15	Regier [12]	2011	1,5	Achieva, Philips	DWI (ADC)
16	Satoh [13]	2008	1,5	Intera NovoDual, Philips	DWI (ADC)
17	Schaefer [14]	2006	1,0	Magnetom Expert, Siemens	PDWI
18	Schroeder [15]	2005	1,5	Magnetom Sonata, Siemens	HASTE
19	Sommer [16]	2014	1,5	Magnetom Avanto, Siemens	HASTE
20	Vogt [17]	2004	1,5	Magnetom Sonata, Siemens	HASTE
21	Yi [18]	2007	3,0	Achieva, Philips	T1WI 3D TFE*

Note. MRI PS: pulse sequences of magnetic resonance imaging

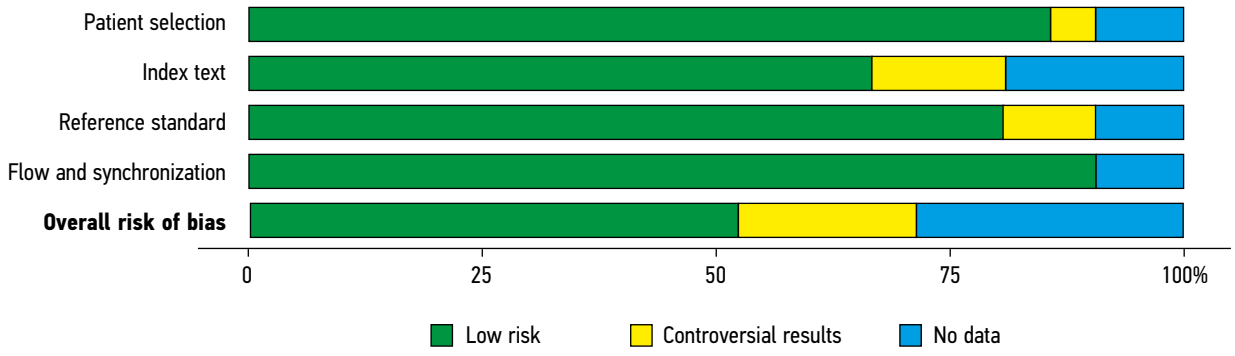

Fig. 2. Histogram of the risk of bias

When the results of the meta-analysis were examined, high sensitivity rates were observed in studies that calculated overall sensitivity and specificity rates for the entire MR protocol rather than separately for each PS (see Table 2). This phenomenon demonstrates the peculiarity of the meta-analysis for MRI as a method in which the signal characteristics are assessed in conjunction with the scanning protocol. These examples may indicate a lack of research into MRI capabilities in the differential diagnosis of SPN, the need for studies of current PS, and the careful tuning of routine PS on a tomograph. This approach will allow for greater MRI efficiency in detecting SPN and studying their characteristics, which is especially important in lung cancer diagnosis.

Lung cancer continues to be the leading cause of death worldwide, including in the Russian Federation, and it is a serious social and economic problem [41, 42]. The presence of cancer among detected SPN ranges from 10% to 70% [2]. In some countries, low-dose CT is performed in high-risk groups as part of screening.

Currently, the coverage of the screening program remains low, and the criteria for inclusion of patients are limited to ensure its economic viability. Thus, many patients will still be diagnosed after the onset of symptoms, rather than at an early stage of disease development and at a high cost of misdiagnosis [41]. Furthermore, radiologists and clinicians continue to face difficulties in monitoring and managing ambiguous SPN. Accordingly, only a comprehensive approach is always used for diagnosis, patient routing, and selection of optimal management and treatment strategies [43].

This meta-analysis revealed an alternative approach for assessing SPN that are suspicious for cancer. In addition, the emphasis was on standard studies that did not make use of contrast enhancement.

Limitations

There were several limitations to this study. For various reasons, the meta-analysis included data with lesions larger than 6 mm. First, nodule sizes greater than 6 mm are the most common in selected studies; second, nodules smaller than 6 mm have a fairly low risk of malignancy according to recent data from Fleischner Society [3]. In addition, the meta-analysis did not compare MRI with histologic data, which could be considered a limitation of the study.

CONCLUSIONS

MRI has the sensitivity and specificity needed for additional diagnosis of SPN that are suspicious for malignancy

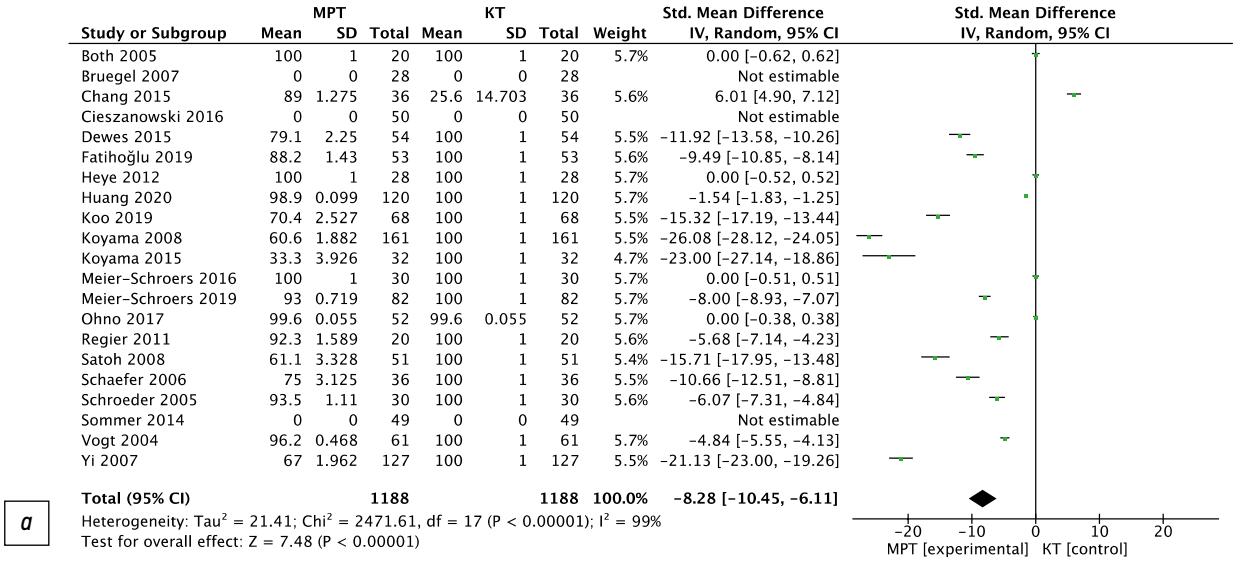

Fig. 3. Forest plot of grouped data for specificity (*a*) and sensitivity (*b*) [40]

Note. SMD: standardized mean difference; CI: confidence interval

Table 2. Characteristics of studies with the highest sensitivity and specificity values

No.	Author, year of study	Sensitivity (general index)	Specificity (general index)	MRI PS	Magnetic field induction, T
1	Both, 2005 [7]	100	100	VIBE, HASTE, T2TSE	1,5
2	Cieszanowski, 2016 [30]	100	-	T2TSE, T2-STIR, T2-HASTE	1,5
3	Meier-Schroers, 2016 [9]	100	100	T2FSE	1,5
4	Regier, 2011 [12]	97	92,3	DWI (ADC)	1,5
5	Heye, 2012 [35]	100	100	VIBE, HASTE	1,5
6	Schaefer, 2006 [14]	100	75	PDWI	1,5

Note. MRI PS: pulse sequences of magnetic resonance imaging

and revealed by CT. The mean MRI sensitivity was 88.3%, while the mean MRI specificity was 71.3%.

MRI is a non-ionizing imaging method that can be used as an additional technique in the evaluation of various PS while resolving controversial cases.

Further research into the most efficient PS, the feasibility of contrast enhancement, and new technological solutions for high-quality diagnostics of SPN is necessary.

ADDITIONAL INFORMATION

Funding source. The study had no sponsorship.

Competing interests. The authors declare that they have no competing interests.

Authors' contribution. Yury A. Vasilev — research concept, writing the manuscript, analysis and expert assessment of research results; Olga Yu. Panina — research concept, search for publications, processing of the results, writing the manuscript; Evgeniia A. Grik — search for publications, processing of the results, Kate A. Akhmad — processing of the results, systematization and final editing of the review; Yulia N. Vasileva — analysis and expert assessment of research results, systematization and final editing of the review. All authors made a substantial contribution to the conception of the work, acquisition, analysis, interpretation of data for the work, drafting and revising the work, final approval of the version to be published and agree to be accountable for all aspects of the work.

REFERENCES

1. Ost D, Fein AM, Feinsilver SH. Clinical practice. The solitary pulmonary nodule. *N Engl J Med*. 2003;348(25):2535–2542. doi: 10.1056/NEJMcp012290

2. Nasim F, Ost DE. Management of the solitary pulmonary nodule. *Curr Opin Pulm Med*. 2019;25(4):344–353. doi: 10.1097/MCP.0000000000000586

3. MacMahon H, Naidich DP, Goo JM, et al. Guidelines for management of incidental pulmonary nodules detected on CT images: From the Fleischner Society 2017. *Radiology*. 2017;284(1):228–243. doi: 10.1148/radiol.2017161659

4. Liberati A, Altman DG, Tetzlaff J, et al. The PRISMA statement for reporting systematic reviews and meta-analyses of studies that evaluate health care interventions: Explanation and elaboration. *PLoS Med*. 2009;6(7):e1000100. doi: 10.1371/journal.pmed.1000100

5. Whiting PF, Rutjes AW, Westwood ME, et al. Quadas-2: A revised tool for the quality assessment of diagnostic accuracy studies. *Ann Intern Med*. 2011;155(8):529–536. doi: 10.7326/0003-4819-155-8-201110180-00009

6. Higgins JP, Thomas J, Chandler J, et al. Cochrane handbook for systematic reviews of interventions. John Wiley & Sons, Hoboken; 2019. doi: 10.1002/9781119536604

7. Both M, Schultze J, Reuter M, et al. Fast T1- and T2-weighted pulmonary MR-imaging in patients with bronchial carcinoma. *Eur J Radiol*. 2005;53(3):478–488. doi: 10.1016/j.ejrad.2004.05.007

8. Bruegel M, Gaa J, Woertler K, et al. MRI of the lung: Value of different turbo spin-echo, single-shot turbo spin-echo, and 3D gradient-echo pulse sequences for the detection of pulmonary metastases. *J Magn Reson Imaging*. 2007;25(1):73–81. doi: 10.1002/jmri.20824

9. Meier-Schroers M, Kukuk G, Homsi R, et al. MRI of the lung using the PROPELLER technique: Artifact reduction, better image quality and improved nodule detection. *Eur J Radiol*. 2016;85(4):707–713. doi: 10.1016/j.ejrad.2015.12.016

10. Meier-Schroers M, Homsi R, Schild HH, Thomas D. Lung cancer screening with MRI: characterization of nodules with different non-enhanced MRI sequences. *Acta Radiol*. 2019;60(2):168–176. doi: 10.1177/0284185118778870

11. Ohno Y, Koyama H, Yoshikawa T, et al. Standard-, reduced-, and nodose thin-section radiologic examinations: Comparison of capability for nodule detection and nodule type assessment in patients suspected of having pulmonary nodules. *Radiology*. 2017;284(2):562–573. doi: 10.1148/radiol.2017161037

12. Regier M, Schwarz D, Henes FO, et al. Diffusion-weighted MR-imaging for the detection of pulmonary nodules at 1.5 Tesla: Intraindividual comparison with multidetector computed tomography. *J Med Imaging Radiat Oncol*. 2011;55(3):266–274. doi: 10.1111/j.1754-9485.2011.02263.x

13. Satoh S, Kitazume Y, Ohdama S, et al. Can malignant and benign pulmonary nodules be differentiated with diffusion-weighted MRI? *Am J Roentgenol*. 2008;191(2):464–470. doi: 10.2214/AJR.07.3133

14. Schaefer JF, Schneider V, Vollmar J, et al. Solitary pulmonary nodules: Association between signal characteristics in dynamic

contrast enhanced MRI and tumor angiogenesis. *Lung Cancer*. 2006;53(1):39–49. doi: 10.1016/j.lungcan.2006.03.010

15. Schroeder T, Ruehm SG, Debatin JF, et al. Detection of pulmonary nodules using a 2D HASTE MR sequence: comparison with MDCT. *Am J Roentgenol*. 2005;185(4):979–984. doi: 10.2214/AJR.04.0814

16. Sommer G, Tremper J, Koenigkam-Santos M, et al. Lung nodule detection in a high-risk population: Comparison of magnetic resonance imaging and low-dose computed tomography. *Eur J Radiol*. 2014;83(3):600–605. doi: 10.1016/j.ejrad.2013.11.012

17. Vogt FM, Herborn CU, Hunold P, et al. HASTE MRI versus chest radiography in the detection of pulmonary nodules: comparison with MDCT. *Am J Roentgenol*. 2004;183(1):71–78. doi: 10.2214/ajr.183.1.1830071

18. Yi CA, Jeon TY, Lee KS, et al. 3-T MRI: usefulness for evaluating primary lung cancer and small nodules in lobes not containing primary tumors. *Am J Roentgenol*. 2007;189(2):386–392. doi: 10.2214/AJR.07.2082

19. Chang S, Hong SR, Kim YJ, et al. Usefulness of thin-section single-shot turbo spin echo with half-fourier acquisition in evaluation of local invasion of lung cancer. *J Magn Reson Imaging*. 2015;41(3):747–754. doi: 10.1002/jmri.24587

20. Schaefer JF, Vollmar J, Schick F, et al. Solitary pulmonary nodules: Dynamic contrast-enhanced MR imaging — Perfusion differences in malignant and benign lesions. *Radiology*. 2004;232(2):544–553. doi: 10.1148/radiol.2322030515

21. Kono R, Fujimoto K, Terasaki H, et al. Dynamic MRI of solitary pulmonary nodules: comparison of enhancement patterns of malignant and benign small peripheral lung lesions. *Am J Roentgenol*. 2007;188(1):26–36. doi: 10.2214/AJR.05.1446

22. Feng H, Shi G, Liu H, et al. Free-breathing radial volumetric interpolated breath-hold examination sequence and dynamic contrast-enhanced MRI combined with diffusion-weighted imaging for assessment of solitary pulmonary nodules. *Magn Reson Imaging*. 2021;75:100–106. doi: 10.1016/j.mri.2020.10.009

23. Kim JH, Kim HJ, Lee KH, et al. Solitary pulmonary nodules: A comparative study evaluated with contrast-enhanced dynamic MR imaging and CT. *J Comput Assist Tomogr*. 2004;28(6):766–775. doi: 10.1097/00004728-200411000-00007

24. Ohno Y, Nishio M, Koyama H, et al. Solitary pulmonary nodules: Comparison of dynamic first-pass contrast-enhanced perfusion area-detector CT, dynamic first-pass contrast-enhanced MR imaging, and FDG PET/CT. *Radiology*. 2015;274(2):563–575. doi: 10.1148/radiol.14132289

25. Heye T, Sommer G, Miedinger D, et al. Ultrafast 3D balanced steady-state free precession MRI of the lung: Assessment of anatomic details in comparison to low-dose CT. *J Magn Reson Imaging*. 2015;42(3):602–609. doi: 10.1002/jmri.24836

26. Akata S, Kajiwara N, Park J, et al. Evaluation of chest wall invasion by lung cancer using respiratory dynamic MRI. *J Med Imaging Radiat Oncol*. 2008;52(1):36–39. doi: 10.1111/j.1440-1673.2007.01908.x

27. Hittmair K, Eckersberger F, Klepetko W, et al. Evaluation of solitary pulmonary nodules with dynamic contrast-enhanced MR imaging-a promising technique? *Magn Reson Imaging*. 1995;13(7):923–933. doi: 10.1016/0730-725x(95)02010-q

28. Alper F, Kurt AT, Aydin Y, et al. The role of dynamic magnetic resonance imaging in the evaluation of pulmonary nodules and masses. *Med Princ Pract*. 2013;22(1):80–86. doi: 10.1159/000339475

29. Frericks BB, Meyer BC, Martus P, et al. MRI of the thorax during whole-body MRI: Evaluation of different MR sequences and comparison to thoracic multidetector computed tomography (MDCT). *J Magn Reson Imaging*. 2008;27(3):538–545. doi: 10.1002/jmri.21218

30. Cieszanowski A, Lisowska A, Dabrowska M, et al. MR imaging of pulmonary nodules: Detection rate and accuracy of size estimation in comparison to computed tomography. *PLoS One*. 2016;11(6):e0156272. doi: 10.1371/journal.pone.0156272

31. Ohno Y, Hatabu H, Takenaka D, et al. Solitary pulmonary nodules: Potential role of dynamic MR imaging in management — Initial experience. *Radiology*. 2002;224(2):503–511. doi: 10.1148/radiol.2242010992

32. Zou Y, Zhang M, Wang Q, et al. Quantitative investigation of solitary pulmonary nodules: dynamic contrast-enhanced MRI and histopathologic analysis. *Am J Roentgenol*. 2008;191(1):252–259. doi: 10.2214/AJR.07.2284

33. Dewes P, Frellesen C, Al-Butmeh F, et al. Comparative evaluation of non-contrast CAIPIRINHA-VIBE 3T-MRI and multidetector CT for detection of pulmonary nodules: In vivo evaluation of diagnostic accuracy and image quality. *Eur J Radiol*. 2016;85(1):193–198. doi: 10.1016/j.ejrad.2015.11.020

34. Fatihoglu E, Biri S, Aydın S, et al. MRI in evaluation of solitary pulmonary nodules. *Turkish Thorac J*. 2019;20(2):90–96. doi: 10.5152/TurkThoracJ.2018.18049

35. Heye T, Ley S, Heussel CP, et al. Detection and size of pulmonary lesions: How accurate is MRI? A prospective comparison of CT and MRI. *Acta Radiol*. 2012;53(2):153–160. doi: 10.1258/ar.2011.110445

36. Koo CW, Lu A, Takahashi EA, et al. Can MRI contribute to pulmonary nodule analysis? *J Magn Reson Imaging*. 2019;49(7):e256–e264. doi: 10.1002/jmri.26587

37. Koyama H, Ohno Y, Kono A, et al. Quantitative and qualitative assessment of non-contrast-enhanced pulmonary MR imaging for management of pulmonary nodules in 161 subjects. *Eur Radiol*. 2008;18(10):2120–2131. doi: 10.1007/s00330-008-1001-2

38. Koyama H, Ohno Y, Seki S, et al. Value of diffusion-weighted MR imaging using various parameters for assessment and characterization of solitary pulmonary nodules. *Eur J Radiol*. 2015;84(3):509–515. doi: 10.1016/j.ejrad.2014.11.024

39. Huang YS, Niisato E, Su MY, et al. Detecting small pulmonary nodules with spiral ultrashort echo time sequences in 1.5 T MRI. *MAGMA*. 2021;34(3):399–409. doi: 10.1007/s10334-020-00885-x

40. Ying GS, Maguire MG, Glynn RJ,et al. Calculating sensitivity, specificity, and predictive values for correlated eye data. *Investig Ophthalmol Vis Sci*. 2020;61(11):29. doi: 10.1167/iovs.61.11.29

41. Bradley SH, Kennedy MP, Neal RD. Recognising lung cancer in primary care. *Adv Ther*. 2019;36(1):19–30. doi: 10.1007/s12325-018-0843-5

42. Nikolaev E, Gombolevskiy V, Gonchar AP, et al. Incidental findings during lung cancer screening by low-dose computed tomography. *Tuberc Lung Dis*. 2018;96(11):60–67. doi: 10.21292/2075-1230-2018-96-11-60-67

43. Loverdos K, Fotiadis A, Kontogianni C, et al. Lung nodules: A comprehensive review on current approach and management. *Ann Thorac Med*. 2019;14(4):226–238. doi: 10.4103/atm.ATM_110_19

СПИСОК ЛИТЕРАТУРЫ

1. Ost D., Fein A.M., Feinsilver S.H. Clinical practice. The solitary pulmonary nodule // N Engl J Med. 2003. Vol. 348, N 25. P. 2535–2542. doi: 10.1056/NEJMcp012290

2. Nasim F., Ost D.E. Management of the solitary pulmonary nodule // Curr Opin Pulm Med. 2019. Vol. 25, N 4. P. 344–353. doi: 10.1097/MCP.0000000000000586

3. MacMahon H., Naidich D.P., Goo J.M., et al. Guidelines for management of incidental pulmonary nodules detected on CT images: From the Fleischner Society 2017 // Radiology. 2017. Vol. 284, N 1. P. 228–243. doi: 10.1148/radiol.2017161659

4. Liberati A., Altman D.G., Tetzlaff J., et al. The PRISMA statement for reporting systematic reviews and meta-analyses of studies that evaluate health care interventions: Explanation and elaboration // PLoS Med. 2009. Vol. 6, N 7. P. e1000100. doi: 10.1371/journal.pmed.1000100

5. Whiting P.F., Rutjes A.W., Westwood M.E., et al. Quadas-2: A revised tool for the quality assessment of diagnostic accuracy studies // Ann Intern Med. 2011. Vol. 155, N 8. P. 529–536. doi: 10.7326/0003-4819-155-8-201110180-00009

6. Higgins J.P., Thomas J., Chandler J., et al. Cochrane handbook for systematic reviews of interventions. John Wiley & Sons, Hoboken; 2019. doi: 10.1002/9781119536604

7. Both M., Schultze J., Reuter M., et al. Fast T1- and T2-weighted pulmonary MR-imaging in patients with bronchial carcinoma // Eur J Radiol. 2005. Vol. 53, N 3. P. 478–488. doi: 10.1016/j.ejrad.2004.05.007

8. Bruegel M., Gaa J., Woertler K., et al. MRI of the lung: Value of different turbo spin-echo, single-shot turbo spin-echo, and 3D gradient-echo pulse sequences for the detection of pulmonary metastases // J Magn Reson Imaging. 2007. Vol. 25, N 1. P. 73–81. doi: 10.1002/jmri.20824

9. Meier-Schroers M., Kukuk G., Homsi R., et al. MRI of the lung using the PROPELLER technique: Artifact reduction, better image quality and improved nodule detection // Eur J Radiol. 2016. Vol. 85, N 4. P. 707–713. doi: 10.1016/j.ejrad.2015.12.016

10. Meier-Schroers M., Homsi R., Schild H.H., Thomas D. Lung cancer screening with MRI: characterization of nodules with different non-enhanced MRI sequences // Acta Radiol. 2019. Vol. 60, N 2. P. 168–176. doi: 10.1177/0284185118778870

11. Ohno Y., Koyama H., Yoshikawa T., et al. Standard-, reduced-, and nodose thin-section radiologic examinations: Comparison of capability for nodule detection and nodule type assessment in patients suspected of having pulmonary nodules // Radiology. 2017. Vol. 284, N 2. P. 562–573. doi: 10.1148/radiol.2017161037

12. Regier M., Schwarz D., Henes F.O., et al. Diffusion-weighted MR-imaging for the detection of pulmonary nodules at 1.5 Tesla: Intra-individual comparison with multidetector computed tomography // J Med Imaging Radiat Oncol. 2011. Vol. 55, N 3. P. 266–274. doi: 10.1111/j.1754-9485.2011.02263.x

13. Satoh S., Kitazume Y., Ohdama S., et al. Can malignant and benign pulmonary nodules be differentiated with diffusion-weighted MRI? // Am J Roentgenol. 2008. Vol. 191, N 2. P. 464–470. doi: 10.2214/AJR.07.3133

14. Schaefer J.F., Schneider V., Vollmar J., et al. Solitary pulmonary nodules: Association between signal characteristics in dynamic contrast enhanced MRI and tumor angiogenesis // Lung Cancer. 2006. Vol. 53, N 1. P. 39–49. doi: 10.1016/j.lungcan.2006.03.010

15. Schroeder T., Ruehm S.G., Debatin J.F., et al. Detection of pulmonary nodules using a 2D HASTE MR sequence: comparison with MDCT // Am J Roentgenol. 2005. Vol. 185, N 4. P. 979–984. doi: 10.2214/AJR.04.0814

16. Sommer G., Tremper J., Koenigkam-Santos M., et al. Lung nodule detection in a high-risk population: Comparison of magnetic resonance imaging and low-dose computed tomography // Eur J Radiol. 2014. Vol. 83, N 3. P. 600–605. doi: 10.1016/j.ejrad.2013.11.012

17. Vogt F.M., Herborn C.U., Hunold P., et al. HASTE MRI versus chest radiography in the detection of pulmonary nodules: comparison with MDCT // Am J Roentgenol. 2004. Vol. 183, N 1. P. 71–78. doi: 10.2214/ajr.183.1.1830071

18. Yi C.A., Jeon T.Y., Lee K.S., et al. 3-T MRI: usefulness for evaluating primary lung cancer and small nodules in lobes not containing primary tumors // Am J Roentgenol. 2007. Vol. 189, N 2. P. 386–392. doi: 10.2214/AJR.07.2082

19. Chang S., Hong S.R., Kim Y.J., et al. Usefulness of thin-section single-shot turbo spin echo with half-fourier acquisition in evaluation of local invasion of lung cancer // J Magn Reson Imaging. 2015. Vol. 41, N 3. P. 747–754. doi: 10.1002/jmri.24587

20. Schaefer J.F., Vollmar J., Schick F., et al. Solitary pulmonary nodules: Dynamic contrast-enhanced MR imaging — Perfusion differences in malignant and benign lesions // Radiology. 2004. Vol. 232, N 2. P. 544–553. doi: 10.1148/radiol.2322030515

21. Kono R., Fujimoto K., Terasaki H., et al. Dynamic MRI of solitary pulmonary nodules: comparison of enhancement patterns of malignant and benign small peripheral lung lesions // Am J Roentgenol. 2007. Vol. 188, N 1. P. 26–36. doi: 10.2214/AJR.05.1446

22. Feng H., Shi G., Liu H., et al. Free-breathing radial volumetric interpolated breath-hold examination sequence and dynamic contrast-enhanced MRI combined with diffusion-weighted imaging for assessment of solitary pulmonary nodules // Magn Reson Imaging. 2021. Vol. 75. P. 100–106. doi: 10.1016/j.mri.2020.10.009

23. Kim J.H., Kim H.J., Lee K.H., et al. Solitary pulmonary nodules: A comparative study evaluated with contrast-enhanced dynamic MR imaging and CT // J Comput Assist Tomogr. 2004. Vol. 28, N 6. P. 766–775. doi: 10.1097/00004728-200411000-00007

24. Ohno Y., Nishio M., Koyama H., et al. Solitary pulmonary nodules: Comparison of dynamic first-pass contrast-enhanced perfusion area-detector CT, dynamic first-pass contrast-enhanced MR imaging, and FDG PET/CT // Radiology. 2015. Vol. 274, N 2. P. 563–575. doi: 10.1148/radiol.14132289

25. Heye T., Sommer G., Miedinger D., et al. Ultrafast 3D balanced steady-state free precession MRI of the lung: Assessment of anatomic details in comparison to low-dose CT // J Magn Reson Imaging. 2015. Vol. 42, N 3. P. 602–609. doi: 10.1002/jmri.24836

26. Akata S., Kajiwara N., Park J., et al. Evaluation of chest wall invasion by lung cancer using respiratory dynamic MRI // J Med Imaging Radiat Oncol. 2008. Vol. 52, N 1. P. 36–39. doi: 10.1111/j.1440-1673.2007.01908.x

27. Hittmair K., Eckersberger F., Klepetko W., et al. Evaluation of solitary pulmonary nodules with dynamic contrast-enhanced MR imaging-a promising technique? // Magn Reson Imaging. 1995. Vol. 13, N 7. P. 923–933. doi: 10.1016/0730-725x(95)02010-q

28. Alper F., Kurt A.T., Aydin Y., et al. The role of dynamic magnetic resonance imaging in the evaluation of pulmonary nodules and masses // Med Princ Pract. 2013. Vol. 22, N 1. P. 80–86. doi: 10.1159/000339475
29. Frericks B.B., Meyer B.C., Martus P., et al. MRI of the thorax during whole-body MRI: Evaluation of different MR sequences and comparison to thoracic multidetector computed tomography (MDCT) // J Magn Reson Imaging. 2008. Vol. 27, N 3. P. 538–545. doi: 10.1002/jmri.21218
30. Cieszanowski A., Lisowska A., Dabrowska M., et al. MR imaging of pulmonary nodules: Detection rate and accuracy of size estimation in comparison to computed tomography // PLoS One. 2016. Vol. 11, N 6. P. e0156272. doi: 10.1371/journal.pone.0156272
31. Ohno Y., Hatabu H., Takenaka D., et al. Solitary pulmonary nodules: Potential role of dynamic MR imaging in management — Initial experience // Radiology. 2002. Vol. 224, N 2. P. 503–511. doi: 10.1148/radiol.2242010992
32. Zou Y., Zhang M., Wang Q., et al. Quantitative investigation of solitary pulmonary nodules: dynamic contrast-enhanced MRI and histopathologic analysis // Am J Roentgenol. 2008. Vol. 191, N 1. P. 252–259. doi: 10.2214/AJR.07.2284
33. Dewes P., Frellesen C., Al-Butmeh F., et al. Comparative evaluation of non-contrast CAIPIRINHA-VIBE 3T-MRI and multidetector CT for detection of pulmonary nodules: In vivo evaluation of diagnostic accuracy and image quality // Eur J Radiol. 2016. Vol. 85, N 1. P. 193–198. doi: 10.1016/j.ejrad.2015.11.020
34. Fatihoğlu E., Biri S., Aydın S., et al. MRI in evaluation of solitary pulmonary nodules // Turkish Thorac J. 2019. Vol. 20, N 2. P. 90–96. doi: 10.5152/TurkThoracJ.2018.18049
35. Heye T., Ley S., Heussel C.P., et al. Detection and size of pulmonary lesions: How accurate is MRI? A prospective comparison of CT and MRI // Acta Radiol. 2012. Vol. 53, N 2. P. 153–160. doi: 10.1258/ar.2011.110445
36. Koo C.W., Lu A., Takahashi E.A., et al. Can MRI contribute to pulmonary nodule analysis? // J Magn Reson Imaging. 2019. Vol. 49, N 7. P. e256–e264. doi: 10.1002/jmri.26587
37. Koyama H., Ohno Y., Kono A., et al. Quantitative and qualitative assessment of non-contrast-enhanced pulmonary MR imaging for management of pulmonary nodules in 161 subjects // Eur Radiol. 2008. Vol. 18, N 10. P. 2120–2131. doi: 10.1007/s00330-008-1001-2
38. Koyama H., Ohno Y., Seki S., et al. Value of diffusion-weighted MR imaging using various parameters for assessment and characterization of solitary pulmonary nodules // Eur J Radiol. 2015. Vol. 84, N 3. P. 509–515. doi: 10.1016/j.ejrad.2014.11.024
39. Huang Y.S., Niisato E., Su M.Y., et al. Detecting small pulmonary nodules with spiral ultrashort echo time sequences in 1.5 T MRI // MAGMA. 2021. Vol. 34, N 3. P. 399–409. doi: 10.1007/s10334-020-00885-x
40. Ying G.S., Maguire M.G., Glynn R.J., et al. Calculating sensitivity, specificity, and predictive values for correlated eye data // Investig Ophthalmol Vis Sci. 2020. Vol. 61, N 11. P. 29. doi: 10.1167/iovs.61.11.29
41. Bradley S.H., Kennedy M.P., Neal R.D. Recognising lung cancer in primary care // Adv Ther. 2019. Vol. 36, N 1. P. 19–30. doi: 10.1007/s12325-018-0843-5
42. Nikolaev E., Gombolevskiy V, Gonchar AP, et al. Incidental findings during lung cancer screening by low-dose computed tomography // Tuberc Lung Dis. 2018. Vol. 96, N 11. P. 60–67. doi: 10.21292/2075-1230-2018-96-11-60-67
43. Loverdos K., Fotiadis A., Kontogianni C., et al. Lung nodules: A comprehensive review on current approach and management // Ann Thorac Med. 2019. Vol. 14, N 4. P. 226–238. doi: 10.4103/atm.ATM_110_19

AUTHORS' INFO

*** Olga Yu. Panina,** MD;
address: 24/1 Petrovka str., 127051, Moscow, Russia;
ORCID: https://orcid.org/0000-0002-8684-775X;
eLibrary SPIN: 5504-8136; e-mail: o.panina@npcmr.ru

Yuriy A. Vasilev, MD, Cand. Sci. (Med.);
ORCID: https://orcid.org/0000-0002-0208-5218;
eLibrary SPIN: 4458-5608; e-mail: dr.vasilev@me.com

Evgeniia A. Grik, MD;
ORCID: http://orcid.org/0000-0002-7908-3982;
eLibrary SPIN: 5558-7307; e-mail: evgeniyagrik@gmail.com

Kate S. Akhmad;
ORCID: http://orcid.org/0000-0002-8235-9361;
eLibrary SPIN: 5891-4384; e-mail: e.ahmad@npcmr.ru

Yulia N. Vasileva, MD, Cand. Sci. (Med.);
ORCID: http://orcid.org/0000-0002-1066-3989;
eLibrary SPIN: 9777-2067; e-mail: drugya@yandex.ru

ОБ АВТОРАХ

*** Панина Ольга Юрьевна,**
адрес: Россия, 127051, Москва, ул. Петровка, д. 24, стр. 1;
ORCID: https://orcid.org/0000-0002-8684-775X;
eLibrary SPIN: 5504-8136; e-mail: o.panina@npcmr.ru

Васильев Юрий Александрович, к.м.н.;
ORCID: https://orcid.org/0000-0002-0208-5218;
eLibrary SPIN: 4458-5608; e-mail: dr.vasilev@me.com

Грик Евгения Андреевна;
ORCID: http://orcid.org/0000-0002-7908-3982;
eLibrary SPIN: 5558-7307; e-mail: evgeniyagrik@gmail.com

Ахмад Екатерина Сергеевна;
ORCID: http://orcid.org/0000-0002-8235-9361;
eLibrary SPIN: 5891-4384; e-mail: e.ahmad@npcmr.ru

Васильева Юлия Николаевна, к.м.н.;
ORCID: http://orcid.org/0000-0002-1066-3989;
eLibrary SPIN: 9777-2067; e-mail: drugya@yandex.ru

* Corresponding author / Автор, ответственный за переписку

DOI: https://doi.org/10.17816/DD62572

Двухэнергетическая компьютерная томография рака головы и шеи

В.С. Петровичев[1], М.В. Неклюдова[1], В.Е. Синицын[2], И.Г. Никитин[1]

[1] Национальный медицинский исследовательский центр «Лечебно-реабилитационный центр», Москва, Российская Федерация
[2] Московский государственный университет имени М.В. Ломоносова, Москва, Российская Федерация

АННОТАЦИЯ

Выполнен обзор публикаций по диагностике рака области головы и шеи методом двухэнергетической компьютерной томографии (ДЭКТ); изучены результаты качественного и количественного анализа данных, полученных методом ДЭКТ с внутривенным контрастированием при опухолях данной локализации; показана важность построения йодных карт для получения дополнительной диагностической информации; описаны аспекты улучшения визуализации орофарингеальной области на фоне артефактов от стоматологических имплантатов. Ряд приведённых в статье научных работ освещает современное состояние вопроса и роль постпроцессинга «сырых данных» ДЭКТ, получения диапазона монохроматических изображений опухолевых и иных патологических изменений области головы и шеи, в том числе сравниваются ДЭКТ с внутривенным контрастированием и рутинная компьютерная томография с точки зрения уменьшения лучевой нагрузки на пациентов, в частности за счёт получения в ходе постобработки виртуальных нативных диагностических изображений из контрастной серии объёмов ДЭКТ. Обзор, помимо последних актуальных научных данных, включает также ссылки на работы по истории развития ДЭКТ как метода. Кратко изложены физические принципы, лежащие в основе ДЭКТ, и перспективы развития метода.

Ключевые слова: двухэнергетическая компьютерная томография; спектральная компьютерная томография; ДЭКТ; рак головы и шеи; плоскоклеточный рак.

Как цитировать

Петровичев В.С., Неклюдова М.В., Синицын В.Е., Никитин И.Г. Двухэнергетическая компьютерная томография рака головы и шеи // *Digital Diagnostics.* 2021. Т. 2, № 3. С. 343–355. DOI: https://doi.org/10.17816/DD62572

Рукопись получена: 03.03.2021 **Рукопись одобрена:** 15.06.2021 **Опубликована:** 01.07.2021

ЭКО•ВЕКТОР

DOI: https://doi.org/10.17816/DD62572

Dual-energy computed tomography for head and neck cancer

Victor S. Petrovichev[1], Marina V. Neklyudova[1], Valentin E. Sinitsyn[2], Igor G. Nikitin[1]

[1] Radiology Department, National Medical Research Treatment and Rehabilitation Centre of the Ministry of Health of Russia, Moscow, Russian Federation
[2] Lomonosov Moscow State University, Moscow, Russian Federation

ABSTRACT

This study reviewed the head and neck cancer diagnosis publications using dual-energy computed tomography (DECT). The qualitative and quantitative analysis of the data was DECT obtained using intravenous contrast enhancement for localized tumors, which shows the importance of constructing iodine maps for obtaining additional diagnostic information, described aspects of improving visualization of the oropharyngeal region against the background of artifacts from dental implants. Several research articles highlight the current state of the issue and the role of post-processing of "raw data" DECT, obtaining a range of monochromatic images of a tumor and other pathological changes in the head and neck region in the article. Several learned treatises were also reflected. DECT with intravenous contrast enhancement and routine computed tomography to reduce radiation exposure to patients were compared particularly due to the possibility of obtaining virtual native diagnostic images from a contrasting series of DECT volumes during post-processing. In addition, this review also includes references to works that highlight the development of DECT as the method. Finally, the physical principles underlying DECT and the prospects for the development of the method are briefly represented.

Keywords: dual energy computed tomography; spectral computed tomography; DECT; head and neck cancer; squamous cell carcinoma; SCC.

To cite this article
Petrovichev VS, Neklyudova MV, Sinitsyn VE, Nikitin IG. Dual-energy computed tomography for head and neck cancer. *Digital Diagnostics.* 2021;2(3):343–355. DOI: https://doi.org/10.17816/DD62572

Received: 03.03.2021 **Accepted:** 15.06.2021 **Published:** 01.07.2021

DOI: https://doi.org/10.17816/DD62572

双能计算机断层扫描用于头和颈癌

Victor S. Petrovichev[1], Marina V. Neklyudova[1], Valentin E. Sinitsyn[2], Igor G. Nikitin[1]

[1] Radiology Department, National Medical Research Treatment and Rehabilitation Centre of the Ministry of Health of Russia, Moscow, Russian Federation
[2] Lomonosov Moscow State University, Moscow, Russian Federation

简评

对使用双能计算机断层扫描（DECT）诊断头颈癌的出版物进行了审查； 研究了通过 DECT 方法获得的数据的定性和定量分析结果，并在该定位的肿瘤中进行了静脉对比增强； 显示了构建碘图以获得额外诊断信息的重要性； 描述了在牙种植体伪影的背景下改善口咽区域可视化的方面。 文章中介绍的许多科学作品强调了当前的技术水平和“原始数据”DECT 后处理的作用，获得了一系列头颈部肿瘤和其他病理变化的单色图像，包括将 DECT 与静脉造影增强和常规计算机断层扫描在减少患者辐射负荷方面进行比较，特别是由于在后处理期间从 DECT 体积的对比系列中获取虚拟原生诊断图像。 除了最新的相关科学数据外，该评论还包括对 DECT 作为一种方法的发展历史的著作的参考。 简要概述了 DECT 的物理原理和该方法的发展前景。

关键词：双能计算机断层扫描； 光谱计算机断层扫描； DECT; 头和颈癌； 鳞状细胞癌。

引用本文

Petrovichev VS, Neklyudova MV, Sinitsyn VE, Nikitin IG. 双能计算机断层扫描用于头和颈癌. *Digital Diagnostics*. 2021;2(3):343–355. DOI: https://doi.org/10.17816/DD62572

收到： 03.03.2021 **接受：** 15.06.2021 **发布日期：**01.07.2021

BACKGROUND

The importance of early diagnosis in head and neck cancer stems from the pathology's dominance in the morbidity structure of malignant neoplasms worldwide [1]. In Russia, the number of patients with newly diagnosed malignant neoplasms of the head and neck region is steadily increasing [2].

Obviously, clinical and endoscopic examinations allow for evaluation of the mucosa of the oral cavity and tongue, as well as the larynx and pharynx. However, the submucosal areas remain unprotected. Moreover, exophytic and endophytic growth can occur in squamous cell cancer, but a mixed type is more common. If a primary or recurrent tumor is found in the mucosa, the submucosal component cannot be reliably assessed (only indirectly through palpation) [3, 4]. Following chemoradiotherapy, a zone of vitreous edema develops, altering the normal anatomy, appearance, and density of the mucosa. Because of their thickening and increase in volume, the root of the tongue, parapharyngeal and paraesophageal areas, and laryngeal and laryngopharyngeal elements may cause dysphagia and dyspnea and complicate endoscopic examination [5]. After immunotherapy of head and neck squamous cell cancer, pseudoprogression is possible, particularly an increase in tumor size and extent, which requires strict dynamic control to rule out true disease progression [6, 7]. All this necessitates the use of objective dynamic monitoring methods such as computed tomography (CT) and magnetic resonance imaging (MRI). Due to a lack of scanners to cover the population and the higher cost of the study, hybrid imaging techniques (positron emission tomography or single-photon emission computed tomography combined with CT) are less accessible. In addition, the timing of hybrid diagnosis during treatment is limited. Thus, for a more reliable differentiation between inflammatory and tumor changes, at least 3 months should elapse after chemoradiotherapy and surgery [8, 9].

MRI is a useful tool for detecting head and neck tumors. The application of current basic pulse sequences resolves a variety of diagnostic issues. Thus, T1, contrast-enhanced T1-weighted images, and T2 weighted sequences and fat-suppressed sequences are the best for visualizing inflammatory changes, staging tumor lesions, and revealing developmental embryonic tumors. Vascular and perfusion sequences are used to rule out vascular malformations and assess microcirculatory parameters of tissue perfusion. Diffusion-weighted images may be useful for imaging cholesteatomas, assessing malignancy and treatment response, and detecting recurrent or residual tumors in head and neck cancers [10, 11]. Aside from the obvious advantages of the method, the time required to perform a full MRI, including various pulse sequences, is longer than CT, limiting the scanner's throughput and the number of possible examinations within a day.

CURRENT DUAL-ENERGY IMAGING TECHNIQUES

The physical methods that underpin the interaction of X-rays with substance and provide a dual-energy scanning are the photoelectric effect, Compton effect, and Thomson scattering.

The fundamental principle of dual-energy computed tomography (DECT) is based on the fact that different anatomical structures and tissues may have the same or different density depending on the X-ray energy under which they are exposed, that is, in the range between high and low kW values. The primary advantage of using dual-energy systems is the ability to decompose the images into underlying materials. In this case, different attenuations at various X-ray energies are recorded. This reveals how much of each material is present in a particular voxel of the image and expands the possibilities for postprocessing the obtained image volumes (Figure). For example, the construction of virtual non-contrast images, subtraction of bone structures, and analysis of radiopaque stones are possible. In addition, iodine maps with isolated iodine images may be generated.

The DECT method has been known since the early days of CT, but its applications were mostly limited to determining bone mineral density [12, 13]. Recently, DECT has been introduced into clinical practice to examine patients with malignant head and neck tumors. When scanning, this method employs either scanners with two energy sources or rapid current switching on the tomograph X-ray tube.

DUAL-ENERGY TOMOGRAPHY OF THE HEAD AND NECK REGION

An early scientific paper discovered no statistically significant difference in the quality of anatomical images of the head and neck region when using dual-energy (80 and 140 kW tube currents) versus routine multispiral computed tomography (MSCT, 120 kW tube current). In addition, a lower radiation load on patients was observed in DECT [14]. Concurrently, since 2010, numerous studies have been conducted to evaluate the dual-energy computed angiography possibilities of the brachycephalic arterial pathology [15–25]. According to A. Schwahofer et al. [26], the use of monoenergetic reconstructions obtained during DECT volume post processing allows to reduce artifacts from metal in the oral cavity only if the density of the latter does not exceed 4.5 g/cm^3 (e.g., titanium or aluminum). This has little application in calculating total radiation dose; however, it may be useful for delineating anatomical landmarks of the area of interest when planning radiotherapy. For artifacts from dental metal with a source density of >4.5 g/cm^3, only a slight reduction in artifacts was observed. The majority of the patients included had metal-containing dentures or other dental hardware with an even higher density (>10 g/cm^3). Thus, monoenergetic reconstructions are not

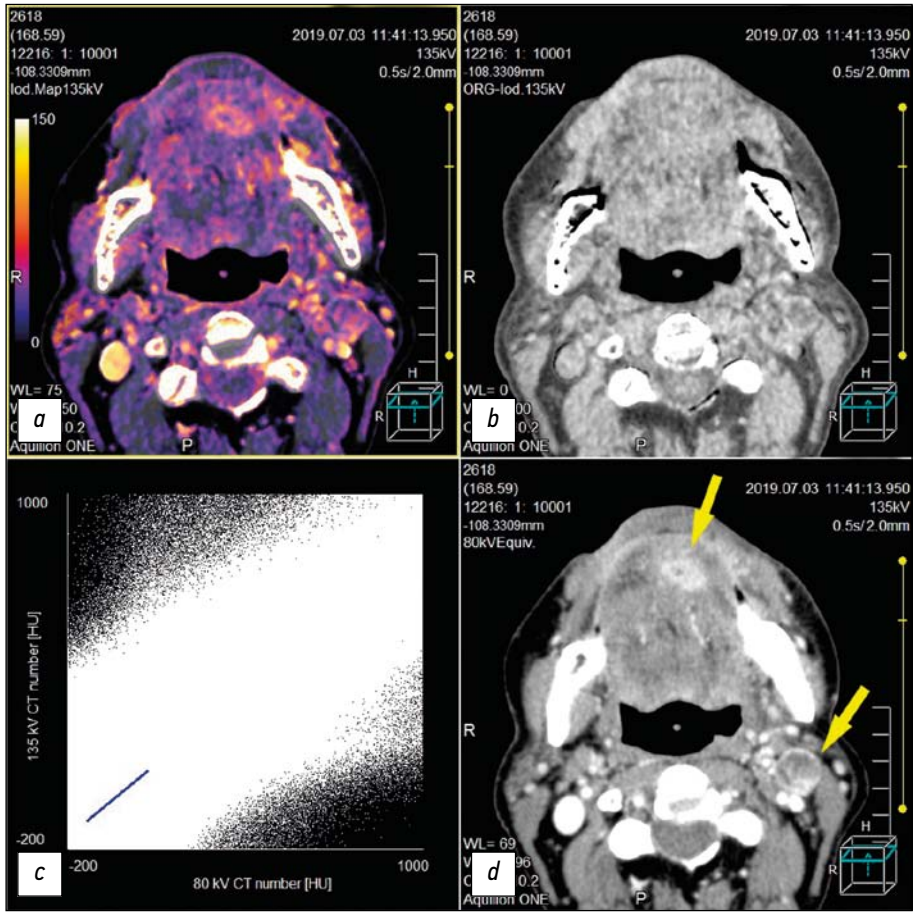

Fig. Dual-energy computed tomography after chemo radiotherapy for squamous cell cancer of the mouth floor that had spread to the tongue. Residual tumor on the lower surface of the tongue and metastasis with decay to the submandibular lymph node on the left (yellow arrows). *a*, iodine map; *b*, virtual non-contrast image; *c*, pixel distribution plot for an individual slice between high and low kV values; *d*, monochromatic image with a low value equal to 80 kV

a universal tool for reducing metal artifacts in radiotherapy planning [26].

In contrast, J. Weiβ et al. [27] reported that the iterative metal artifact reduction mode allows for improved visualization of the oral cavity area and surrounding anatomical structures in the presence of dental implant artifacts. The images and diagnostic significance were assessed both qualitatively according to the Likert scale and quantitatively using Hounsfield units (HU). The study discovered that in 30 cases, using metal artifact reduction made images more informative when compared to not using this mode (3.8 ± 0.5 versus 2.6 ± 0.5, respectively; $p < 0.0001$). When the degree of artifacts was quantified using HU, correlated results were obtained. The findings for metal artifact reduction were significantly lower than for standard reconstruction (0.9 ± 1.6 versus 20 ± 47, respectively; $p < 0.05$) [27].

According to N. Große Hokamp et al. [28], hypo- and hyperattenuating artifacts in virtual monoenergetic images (VMI) with high kiloelectronvolt (keV) values showed increased and decreased HU values compared to conventional CT imaging (CI) (CI/$VMI_{200\ keV}$: –218.7/–174.4 HU, $p = 0.1$ and 309.8/119.2, $p = 0.05$, respectively). In addition, artifacts in fat decreased on VMI with high keV values (CI/$VMI_{200\ keV}$: 23.9/16.4, $p = 0.05$). Moreover, a qualitative decrease in superdense artifacts on VMI with high (≥100) keV values (e.g., CI/$VMI_{200\ keV}$: 2(1-3)/3(1-5), $p = 0.05$) was observed. Reduced artifact evidence improved imaging of the soft palate and cheeks (e.g., CI/$VMI_{200\ keV}$: 2(1-4)/3(1-5) and 2(1-5)/3(1-5), $p \leq 0.05$). In general, VMI obtained during postprocessing of DECT volumes reduces the intensity of artifacts from dental implants and improves diagnosis of the surrounding soft tissues [28].

Another study found that using high-energy VMI reduces artifacts while weakening the visualization of iodine-containing contrast agents in tumor tissue. In general, high-energy VMI (<100 keV) as useful additional diagnostic images for assessing head and neck cancer may achieve a moderate reduction in artifacts while maintaining sufficient visualization of iodine-containing contrast agents [29]. This is supported by the study of E. Liao [30], which found that DECT improves visualization of the head, neck, and spine in the presence of artifacts from metal implants. According to some other authors, spectral CT improves radial diagnosis of malignant head and neck neoplasms [31–36].

A.M. Tawfik et al. [37] conducted a study to improve imaging of head and neck tumors. This included the assessment

of images obtained with different weighting factors (0.3, 0.6, and 0.8) for 80 and 140 kW, as well as the assessment of tumor lines. The study included 35 people with malignant head and neck neoplasms who were selected from a group of 60 patients with suspected cancer. The authors compared such parameters as signal-to-noise ratio, signal attenuation measurements, and objective noise between different sets of head and neck images. The results were analyzed by two independent radiologists who assessed the following parameters on a five-point scale: lesion contours, image sharpness, and subjective noise. The scientists concluded that combining DECT diagnostic data obtained at 80 kW and 140 kW tube currents with a weighting factor of 0.6 (60% of the 80 kW data) improves the signal-to-noise ratio from the tumor focus and subjectively increases the overall image quality, including tumor borders. This weighting factor showed more diagnostic information than the 0.3 coefficient, which simulates current values on a 120 kW tube and is as close as possible to standard MSCT images [37].

According to M. Li et al. [38], using DECT to analyze material composition in conjunction with reconstructed monochromatic images has a promising potential for differential diagnosis of thyroid nodules and tumor grade clarification.

When assessing the local spread of laryngeal cancer, determination of the degree of thyroid cartilage invasion is critical. In the study of this diagnostic problem, the invasion degree was assessed on a five-point scale: true invasion began with erosion (3 points) and ended with cartilage invasion (5 points). These data were used to generate iodine maps and weighted average images. Further, weighted average images and iodine maps had 100% sensitivity, specificity, and accuracy in assessing thyroid cartilage invasion. In only one case, the weighted average images missed the complete invasion of the thyroid cartilage by squamous cell cancer of the laryngeal fold; however, the prevalence was clarified on the iodine maps [39].

The potential of the method in assessing the cartilaginous structure of the larynx was described in several other studies. In particular, R. Forghani et al. [40] noted differences in signal attenuation on VMI (≥ 95 keV) of head and neck squamous cell cancer versus unossified thyroid cartilage of the larynx. In another study, a group of scientists from Japan and the United States compared MRI and DECT in assessing the cartilaginous structure of the larynx in general and the thyroid cartilage in particular in head and neck squamous cell cancer. DECT had a higher specificity when compared to MRI. Such data were obtained for both the invasion of the entire cartilaginous structure of the larynx (84% for MRI versus 98% for DECT, $p < 0.004$) and the thyroid cartilage (64% versus 100%, respectively, $p < 0.001$). The mean area under ROC curve (0.94 vs. 0.95, $p = 0.70$) was calculated. The sensitivity of the methods for a similar task was not significantly different for the entire cartilaginous structure of the larynx (97% for MRI versus 81% for DECT, $p = 0.16$) and separately for the thyroid cartilage (100% versus 89%, respectively, $p = 0.50$); however, there was a tendency toward a higher sensitivity for MRI. DECT allows for the avoidance of overestimation of the extent of laryngeal cartilage invasion caused by inflammatory changes. This is achieved by employing appropriate diagnostic criteria on weighted average images and iodine maps for both ossified and unossified laryngeal cartilage. Concurrently, DECT may miss small tumor invasion of ossified laryngeal cartilages, which determines the efficiency of the method precisely in the absence of overestimation of the invasion degree of cartilaginous structure of the larynx and thus contributes to the growth of organ-preserving approaches to the treatment of laryngeal and laryngopharyngeal squamous cell cancer [41].

J.L. Wichmann et al. [42] investigated the diagnostic accuracy of a series of DECT images (80 kW and linear-mixed 120 kW) in 170 cases of various head and neck pathologies. Subsequent analyses were carried out by three independent radiologists who had been referred for clinical trials. Other data, such as images from other diagnostic modalities, were not available to the examiners. The findings were compared with medical records, CT scans, and histologic reports. Sensitivity, specificity, positive predictive value, and negative predictive value were calculated separately for each examiner. Agreement between radiologists was assessed by using intraclass correlation coefficients. The following clinical nosologies were assigned to the diagnostic groups: squamous cell cancer ($n = 107$; presence/absence for primary/recurrent squamous cell cancer), lymphoma ($n = 40$; presence/absence for primary/recurrent lymphoma), and benign diseases ($n = 23$; e.g., abscess). For the 80 kW imaging series and the 120 kW line-mixed images, the cumulative sensitivity, specificity, positive predictive value, and negative predictive value were 94.8, 93.0, 95.9, and 91.1, respectively. Moreover, the results (%) for the group of patients with squamous cell cancer were extremely high (94.8/95.3, 89.1/89.1, 94.3/94.4, and 90.1/91.0); a similar pattern with lymphoma-related disease (95.0, 100.0, 100.0, and 95.2 for the 80/120 kW image series) was noted. The agreement between investigators was nearly perfect (intraclass correlation coefficients of 0.82 and 0.80; 95% CI: 0.76–0.74 and 0.86–0.85). The absorbed dose per scan length was approximately 48% lower at 80 kW when compared to standard 120 kW scans (135.5 versus 282.2 mGy/cm). The researchers concluded that low-kilovoltage CT (80 kW) has high resolution, providing good diagnostic accuracy for routine clinical practice while significantly reducing the radiation load on the patient [42].

Several other studies provided similar evidence of improved imaging of primary head and neck cancers in DECT data postprocessing with two energy sources when constructing nonlinear image mixing compared to linear image mixing at low and high energies (80/140 kW) [43]. According to S. Lam et al. [44], the optimal soft tissue imaging of the head and neck region on VMI is at 65 keV, while the optimal contrast-to-noise ratio for squamous cell cancer imaging

is at 40 keV. This is because there is a difference in signal attenuation between the tumor and unaffected surrounding soft tissues ($p = 0.03$).

A group of scientists from China investigated the use of DECT in the detection and differential diagnosis of metastatically affected cervical lymph nodes in squamous cell head and neck cancer and other lymphoproliferative diseases. The authors concluded that optimal visualization of the affected lymph nodes was achieved on 70 keV monoenergetic images. In addition, the study design included the slope of the spectral curve of soft tissue radiability for iodine molecules depending on the kW value [45]. According to F. Fu et al. [46], virtual noncontrast images obtained in DECT postprocessing for visualization of metastatically affected cervical lymph nodes are of comparable quality to a full-scale native study. Moreover, such images have a lower effective dose of radiation to the patient when compared to the standard native study ($p < 0.05$). The combination of DECT with intravenous contrast enhancement and subsequent construction of virtual native images allows adequate visualization of the secondary affected lymph nodes with a lower radiation exposure to the patient [46].

R. Forghani (Canada) [47] compared the reconstructions and postprocessing potential of DECT with one energy source and fast switching kilovoltage (kW) on an X-ray tube and DECT with two energy sources and suggested that post processing be used for optimal imaging of soft neck tissues. Thus, virtual monoenergetic reconstructions for all neck area scans were performed at 65 and 40 keV minimum; for laryngeal tumor diagnosis, similar reconstructions and iodine mapping and virtual monoenergetic reconstructions at 95 keV (or at higher values) were used. The author proposes using all of the above, except for iodine maps, to visualize tumors of the oral cavity and oropharynx and reduce dental artifacts [47]. Further, another group of scientists provides comparable data [48].

The differential diagnosis of spectral imaging in the exclusion of residual or recurrent tumors after special treatment is given in the study of the international group of authors. Thus, according to a small cohort study by Yamauchi et al. [49], when comparing virtual monoenergetic reconstructions at 40 and 70 keV, the former allows for a better differential diagnosis of recurrent or residual tumors from benign changes caused by the performed treatment. In addition, L. Yang et al. [50] discovered differences in iodine concentration, water, and spectral curve slope in affected cervical lymph nodes from patients with various nosological diseases, including thyroid and salivary gland cancer, lymphoma, and squamous cell cancer.

M.S. May et al. [51] compared dual-energy and monoenergy (70 kW) DECT scanning with two energy sources in patients with head and neck cancer. When constructing monoenergetic reconstructions at 40 keV, the former allows for better visualization of tumor borders, whereas a 70-kW monoenergetic scanning is appropriate to reduce artifacts in the presence of metal implants in the oral cavity. A group of Canadian scientists found similar results when comparing dual-energy and standard CT scanning of patients with squamous cell head and neck cancer [52].

According to R. Forghani et al. [53–55], various DECT reconstructions combined with subsequent quantitative analysis may improve the characteristics of tissue assessment and tumor imaging, including invasion into anatomical structures, which may impact patient management. L. Yang et al. [56] used DECT to assess therapeutic response to chemoradiotherapy in two groups of patients with laryngeal and pharyngeal cancer in complete and incomplete remission. The spectral curve had a different slope depending on whether or not residual tumor was. A ROC analysis of diagnostic efficiency showed an area under the curve of 0.83. When assessing the effects for esophageal cancer radiation therapy before and after, a group of other scientists proposed that the construction of iodine maps in DECT postprocessing allows them to assess iodine concentration in both cases. In addition, the effect of chemoradiation therapy may be analyzed while avoiding an increased radiation dose during treatment [57].

An interesting method for assessing nasopharyngeal cancer in DECT was proposed by measuring the concentration of gold nanoparticles that were attached to folic acid as a linker. DECT has the ability to decompose the studied material, allowing for the separation and identification of different elements in the examined tissues, particularly gold nanoparticles. Actually, this diagnostic method is molecular targeted imaging of nasopharyngeal cancer cells [58].

Recently, machine learning has gained prominence in the treatment of head and neck cancer. One group of authors described the advantages of the automated multi-energy texture analysis of soft tissues of all image series compared to the analysis of individual monoenergetic reconstructions to predict metastatic lesions of loco regional lymph nodes [59]. Another group of scientists studied the DECT potential in assessing lymph nodes in the neck region in various neoplastic lesions using machine learning, including lymphoproliferative diseases [60]. This research avenue is both scientific and practical in nature, and it merits further study.

CONCLUSIONS

Thus, in addition to the examination of patients with suspected head and neck cancer, DECT with intravenous bolus contrast provides more detailed information when compared to conventional contrast MSCT. DECT enables the decomposition of the obtained images into underlying materials, in particular, to obtain both isolated and mixed iodine maps of the area of interest, i.e., tumors and metastatically affected regional lymph nodes. This information may be of diagnostic value in dynamic examination of patients following special antitumor treatment, such as remote radiation, chemotherapy, and immunotherapy.

ADDITIONAL INFORMATION

Funding source. This study was not supported by any external sources of funding.

Competing interests. The authors declare no obvious and potential conflicts of interest related to the publication of this article.

Authors' contribution. V.S. Petrovichev — literature review, collection and analysis of literary sources, text writing and article editing; M.V. Neklyudova — review of literature, preparation and writing of the text of the article; V.E. Sinitsyn — literature review, collection and analysis of literary sources, preparation and editing of the article; I.G. Nikitin — collection and analysis of literary sources, article editing. All authors made a substantial contribution to the conception of the work, acquisition, analysis, interpretation of data for the work, drafting and revising the work, final approval of the version to be published and agree to be accountable for all aspects of the work.

Acknowledgements. The authors express their gratitude to Nataliya G. Pokrovskaya for support in stylistic editing of the article text.

REFERENCES

1. Bray F, Ferlay J, Soerjomataram I, et al. Global cancer statistics 2018: GLOBOCAN estimates of incidence and mortality worldwide for 36 cancers in 185 countries. *CA: A Cancer Journal for Clinicians*. 2018;68(6):394–424. doi: 10.3322/caac.21492

2. Socially significant diseases of the Russian population in 2018. Statistical materials. Moscow; 2019. P. 15–17. (In Russ).

3. Pynnonen MA, Gillespie MB, Roman B, et al. Clinical practice guideline: evaluation of the neck mass in adults. *Otolaryngol Head Neck Surg*. 2017;157(2 Suppl):S1–S30. doi: 10.1177/0194599817722550

4. Mannelli G, Cecconi L, Gallo O. Laryngeal preneoplastic lesions and cancer: challenging diagnosis. Qualitative literature review and meta-analysis. *Critical Reviews in Oncology Hematology*. 2016;106:64–90. doi: 10.1016/j.critrevonc.2016.07.004

5. Hinther A, Samson N, Lau H, et al. Volumetric changes in pharyngeal structures following head and neck cancer chemoradiation therapy. *The Laryngoscope*. 2020;130(3):597–602. doi: 10.1002/lary.28164

6. Baxi SS, Dunn LA, Burtness BA. Amidst the excitement: A cautionary tale of immunotherapy, pseudoprogression and head and neck squamous cell carcinoma. *Oral Oncology*. 2016;62:147–148. doi: 10.1016/j.oraloncology. 2016.10.007

7. Szturz P, Vermorken JB. Immunotherapy in head and neck cancer: aiming at EXTREME precision. *BMC Med*. 2017;15(1):110. doi: 10.1186/s12916-017-0879-4

8. Abgral R, Querellou S, Potard G, et al. Does 18f-fdg pet/ct improve the detection of posttreatment recurrence of head and neck squamous cell carcinoma in patients negative for disease on clinical follow-up? *Journal of Nuclear Medicine*. 2008;50(1):24–29. doi: 10.2967/jnumed.108.055806

9. Greven KM, Williams DW, Keyes JW, et al. Positron emission tomography of patients with head and neck carcinoma before and after high dose irradiation. *Cancer*. 1994;74(4):1355–1359. doi: 10.1002/1097-0142(19940815)74:4<1355::aid-cncr2820740428>3.0.co;2-i

10. Widmann G, Henninger B, Kremser C, Jaschke W. MRI sequences in head & neck radiology – state of the art. *Fortschr Röntgenstr*. 2017;189(05):413–422. doi: 10.1055/s-0043-103280

11. Dai YL, King AD. State of the art MRI in head and neck cancer. *Clinical Radiology*. 2018;73(1):45–59. doi: 10.1016/j.crad.2017.05.020

12. Genant HK, Boyd D. Quantitative bone mineral analysis using dual energy computed tomography. *Investigative Radiology*. 1977;12(6):545–551. doi: 10.1097/00004424-197711000-00015

13. Raymakers JA, Hoekstra O, van Putten J, et al. Fracture prevalence and bone mineral mass in osteoporosis measured with computed tomography and dual energy photon absorptiometry. *Skeletal Radiol*. 1986;15(3):191–197. doi: 10.1007/BF00354059

14. Tawfik AM, Kerl JM, Razek AA, et al. Image quality and radiation dose of dual-energy ct of the head and neck compared with a standard 120-kvp acquisition. *AJNR Am J Neuroradiol*. 2011;32(11):1994–1999. doi: 10.3174/ajnr.A2654

15. Deng K, Liu C, Ma R, et al. Clinical evaluation of dual-energy bone removal in CT angiography of the head and neck: comparison with conventional bone-subtraction CT angiography. *Clinical Radiology*. 2009;64(5):534–541. doi: 10.1016/j.crad.2009.01.007

16. Lell MM, Kramer M, Klotz E, et al. Carotid computed tomography angiography with automated bone suppression: a comparative study between dual energy and bone subtraction techniques. *Investigative Radiology*. 2009;44(6):322–328. doi: 10.1097/RLI.0b013e31819e8ad9

17. Thomas C, Korn A, Krauss B, et al. Automatic bone and plaque removal using dual energy CT for head and neck angiography: Feasibility and initial performance evaluation. *European Journal of Radiology*. 2010;76(1):61–67. doi: 10.1016/j.ejrad.2009.05.004

18. Lell MM, Hinkmann F, Nkenke E, et al. Dual energy CTA of the supraaortic arteries: Technical improvements with a novel dual source CT system. *European Journal of Radiology*. 2010;76(2):e6–e12. doi: 10.1016/j.ejrad.2009.09.022

19. Chen Y, Xue H, Liu W, et al. [Dual-energy computed tomographic angiography of head and neck arteries with different contrast material doses in second generation dual-source computed tomography system]. *Zhongguo Yi Xue Ke Xue Yuan Xue Bao*. 2010;32(6):628–633. doi: 10.3881/j.issn.1000.503X.2010.06.008

20. Korn A, Fenchel M, Bender B, et al. High-pitch dual-source CT angiography of supra-aortic arteries: assessment of image quality and radiation dose. *Neuroradiology*. 2013;55(4):423–430. doi: 10.1007/s00234-012-1120-y

21. Chen Y, Xue H, Jin Z, et al. 128-slice acceletated-pitch dual energy ct angiography of the head and neck: comparison of different low contrast medium volumes. *PLoS ONE*. 2013;8(11):e80939. doi: 10.1371/journal.pone.0080939

22. Korn A, Bender B, Schabel C, et al. Dual-source dual-energy ct angiography of the supra-aortic arteries with tin filter. *Academic Radiology*. 2015;22(6):708–713. doi: 10.1016/j.acra.2015.01.016

23. Kaemmerer N, Brand M, Hammon M, et al. Dual-energy computed tomography angiography of the head and neck with single-source computed tomography: a new technical (Split filter) approach for bone removal. *Invest Radiol*. 2016;51(10):618–623. doi: 10.1097/RLI.0000000000000290

24. Ma G, Yu Y, Duan H, et al. Subtraction CT angiography in head and neck with low radiation and contrast dose dual-energy spectral CT using rapid kV-switching technique. *BJR*. 2018;20170631. doi: 10.1259/bjr.20170631
25. Wu Q, Shi D, Cheng T, et al. Improved display of cervical intervertebral discs on water (Iodine) images: incidental findings from single-source dual-energy CT angiography of head and neck arteries. *Eur Radiol*. 2019;29(1):153–160. doi: 10.1007/s00330-018-5603-z
26. Schwahofer A, Bär E, Kuchenbecker S, et al. The application of metal artifact reduction (Mar) in CT scans for radiation oncology by monoenergetic extrapolation with a DECT scanner. *Zeitschrift für Medizinische Physik*. 2015;25(4):314–325. doi: 10.1016/j.zemedi.2015.05.004
27. Weiß J, Schabel C, Bongers M, et al. Impact of iterative metal artifact reduction on diagnostic image quality in patients with dental hardware. *Acta Radiol*. 2017;58(3):279–285. doi: 10.1177/0284185116646144
28. Große Hokamp N, Laukamp KR, Lennartz S, et al. Artifact reduction from dental implants using virtual monoenergetic reconstructions from novel spectral detector CT. *European Journal of Radiology*. 2018;104:136–142. doi: 10.1016/j.ejrad.2018.04.018
29. Nair JR, DeBlois F, Ong T, et al. Dual-energy ct: balance between iodine attenuation and artifact reduction for the evaluation of head and neck cancer. *Journal of Computer Assisted Tomography*. 2017;41(6):931–936. doi: 10.1097/RCT.0000000000000617
30. Liao E, Srinivasan A. Applications of dual-energy computed tomography for artifact reduction in the head, neck, and spine. *Neuroimaging Clinics of North America*. 2017;27(3):489–497. doi: 10.1016/j.nic.2017.04.004
31. Vogl TJ, Schulz B, Bauer RW, et al. Dual-energy ct applications in head and neck imaging. *American Journal of Roentgenology*. 2012;199(5 Suppl):S34–S39. doi: 10.2214/AJR.12.9113
32. Srinivasan A, Parker RA, Manjunathan A, et al. Differentiation of benign and malignant neck pathologies: preliminary experience using spectral computed tomography. *Journal of Computer Assisted Tomography*. 2013;37(5):666–672. doi: 10.1097/RCT.0b013e3182976365
33. Tawfik AM, Razek AA, Kerl JM, et al. Comparison of dual-energy CT-derived iodine content and iodine overlay of normal, inflammatory and metastatic squamous cell carcinoma cervical lymph nodes. *Eur Radiol*. 2014;24(3):574–580. doi: 10.1007/s00330-013-3035-3
34. Kuno H, Onaya H, Fujii S, et al. Primary staging of laryngeal and hypopharyngeal cancer: CT, MR imaging and dual-energy CT. *European Journal of Radiology*. 2014;83(1):e23–e35. doi: 10.1016/j.ejrad.2013.10.022
35. Toepker M, Czerny C, Ringl H, et al. Can dual-energy CT improve the assessment of tumor margins in oral cancer? *Oral Oncology*. 2014;50(3):221–227. doi: 10.1016/j.oraloncology.2013.12.001
36. Ginat DT, Mayich M, Daftari-Besheli L, Gupta R. Clinical applications of dual-energy CT in head and neck imaging. *Eur Arch Otorhinolaryngol*. 2016;273(3):547–553. doi: 10.1007/s00405-014-3417-4
37. Tawfik AM, Kerl JM, Bauer RW, et al. Dual-energy CT of head and neck cancer: average weighting of low- and high-voltage acquisitions to improve lesion delineation and image quality –initial clinical experience. *Investigative Radiology*. 2012;47(5):306–311. doi: 10.1097/RLI.0b013e31821e3062
38. Li M, Zheng X, Li J, et al. Dual-energy computed tomography imaging of thyroid nodule specimens: comparison with pathologic findings. *Investigative Radiology*. 2012;47(1):58–64. doi: 10.1097/RLI.0b013e318229fef3
39. Kuno H, Onaya H, Iwata R, et al. Evaluation of cartilage invasion by laryngeal and hypopharyngeal squamous cell carcinoma with dual-energy CT. *Radiology*. 2012;265(2):488–496. doi: 10.1148/radiol.12111719
40. Forghani R, Levental M, Gupta R, et al. Different spectral hounsfield unit curve and high-energy virtual monochromatic image characteristics of squamous cell carcinoma compared with nonossified thyroid cartilage. *AJNR Am J Neuroradiol*. 2015;36(6):1194–1200. doi: 10.3174/ajnr.A4253
41. Kuno H, Sakamaki K, Fujii S, et al. Comparison of MR imaging and dual-energy CT for the evaluation of cartilage invasion by laryngeal and hypopharyngeal squamous cell carcinoma. *AJNR Am J Neuroradiol*. 2018;39(3):524–531. doi: 10.3174/ajnr.A5530
42. Wichmann JL, Kraft J, Nöske EM, et al. Low-tube-voltage 80-kvp neck ct: evaluation of diagnostic accuracy and interobserver agreement. *AJNR Am J Neuroradiol*. 2014;35(12):2376–2381. doi: 10.3174/ajnr.A4052
43. Scholtz JE, Hüsers K, Kaup M, et al. Non-linear image blending improves visualization of head and neck primary squamous cell carcinoma compared to linear blending in dual-energy CT. *Clinical Radiology*. 2015;70(2):168–175. doi: 10.1016/j.crad.2014.10.018
44. Lam S, Gupta R, Levental M, et al. Optimal virtual monochromatic images for evaluation of normal tissues and head and neck cancer using dual-energy CT. *AJNR Am J Neuroradiol*. 2015;36(8):1518–1524. doi: 10.3174/ajnr.A4314
45. Wang X, Zhao Y, Wu N, et al. [Application of single-source dual-energy spectral CT in differentiating lymphoma and metastatic lymph nodes in the head and neck]. *Zhonghua Zhong Liu Za Zhi*. 2015;37(5):361–366.
46. Fu F, He A, Zhang Y, et al. Dua-energy virtual noncontrast imaging in diagnosis of cervical metastasis lymph nodes. *J Can Res Ther*. 2015;11(6):202. doi: 10.4103/0973-1482.168185
47. Forghani R. Advanced dual-energy CT for head and neck cancer imaging. *Expert Review of Anticancer Therapy*. 2015;15(12):1489–1501. doi: 10.1586/14737140.2015.1108193
48. Lam S, Gupta R, Kelly H, et al. Multiparametric evaluation of head and neck squamous cell carcinoma using a single-source dual-energy CT with fast kVp switching: state of the art. *Cancers*. 2015;7(4):2201–2216. doi: 10.3390/cancers7040886
49. Yamauchi H, Buehler M, Goodsitt MM, et al. Dual-energy CT-based differentiation of benign posttreatment changes from primary or recurrent malignancy of the head and neck: comparison of spectral hounsfield units at 40 and 70 kev and iodine concentration. *American Journal of Roentgenology*. 2016;206(3):580–587. doi: 10.2214/AJR.15.14896
50. Yang L, Luo D, Li L, et al. Differentiation of malignant cervical lymphadenopathy by dual-energy CT: a preliminary analysis. *Sci Rep*. 2016;6(1):31020. doi: 10.1038/srep31020
51. May MS, Bruegel J, Brand M, et al. Computed tomography of the head and neck region for tumor staging – comparison of dual-source, dual-energy and low-kilovolt, single-energy acquisitions. *Invest Radiol*. 2017;52(9):522–528. doi: 10.1097/RLI.0000000000000377
52. Forghani R, Kelly H, Yu E, et al. Low-energy virtual monochromatic dual-energy computed tomography images for the evaluation of head and neck squamous cell carcinoma: a study of tumor visibility compared with single-energy computed tomography

and user acceptance. *Journal of Computer Assisted Tomography*. 2017;41(4):565–571. doi: 10.1097/RCT.0000000000000571
53. Forghani R, Kelly HR, Curtin HD. Applications of dual-energy computed tomography for the evaluation of head and neck squamous cell carcinoma. *Neuroimaging Clinics of North America*. 2017;27(3):445–459. doi: 10.1016/j.nic.2017.04.001
54. Pérez-Lara A, Forghani R. Spectral computed tomography. *Magnetic Resonance Imaging Clinics of North America*. 2018;26(1):1–17. doi: 10.1016/j.mric.2017.08.001
55. Forghani R, Mukherji SK. Advanced dual-energy CT applications for the evaluation of the soft tissues of the neck. *Clinical Radiology*. 2018;73(1):70–80. doi: 10.1016/j.crad.2017.04.002
56. Yang L, Luo D, Yi J, et al. Therapy effects of advanced hypopharyngeal and laryngeal squamous cell carcinoma: evaluated using dual-energy CT quantitative parameters. *Sci Rep*. 2018;8(1):9064. doi: 10.1038/s41598-018-27341-0
57. Ge X, Yu J, Wang Z, et al. Comparative study of dual energy CT iodine imaging and standardized concentrations before and after chemoradiotherapy for esophageal cancer. *BMC Cancer*. 2018;18(1):1120. doi: 10.1186/s12885-018-5058-2
58. Khademi S, Sarkar S, Shakeri-Zadeh A, et al. Dual-energy CT imaging of nasopharyngeal cancer cells using multifunctional gold nanoparticles. *IET nanobiotechnol*. 2019;13(9):957–961. doi: 10.1049/iet-nbt.2019.0067
59. Forghani R, Chatterjee A, Reinhold C, et al. Head and neck squamous cell carcinoma: prediction of cervical lymph node metastasis by dual-energy CT texture analysis with machine learning. *Eur Radiol*. 2019;29(11):6172–6181. doi: 10.1007/s00330-019-06159-y
60. Seidler M, Forghani B, Reinhold C, et al. Dual-energy CT texture analysis with machine learning for the evaluation and characterization of cervical lymphadenopathy. *Computational and Structural Biotechnology Journal*. 2019;17:1009–1015. doi: 10.1016/j.csbj.2019.07.004

СПИСОК ЛИТЕРАТУРЫ

1. Bray F., Ferlay J., Soerjomataram I., et al. Global cancer statistics 2018: GLOBOCAN estimates of incidence and mortality worldwide for 36 cancers in 185 countries // CA: A Cancer Journal for Clinicians. 2018. Vol. 68, N 6. P. 394–424. doi: 10.3322/caac.21492
2. Социально значимые заболевания населения России в 2018 году. Статистические материалы. Москва, 2019. С. 15–17.
3. Pynnonen M.A., Gillespie M.B., Roman B., et al. Clinical practice guideline: evaluation of the neck mass in adults // Otolaryngol Head Neck Surg. 2017. Vol. 157, N 2, Suppl. P. S1–S30. doi: 10.1177/0194599817722550
4. Mannelli G., Cecconi L., Gallo O. Laryngeal preneoplastic lesions and cancer: challenging diagnosis. Qualitative literature review and meta-analysis // Critical Reviews in Oncology/Hematology. 2016. Vol. 106. P. 64–90. doi: 10.1016/j.critrevonc.2016.07.004
5. Hinther A., Samson N., Lau H., et al. Volumetric changes in pharyngeal structures following head and neck cancer chemoradiation therapy // The Laryngoscope. 2020. Vol. 130, N 3. P. 597–602. doi: 10.1002/lary.28164
6. Baxi S.S., Dunn L.A., Burtness B.A. Amidst the excitement: A cautionary tale of immunotherapy, pseudoprogression and head and neck squamous cell carcinoma // Oral Oncology. 2016. Vol. 62. P. 147–148. doi: 10.1016/j.oraloncology. 2016.10.007
7. Szturz P., Vermorken J.B. Immunotherapy in head and neck cancer: aiming at EXTREME precision // BMC Med. 2017. Vol. 15, N 1. P. 110. doi: 10.1186/s12916-017-0879-4
8. Abgral R., Querellou S., Potard G., et al. Does 18f-fdg pet/ct improve the detection of posttreatment recurrence of head and neck squamous cell carcinoma in patients negative for disease on clinical follow-up? // Journal of Nuclear Medicine. 2008. Vol. 50, N 1. P. 24–29. doi: 10.2967/jnumed.108.055806
9. Greven KM, Williams DW, Keyes JW, et al. Positron emission tomography of patients with head and neck carcinoma before and after high dose irradiation // Cancer. 1994. Vol. 74, N 4. P. 1355–1359. doi: 10.1002/1097-0142(19940815)74:4<1355::aid-cncr2820740428>3.0.co;2-i
10. Widmann G., Henninger B., Kremser C., Jaschke W. MRI sequences in head & neck radiology – state of the art // Fortschr Röntgenstr. 2017. Vol. 189, N 5. P. 413–422. doi: 10.1055/s-0043-103280
11. Dai Y.L., King A.D. State of the art MRI in head and neck cancer // Clinical Radiology. 2018. Vol. 73, N 1. P. 45–59. doi: 10.1016/j.crad.2017.05.020
12. Genant H.K., Boyd D. Quantitative bone mineral analysis using dual energy computed tomography // Investigative Radiology. 1977. Vol. 12, N 6. P. 545–551. doi: 10.1097/00004424-197711000-00015
13. Raymakers J.A., Hoekstra O., van Putten J., et al. Fracture prevalence and bone mineral mass in osteoporosis measured with computed tomography and dual energy photon absorptiometry // Skeletal Radiol. 1986. Vol. 15, N 3. P. 191–197. doi: 10.1007/BF00354059
14. Tawfik A.M., Kerl J.M., Razek A.A., et al. Image quality and radiation dose of dual-energy CT of the head and neck compared with a standard 120-kVp acquisition // AJNR Am J Neuroradiol. 2011. Vol. 32, N 11. P. 1994–1999. doi: 10.3174/ajnr.A2654
15. Deng K., Liu C., Ma R., et al. Clinical evaluation of dual-energy bone removal in CT angiography of the head and neck: comparison with conventional bone-subtraction CT angiography // Clinical Radiology. 2009. Vol. 64, N 5. P. 534–541. doi: 10.1016/j.crad.2009.01.007
16. Lell M.M., Kramer M., Klotz E., et al. Carotid computed tomography angiography with automated bone suppression: a comparative study between dual energy and bone subtraction techniques // Investigative Radiology. 2009. Vol. 44, N 6. P. 322–328. doi: 10.1097/RLI.0b013e31819e8ad9
17. Thomas C., Korn A., Krauss B., et al. Automatic bone and plaque removal using dual energy CT for head and neck angiography: Feasibility and initial performance evaluation // European Journal of Radiology. 2010. Vol. 76, N 1. P. 61–67. doi: 10.1016/j.ejrad.2009.05.004
18. Lell M.M., Hinkmann F., Nkenke E., et al. Dual energy CTA of the supraaortic arteries: Technical improvements with a novel dual source CT system // European Journal of Radiology. 2010. Vol. 76, N 2. P. e6–e12. doi: 10.1016/j.ejrad.2009.09.022
19. Chen Y., Xue H., Liu W., et al. [Dual-energy computed tomographic angiography of head and neck arteries with different contrast material doses in second generation dual-source computed tomography system] // Zhongguo Yi Xue Ke Xue Yuan Xue Bao. 2010. Vol. 32, N 6. P. 628–633. doi: 10.3881/j.issn.1000.503X.2010.06.008

20. Korn A., Fenchel M., Bender B., et al. High-pitch dual-source CT angiography of supra-aortic arteries: assessment of image quality and radiation dose // Neuroradiology. 2013. Vol. 55, N 4. P. 423–430. doi: 10.1007/s00234-012-1120-y
21. Chen Y., Xue H., Jin Z., et al. 128-slice acceletated-pitch dual energy ct angiography of the head and neck: comparison of different low contrast medium volumes // PLoS ONE. 2013. Vol. 8, N 11. P. e80939. doi: 10.1371/journal.pone.0080939
22. Korn A., Bender B., Schabel C., et al. Dual-source dual-energy ct angiography of the supra-aortic arteries with tin filter // Academic Radiology. 2015. Vol. 22, N 6. P. 708–713. doi: 10.1016/j.acra.2015.01.016
23. Kaemmerer N., Brand M., Hammon M., et al. Dual-energy computed tomography angiography of the head and neck with single-source computed tomography: a new technical (Split filter) approach for bone removal // Invest Radiol. 2016. Vol. 51, N 10. P. 618–623. doi: 10.1097/RLI.0000000000000290
24. Ma G., Yu Y., Duan H., et al. Subtraction CT angiography in head and neck with low radiation and contrast dose dual-energy spectral CT using rapid kV-switching technique // BJR. 2018. P. 20170631. doi: 10.1259/bjr.20170631
25. Wu Q., Shi D., Cheng T., et al. Improved display of cervical intervertebral discs on water (Iodine) images: incidental findings from single-source dual-energy CT angiography of head and neck arteries // Eur Radiol. 2019. Vol. 29, N 1. P. 153–160. doi: 10.1007/s00330-018-5603-z
26. Schwahofer A., Bär E., Kuchenbecker S., et al. The application of metal artifact reduction (MAR) in CT scans for radiation oncology by monoenergetic extrapolation with a DECT scanner // Zeitschrift für Medizinische Physik. 2015. Vol. 25, N 4. P. 314–325. doi: 10.1016/j.zemedi.2015.05.004
27. Weiβ J., Schabel C., Bongers M., et al. Impact of iterative metal artifact reduction on diagnostic image quality in patients with dental hardware // Acta Radiol. 2017. Vol. 58, N 3. P. 279–285. doi: 10.1177/0284185116646144
28. Große Hokamp N., Laukamp K.R., Lennartz S., et al. Artifact reduction from dental implants using virtual monoenergetic reconstructions from novel spectral detector CT // European Journal of Radiology. 2018. Vol. 104. P. 136–142. doi: 10.1016/j.ejrad.2018.04.018
29. Nair J.R., DeBlois F., Ong T., et al. Dual-energy ct: balance between iodine attenuation and artifact reduction for the evaluation of head and neck cancer // Journal of Computer Assisted Tomography. 2017. Vol. 41, N 6. P. 931–936. doi: 10.1097/RCT.0000000000000617
30. Liao E., Srinivasan A. Applications of dual-energy computed tomography for artifact reduction in the head, neck, and spine // Neuroimaging Clinics of North America. 2017. Vol. 27, N 3. P. 489–497. doi: 10.1016/j.nic.2017.04.004
31. Vogl T.J., Schulz B., Bauer R.W., et al. Dual-energy ct applications in head and neck imaging // American Journal of Roentgenology. 2012. Vol. 199, N 5, Suppl. P. S34–S39. doi: 10.2214/AJR.12.9113
32. Srinivasan A., Parker R.A., Manjunathan A., et al. Differentiation of benign and malignant neck pathologies: preliminary experience using spectral computed tomography // Journal of Computer Assisted Tomography. 2013. Vol. 37, N 5. P. 666–672. doi: 10.1097/RCT.0b013e3182976365
33. Tawfik A.M., Razek A.A., Kerl J.M., et al. Comparison of dual-energy CT-derived iodine content and iodine overlay of normal, inflammatory and metastatic squamous cell carcinoma cervical lymph nodes // Eur Radiol. 2014. Vol. 24, N 3. P. 574–580. doi: 10.1007/s00330-013-3035-3
34. Kuno H., Onaya H., Fujii S., et al. Primary staging of laryngeal and hypopharyngeal cancer: CT, MR imaging and dual-energy CT // European Journal of Radiology. 2014. Vol. 83, N 1. P. e23–e35. doi: 10.1016/j.ejrad.2013.10.022
35. Toepker M., Czerny C., Ringl H., et al. Can dual-energy CT improve the assessment of tumor margins in oral cancer? // Oral Oncology. 2014. Vol. 50, N 3. P. 221–227. doi: 10.1016/j.oraloncology.2013.12.001
36. Ginat D.T., Mayich M., Daftari-Besheli L., Gupta R. Clinical applications of dual-energy CT in head and neck imaging // Eur Arch Otorhinolaryngol. 2016. Vol. 273, N 3. P. 547–553. doi: 10.1007/s00405-014-3417-4
37. Tawfik A.M., Kerl J.M., Bauer R.W., et al. Dual-energy CT of head and neck cancer: average weighting of low- and high-voltage acquisitions to improve lesion delineation and image quality –initial clinical experience // Investigative Radiology. 2012. Vol. 47, N 5. P. 306–311. doi: 10.1097/RLI.0b013e31821e3062
38. Li M., Zheng X., Li J., et al. Dual-energy computed tomography imaging of thyroid nodule specimens: comparison with pathologic findings // Investigative Radiology. 2012. Vol. 47, N 1. P. 58–64. doi: 10.1097/RLI.0b013e318229fef3
39. Kuno H., Onaya H., Iwata R., et al. Evaluation of cartilage invasion by laryngeal and hypopharyngeal squamous cell carcinoma with dual-energy CT // Radiology. 2012. Vol. 265, N 2. P. 488–496. doi: 10.1148/radiol.12111719
40. Forghani R., Levental M., Gupta R., et al. Different spectral hounsfield unit curve and high-energy virtual monochromatic image characteristics of squamous cell carcinoma compared with nonossified thyroid cartilage // AJNR Am J Neuroradiol. 2015. Vol. 36, N 6. P. 1194–1200. doi: 10.3174/ajnr.A4253
41. Kuno H., Sakamaki K., Fujii S., et al. Comparison of MR imaging and dual-energy CT for the evaluation of cartilage invasion by laryngeal and hypopharyngeal squamous cell carcinoma // AJNR Am J Neuroradiol. 2018. Vol. 39, N 3. P. 524–531. doi: 10.3174/ajnr.A5530
42. Wichmann J.L., Kraft J., Nöske E.M., et al. Low-tube-voltage 80-kVp neck CT: evaluation of diagnostic accuracy and interobserver agreement // AJNR Am J Neuroradiol. 2014. Vol. 35, N 12. P. 2376–2381. doi: 10.3174/ajnr.A4052
43. Scholtz J.E., Hüsers K., Kaup M., et al. Non-linear image blending improves visualization of head and neck primary squamous cell carcinoma compared to linear blending in dual-energy CT // Clinical Radiology. 2015. Vol. 70, N 2. P. 168–175. doi: 10.1016/j.crad.2014.10.018
44. Lam S., Gupta R., Levental M., et al. Optimal virtual monochromatic images for evaluation of normal tissues and head and neck cancer using dual-energy CT // AJNR Am J Neuroradiol. 2015. Vol. 36, N 8. P. 1518–1524. doi: 10.3174/ajnr.A4314
45. Wang X., Zhao Y., Wu N., et al. [Application of single-source dual-energy spectral CT in differentiating lymphoma and metastatic lymph nodes in the head and neck] // Zhonghua Zhong Liu Za Zhi. 2015. Vol. 37, N 5. P. 361–366.
46. Fu F., He A., Zhang Y., et al. Dua-energy virtual noncontrast imaging in diagnosis of cervical metastasis lymph nodes // J Can Res Ther. 2015. Vol. 11, N 6. P. 202. doi: 10.4103/0973-1482.168185
47. Forghani R. Advanced dual-energy CT for head and neck cancer imaging // Expert Review of Anticancer Therapy. 2015. Vol. 15, N 12. P. 1489–1501. doi: 10.1586/14737140.2015.1108193

48. Lam S., Gupta R., Kelly H., et al. Multiparametric evaluation of head and neck squamous cell carcinoma using a single-source dual-energy CT with fast kVp switching: state of the art // Cancers. 2015. Vol. 7, N 4. P. 2201–2216. doi: 10.3390/cancers7040886
49. Yamauchi H., Buehler M., Goodsitt M.M., et al Dual-energy CT-based differentiation of benign posttreatment changes from primary or recurrent malignancy of the head and neck: comparison of spectral hounsfield units at 40 and 70 kev and iodine concentration // American Journal of Roentgenology. 2016. Vol. 206, N 3. P. 580–587. doi: 10.2214/AJR.15.14896
50. Yang L., Luo D., Li L., et al. Differentiation of malignant cervical lymphadenopathy by dual-energy CT: a preliminary analysis // Sci Rep. 2016. Vol. 6, N 1. P. 31020. doi: 10.1038/srep31020
51. May M.S., Bruegel J., Brand M., et al. Computed tomography of the head and neck region for tumor staging – comparison of dual-source, dual-energy and low-kilovolt, single-energy acquisitions // Invest Radiol. 2017. Vol. 52, N 9. P. 522–528. doi: 10.1097/RLI.0000000000000377
52. Forghani R., Kelly H., Yu E., et al. Low-energy virtual monochromatic dual-energy computed tomography images for the evaluation of head and neck squamous cell carcinoma: a study of tumor visibility compared with single-energy computed tomography and user acceptance // Journal of Computer Assisted Tomography. 2017. Vol. 41, N 4. P. 565–571. doi: 10.1097/RCT.0000000000000571
53. Forghani R., Kelly H.R., Curtin H.D. Applications of dual-energy computed tomography for the evaluation of head and neck squamous cell carcinoma // Neuroimaging Clinics of North America. 2017. Vol. 27, N 3. P. 445–459. doi: 10.1016/j.nic.2017.04.001
54. Pérez-Lara A., Forghani R. Spectral computed tomography // Magnetic Resonance Imaging Clinics of North America. 2018. Vol. 26, N 1. P. 1–17. doi: 10.1016/j.mric.2017.08.001
55. Forghani R., Mukherji S.K. Advanced dual-energy CT applications for the evaluation of the soft tissues of the neck // Clinical Radiology. 2018. Vol. 73, N 1. P. 70–80. doi: 10.1016/j.crad.2017.04.002
56. Yang L., Luo D., Yi J., et al. Therapy effects of advanced hypopharyngeal and laryngeal squamous cell carcinoma: evaluated using dual-energy CT quantitative parameters // Sci Rep. 2018. Vol. 8, N 1. P. 9064. doi: 10.1038/s41598-018-27341-0
57. Ge X., Yu J., Wang Z., et al. Comparative study of dual energy CT iodine imaging and standardized concentrations before and after chemoradiotherapy for esophageal cancer // BMC Cancer. 2018. Vol. 18, N 1. P. 1120. doi: 10.1186/s12885-018-5058-2
58. Khademi S., Sarkar S., Shakeri-Zadeh A., et al. Dual-energy CT imaging of nasopharyngeal cancer cells using multifunctional gold nanoparticles // IET nanobiotechnol. 2019. Vol. 13, N 9. P. 957–961. doi: 10.1049/iet-nbt.2019.0067
59. Forghani R., Chatterjee A., Reinhold C., et al. Head and neck squamous cell carcinoma: prediction of cervical lymph node metastasis by dual-energy CT texture analysis with machine learning // Eur Radiol. 2019. Vol. 29, N 11. P. 6172–6181. doi: 10.1007/s00330-019-06159-y
60. Seidler M., Forghani B., Reinhold C., et al. Dual-energy CT texture analysis with machine learning for the evaluation and characterization of cervical lymphadenopathy // Computational and Structural Biotechnology Journal. 2019. Vol. 17. P. 1009–1015. doi: 10.1016/j.csbj.2019.07.004

AUTHORS' INFO

*** Victor S. Petrovichev,** MD, Cand. Sci. (Med.);
address: 3 Ivan'kovskoe shosse, 125367, Moscow, Russia;
ORCID: http://orcid.org/0000-0002-8391-2771;
eLibrary SPIN: 7730-7420; e-mail: petrovi4ev@gmail.com

Marina V. Neklyudova, MD, Cand. Sci. (Med.);
ORCID: https://orcid.org/0000-0003-4224-2975;
eLibrary SPIN: 7450-6800; e-mail: mneklyudova@med-rf.ru

Valentin E. Sinitsyn, MD, Dr. Sci. (Med.), Professor;
ORCID: https://orcid.org/0000-0002-5649-2193;
eLibrary SPIN: 8449-6590; e-mail: vsini@mail.ru

Igor G. Nikitin, MD, Dr. Sci. (Med.), Professor;
ORCID: https://orcid.org/0000-0003-1699-0881;
eLibrary SPIN: 3595-1990; e-mail: igor.nikitin.64@mail.ru

ОБ АВТОРАХ

*** Петровичев Виктор Сергеевич,** к.м.н.;
адрес: Россия, 125367, Москва, Иваньковское шоссе, д. 3;
ORCID: http://orcid.org/0000-0002-8391-2771;
eLibrary SPIN: 7730-7420; e-mail: petrovi4ev@gmail.com

Неклюдова Марина Викторовна, к.м.н.;
ORCID: https://orcid.org/0000-0003-4224-2975;
eLibrary SPIN: 7450-6800; e-mail: mneklyudova@med-rf.ru

Синицын Валентин Евгеньевич, д.м.н., профессор;
ORCID: https://orcid.org/0000-0002-5649-2193;
eLibrary SPIN: 8449-6590; e-mail: vsini@mail.ru

Никитин Игорь Геннадиевич, д.м.н., профессор;
ORCID: https://orcid.org/0000-0003-1699-0881;
eLibrary SPIN: 3595-1990; e-mail: igor.nikitin.64@mail.ru

* Corresponding author / Автор, ответственный за переписку

DOI: https://doi.org/10.17816/DD77446

К вопросу об этических аспектах внедрения систем искусственного интеллекта в здравоохранении

Д.Е. Шарова, В.В. Зинченко, Е.С. Ахмад, О.А. Мокиенко, А.В. Владзимирский, С.П. Морозов

Научно-практический клинический центр диагностики и телемедицинских технологий Департамента здравоохранения г. Москвы, Москва, Российская Федерация

АННОТАЦИЯ

Рассматриваются этические вопросы применения в ходе жизненного цикла систем искусственного интеллекта; представлена актуальная информация о мировых и отечественных тенденциях в этой сфере. Описан международный и национальный опыт в области этических вопросов применения систем искусственного интеллекта в здравоохранении; разобраны международные и национальные стратегии развития искусственного интеллекта в здравоохранении, где особое внимание уделяется национальному развитию, и выявлены основные тенденции, сходства и различия между стратегиями. Описаны также этические составляющие процесса клинических испытаний систем искусственного интеллекта в России, в рамках которых оцениваются их безопасность и эффективность. В рамках передового отечественного опыта по техническому регулированию систем искусственного интеллекта, аналогов которому нет в мире, представлены работы по унификации и стандартизации требований, используемые при разработке, тестировании и эксплуатации систем искусственного интеллекта в здравоохранении и уникальный опыт России в части сертификационных требований к медицинским изделиям, использующим технологии искусственного интеллекта.

Особо подчёркнута важность построения успешной системы здравоохранения в области технологий искусственного интеллекта, которая способствует укреплению доверия и соблюдению этических норм.

Ключевые слова: клиническая этика; искусственный интеллект; стандартизация; клинические испытания.

Как цитировать

Шарова Д.Е., Зинченко В.В., Ахмад Е.С., Мокиенко О.А, Владзимирский А.В., Морозов С.П. К вопросу об этических аспектах внедрения систем искусственного интеллекта в здравоохранении // *Digital Diagnostics*. 2021. Т. 2, № 3. С. 356–368. DOI: https://doi.org/10.17816/DD77446

Рукопись получена: 06.08.2021 **Рукопись одобрена:** 08.09.2021 **Опубликована:** 22.09.2021

ЭКО•ВЕКТОР

DOI: https://doi.org/10.17816/DD77446

On the issue of ethical aspects of the artificial intelligence systems implementation in healthcare

Daria S. Sharova, Viktoria V. Zinchenko, Ekaterina S. Akhmad, Olesia A. Mokienko, Anton V. Vladzymyrskyy, Sergey P. Morozov

Moscow Center for Diagnostics and Telemedicine, Moscow, Russian Federation

ABSTRACT

This article aimed to analyze the ethical issues associated with different stages in the life-cycle of artificial intelligence (AI) systems and provide up-to-date information about global and domestic trends in this subject. Described herein are the international and national experiences with ethical issues of AI systems used in healthcare. In addition, the international and national strategies for the development of AI in healthcare are analyzed, with a focus on national development. Moreover, the main trends, similarities, and differences between strategies are identified. Furthermore, the ethical components of the clinical trial process are described to evaluate the safety and efficacy of AI systems in Russia. Domestic, state-of-the-art, and globally unique experience in the technical regulation of AI systems is shown on unification papers and standardization of requirements for the development, testing, and operation of AI systems in healthcare are presented; finally, the unparalleled Russian experience in certification requirements for AI-based medical devices is demonstrated. Furthermore, the article summarizes the main conclusions and emphasizes the importance of a strong successful healthcare system based on AI technologies that build trust and compliance with ethical standards.

Keywords: clinical ethics; artificial intelligence; standardization; clinical trial

To cite this article

Sharova DS, Zinchenko VV, Akhmad ES, Mokienko OA, Vladzymyrskyy AV, Morozov SP. On the issue of ethical aspects of the artificial intelligence system implementation in healthcare. *Digital Diagnostics*. 2021;2(3)356–368. DOI: https://doi.org/10.17816/DD77446

Received: 06.08.2021 **Accepted:** 08.09.2021 **Published:** 22.09.2021

ECO•VECTOR

DOI: https://doi.org/10.17816/DD77446

关于在医疗保健中实施人工智能系统的伦理方面

Daria S. Sharova, Viktoria V. Zinchenko, Ekaterina S. Akhmad, Olesia A. Mokienko, Anton V. Vladzymyrskyy, Sergey P. Morozov

Moscow Center for Diagnostics and Telemedicine, Moscow, Russian Federation

简评

考虑了人工智能系统在生命周期中使用的伦理问题，介绍了该领域世界和国内趋势的相关信息。 描述了在医疗保健中使用人工智能系统的伦理问题领域的国际和国家经验； 分析了医疗保健人工智能发展的国际和国家战略，特别关注国家发展，并确定了战略之间的主要趋势、异同。 还描述了俄罗斯人工智能系统临床试验过程的伦理组成部分，并在其框架内评估了其安全性和有效性。 人工智能系统技术监管方面国内先进经验的框架下，致力于在医疗领域人工智能系统的开发、测试和运行中使用的要求的统一和标准化，以及独特的人工智能系统的技术规范。介绍了俄罗斯在医疗器械认证要求方面的经验，使用人工智能技术。

特别强调了在人工智能技术领域建立成功的医疗保健系统的重要性，这有助于建立信任和遵守道德标准。

关键词：临床伦理； 人工智能；标准化；临床试验。

引用本文

Sharova DS, Zinchenko VV, Akhmad ES, Mokienko OA, Vladzymyrskyy AV, Morozov SP. 关于在医疗保健中实施人工智能系统的伦理方面. *Digital Diagnostics*. 2021;2(3)356–368. DOI: https://doi.org/10.17816/DD77446

收到： 06.08.2021 **接受：** 08.09.2021 **发布日期：**22.09.2021

INTRODUCTION

According to GOST R 59277-2020, artificial intelligence (AI) is defined as a set of technological solutions that simulates human cognitive functions, including self-learning, identifying solutions without a predetermined algorithm, and achieving insight, thereby obtaining results that are comparable at least to human intellectual activity. Thus, systems based on AI technologies have certain characteristics, such as the ability to "evolve" and apply "new knowledge." This imposes on society the responsibility to develop new ethical standards for the application of such systems, such as those that help physicians diagnose diseases and make decisions to provide substantial help in medicine. AI systems must be effective (due to their variety of options), safe, and assured by regulatory control, including ethical standards (development of a code of ethics and national and international ethical standards for using AI technologies in medicine) and technical regulation that are subjected to reforms and updates. Despite their similarity to a black box, AI systems should not cause distrust as their use the benefits are much greater, such as handling staff shortages and obtaining independent second opinion due to the emerging well-established norms and rules.

The development of AI systems brings forth ethical issues regarding the impact on decision-making processes and interactions in medicine and the overall healthcare system [1]. Even with the use of AI systems, human rights should be respected, which requires systematic ethical discussions; certain ethical standards must be established for their global application [2].

The ethical part is a characteristic of all stages of the AI lifecycle, a set of processes from the development (scientific and clinical research, design, and creation) and operation (market launch, financing, maintenance, monitoring, and performance evaluation) to the withdrawal from an operation. Bearing in mind the ethical issues during the interaction of objects with AI systems is of particular relevance. In this case, objects involved with AI systems are defined as any party that is involved in any of the stages of the AI lifecycle, such as legal and physical persons, including researchers, scientists, physicians, data processing specialists, engineers, information technology (IT) specialists, commercial and public companies, universities, and research centers.

Particularly, the ethical issues of AI application in global and national healthcare systems are worth mentioning [3, 4]. AI systems that involve medical products are increasing. Therefore, minimizing the potential for errors associated with medical and personal patient data that are used to develop and test AI technologies is necessary. To perform these tasks, access to sufficient verified, high-quality medical data of patients is required, which may be used for disease prediction, diagnosis, treatment optimization, as well as external and internal testing algorithms [5–7]. Thus, a set of solutions is needed, including state regulation, involvement of highly qualified experts (engineers, physicians, and IT specialists); raising patient awareness to solve the ethical problems associated with the development and implementation of medical AI systems is also warranted.

Therefore, this study aimed to present the currently available documents that regulate the ethical aspects and norms of the global AI application, particularly in the healthcare industry. Moreover, the normative legal and technical regulatory documents for AI systems worldwide were studied, along with the presentation of the Russian experience of the first national standards that will control the development and application of AI technologies in healthcare.

INTERNATIONAL AND NATIONAL EXPERIENCE TO SOLVE THE ETHICAL ISSUES OF AI APPLICATION IN HEALTHCARE: GENERAL PROVISIONS

Data privacy concerns are raised with the widespread use of patient data for AI training. Improving healthcare by maintaining a balance between the secondary use of data from other patients and the privacy of personal information presents several challenges. For example, the challenge at the individual level is to understand the extent to which personal data may be used at the secondary level and what elements are involved, who can access these data, how effective and complete their anonymity is, the potential use of data to harm the patients, the financial use of data, and the effect of the data privacy policy on the care received [6]. In addition, the issue of "liability awareness" for the ownership of personal data may arise at the level of medical institutions that share medical data, and such sharing may be problematic.

However, in case of a misdiagnosis made by a physician when using an AI system, the extent to which the involved party (physician, institution, healthcare system, or AI manufacturer) is ethically responsible is unclear. According to the existing normative legal acts (Federal Law of November 21, 2011, No. 323-FZ, Art. 98 [as amended on July 2, 2021] on Fundamentals of Healthcare in the Russian Federation), the responsibility of violations of various legal norms in healthcare lies on the medical organization and the physician.

The responsibility for medical errors becomes more ambiguous at the state level. Thus, AI systems may not meet all the established requirements, and risks are present when using medical devices, including AI systems, for diagnoses. The United State Food and Drug Administration states that these medical devices may be risky due to the following five reasons: increased false positives leading to unnecessary additional procedures, increased false negatives, use in unsuitable settings, misuse by people, and malfunction due to improper product (AI system) introduction in the market [8]. Thus, a transparent and well-established state regulatory system is needed to minimize the risks, thereby partially

removing or controlling the ethical issues associated with using AI systems at the state level.

By definition, a regulatory system is a set of rules. For products manufactured by an industry, such as drugs, vaccines, medical devices, and AI systems, the role of regulations is to limit the risks associated with the product, such as an unsafe product, the product not meeting the purpose for which the product was intended for (inefficient product), or the risk of not meeting up with quality standards based on the global report of the World Health Organization (WHO) on Ethics and Governance of Artificial Intelligence for Health [9]. The national legislation is responsible for developing such rules and creating the conditions to ensure compliance with these laws. Among those who are required to follow these rules are manufacturers and users of AI systems (medical organizations, physicians, and other medical staff). For example, the AI manufacturer is recommended to use the accepted classification of pathologies according to approved thesauruses and the International Classification of Diseases or name the phenomena as recommended by professional associations.

GENERAL APPROACHES TO SOLVE ETHICAL ISSUES

WHO experts have formulated principles to address ethical issues, which apply to AI systems in healthcare [9].

1. Protecting autonomy

With AI development, physicians began to raise concerns about being replaced by these technologies. However, the proposed principle of protecting autonomy implies that AI systems should be designed to help in decision-making and be fully controllable when operated by medical staff. In addition, this principle requires data protection and privacy on the part of AI manufacturers, dataset creators, and national governments, which should be enshrined in regulations. In Russia, an experimental regime of personal data processing was introduced in Moscow (Federal Law No. 152-FZ of July 27, 2006, on Personal Data), which allowed changes in the informed consent of patients. Moreover, changes were initiated in the regulatory legal documents related to medical devices in 2020. These amendments outlined the role of the AI system as an aid to physician decision-making, thereby removing the issue of using AI without physician interventions.

2. Ensuring patient safety and well-being

AI systems should be designed not to cause physical or mental harm to the patient and must meet the approved requirements for safety, efficiency, and quality throughout the life cycle. Therefore, quality control and monitoring mechanisms will be put in place to ensure that AI systems function as intended. The recommendations of the International Medical Device Regulators Forum to perform a clinical evaluation of software were approved and are being adopted in Russia [10]. In addition, standards for protocols and reports on clinical trial results are being developed. For example, randomized controlled studies are considered the gold standard of experimental design to provide evidence on the safety and efficiency of AI systems. In this regard, the extension of Consolidated Standards of Reporting Trials—AI (CONSORT-AI) to CONSORT 2010 and Standard Protocol Items: Recommendations for Interventional Trials—AI (SPIRIT-AI) was developed [11].

3. Ensuring transparency, explainability, and intelligibility of AI systems

The intelligibility of AI systems includes ensured transparency and explainability. AI manufacturers must demonstrate transparency by publishing and presenting data to the professional community on how the AI model was developed, its application scenario, the parameters of data sets that were used to develop and validate the AI system, and clinical studies that are conducted to demonstrate the efficiency of this system [10].

AI algorithms and the principle of data processing and decision-making should be explained as much as possible to inform the individuals and patients.

In addition, the specified principle of AI intelligibility is related to the principle of safety as it requires disclosure of information about the performed tests and their completeness and quality.

4. Enhancing responsibility and accountability

Engineers and manufacturers of AI systems along with medical experts must develop and visualize scenarios for applying this technology, including the efficiency and performance results obtained. In this case, concerned parties are responsible to use the AI system for its intended purpose and within the stated conditions, and all its incorrect operations must be documented and further monitored.

5. Ensuring equity

AI technologies should be available to all segments of society, irrespective of age, gender, race, financial status, and social status. AI manufacturers must ensure and provide information that the data sets for AI training and testing are free from systematic sampling errors (biases) and are therefore accurate, complete, and diverse, which give equal parameters for the AI efficiency within the entire population.

6. Promoting AI that is responsive and sustainable

Responsiveness requires the manufacturer and user of the AI system to continuously collect and analyze information on its use to monitor the compliance of its performance with the stated requirements. The parameters of resources and external systems for the AI functioning, as well as its integration (such as medical information systems), should be ensured. Responsiveness is relevant in assessing the place of a particular AI system in healthcare, the opinions of physicians, and the execution and efficiency of anticipated scenarios for AI applications.

The principles presented for solving ethical problems are general and should be adapted to national contexts. Many world powers presented their national strategies with

consolidation of basic principles of AI development, which includes those previously mentioned.

INTERNATIONAL STRATEGIES FOR AI DEVELOPMENT IN HEALTHCARE

Main documents from the world-leading powers were reviewed to study the international strategies for AI use and development in healthcare.

Most world powers, such as the United States, China, Japan, South Korea, the European countries, and Russia, recently developed and published national strategies or policy documents defining the goals, objectives, and plans for AI development, all of which emphasized the ethical component in healthcare (Fig. 1) [12, 13].

Japan, being one of the first countries to develop a national AI strategy and a report on the Artificial Intelligence Technology Strategy in 2017, identified healthcare as a major industry for further development [14]. In the same year, Singapore launched an AI Singapore National Program, which focused on the national health system [15]. In addition, South Korea published its AI Development National Strategy in 2019, which also prioritized the healthcare system [16].

The European Commission adopted the AI for Europe strategy in 2018, which presented an initiative aimed at ensuring appropriate ethical and legal approaches by creating a European AI Alliance and developing guidelines for AI ethics [17].

Moreover, the United States published the National AI R&D Strategic Plan (2019 Update), which identified eight strategic priorities, namely, long-term investments, effective methods of human-AI interaction, regulation of legal and ethical AI implications, AI safety and security, publicly available data sets, AI standardization and testing, advancing the AI R&D workforce, and public-private partnerships [12]. In the same year, the report on Current State and Near-Term Priorities for AI-Enabled Diagnostic Support Software in Health Care was published. Therein, experts substantiated the need for changes in government policy and regulation to ensure safer and more effective AI applications in healthcare [18]. This paper provides an overview of the current regulatory framework that governs the development and use of clinical decision support systems, as well as diagnostic support. The experts concluded that regulatory changes for AI systems in healthcare based on the following tenets are needed:

First, providing evidence that AI systems improve patient outcomes, increase the quality of life, and reduce the cost of care, as well as provide physicians with relevant information that is "useful and trustworthy."

Second, assessing the potential risks of using AI products in clinical settings. "The degree to which a software product comes with information that explains how it works and the types of populations used to train the software will have significant impact on regulators' and clinicians' assessment of the risk to patients

Fig. 1. Timeline to develop and approve artificial intelligence strategies worldwide

when clinicians use this software," the researchers note. "Product labeling may need to be reconsidered and the risks and benefits of continuous learning versus locked models must be discussed."

A White Paper on Ethical and Legal Issues Related to Artificial Intelligence in Radiology was published in Canada in 2019 [6]. This official document of the Canadian Association of Radiologists provides a framework for exploring legal and ethical AI issues in medical imaging. Particular attention was paid to patient data privacy, AI systems (levels of autonomy, liability, and legal aspects), Canadian healthcare practices (best practices and current legal framework), and the projected opportunities that AI may provide for healthcare.

Ethics Guidelines for Trustworthy AI published by a group of experts of the European Commission in 2019 contain a set of key requirements, which elevates AI systems to the level of trustworthy technologies, such as human agency and oversight, technical robustness and safety, privacy and data governance, transparency, diversity, non-discrimination and fairness, societal and environmental well-being, and accountability [19].

In 2020, the European Parliament postulated the creation of a new legal framework that outlines ethical principles and legal obligations for the development of AI and robotics, and their deployment and use were all described in a White Paper on Artificial Intelligence Regulation [3].

The Council of Europe (the Ad hoc Committee on Artificial Intelligence, CAHAI), including the representatives of Russia, actively developed approaches to European regulation [20].

Moreover, UNESCO developed draft guidelines on AI ethics to be adopted by its member countries at the end of 2021 [21]. Thus, Europe is becoming a global player in AI ethics and actively developing documents in this sphere, including those for the intended use of AI systems in healthcare [20].

Notably, the United States has a freer market approach to AI compared with Europe, and the United States market for medical devices using AI-based software is one of the largest around the world. AI is predicted to contribute up to 13.33 trillion euros to the global economy in 2030, and the regions estimated to benefit most are China and North America, followed by Southern Europe [22].

China's strategy for AI development correlates with that of the scientific and technological development of the Russian Federation that focused on the transition to "digital and intelligent production technologies, robotic systems, new materials, and methods of construction, as well as creating systems for processing large data volumes, machine learning, and artificial intelligence" [23]. The State Council of China published a New Generation Artificial Intelligence Development Plan in 2017, which outlined step-by-step goals for AI development; subsequently, China AI Industry White Paper was developed in 2018 [24]. Both documents listed healthcare and ethics among their priorities.

Separate studies raise the issue of ethical development and implementation of AI systems in the medical community. For example, a joint statement by the European and North American communities addressed basic ethical principles similar to those proposed by the WHO, whereas the radiology community stated its intention to develop a unified code of ethics to create a sound ethical foundation with rapid technological advancements [25, 26].

In Russia, the current priority is AI development and implementation in healthcare, which could help in achieving strategic goals and objectives of the Healthcare National Project, including decreased morbidity and mortality and increased life expectancy. This strategy will be discussed in more detail in the following section.

NATIONAL STRATEGY FOR THE AI DEVELOPMENT IN HEALTHCARE

National processes of AI development in Russia, including AI in healthcare, are built on the principles of openness with the involvement of researchers, AI manufacturers, and government agencies. The work on the Code of AI ethics was initiated in 2020 by the order of the President of the Russian Federation [27].

Russia attaches great importance to international cooperation in AI development [28]. Concurrently, proper management of AI potential and the creation of necessary foundations and standardized approaches for the safe and ethical development of AI systems, which should include creative force and contribute to the development of human potential and abilities, is important.

Russia is an active participant in AI development and follows all global trends. Thus, the Russian government developed and adopted a comprehensive policy that allowed the national strategy to be further implemented [29]. In October 2019, the Russian President signed a Decree on the Development of Artificial Intelligence in the Russian Federation, which introduced the National Strategy for the Development of Artificial Intelligence until 2030 and approved the plans for initiating the AI Federal Project (introduced in 2020 as part of the national project for Digital Economy of the Russian Federation) [30]. The Federal project includes six main blocks, namely, support for scientific research, creation of a comprehensive legal regulation system, software design and development, improvement in data accessibility and quality, increased hardware accessibility, staff training, and increased public awareness on AI technologies.

The uniqueness of the Russian national strategy, which differs from the strategies of other countries, is their priority in the development of AI in healthcare, including the need to move from general principles to a more practical level. One of such routes is the creation of normative legal and technical regulations (standardization). In Russia, software, created using AI technologies and intended by the manufacturer

to provide medical care refers to medical devices (software as a medical device).

The Technical Artificial Intelligence Committee for Standardization (TC164) was created in July 2019 to develop technical regulations and improve the AI standardization efficiency [31]. In addition, Artificial Intelligence in Healthcare PC01 Subcommittee was created within the TC164 Committee to elaborate the national and international standards that cover the requirements for the development, testing, application, and operation of medical AI software and coordinate the work on unification and standardization of requirements used in the development, testing, and operation of AI systems in healthcare, as well as set certification requirements for medical products based on AI technologies [32].

Russian experts recently developed and prepared a corresponding standard for approval to regulate the process of AI clinical trials (as part of clinical assessment for independent testing of AI systems), where their safety and efficiency are evaluated, and AI systems are registered as medical devices. Ethical review is recommended before conducting clinical trials of unregistered medical devices (AI systems). This review includes issues related to the ethical components and analysis of possible adverse events arising from the AI application. Moreover, the Ethical Committee should review the clinical trial program (in the trial design approval and formation of data sets monitoring), and evaluate the compliance of the qualifications of investigators with the proposed trial.

Remarkably, the challenge of recent years, namely, the coronavirus disease-2019 (COVID-19) pandemic, has increased the understanding of the ethical AI application aspects in healthcare, including in the diagnosis of this disease using chest computed tomography [33]. The paper shows that AI technologies may adjust the patient flow by tracking radiological sign categories of pulmonary changes in COVID-19, which influences the tactics for managing such patients, because AI systems automatically process patient images and, accordingly, assess the volume of changes in the lungs more accurately; physicians perform such an assessment visually. Another ethical aspect of AI application during the COVID-19 pandemic was the issues of privacy, data protection, and their use for virus tracking [21].

CONCLUSIONS

Currently, standards for AI regulation in healthcare are actively developed at the national and international levels. However, these regulatory agencies did not form a full-fledged legal framework and control systems and have insufficient experience in using AI technologies. Therefore, ethical aspects of this process remain unresolved or controversial.

Russia actively develops legal and technical AI regulation, as well as issues of assessment, measurement, and standardization of AI technologies to improve and finalize normative and legal documents. The most active work is performed in the national industry standardization of healthcare. The unification of best practices will structure the development, evaluation, regulation, and security control in the application and development of AI technologies, thereby increasing public confidence.

A system based on ethical performance must be created to achieve the desired public goal for AI systems to benefit the society. Therefore, the existing legal framework must be reviewed and updated for new technological advancements. Regulations and industry standards in clinical medicine require that AI systems be developed and evaluated according to ethical standards, especially those intended for physicians and other members of the medical community. AI systems must be "transparent" in understanding by healthcare providers and protect the interests of physicians and patients, especially in the area of ethical regulation. Only by this can a trustworthy and ethically safe relationship be built between the physician, patient, and AI manufacturer.

The international community and private companies should develop ethical monitoring and verification mechanisms to identify, prevent, and minimize the impact of AI systems in human rights, good scientific practice, legality, and protection, and evaluate the efficiency of such mechanisms. States are encouraged to consider forms of governance, such as AI certification mechanisms and mutual recognition of standardization while considering the healthcare industry and the use of AI systems and their potential impact on human lives, as well as other ethical aspects.

The AI safety and security may be improved by developing reliable systems against unauthorized access to personal information complex solutions that will provide more effective training of AI models based on quality data.

Importantly, public and political discussions should focus on the ethics of healthcare. AI has enormous potential to improve healthcare. However, its realization will be possible if ethical problems facing society are addressed as soon as possible.

Whether the use of AI systems is ethically acceptable depends on the extent to which AI technologies contribute positively to individual patients and the entire society, including medical organizations and physicians (users). All levels of interaction should be guided by a relative level of equity between the principles of fairness and expected positive outcomes.

ADDITIONAL INFORMATION

Funding source. This article was prepared with the support of the Moscow Healthcare Department as a part of Program "Scientific Support of the Capital's Healthcare" for 2020–2022 (Unified State Information System for Accounting of Research, Development, and Technological Works No: AAAA-A21-121012290079-2).

Competing interests. The authors declare the absence of obvious and potential conflicts of interest related to the publication of this article.

Authors' contribution. Concept of the article — D. Sharova, V. Zinchenko, E. Akhmad; collection and processing of the materials, writing the paper — D. Sharova, V. Zinchenko, E. Akhmad; compilation of the reference list — D. Sharova, E. Akhmad; editing — D. Sharova, V. Zinchenko, E. Akhmad, O. Mokienko, A. Vladzymyrskyy, S. Morozov. The final version of the article was approved by all co-authors, who equally share a responsibility for the integrity of all parts of the article. All authors confirm their authorship in accordance with the international ICMJE criteria. All authors made a substantial contribution to the concept development, research and article preparation, read and approved the final version before the publication.

REFERENCES

1. Top 10 principles for ethical artificial intelligence [Electronic resource]. UNI Global Union; 2017. 10 p. Available from: http://www.thefutureworldofwork.org/media/35420/uni_ethical_ai.pdf. Accessed: 11.07.2021.

2. World Medical Association, Inc. WMA Declaration of Helsinki — Ethical Principles for Medical Research Involving Human Subjects [Electronic resource]. Available from: https://web.archive.org/web/20140101202246/http://www.wma.net/en/30publications/10policies/b3/. Accessed: 11.07.2021.

3. Gerke S, Minssen T, Cohen G. Ethical and legal challenges of artificial intelligence-driven healthcare. In: Artificial Intelligence in Healthcare. 2020. P. 295–336. doi: 10.1016/B978-0-12-818438-7.00012-5

4. The state of the industry in Russia and the world. Strategy of Russia. In: Almanac "Artificial Intelligence": a collection of analytical materials on the field of artificial intelligence in Russia and the world. NTI Competence Center in the direction of "Artificial Intelligence" on the basis of Moscow Institute of Physics and Technology. 2019;1:7–136. (In Russ).

5. Pavlov NA, Andreychenko AE, Vladzymyrskyy AV, et al. Reference medical datasets (MosMedData) for independent external evaluation of algorithms based on artificial intelligence in diagnostics. *Digital Diagnostics.* 2021;2(1):49–66. (In Russ).

6. Jaremko JL, Azar M, Bromwich R, et al. Canadian Association of Radiologists white paper on ethical and legal issues related to artificial intelligence in radiology. *Can Assoc Radiol J.* 2019;70(2):107–118. doi: 10.1016/j.carj.2019.03.001

7. Morozov SP, Vladzymyrskyy AV, Klyashtornyy VG, et al. Clinical acceptance of software based on artificial intelligence technologies (radiology). The series " Best practices in medical imaging". Issue 57. Moscow; 2019. 51 p. (In Russ).

8. FDA. Factors to consider regarding benefit-risk in medical device product availability, compliance, and enforcement decisions [Electronic resource]. Available from: https://www.fda.gov/ regulatory-information/search-fda-guidance-documents/factors-consider-regarding-benefit-risk-medical-device-product-availability-compliance-and. Accessed: 11.07.2021.

9. WHO guidance. Ethics and governance of artificial intelligence for health. 2020 [Electronic resource]. Available from: https://www.who.int/publications/i/item/9789240029200. Accessed: 11.07.2021.

10. Morozov SP, Zinchenko VV, Khoruzhaya AN, et al. Standardization of artificial intelligence in healthcare: Russia becomes the leader. *Medical Doctor and Information Technology.* 2021;(2):12–19. (In Russ). doi: 1025881/18110193_2021_2_12

11. Liu X, Cruz Rivera S, Moher D, et al.; SPIRIT-AI and CONSORT-AI Working Group. Reporting guidelines for clinical trial reports for interventions involving artificial intelligence: the CONSORT-AI extension. *Nat Med.* 2020;26(9):1364–1374. doi: 10.1038/s41591-020-1034-x

12. Select Committee on artificial intelligence: a report. In: The national artificial intelligence research and development strategic plan: 2019 update [Electronic resource]. 2019. Available from: https://www.nitrd.gov/pubs/National-AI-RD-Strategy-2019.pdf. Accessed: 11.07.2021.

13. Konrad Adenauer Stiftung. Comparison of national strategies to promote artificial intelligence [Electronic resource]. Available from: https://www.kas.de/en/single-title/-/content/vergleich-nationaler-strategien-zur-forderung-von-kunstlicher-intellige-1. Accessed: 11.07.2021.

14. Artificial Intelligence Technology Strategy (Report of Strategic Council for AI Technology). Strategic Council for AI Technology; 2017 [Electronic resource]. Available from: https://pdf4pro.com/view/artificial-intelligence-technology-strategy-nedo-6dc4e.html. Accessed: 11.07.2021.

15. National Research Foundation. AI Singapore [Electronic resource]. Available from: https://www.nrf.gov.sg/programmes/artificial-intelligence-r-d-programme. Accessed: 11.07.2021.

16. The International Trade Administration (ITA). Korea — Artificial Intelligence [Electronic resource]. Available from: https://www.privacyshield.gov/article?id=Korea-Artificial-Intelligence. Accessed: 11.07.2021.

17. European Commission website. Shaping Europe's digital future. Communication artificial intelligence for Europe [Electronic resource]. Available from: https://digital-strategy.ec.europa.eu/en/library/communication-artificial-intelligence-europe. Accessed: 11.07.2021.

18. Current state and near-term priorities for AI-enabled diagnostic support software in health care [Electronic resource]. Duke-Margolis Center for Health Policy; 2019. Available from: https://healthpolicy.duke.edu/sites/default/files/2019-11/dukemargolisaienableddxss.pdf. Accessed: 11.07.2021.

19. European Commission website. Shaping Europe's digital future. Ethics guidelines for trustworthy AI [Electronic resource]. Available from: https://digital-strategy.ec.europa.eu/en/library/ ethics-guidelines-trustworthy-ai. Accessed: 11.07.2021.

20. Council of Europe and Artificial Intelligence [Electronic resource]. Available from: https://www.coe.int/en/web/artificial-intelligence. Accessed: 11.07.2021.

21. United Nations Educational, Cultural and Scientific Organization. SHS/BIO/AHEG-AI/2020/4 REV.2. The first draft of the recommendation on the ethical aspects of artificial intelligence [Electronic resource]. 2020. (In Russ). Available from: https://ifap.ru/ pr/2020/n201116a.pdf. Accessed: 11.07.2021.

22. European Commission website. USA-China-EU plans for AI: where do we stand? [Electronic resource]. 2018. Available from: https://ati.ec.europa.eu/sites/default/files/2020-07/USA-China-EU%20plans%20for%20AI%20-%20where%20do%20we%20stand%20%28v5%29.pdf. Accessed: 11.07.2021.

23. Decree of the President of the Russian Federation No. 642 dated 01.12.2016 "On the strategy of scientific and technological development of the Russian Federation". Available from: http://www.kremlin.ru/acts/bank/41449. Accessed: 11.07.2021.
24. Global Artificial Intelligence Industry Whitepaper [Electronic resource]. Deloitte Technology, Media and Telecommunications Industry; 2019. Available from: https://www2.deloitte.com/cn/ en/pages/technology-media-and-telecommunications/articles/ global-ai-development-white-paper.html. Accessed: 11.07.2021.
25. Geis JR, Brady AP, Wu CC, et al. Ethics of artificial intelligence in radiology: summary of the Joint European and North American Multisociety Statement. *Radiology*. 2019;293(2):436–440. doi: 10.1148/radiol.2019191586
26. Safdar NM, Banja JD, Meltzer CC. Ethical considerations in artificial intelligence. *Eur J Radiol*. 2020;122:108768. doi: 10.1016/j.ejrad.2019.108768
27. Website of the President of Russia. List of assignments based on the results of the conference on artificial intelligence [Electronic resource]. (In Russ). Available from: http://www.kremlin.ru/acts/assignments/orders/64859. Accessed: 11.07.2021.
28. The expert center of the electronic state. Actual tasks of international cooperation on the development and regulation of artificial intelligence [Electronic resource]. (In Russ). Available from: http://d-russia.ru/aktualnye-zadachi-mezhdunarodnogo-vzaimodejstviya-po-razvitiyu-i-regulirovaniyu-iskusstvennogo-intellekta.html. Accessed: 11.07.2021.
29. Order of the Government of the Russian Federation No. 2129-r of 19.08.2020. (In Russ). Available from: http://publication.pravo.gov.ru/Document/View/0001202008260005?index=0&rangeSize=1 Accessed: 11.07.2021.
30. Decree of the President of the Russian Federation No. 490 dated 10.10.2019 "On the development of artificial intelligence in the Russian Federation". (In Russ). Available from: http://www.kremlin.ru/ acts/bank/44731. Accessed: 11.07.2021.
31. Ministry of Industry and Trade of the Russian Federation. Federal Agency for Technical Regulation and Metrology. Order No. 1732 of July 25, 2019 "On the establishment of the technical Committee for Standardization "Artificial Intelligence". (In Russ). Available from: https://docs.cntd.ru/document/560916332. Accessed: 11.07.2021.
32. Technical Committee for Standardization "Artificial Intelligence" (TC164). Order No. 1 of 13.01.2020 "On determining the basic organization of the subcommittee "Artificial Intelligence in Healthcare". (In Russ). Available from: https://tele-med.ai/media/uploads/2021/03/18/01_-2-2.pdf. Accessed: 11.07.2021.
33. Morozov SP, Chernina VYu, Andreychenko AE, et al. How does artificial intelligence effect on the assessment of lung damage in COVID-19 on chest CT scan? *Digital Diagnostics*. 2020;2(1):27–38. (In Russ). doi: 10.17816/DD60040

СПИСОК ЛИТЕРАТУРЫ

1. Top 10 principles for ethical artificial intelligence [электронный ресурс]. UNI Global Union; 2017. Режим доступа: http://www.thefutureworldofwork.org/media/35420/uni_ethical_ai.pdf. Дата обращения: 11.07.2021.
2. World Medical Association, Inc. WMA Declaration of Helsinki — Ethical Principles for Medical Research Involving Human Subjects [электронный ресурс]. Режим доступа: https://web.archive.org/web/20140101202246/http://www.wma.net/en/30publications/10policies/b3/. Дата обращения: 11.07.2021.
3. Gerke S, Minssen T, Cohen G. Ethical and legal challenges of artificial intelligence-driven healthcare // Artificial Intelligence in Healthcare. 2020. P. 295–336. doi: 10.1016/B978-0-12-818438-7.00012-5
4. Состояние отрасли в России и мире. Стратегия России // Альманах «Искусственный интеллект»: сборник аналитических материалов по отрасли искусственного интеллекта в России и мире. Центр компетенций НТИ по направлению «Искусственный интеллект» на базе МФТИ. 2019. № 1. С. 7–136.
5. Павлов Н.А., Андрейченко А.Е., Владзимирский А.В., и др. Эталонные медицинские датасеты (MosMedData) для независимой внешней оценки алгоритмов на основе искусственного интеллекта в диагностике // Digital Diagnostics. 2021. Т. 2, № 1. С. 49–66.
6. Jaremko J.L., Azar M., Bromwich R., et al. Canadian Association of Radiologists white paper on ethical and legal issues related to artificial intelligence in radiology // Can Assoc Radiol J. 2019. Vol. 70, N 2. P. 107–118. doi: 10.1016/j.carj.2019.03.001
7. Морозов С.П., Владзимирский А.В., Кляшторный В.Г., и др. Клинические испытания программного обеспечения на основе интеллектуальных технологий (лучевая диагностика). Серия «Лучшие практики лучевой и инструментальной диагностики». Вып. 57. Москва, 2019. 51 с.
8. FDA. Factors to consider regarding benefit-risk in medical device product availability, compliance, and enforcement decisions [электронный ресурс]. Режим доступа: https://www.fda.gov/regulatory-information/search-fda-guidance-documents/factors-consider-regarding-benefit-risk-medical-device-product-availability-compliance-and. Дата обращения: 11.07.2021.
9. WHO guidance. Ethics and governance of artificial intelligence for health [электронный ресурс]. 2020. Режим доступа: https://www.who.int/publications/i/item/9789240029200. Дата обращения: 11.07.2021.
10. Морозов С.П., Зинченко В.В., Хоружая А.Н., и др. Стандартизация искусственного интеллекта в здравоохранении: Россия выходит в лидеры // Врач и информационные технологии. 2021. № 2. С. 12–19. doi: 1025881/18110193_2021_2_12
11. Liu X., Cruz Rivera S., Moher D., et al.; SPIRIT-AI and CONSORT-AI Working Group. Reporting guidelines for clinical trial reports for interventions involving artificial intelligence: the CONSORT-AI extension // Nat Med. 2020. Vol. 26, N 9. P. 1364–1374. doi: 10.1038/s41591-020-1034-x
12. Select Committee on artificial intelligence: a report // The national artificial intelligence research and development strategic plan: 2019 update [электронный ресурс]. 2019. Режим доступа: https://www.nitrd.gov/pubs/National-AI-RD-Strategy-2019.pdf. Дата обращения: 11.07.2021.
13. Konrad Adenauer Stiftung. Comparison of national strategies to promote artificial intelligence [электронный ресурс]. Режим доступа: https://www.kas.de/en/single-title/-/content/vergleich-nationaler-strategien-zur-forderung-von-kunstlicher-intellige-1. Дата обращения: 11.07.2021.
14. Artificial Intelligence Technology Strategy (Report of Strategic Council for AI Technology) [электронный ресурс]. Strategic Council

for AI Technology; 2017. Режим доступа: https://pdf4pro.com/view/artificial-intelligence-technology-strategy-nedo-6dc4e.html. Дата обращения: 11.07.2021.
15. National Research Foundation. AI Singapore [электронный ресурс]. Режим доступа: https://www.nrf.gov.sg/programmes/artificial-intelligence-r-d-programme. Дата обращения: 11.07.2021.
16. The International Trade Administration (ITA). Korea — Artificial Intelligence [электронный ресурс]. Режим доступа: https://www.privacyshield.gov/article?id=Korea-Artificial-Intelligence. Дата обращения: 11.07.2021.
17. European Commission website. Shaping Europe's digital future. Communication artificial intelligence for Europe [электронный ресурс]. Режим доступа: https://digital-strategy.ec.europa.eu/en/library/communication-artificial-intelligence-europe. Дата обращения: 11.07.2021.
18. Current state and near-term priorities for AI-enabled diagnostic support software in health care [электронный ресурс]. Duke-Margolis Center for Health Policy; 2019. Режим доступа: https://healthpolicy.duke.edu/sites/default/files/2019-11/dukemargolisaienableddxss.pdf. Дата обращения: 11.07.2021.
19. European Commission website. Shaping Europe's digital future. Ethics guidelines for trustworthy AI [электронный ресурс]. Режим доступа: https://digital-strategy.ec.europa.eu/en/library/ethics-guidelines-trustworthy-ai. Дата обращения: 11.07.2021.
20. Council of Europe and Artificial Intelligence [электронный ресурс]. Режим доступа: https://www.coe.int/en/web/artificial-intelligence. Дата обращения: 11.07.2021.
21. ООН по вопросам образования, культуры и науки. SHS/BIO/AHEG-AI/2020/4 REV.2. Первый проект рекомендации об этических аспектах искусственного интеллекта [электронный ресурс]. 2020. Режим доступа: https://ifap.ru/pr/2020/n201116a.pdf. Дата обращения: 11.07.2021.
22. European Commission website. USA-China-EU plans for AI: where do we stand? [электронный ресурс]. 2018. Режим доступа: https://ati.ec.europa.eu/sites/default/files/2020-07/USA-China-EU%20plans%20for%20AI%20-%20where%20do%20we%20stand%20%28v5%29.pdf. Дата обращения: 11.07.2021.
23. Указ Президента Российской Федерации от 01.12.2016 № 642 «О стратегии научно-технологического развития Российской Федерации». Режим доступа: http://www.kremlin.ru/acts/bank/41449. Дата обращения: 11.07.2021.
24. Global Artificial Intelligence Industry Whitepaper [электронный ресурс]. Deloitte Technology, Media and Telecommunications Industry; 2019. Режим доступа: https://www2.deloitte.com/cn/en/pages/technology-media-and-telecommunications/articles/global-ai-development-white-paper.html. Дата обращения: 11.07.2021.
25. Geis J.R., Brady A.P., Wu C.C., et al. Ethics of artificial intelligence in radiology: summary of the Joint European and North American Multisociety Statement // Radiology. 2019. Vol. 293, N 2. P. 436–440. doi: 10.1148/radiol.2019191586
26. Safdar N.M., Banja J.D., Meltzer C.C. Ethical considerations in artificial intelligence // Eur J Radiol. 2020. Vol. 122. P. 108768. doi: 10.1016/j.ejrad.2019.108768
27. Сайт Президента России. Перечень поручений по итогам конференции по искусственному интеллекту [электронный ресурс]. Режим доступа: http://www.kremlin.ru/acts/assignments/orders/64859. Дата обращения: 11.07.2021.
28. Экспертный центр электронного государства. Актуальные задачи международного взаимодействия по развитию и регулированию искусственного интеллекта [электронный ресурс]. Режим доступа: http://d-russia.ru/aktualnye-zadachi-mezhdunarodnogo-vzaimodejstviya-po-razvitiyu-i-regulirovaniyu-iskusstvennogo-intellekta.html. Дата обращения: 11.07.2021.
29. Распоряжение Правительства Российской Федерации от 19.08.2020 № 2129-р. Режим доступа: http://publication.pravo.gov.ru/Document/View/0001202008260005?index=0&rangeSize=1. Дата обращения: 11.07.2021.
30. Указ Президента Российской Федерации от 10.10.2019 № 490 «О развитии искусственного интеллекта в Российской Федерации». Режим доступа: http://www.kremlin.ru/acts/bank/44731. Дата обращения: 11.07.2021.
31. Министерство промышленности и торговли Российской Федерации. Федеральное агентство по техническому регулированию и метрологии. Приказ от 25 июля 2019 года № 1732 «О создании технического комитета по стандартизации "Искусственный интеллект"». Режим доступа: https://docs.cntd.ru/document/560916332. Дата обращения: 11.07.2021.
32. Технический комитет по стандартизации «Искусственный интеллект» (ТК164). Приказ от 13.01.2020 № 1 «Об определении базовой организации подкомитета "Искусственный интеллект в здравоохранении"». Режим доступа: https://tele-med.ai/media/uploads/2021/03/18/01_-2-2.pdf. Дата обращения: 11.07.2021.
33. Морозов С.П., Чернина В.Ю., Андрейченко А.Е., и др. Как искусственный интеллект влияет на оценку поражения легких при COVID-19 по данным КТ грудной клетки? // Digital Diagnostics. 2021. Vol. 2, № 1. P. 27–38. doi: 10.17816/DD60040

AUTHORS' INFO

*** Daria E. Sharova**;
address: 28-1 Srednyaya Kalitnikovskaya str.,
109029 Moscow, Russia;
ORCID: https://orcid.com/0000-0001-5792-3912;
eLibrary SPIN: 1811-7595; e-mail: d.sharova@npcmr.ru

Victoria V. Zinchenko,
ORCID: https://orcid.com/0000-0002-2307-725X;
eLibrary SPIN: 4188-0635; e-mail: v.zinchenko@npcmr.ru

ОБ АВТОРАХ

*** Шарова Дарья Евгеньевна;**
адрес: Россия, 109029, Москва,
Средняя Калитниковская ул., д. 28, стр. 1;
ORCID: https://orcid.com/0000-0001-5792-3912;
eLibrary SPIN: 1811-7595; e-mail: d.sharova@npcmr.ru

Зинченко Виктория Валерьевна,
ORCID: https://orcid.com/0000-0002-2307-725X;
eLibrary SPIN: 4188-0635; e-mail: v.zinchenko@npcmr.ru

* Corresponding author / Автор, ответственный за переписку

Ekaterina S. Akhmad,
ORCID: https://orcid.com/0000-0002-8235-9361;
eLibrary SPIN: 5891-4384; e-mail: e.ahmad@npcmr.ru

Olesia A. Mokienko, MD, Cand. Sci. (Med.);
ORCID: https://orcid.com/0000-0002-7826-5135;
eLibrary SPIN: 8088-9921; e-mail: o.mokienko@npcmr.ru

Anton V. Vladzymyrskyy, MD;
ORCID: https://orcid.com/0000-0002-2990-7736;
eLibrary SPIN: 3602-7120; e-mail: a.vladzimirsky@npcmr.ru

Sergey P. Morozov, MD, Dr. Sci. (Med.), Professor;
ORCID: https://orcid.com/0000-0001-6545-6170;
eLibrary SPIN: 8542-1720; e-mail: morozov@npcmr.ru

Ахмад Екатерина Сергеевна,
ORCID: https://orcid.com/0000-0002-8235-9361;
eLibrary SPIN: 5891-4384; e-mail: e.ahmad@npcmr.ru

Мокиенко Олеся Александровна, к.м.н.;
ORCID: https://orcid.com/0000-0002-7826-5135;
eLibrary SPIN: 8088-9921; e-mail: o.mokienko@npcmr.ru

Владзимирский Антон Вячеславович, д.м.н.;
ORCID: https://orcid.com/0000-0002-2990-7736;
eLibrary SPIN: 3602-7120; e-mail: a.vladzimirsky@npcmr.ru

Морозов Сергей Павлович, д.м.н., профессор;
ORCID: https://orcid.com/0000-0001-6545-6170;
eLibrary SPIN: 8542-1720; e-mail: morozov@npcmr.ru

DOI: https://doi.org/10.17816/DD71434

Современные технологии визуализации и термоаблации очагов гиперпаратиреоза

П.О. Румянцев[1], А.А. Бубнов[2, 3], М.В. Дегтярев[2], К.Ю. Слащук[2], С.М. Захарова[2], Д.Ю. Агибалов[3], В.Ю. Тимошенко[3, 4]

[1] Международный медицинский центр «СОГАЗ МЕДИЦИНА», Санкт-Петербург, Российская Федерация
[2] Национальный медицинский исследовательский центр эндокринологии, Москва, Российская Федерация
[3] Национальный исследовательский ядерный университет МИФИ, Москва, Российская Федерация
[4] Московский государственный университет имени М.В. Ломоносова, Москва, Российская Федерация

АННОТАЦИЯ

Патология околощитовидных желёз по частоте встречаемости находится на третьем месте среди эндокринных болезней, уступая сахарному диабету и заболеваниям щитовидной железы. На сегодняшний день в клинической практике широко применяются только два метода лечения гиперпаратиреоза — консервативный и хирургический. Однако в последние время помимо них появились способы транскутанной термодеструкции (аблации), основанные на прицельном физическом воздействии — лазерном, радиочастотном, микроволновом, ультразвуковом. Настоящий обзор посвящён критическому анализу современного арсенала методов локальной термодеструкции гиперфункции околощитовидных желёз при гиперпаратиреозе. Цель обзора — показать возможности современных неинвазивных и малоинвазивных методов лечения гиперпаратиреоза без противопоставления их хирургическому методу. В обзор включены данные рандомизированных клинических исследований за период с 2012 по 2021 г., найденных в Google Scholar, Pubmed. Общее количество пациентов — 1938 (лазерная аблация — 216, радиочастотная аблация — 225, микроволновая аблация — 1467, аблация ультразвуком высокой плотности — 30). Получены критерии применимости методов термодеструкции. Составлен алгоритм по лечению гиперпаратиреоза. Таким образом, в качестве альтернативы хирургическому вмешательству проанализированы четыре современных метода термодеструкции патологически изменённых околощитовидных желёз, каждый из которых имеет преимущества и недостатки, свой профиль эффективности и безопасности. Как показывает анализ существующей доказательной практики, наибольшей популярностью среди клиницистов пользуется метод микроволновой аблации, однако более эффективным методом термодеструкции гиперфункционирующих околощитовидных желёз является лазерная аблация.

Ключевые слова: гиперпаратиреоз; термодеструкция; аблация околощитовидных желёз; лазерная аблация; радиочастотная аблация; микроволновая аблация; HIFU-аблация.

Как цитировать

Румянцев П.О., Бубнов А.А., Дегтярев М.В., Слащук К.Ю., Захарова С.М., Агибалов Д.Ю., Тимошенко В.Ю. Современные технологии визуализации и термоаблации очагов гиперпаратиреоза // *Digital Diagnostics*. 2021. Т. 2, № 3. С. 369–385. DOI: https://doi.org/10.17816/DD71434

Рукопись получена: 13.08.2021 **Рукопись одобрена:** 24.08.2021 **Опубликована:** 02.09.2021

ЭКО•ВЕКТОР

DOI: https://doi.org/10.17816/DD71434

Methods of medical visualization and thermal ablation as a new approach to treatment of hyperparathyroidism

Pavel O. Rumyantsev[1], Aleksandr A. Bubnov[2, 3], Mikhail V. Degtyarev[2], Konstantin Yu. Slashchuk[2], Svetlana M. Zakharova[2], Dmitry Yu. Agibalov[3], Viktor Yu. Timoshenko[3, 4]

[1] International Medical Center "SOGAZ", Saint-Petersburg, Russian Federation
[2] Endocrinology Research Centre, Moscow, Russian Federation
[3] National Research Nuclear University MEPhI (Moscow Engineering Physics Institute), Moscow, Russian Federation
[4] Lomonosov Moscow State University, Moscow, Russian Federation

ABSTRACT

The pathologies of parathyroid glands are widespread among endocrine system diseases, excluding diabetes and thyroid pathology. There are only two methods that are used to treat hyperparathyroidisms, such as surgery and conservative therapy. However, transracial thermal destruction methods (ablation) have recently appeared in clinical practice. The methods have good precision and connect with physical phenomena, such as interaction laser, radiofrequency, microwave, and HIFU irradiation with bio substance. The review is dedicated to critically analyze the modern methods for local thermal destruction of the hyper-functioning parathyroid glands. The review includes data from randomized clinical trials from 2012 to 2021. The studies were from Google Scholar and Pubmed with a total number of 1,938 patients (laser ablation — 216 patients, radiofrequency ablation — 225, microwave ablation — 1467, high-density ultrasound ablation — 30 patients). Recommendations methods of thermal destruction application were obtained during the review. Furthermore, we have designed some algorithms for hyperparathyroidism treatment. Moreover, thermal destruction methods were observed. There are four modern methods of thermal destruction which have been analyzed like alternatives to surgery. Each of them has advantages and disadvantages, its profile of safety and effectiveness. After processing information from a proven database, the most popular among specialists is methods of microwave ablation. However, laser ablation is more effective than other ways.

Keywords: hyperparathyroidism; thermal destruction; ablation of parathyroid glands; laser ablation; radiofrequency ablation; microwave ablation; HIFU ablation.

To cite this article

Rumyantsev PO, Bubnov AA, Degtyarev MV, Slashchuk KY, Zakharova SM, Agibalov DYu, Timoshenko VY. Methods of medical visualization and thermal ablation as a new approach to treatment of hyperparathyroidism. *Digital Diagnostics*. 2021;2(3):369–385. DOI: https://doi.org/10.17816/DD71434

Received: 13.08.2021 **Accepted:** 24.08.2021 **Published:** 02.09.2021

DOI: https://doi.org/10.17816/DD71434

甲状旁腺功能亢进病灶可视化和热消融的现代技术

Pavel O. Rumyantsev[1], Aleksandr A. Bubnov[2, 3], Mikhail V. Degtyarev[2], Konstantin Yu. Slashchuk[2], Svetlana M. Zakharova[2], Dmitry Yu. Agibalov[3], Viktor Yu. Timoshenko[3, 4]

[1] International Medical Center "SOGAZ", Saint-Petersburg, Russian Federation
[2] Endocrinology Research Centre, Moscow, Russian Federation
[3] National Research Nuclear University MEPhI (Moscow Engineering Physics Institute), Moscow, Russian Federation
[4] Lomonosov Moscow State University, Moscow, Russian Federation

简评

甲状旁腺病理学在内分泌疾病中居第三位，仅次于糖尿病和甲状腺疾病。 目前，只有两种治疗甲状腺功能亢进的方法被广泛应用于临床：保守的和手术的。然而，最近还出现了基于激光、射频、微波等目标物理效应的跨层热分解（消融）方法，超声波。本综述致力于对甲状腺功能亢进的局部热分解方法的现代武库进行批判性分析。本综述的目的是展示现代无创和微创方法治疗甲状旁腺功能亢进的可能性，同时又不反对手术方法。 该综述包括2012年至2021年期间在谷歌学者（Google Scholar，PubMed）中发现的随机临床研究数据。患者总数-1938人（激光消融216人，射频消融225人，微波消融1467人，高密度超声消融30人）。获得了热分解方法的适用性标准。建立了治疗甲状腺功能亢进的算法。因此，作为手术干预的替代方法，已经分析了四种现代热破坏病理改变的甲状旁腺方法，每种方法都有优点和缺点，其自身的有效性和安全性。 对现有循证实践的分析表明，最受临床医生欢迎的是微波消融方法，而激光消融是一种更有效的热破坏功能亢进的甲状旁腺的方法。

关键词：甲状旁腺功能亢进； 热破坏； 甲状旁腺消融； 激光烧蚀； 射频消融； 微波消融； HIFU 消融。

引用本文

Rumyantsev PO, Bubnov AA, Degtyarev MV, Slashchuk KY, Zakharova SM, Agibalov DYu, Timoshenko VY. 甲状旁腺功能亢进病灶可视化和热消融的现代技术. *Digital Diagnostics*. 2021;2(3):369–385. DOI: https://doi.org/10.17816/DD71434

收到：13.08.2021 **接受：**24.08.2021 **发布日期：**02.09.2021

INTRODUCTION

Hyperparathyroidism (HPT) is an autonomous hyperfunction of one or more parathyroid glands. Primary HPT (PHPT) results from primary autonomous hyperfunction, mostly of a single parathyroid gland of neoplastic nature. Secondary (SHPT) and tertiary HPT, which are most common with multiple hyperfunctioning parathyroid glands, occur in response to chronically low blood calcium concentrations due to chronic renal failure [1].

PHPT is characterized by excessive secretion of parathyroid hormone (parathormone) with upper normal or increased blood calcium concentrations due to primary parathyroid gland pathology. The worldwide PHPT prevalence ranges between 1–40 cases per 100,000 population [2]. In addition, PHPT is more common in the working age. In the age group of up to 45 years, the probability of developing the disease is equal for both genders, whereas after 45 years, this pathology becomes more typical for women [3].

SHPT results from a compensatory increased parathormone production in response to decreased serum calcium concentrations [4] and is most frequently observed in the end-stage renal disease. Up to 75% of patients with renal failure have clinically evident SHPT; of these patients, 5% require surgical treatment [5].

The main methods for diagnosing HPT are biochemical blood test (parathyroid hormone, calcium, phosphorus, creatinine, and vitamin D concentrations) and a 24 h urine test (calcium). Once the diagnosis is confirmed, and if radical treatment is indicated, instrumental examinations (ultrasound (US), contrast-enhanced X-ray computed tomography, and radioisotope scanning) are performed, including hybrid methods of molecular imaging (planar scintigraphy and single-photon emission computed tomography/computed tomography [SPECT/CT]) with technetril staining (^{99m}Tc-MIBI) or 18F-choline positron emission tomography/CT (PET/CT) [6, 7].

Currently, two methods of HPT treatment are widely used in clinical practice, that is, conservative therapy and surgery (Table 1). Conservative therapy includes drug treatment [8] to reduce hypercalcemia and prevent hypercalcemic crises and fractures. This method lacks a radical HPT treatment and is used mostly in mild, uncomplicated HTP forms, the impossibility of parathyroidectomy, or refusal of the patient to undergo surgery. The surgical treatment can radically eliminate parathormone hyperproduction; however, this method is associated with hospitalization, anesthesia, risk of surgical complications, scarring on the neck, and recovery period [9, 10].

The introduction of new algorithms for imaging parathyroid glands in HPT into surgical practice improved the topical differential diagnosis, increased the precision, and reduced the number of surgical injuries. [11]. Endoscopic technologies, intraoperative neuromonitoring, and fluorescence imaging of the periothyroid glands allow improved efficiency and safety of interventions [12]. The efficiency of surgical treatment is 92%–94% [13]. However, not all patients are willing to be operated on, and others have no opportunity to undergo surgery (contraindications and risk to life with anesthesia and surgery).

Thus, in the study by B. Wu et al. [14], surgical HPT treatment was performed in only 29% of patients with absolute indications. Most frequently, patients aged up to 60 years undergo surgery, whereas in older age groups, the proportion of surgical interventions decreases by 1.5–3 times every decade.

Table 1. Conventional HPT treatments

Treatment	Indications	Approach	Imaging
Conservative therapy	• Correction of hypercalcemia • Prevention of hypercalcemic crises • Prevention of low traumatic fractures	• Palliative • Symptomatic	-
Surgery	• Serum total calcium concentration of 0.25 mmol/L (1 mg%) exceeding the laboratory norm • Decreased glomerular filtration rate (<60 mL/min/1.73 m^2) • Visceral PHPT manifestations (ICD) • Daily calcium excretion (>400 mg/10 mmol per day) • Decreased bone mineral density in radius, femur, or vertebrae (<–2.5 SD by T-criterion) • A history of low traumatic fractures and/or radiologically detectable vertebral body fractures (based on MSCT or MRI) • Age of <50 years	• Radical	• US, scintigraphy (SPECT/CT, PET/CT) • Contrast-enhanced CT, PET/CT

Note. PHPT (ICD), primary hyperparathyroidism; MSCT, multispiral computed tomography; MRI, magnetic resonance imaging; SPECT/CT, single-photon emission computed tomography/computed tomography; PET/CT, positron emission tomography/computed tomography.

In this regard, the development of alternative methods of destruction (ablation) of hyperfunctioning parathyroid glands is necessary.

In addition to surgical treatment, methods of transcutaneous thermal destruction (ablation) based on targeted physical effects (laser, radio frequency, microwaves, and US), appeared in clinical practice (Table 2) [15–17].

According to the Google Scholar database, microwave ablation was used in the largest number of papers on thermal destruction of hyperfunctioning parathyroid glands, whereas high-intensity focused US (HIFU) ablation was used in the smallest number (Fig. 1).

Radiofrequency and laser ablation occupy an intermediate position. The high popularity and accumulated wide experience of microwave ablation is due to the leading position among all currently known methods for thermal destruction of the parathyroid glands.

CURRENT PREOPERATIVE IMAGING AND INTRAOPERATIVE NAVIGATION OPTIONS

Before considering alternative surgical methods of parathyroid gland destruction in HTP, the current possibilities of their imaging at the preoperative and intraoperative stages should be highlighted.

Preoperative parathyroid gland imaging

US is the standard, most accessible, and safe method for preoperative imaging in HTP (Fig. 2).

In addition to US, either single-isotope biphasic scintigraphy with ^{99m}Tc-MIBI or dual-isotope scintigraphy in SPECT/CT mode with ^{99m}Tc-MIBI and $^{99m}TcO_4$ (pertechnetate) is performed [18, 19] (Fig. 3).

Table 2. Characteristics of different methods for thermal destruction of hyperfunctioning parathyroid glands in verified HPT (based on international recommendations)

Ablation	*n*	Applicability criteria	Operating mode	Efficiency	Side effects
Laser	216	• Lesion diameter (≤30 mm) • Contraindications to surgery • Restrictions on ectopia • Age over 18 years	3 W 6–10 min	92%	8% (dysphonia)
Radio frequency	225	• Parathormone (≥800 ng/mL) • Number of parathyroid hyperplasias (<4) • Uncontrolled SHPT with drug treatment • No serious clotting disorders, heart failure, or uncontrolled hypertension	10–50 W 1–2 min	83,6%	2,1% (transient hypocalcemia, transient hoarseness)
Microwaves	1467	• Renal failure with hyperparathyroidism • Inefficient conservative treatment (despite adequate drug therapy) • Parathormone concentrations (≥600 pg/mL) • At least one enlarged parathyroid gland • Minimum gland diameter (≥6 mm) • Not applicable for surgical resection • Parathyroid glands in an area that is difficult to access for resection	30 W 3–5 min	89,4%	6% (hoarseness)
High-intensity focused US	30	• Serum calcium concentrations (≥2.60 mmol/L) • A cytologically proved lesion of parathyroid origin • Adenoma depth (<23 mm) between posterior margin and skin surface • Adenoma thickness (>8 mm) • Distance from trachea (>3 mm), distance from esophagus and carotid artery (>2 mm) • No significant macrocalcifications at <10 mm distance from the target • Age over 18 years	5 W 2–3 min	Complete remission in 23% after one year; good control of the disease in 69%	Temporary side effects included impaired vocal cord mobility (23.1%), subcutaneous swelling (23.1%), and combined effect (15.2%)

Note. *n,* the total number of patients treated at the date of writing.

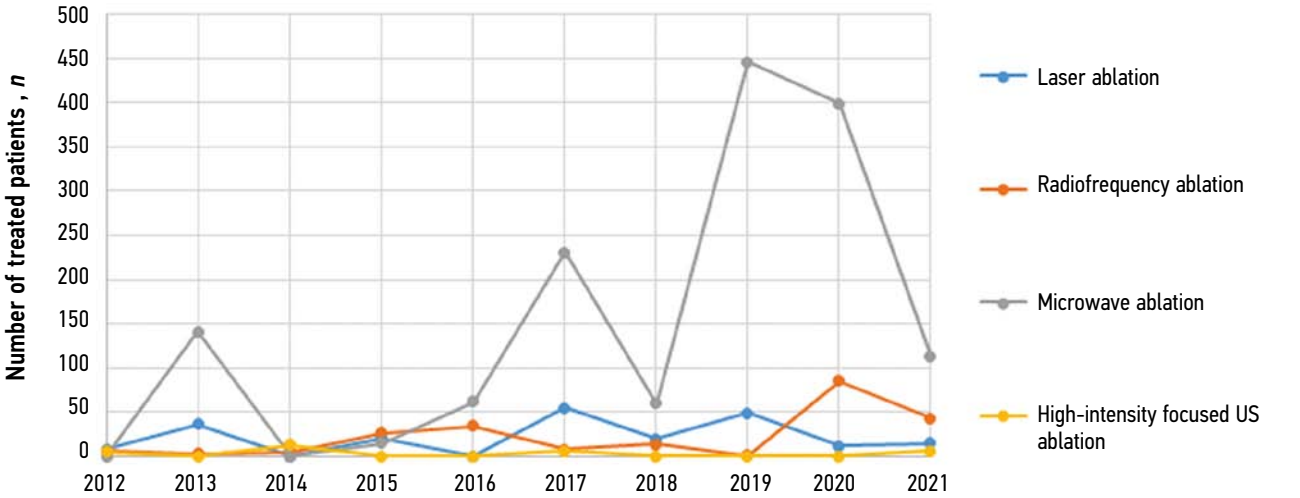

Fig. 1. Dynamics of publications on the use of alternative methods for periothyroid gland destruction.

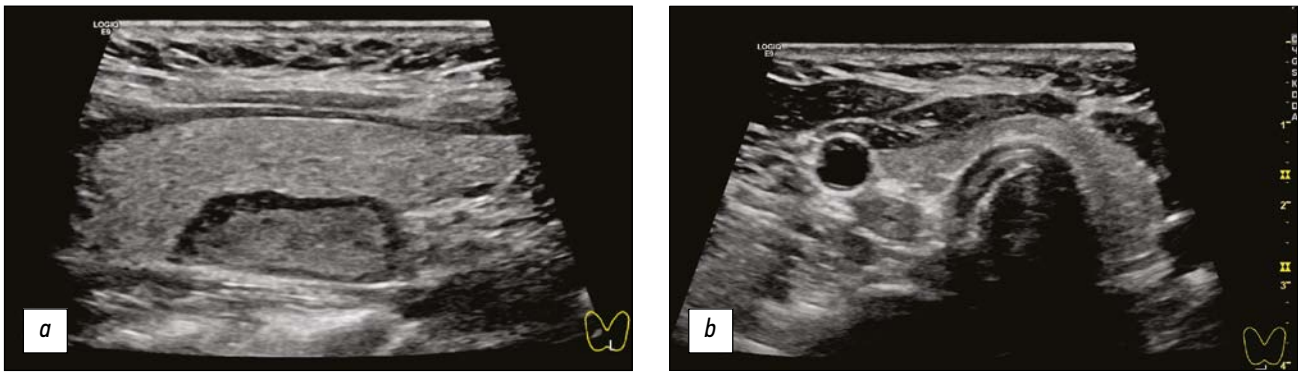

Fig. 2. US imaging of hyperfunctioning parathyroid glands in HPT: *a*, PHPT; *b*, SHPT.

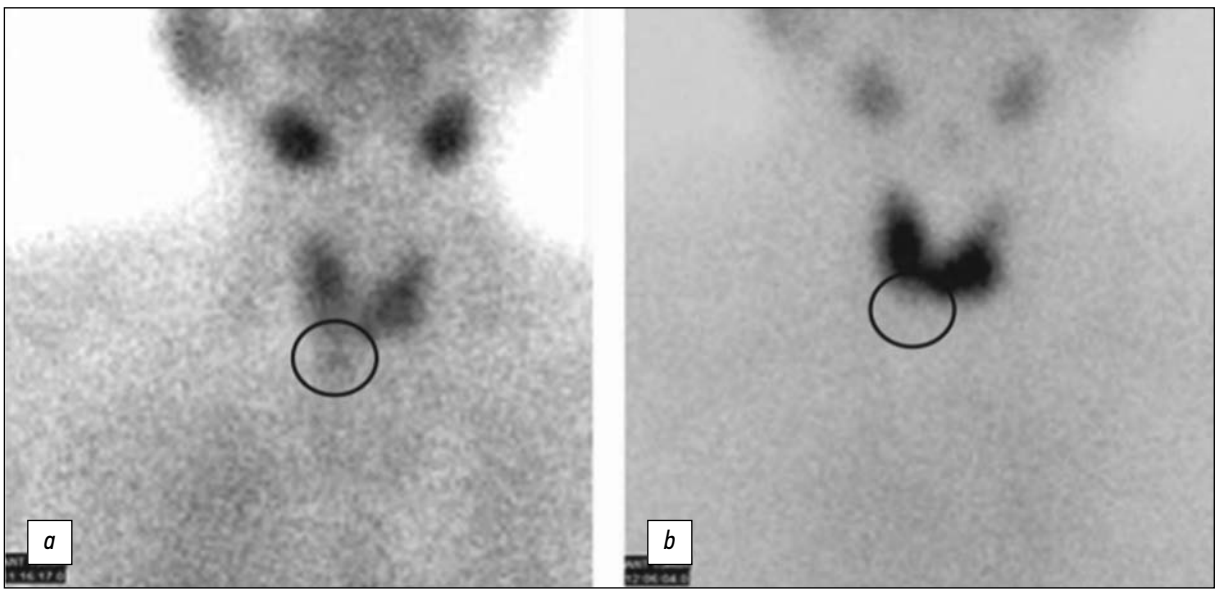

Fig. 3. Dual-isotope scintigraphy: *a*, ^{99m}Tc-MIBI scintigraphy; *b*, ^{99m}Tc-TcO4 scintigraphy.

The most informative method for topical HPT diagnosis is ^{99m}Tc-MIBI radionuclide diagnostics, especially in SPECT/CT mode (Fig. 4). On average, the sensitivity of the method reaches 88% (with a positive prognostic value of 96%) [20].

According to the literature, the sensitivity of ^{99m}Tc-MIBI studies in patients with PHPT is 88% [21], whereas a combination of diagnostic methods gives better results. Thus, a combination of ^{99m}Tc-MIBI scintigraphy and US has a sensitivity of 95% compared with the 80% and 87% for US and separate radionuclide diagnosis, respectively [22].

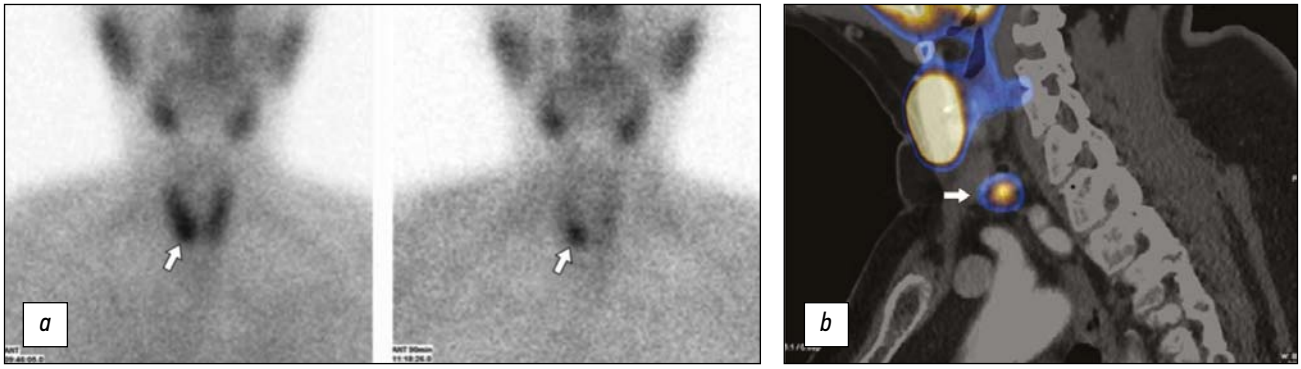

Fig. 4. ^{99m}Tc-MIBI radionuclide examinations (technetril): *a*, dual-phase planar scintigraphy (early and delayed scans). A parathyroid mass is visualized in the right lobe projection (arrows) with preserved and increased accumulation of radiopharmaceuticals on the delayed scan; *b*, ^{99m}Tc-MIBI SPECT/CT. A periothyroid mass is visualized behind and downward from the lower pole of the left lobe (arrow), which accumulates radiopharmaceuticals.

Intraoperative imaging for minimally invasive parathyroid removal techniques

The complementarity of preoperative and intraoperative imaging methods is an important factor for the localization of pathological structures when using minimally invasive techniques for the removal of parathyroid glands (Fig. 5).

Among intraoperative imaging methods, US is most commonly used to obtain real-time information about the region

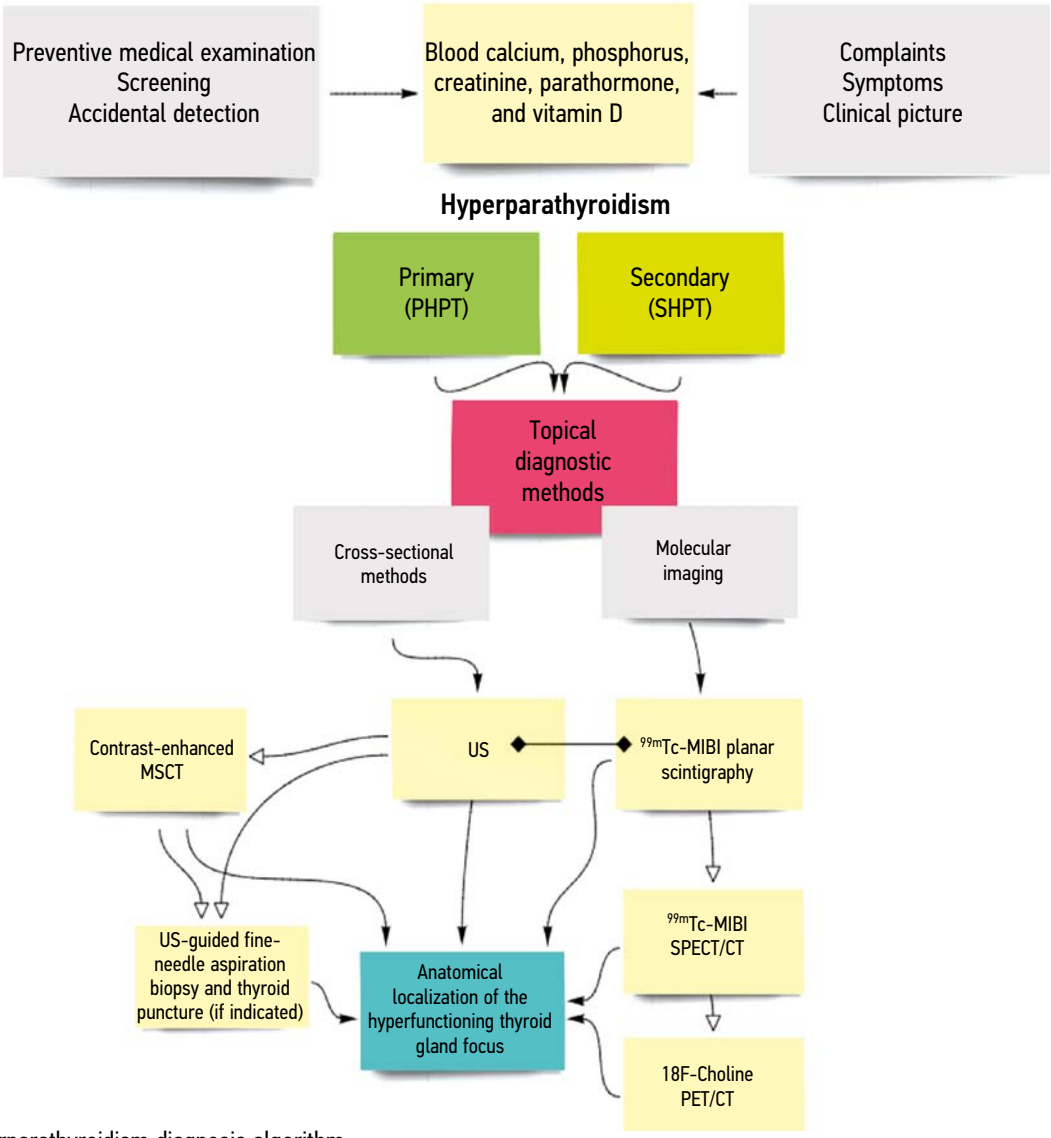

Fig. 5. Hyperparathyroidism diagnosis algorithm.

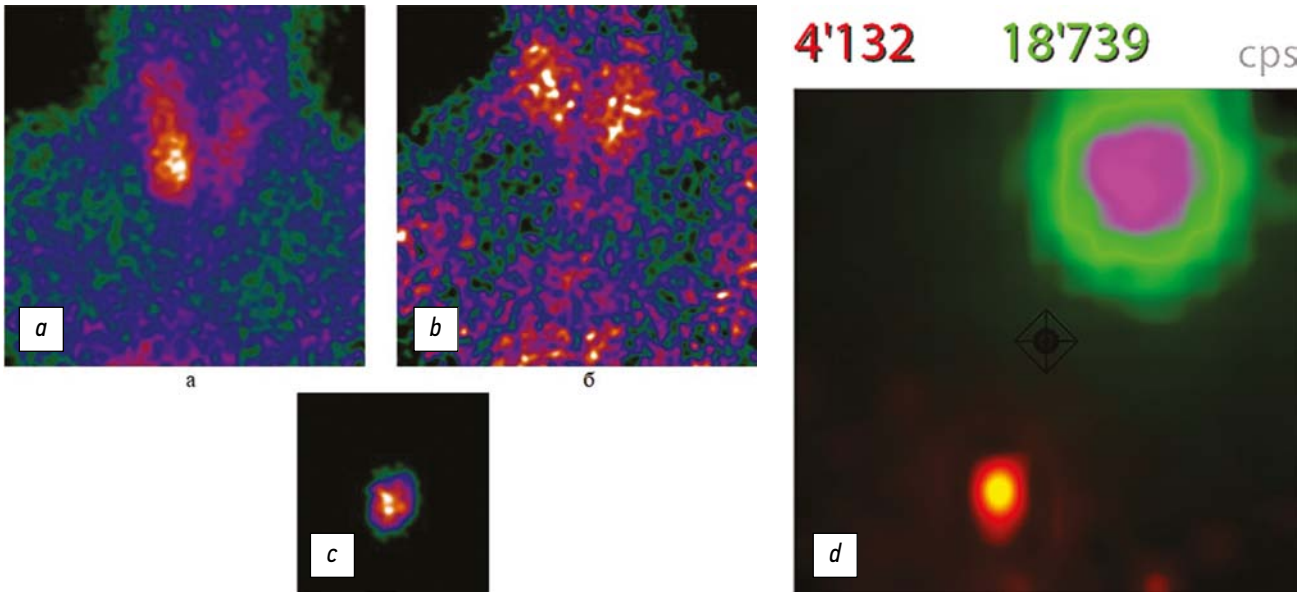

Fig. 6. Images obtained with Sentinella-102 (*a–c*) and CrystalCam (*d*) multichannel gamma probes.

of interest. However, with advances in technologies, multichannel gamma probes, including portable (Sentinella-102) and handheld (CrystalCam) gamma cameras, may be used in addition to US (Fig. 6).

These devices are based on the same physical principles. However, they implement different technical solutions, which make the use of handheld gamma cameras more promising (Table 3). Given the better characteristics, CrystalCam provides higher-quality (contrast) images as opposed to Sentinella-102.

Thus, intraoperative imaging techniques allow to control the thyroid bed area and use parathyroid gland destruction methods, which are alternatives to parathyroidectomy.

MINIMALLY INVASIVE THERMAL ABLATION OF HYPERFUNCTIONING PARATHYROID GLANDS

Thermal ablation has uncontrolled effects on surrounding tissues to varying degrees, and the location of the parathyroid glands may be adjacent to the recurrent laryngeal nerve. The need to assess the risk of recurrent laryngeal nerve damage during thermal ablation creates additional difficulties in the choice of treatment, given that the loss of vocal function is a highly undesirable complication. The more focused and controlled the thermal exposure, the lower the risk of surrounding tissue damage. For example, the MRgFUS method (InSightec, Israel) uses MR-guided focused US by heating the object of thermal destruction (see below). Currently, no sufficient evidence exists for the full comparison of thermal ablation and surgical treatment in terms of risk of recurrent laryngeal nerve damage. However, the evidence base will continually grow.

Laser destruction (ablation)

The invention of the ruby crystal laser by the American physicist Theodore H. Maiman in 1960 ushered in an era of using this technology in various fields of human life, including medicine [23]. The laser found its first practical application in medicine for microadhesion during retinal surgery in 1962. Historically, lasers were originally used in ophthalmology, given that the eye and its interior are among the

Table 3. Characteristics of gamma probes

Parameters	Installation	
	Portable gamma camera	Handheld gamma camera
Model	Sentinella-102	CrystalCam
Sensitivity, count rate, MBq	300–200	5000
Count rate, 10^6	1,7	6,2
Spatial resolution with collimator (native), mm	4–10 at 10 cm distance with different collimators	5,4–9,2
Energy resolution, %	16	<7
Dynamic range of detectable energies, keV	50–200	40–250

most accessible organs due to their transparency. The first procedure that may be called laser ablation was performed at the National Medical Laser Centre in London in 1984. A patient with skin cancer underwent a 10 min surgery using Nd-YAG laser radiation with a 20 W output power [24].

Laser ablation is based on heating pathological biostructures by the application of energy to cause irreversible damage at the cellular level (tissue necrosis due to fluid heating in cells and its subsequent evaporation). Typically, tissues are heated to a temperature of 50 °C–54 °C to achieve coagulation within the region of interest.

Currently, laser ablation is increasingly used to remove parathyroid glands. The technique is based on the US-guided introduction of fibers into the periothyroid gland (Fig. 7). Then, the laser is switched on, and energy is brought in through the fiber to further coagulate the tissue. For laser ablation, a hybrid system is commonly used (EchoLaser X4, Esaote, Genova, Italy), and it combines US with a linear sensor and four independent fibers to deliver laser radiation to the periothyroid gland. The radiation is generated by a diode laser with a wavelength of 1064 nm, a beam diameter of 0.3 mm, and an output power level of 1–7 W. Optical fibers 1.5 m long with a 300 μm core are inserted percutaneously into the target using a 21G needle.

The use of laser ablation to treat patients with functional adenomas of parathyroid glands demonstrates high levels of sustained complete response with a clinically significant follow-up period within 24 months. Clinical HPT symptoms disappeared by 6 months. Alternatively, persistent serologic normalization of parathormone and calcium was observed by the same period [25].

Radiofrequency ablation

The capability of radiofrequency waves to pass through biological tissues was discovered in 1891. However, an increase in tissue temperature did not result in neuromuscular excitation. Thus, this discovery became the starting point for the development of the radiofrequency ablation method [26]. For a long time, scientists faced the problem of tissue necrosis expansion during exposure to radiofrequency waves and after its solving, had difficulties associated with the uncontrollable form and unpredictability of necrosis development. This problem was solved only by the end of the XX century, with the invention of a special electrode type that allowed the prediction of necrosis in tissues more accurately [27].

The physical basis of the method is resistive heating through an electrically conductive pathway (exposure to alternating current on the tissue), which consists of tissue molecules with most of the particles being water molecules. The dipole moments of the molecules, while attempting to remain aligned in the direction of the current, are forced to oscillate when the alternating current is rapidly applied and transmit the oscillations to neighboring molecules. Energy losses due to friction between adjacent molecules lead to local energy release and temperature increase above 50 °C, which activates the subsequent tissue necrosis. Radio waves are generated in the frequency range of 450–500 kHz. The main physical limitation of the method is its use in tissues with low electrical conductivity [28].

Radiofrequency ablation is used for various tumors, including those of lungs, kidneys, breasts, bones, thyroid glands, and liver [29–31]. Recently, studies have been conducted to verify the efficiency and safety of this technique in PHPT treatment and consider it as an alternative to open parathyroidectomy [32]. The procedure is US guided. A probe is inserted into the adenoma through a puncture, and the total power delivered to the adenoma varies from 10 W to 70 W, depending on the mass size [33].

The method is an alternative to open parathyroidectomy for patients with comorbidities and a single adenoma that is visible on US and SPECT/CT. Large adenomas that cause discomfort in the neck or cosmetic problems are also good candidates. If periothyroid glands are suspected for a malignancy (US signs of local invasion, size >3 cm, laboratory parathormone >300 pmol/L, and albumin-corrected calcium >3 mmol/L), the procedure is contraindicated. If periothyroid

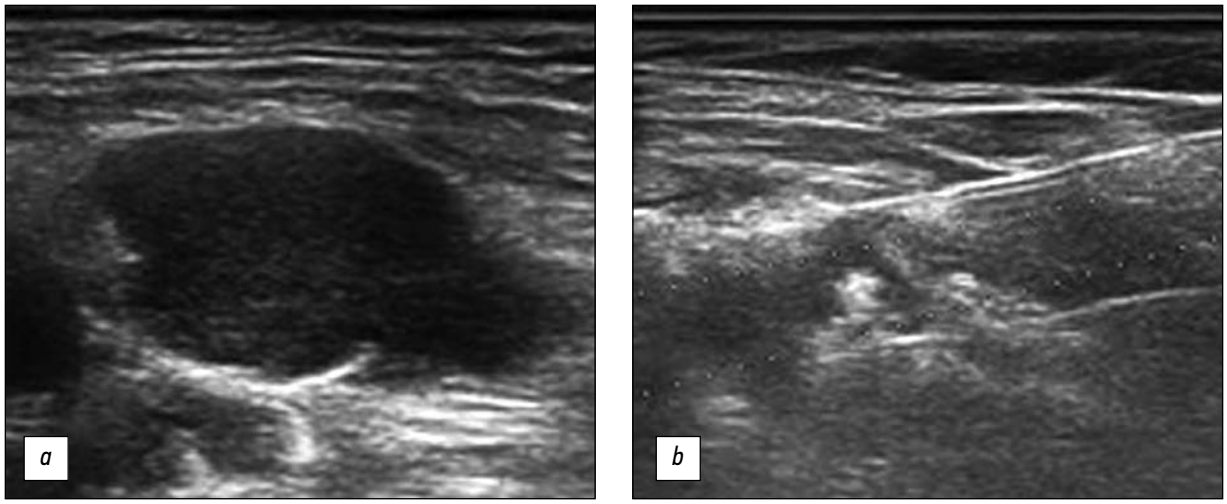

Fig. 7. Laser ablation in primary hyperparathyroidism: *a*, parathyroid adenoma; *b*, two laser fibers and a periothyroid area after ablation.

carcinoma is suspected, then surgical removal and pathomorphologic verification are recommended.

Microwave ablation

Microwave ablation is the "youngest" method. The first references to the use of microwave ablation date back to the 1980s. However, generators applicable for this procedure began to be produced commercially in the XXI century, which largely pushed the development of this area [34].

The mechanism of microwave ablation is based on the effect of electromagnetic fields with high frequencies (915 MHz to 2.45 GHz). This type of radiation is between infrared radiation and radio waves. Water molecules are polar, that is, electric charges on molecules are asymmetrical. The part of molecules that contains two hydrogen atoms is positively charged, whereas that with oxygen is negatively charged. Molecules function as small electric dipoles that rapidly rotate back and forth in spatial orientation and attempt to align with charges of opposite polarity. Polar molecules in the tissue are forced to continuously rearrange with the oscillating electric field and increase their kinetic energy and consequently, the temperature of the tissue. Tissues with a high-water content (such as solid organs and tumors) are the most favorable for this type of heating. When temperatures reach 50 °C–100 °C, protein and enzymatic degradation and denaturation of histone complexes, which are necessary to maintain the tertiary DNA structure, are activated. After exposure to these cytotoxic temperatures, cell death through coagulation necrosis eventually occurs [35].

Microwave ablation for PHPT is US-guided. The surgeon creates access through a 17G needle to bring the applicator antenna to the periothyroid gland. At the end of the applicator, a field is formed through which energy is transmitted to the tissue. Ablation is performed in a fractionation mode with an input power of 30 W for 25–30 s for each point in the volume. The duration of the procedure is 3–5 min, and it is performed until a hypoechogenic picture is obtained on the US image [36].

According to the literature, the incidence of recurrent and persistent HPT after parathyroidectomy was 0.83%–26% and 0.4%–15%, respectively [37]. When microwave ablation was used to remove the parathyroid glands, the rates of local recurrence and new cases were 8.8% and 11.8%, respectively. Ablation implicitly differed from surgical treatment; however, the long-term efficiency was not inferior to parathyroidectomy [38]. The use of microwave ablation as a radical method for treatment in patients with PHPT is safe and effective, whereas the long-term follow-up period showed no increase in the number of complications.

High-intensity focused ultrasound ablation

R.W. Wood and A.L. Loomis first introduced the thermal properties of high-intensity US in 1927. Subsequently, J.G. Lynn described the use of a focused US generator in 1942, and this generator can induce *ex vivo* focal thermal ablation of liver and brain samples through intermediate areas of the skull and cerebral membranes without skin damage [39]. In the 1950s, brothers William and Francis Fry developed a transcranial system based on high-intensity US, and it can be used after craniotomy in animals to target deep parts of the brain, contributing to the development of interest in this type of ablation for the treatment of movement disorders such as Parkinson's disease [40].

The earliest cases of high-intensity US ablation therapy were described in the early 1990s in patients with prostate diseases, and further improvements in imaging techniques (US and MRI) allowed the treatment of a wide range of benign and malignant tumors [41]. Currently, the HIFU method is used to remove benign functionally active nodular neoplasms of the thyroid gland, hyperfunctioning parathyroid glands, and in prostate cancer [42–44].

The formation of ultrasonic waves occurs as a result of the inverse piezoelectric effect. The generator supplies an alternating voltage to the plate covers, which are applied to the piezoelectric crystal (quartz crystal). Consequently, the crystal lattice is deformed when exposed to the electric field, and forced oscillations occur. Resonance of oscillations is observed when the change frequency in the electric field voltage and the natural frequency of the crystal oscillation coincide. As a result, with a decrease in the crystal thickness, rarefaction is developed in the adjacent layers of the surrounding medium, and with its increase, the medium particles thicken. Thus, an ultrasonic wave arises in the medium, and it propagates in the direction perpendicular to the piezoelectric crystal surface.

Ultrasonic waves are generated in the frequency range from 20 kHz to 1 THz. Therapeutic US has an intensity of >5 W/cm^2, which may result in coagulation tissue necrosis and is most commonly used for ablation. Protein denaturation and coagulation necrosis usually occur at 56°C and have a 1 s exposure time, whereas temperatures above 43° for 1 h make tissues more susceptible to chemotherapy and radiation. The increase in temperature of biological tissues, which results from the absorption of ultrasonic radiation, is linearly proportional to sound intensity.

Currently, EchoPulse (Theraclion, Paris, France) is the only system available for high-intensity US ablation in PHPT. The device contains a diagnostic US unit for intraoperative imaging (7.5 MHz) and a therapeutic US component (3 MHz) for delivering the energy to the target volume. A special cooling circuit reduces the temperature between successive pulses. A pulse of therapeutic US creates an elliptical ablation area with the semi-major and semi-minor axes of 4.5 and 1 mm, respectively. After preplanning the procedure, several pulses are delivered to perform ablation. Safe boundaries of the treated area from the trachea, carotid artery, and skin are 3, 2 mm, 5 mm, respectively. The maximum treatable depth from the skin surface is 28 mm. The procedure is usually performed under sedation, during

which the patient is conscious, and local anesthesia is rarely required.

Thus, the size of parathyroid glands and parathyroid hormone level decrease significantly after one month of therapy, whereas the calcium concentrations slowly decrease. Complete remission is noted in 23% after a year, good disease control is achieved in 69%, and the procedure is considered unsuccessful in 8% of the treated patients. The number of sessions largely depends on the therapeutic response [45].

Despite the encouraging results of these studies, high-intensity US therapy still has limiting factors. The procedure is time consuming, and the patient must remain immobile during the entire ablation period because the treatment will have to be restarted when they move. Moreover, additional procedures are needed to treat large and deep lesions, given that the maximum depth at which the method works is only 28 mm from the skin. If scars or moles are present between the transducer and the skin, performing ablation is not possible. Thus, larger studies are needed to introduce HIFU ablation into clinical practice.

DISCUSSION

Importantly, the quality of HPT destruction when using the above-mentioned methods may vary significantly. Adenomas or hyperplasia of parathyroid glands function by every cell, and destruction of only a part of the gland may not give the proper effect. In this regard, the most significant controversy is the determination of destruction volume to achieve the best result and consider the likelihood of complications. In the articles included in this review, the destruction volume was determined under US guidance and compared with the preoperative SPECT/CT data. Persistent complications were either not observed, or the authors did not specify these data in their findings, which further emphasizes the need for direct comparative and randomized clinical studies devoted to this issue.

Practically, the HPT nature must be considered and separately, the use of thermal ablation techniques in PHPT and SHPT (renal origin), when determining the destruction volume. These diseases are different, and the tactics of using minimally invasive techniques therefore may differ. Morphological changes in PHPT and SHPT are fundamentally different; therefore, the destruction volume in these diseases may vary.

A separate concern is the long-term efficiency of thermal ablation methods compared with surgical treatment. In the majority of the analyzed articles, a positive attitude toward the use of alternative treatment methods was observed, and these methods are rarely extremely and critically compared with traditional (radical) ones. However, insufficient data have been accumulated recently on the long-term follow-up of patients after thermal ablation in comparative studies to assess the efficiency in comparison with traditional methods. Therefore, the viability of alternative methods should mainly be considered at this stage, but only if traditional methods cannot be used.

Based on the analyzed information, the algorithm for HPT treatment, which considers the potential of alternative methods, was developed (Fig. 8). This algorithm differs from the clinical PHPT treatment guidelines approved by the Russian Ministry of Health and the recommendations for SHPT treatment proposed by Kidney Disease: Improving Global Outcomes) [46] and Kidney Disease Outcomes Quality Initiative [47]. However, the formulated algorithm is based on more recent data and the results of the latest studies with applications that are described in the technology review, which make them relevant for further discussion without changing or compromising other algorithms.

Thus, the review analyzed four methods of thermal HPT destruction as an alternative to surgical intervention. (Fig. 9). These methods use different physical principles of thermal ablation, and considerable clinical experience in their application has been accumulated. The HPT cause is determined by using functional and topical diagnostic

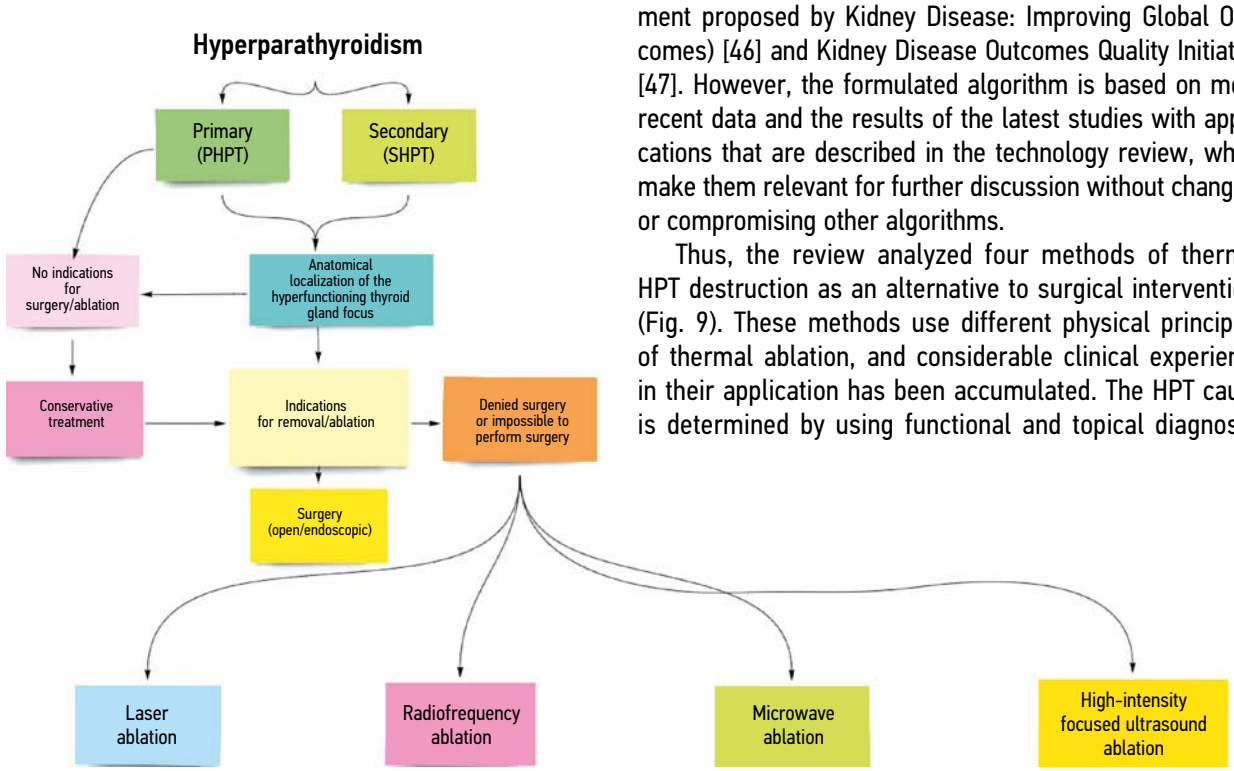

Fig. 8. Hyperparathyroidism treatment algorithm.

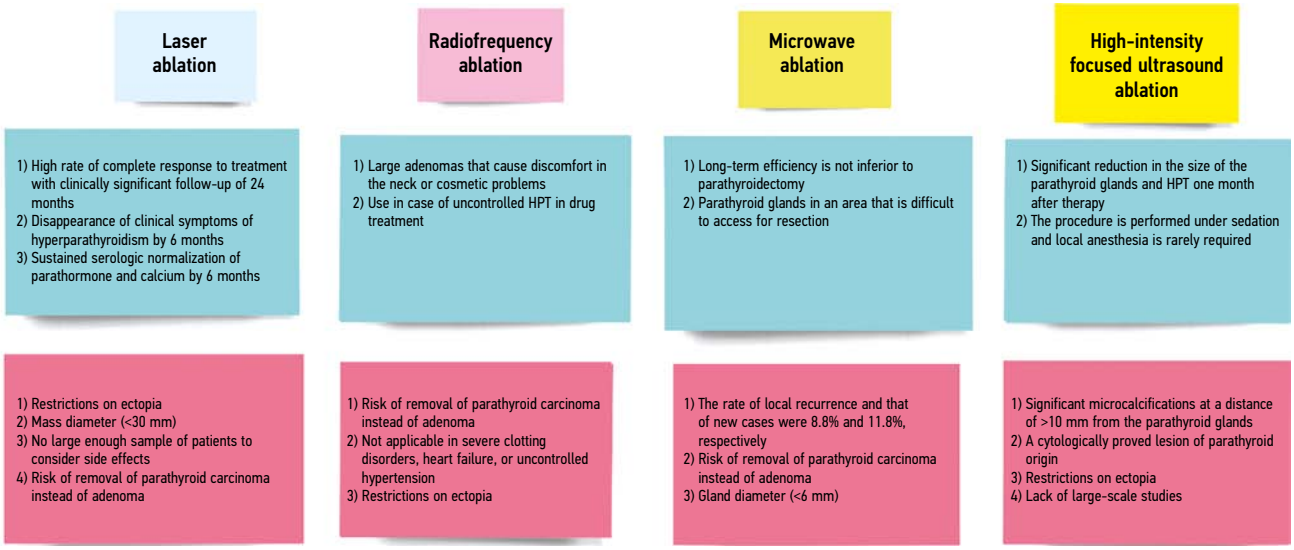

Fig. 9. Summary of the advantages (green) and disadvantages (red) of the methods for thermal destruction of the parathyroid glands.

methods. The current algorithm for preoperative topical HTP diagnosis, including US, MSCT, SPECT/CT, and PET/CT, allows to achieve 95% detection of hyperfunctioning parathyroid glands.

CONCLUSIONS

Thus, any of the selected methods of thermal destruction requires monitoring (US and MRI) of the thermal effect and highly qualified and experienced specialists. Each basic method of thermal destruction of hyperfunctioning parathyroid glands has its advantages and disadvantages, efficiency, and safety profile. The analysis of clinical practice shows that microwave ablation is the most popular (the first and best known) method at present. However, laser ablation is potentially more effective and safer primarily due to the technical capability of the method to perform more targeted and US-guided thermal destruction.

Not all patients with indications for surgical HPT treatment may be operated on. Hence, the interest in improving alternative nonsurgical treatment methods will increase.

ADDITIONAL INFORMATION

Funding source. The authors declare that there is no external funding for the exploration and analysis work.

Competing interests. The authors declare no obvious and potential conflicts of interest related to the publication of this article.

Authors' contribution. Rumiantsev P.O. — study conception and design, data analysis, drafting of the manuscript; Bubnov A.A. — study conception and design, analysis and picking up information, illustrations, drafting of the manuscript; Degtyarev M.V., Slashchuk K.Y. — drafting of the manuscript, illustrations, analysis and picking up information; Zakharova S.M., Agibalov D.Yu. — illustrations, analysis information; Timoshenko V.Yu. — analysis information, drafting of the manuscript. All authors made a substantial contribution to the conception of the work, acquisition, analysis, interpretation of data for the work, drafting and revising the work, final approval of the version to be published and agree to be accountable for all aspects of the work.

REFERENCES

1. Fraser WD. Hyperparathyroidism. *Lancet*. 2009;374(9684):145–158. doi: 10.1016/S0140-6736(09)60507-9

2. Vadiveloo T, Donnan PT, Leese GP. A population-based study of the epidemiology of chronic hypoparathyroidism. *J Bone Miner Res*. 2018;33(3):478–485. doi: 10.1002/jbmr.3329

3. Yanevskaya LG, Karonova TL, Sleptsov IV, et al. Primary hyperparathyroidism: clinical forms and their features. Retrospective study. *Clinical and Experimental Thyroidology*. 2019;15(1):19–29. (In Russ). doi: 10.14341/ket10213

4. Mokrysheva NG, Eremkina AK, Mirnaya SS, et al. Challenges in differential diagnosis between primary and secondary forms of hyperparathyroidism. *Obesity and Metabolism*. 2017;14(3):48–53. (In Russ). doi: 10.14341/omet2017348-53

5. Smorshchok VN, Kuznetsov NS, Artemova AM, et al. Surgical treatment of patients with secondary hyperparathyroidism in chronic renal failure. *Problems of Endocrinology*. 2003;49(6):36–41. (In Russ). doi: 10.14341/probl11761

6. Slashchuk KY, Degtyarev MV, Rumyantsev PO, et al. Imaging methods of the parathyroid glands in primary hyperparathyroidism. Literature review. *Endocrine Surgery*. 2019;13(4):153–174. (In Russ). doi: 10.14341/serg12241

7. Broos WM, van der Zant FM, Knol JJ, Wondergem M. Choline PET/CT in parathyroid imaging: a systematic review. *Nucl Med Commun*. 2019;40(2):96–105. doi: 10.1097/MNM.0000000000000952

8. Yu N, Leese GP, Smith D, Donnan PT. The natural history of treated and untreated primary hyperparathyroidism: the parathyroid

epidemiology and audit research study. *QJM.* 2011;104(6):513–521. doi: 10.1093/qjmed/hcq261

9. Ishii H, Stechman MJ, Watkinson JC, et al. A review of parathyroid surgery for primary hyperparathyroidism from the United Kingdom Registry of Endocrine and Thyroid Surgery (UKRETS). *World J Surg*. 2021;45:782–789. doi: 10.1007/s00268-020-05885-5

10. Kim MS, Kim GH, Lee CH, et al. Surgical outcomes of subtotal parathyroidectomy for renal hyperparathyroidism. *Clin Exp Otorhinolaryngol*. 2020;13(2):173–178. doi: 10.21053/ceo.2019.01340

11. LeBlanc RA, Isaac A, Abele J, et al. Validation of a novel method for localization of parathyroid adenomas using SPECT/CT. *J Otolaryngol Head Neck Surg*. 2018;47(1):65. doi: 10.1186/s40463-018-0307-6

12. Zhao S, Guo X, Taniguchi M, et al. Detection of mediastinal lymph node metastases using indocyanine green (ICG) fluorescence imaging in an orthotopic implantation model. *Anticancer Res*. 2020;40(4):1875–1882. doi: 10.21873/anticanres.14141

13. Kose E, Rudin AV, Kahramangil B, et al. Autofluorescence imaging of parathyroid glands: An assessment of potential indications. *Surgery*. 2020;167(1):173–179. doi: 10.1016/j.surg.2019.04.072

14. Wu B, Haigh PI, Hwang R, et al. Underutilization of parathyroidectomy in elderly patients with primary hyperparathyroidism. *J Clin Endocrinol Metab*. 2010;95(9):4324–4330. doi: 10.1210/jc.2009-2819

15. Kovatcheva RD, Vlahov JD, Stoinov JI, et al. High-intensity focused ultrasound (HIFU) treatment in uraemic secondary hyperparathyroidism. *Nephrol Dial Transplant*. 2012;27(1):76–80. doi: 10.1093/ndt/gfr590

16. Korkusuz H, Nimsdorf F, Happel C, et al. Percutaneous microwave ablation of benign thyroid nodules. Functional imaging in comparison to nodular volume reduction at a 3-month follow-up. *Nuklearmedizin*. 2015;54(1):13–19. doi: 10.3413/Nukmed-0678-14-06

17. Zeng Z, Peng CZ, Liu JB, et al. Efficacy of ultrasound-guided radiofrequency ablation of parathyroid hyperplasia: single session vs. two-session for effect on hypocalcemia. *Sci Rep.* 2020;10(1):6206. doi: 10.1038/s41598-020-63299-8

18. Casara D, Rubello D, Piotto A, Pelizzo MR. 99mTc-MIBI radioguided minimally invasive parathyroid surgery planned on the basis of a preoperative combined 99mTc-pertechnetate/99mTc-MIBI and ultrasound imaging protocol. *Eur J Nucl Med*. 2000;27(9):1300–1304. doi: 10.1007/s002590000297

19. Huang Z, Lou C. 99mTcO4-/99mTc-MIBI dual-tracer scintigraphy for preoperative localization of parathyroid adenomas. *J Int Med Res*. 2019;47(2):836–845. doi: 10.1177/0300060518813742

20. Zhang R, Zhang Z, Huang P, et al. Diagnostic performance of ultrasonography, dual-phase 99mTc-MIBI scintigraphy, early and delayed 99mTc-MIBI SPECT/CT in preoperative parathyroid gland localization in secondary hyperparathyroidism. *BMC Med Imaging*. 2020;20(1):91. doi: 10.1186/s12880-020-00490-3

21. Treglia G, Sadeghi R, Schalin-Jäntti C, et al. Detection rate of 99m Tc-MIBI single photon emission computed tomography (SPECT)/CT in preoperative planning for patients with primary hyperparathyroidism: A meta-analysis. *Head Neck*. 2016;38(Suppl 1):2159–2172. doi: 10.1002/hed.24027

22. Huber GF, Hüllner M, Schmid C, et al. Benefit of 18F-fluorocholine PET imaging in parathyroid surgery. *Eur Radiol*. 2018;28(6):2700–2707. doi: 10.1007/s00330-017-5190-4

23. Pacella CM, Mauri G. History of laser ablation. image-guided laser ablation. Springer, Cham; 2020. doi: 10.1007/978-3-030-21748-8_1

24. Bown SG. Phototherapy in tumors. *World J Surg*. 1983;7(6):700–709. doi: 10.1007/BF01655209

25. Appelbaum L, Goldberg SN, Ierace T, Mauri G. US-guided laser treatment of parathyroid adenomas. *Int J Hyperthermia*. 2020;37(1):366–372. doi: 10.1080/02656736.2020.1750712

26. Rhim H, Goldberg SN, Dodd GD, et al. Essential techniques for successful radio-frequency thermal ablation of malignant hepatic tumors. *Radiographics*. 2001;21:S17–S35. doi: 10.1148/radiographics.21.suppl_1.g01oc11s17

27. McGahan JP, Dodd G. Radiofrequency ablation of the liver. *American Journal of Roentgenology.* 2001;176(1): 3–16 doi: 10.2214 / ajr.176.1.1760003

28. Hong K, Georgiades C. Radiofrequency ablation: mechanism of action and devices. *J Vasc Interv Radiol*. 2010;21(8 Suppl):179–186. doi: 10.1016/j.jvir.2010.04.008

29. Zhang M, Tufano RP, Russell JO. Ultrasound-Guided radiofrequency ablation versus surgery for low-risk papillary thyroid microcarcinoma: results of over 5 years' follow-up. *Thyroid*. 2020;30(3):408–417. doi: 10.1089/thy.2019.0147

30. Schullian P, Johnston EW, Putzer D, et al. Safety and efficacy of stereotactic radiofrequency ablation for very large (≥8 cm) primary and metastatic liver tumors. *Sci Rep*. 2020;10(1):1618. doi: 10.1038/s41598-020-58383-y

31. Marshall HR, Shakeri S, Hosseiny M, et al. Long-term survival after percutaneous radiofrequency ablation of pathologically proven renal cell carcinoma in 100 patients. *J Vasc Interv Radiol*. 2020;31(1):15–24. doi: 10.1016/j.jvir.2019.09.011

32. Laird AM, Libutti SK. Minimally invasive parathyroidectomy versus bilateral neck exploration for primary hyperparathyroidism. *Surg Oncol Clin N Am*. 2016;25(1):103–118. doi: 10.1016/j.soc.2015.08.012

33. Ha EJ, Baek JH, Baek SM. Minimally invasive treatment for benign parathyroid lesions: treatment efficacy and safety based on nodule characteristics. *Korean J Radiol*. 2020;21(12):1383–1392. doi: 10.3348/kjr.2020.0037

34. Sidorov DV, Stepanov SO, Grishin NA, et al. Microwave ablation in the treatment of liver malignancies. *Oncology. Journal named after P.A. Herzen*. 2013;1(2):27–31. (In Russ).

35. Lubner MG, Brace CL, Hinshaw JL, Lee FT. Microwave tumor ablation: mechanism of action, clinical results, and devices. *J Vasc Interv Radiol*. 2010;21(8):192–203 doi: 10.1016/j.jvir.2010.04.007

36. Wei Y, Peng L, Li Y, et al. Clinical study on safety and efficacy of microwave ablation for primary hyperparathyroidism. *Korean J Radiol*. 2020;21(5):572–581. doi: 10.3348/kjr.2019.0593

37. Schlosser K, Bartsch DK, Diener MK, et al. Total parathyroidectomy with routine thymectomy and autotransplantation versus total parathyroidectomy alone for secondary hyperparathyroidism: results of a nonconfirmatory multicenter prospective randomized controlled pilot trial. *Annals of Surgery*. 2016;264(5):745–753. doi: 10.1097/SLA.0000000000001875

38. Zhuo L, Zhang L, Peng LL, et al. Microwave ablation of hyperplastic parathyroid glands is a treatment option for end-stage renal disease patients ineligible for surgical resection. *Int J Hyperthermia*. 2019;36(1):29–35. doi: 10.1080/02656736.2018.1528392

39. Copelan A, Hartman J, Chehab M, Venkatesan AM. High-Intensity focused ultrasound: current status for image-guided therapy. *Semin Intervent Radiol*. 2015;32(4):398–415. doi: 10.1055/s-0035-1564793
40. Suleimanov EA, Filonenko EV, Moskvicheva LI, et al. The possibility of hifu therapy at the present stage. *Research and Practical Medicine Journal*. 2016;3(3):76–82. (In Russ). doi: 10.17709/2409-2231-2016-3-3-8
41. Limani K, Aoun F, Holz S, et al. Single high intensity focused ultrasound session as a whole gland primary treatment for clinically localized prostate cancer: 10-year outcomes. *Prostate Cancer*. 2014;2014:186782. doi: 10.1155/2014/186782
42. Chung SR, Baek JH, Suh CH, et al. Efficacy and safety of high-intensity focused ultrasound (HIFU) for treating benign thyroid nodules: a systematic review and meta-analysis. *Acta Radiologica*. 2020;61(12):1636–1643. doi: 10.1177/0284185120909339
43. Ploussard G. Re: Salvage high-intensity focused ultrasound (HIFU) for locally recurrent prostate cancer after failed radiation therapy: multi-institutional analysis of 418 patients. *Eur Urol*. 2018;73(1):140–141. doi: 10.1016/j.eururo.2017.09.031
44. Tsamatropoulos P, Valcavi R. HIFU and RFA Ablation for thyroid and parathyroid disease. Advanced thyroid and parathyroid ultrasound. Springer, Cham; 2017. doi: 10.1007/978-3-319-44100-9_36
45. Kovatcheva R, Vlahov J, Stoinov J, et al. US-guided high-intensity focused ultrasound as a promising non-invasive method for treatment of primary hyperparathyroidism. *Eur Radiol*. 2014;24(9):2052–2058. doi: 10.1007/s00330-014-3252-4
46. Khwaja A. KDIGO clinical practice guidelines for acute kidney injury. *Nephron Clin Pract*. 2012;120(4):179–184. doi: 10.1159/000339789
47. Daugirdas JT, Depner TA, Inrig J, et al. KDOQI clinical practice guideline for hemodialysis adequacy: 2015 update. *Am J Kidney Dis*. 2015;66(5):884–930. doi: 10.1053/j.ajkd.2015.07.015

СПИСОК ЛИТЕРАТУРЫ

1. Fraser W.D. Hyperparathyroidism // Lancet. 2009. Vol. 374, N 9684. P. 145–158. doi: 10.1016/S0140-6736(09)60507-9
2. Vadiveloo T., Donnan P.T., Leese G.P. A population-based study of the epidemiology of chronic hypoparathyroidism // J Bone Miner Res. 2018. Vol. 33, N 3. P. 478–485. doi: 10.1002/jbmr.3329
3. Яневская Л.Г., Каронова Т.Л., Слепцов И.В., и др. Первичный гиперпаратиреоз: клинические формы и их особенности. Результаты ретроспективного исследования // Клиническая и экспериментальная тиреоидология. 2019. Т. 15, № 1. С. 19–29. doi: 10.14341/ket10213
4. Мокрышева Н.Г., Еремкина А.К., Мирная С.С., Ковалева Е.В. Трудности дифференциальной диагностики между первичной и вторичной формами гиперпаратиреоза // Ожирение и метаболизм. 2017. Т. 14, № 3. С. 48–53. doi: 10.14341/omet2017348-53
5. Сморщок В.Н., Кузнецов Н.С., Артемова А.М., и др. Хирургическое лечение больных с вторичным гиперпаратиреозом при хронической почечной недостаточности // Проблемы эндокринологии. 2003. Т. 49, № 6. С. 36–41. doi: 10.14341/probl11761
6. Слащук К.Ю., Дегтярев М.В., Румянцев П.О., и др. Методы визуализации околощитовидных желез при первичном гиперпаратиреозе. Обзор литературы // Эндокринная хирургия. 2019. Т. 13, № 4. С. 153–174. doi: 10.14341/serg12241
7. Broos W.M., van der Zant F.M., Knol J.J., Wondergem M. Choline PET/CT in parathyroid imaging: a systematic review // Nucl Med Commun. 2019. Vol. 40, N 2. P. 96–105. doi: 10.1097/MNM.0000000000000952
8. Yu N., Leese G.P., Smith D., Donnan P.T. The natural history of treated and untreated primary hyperparathyroidism: the parathyroid epidemiology and audit research study // QJM. 2011. Vol. 104, N 6. P. 513–521. doi: 10.1093/qjmed/hcq261
9. Ishii H., Stechman M.J., Watkinson J.C., et al. A review of parathyroid surgery for primary hyperparathyroidism from the United Kingdom Registry of Endocrine and Thyroid Surgery (UKRETS) // World J Surg. 2021. Vol. 45. P. 782–789. doi: 10.1007/s00268-020-05885-5
10. Kim M.S., Kim G.H., Lee C.H., et al. Surgical outcomes of subtotal parathyroidectomy for renal hyperparathyroidism // Clin Exp Otorhinolaryngol. 2020. Vol. 13, N 2. P. 173–178. doi: 10.21053/ceo.2019.01340
11. LeBlanc R.A., Isaac A., Abele J., et al. Validation of a novel method for localization of parathyroid adenomas using SPECT/CT // J Otolaryngol Head Neck Surg. 2018. Vol. 47, N 1. P. 65. doi: 10.1186/s40463-018-0307-6
12. Zhao S., Guo X., Taniguchi M., et al. Detection of mediastinal lymph node metastases using indocyanine green (ICG) fluorescence imaging in an orthotopic implantation model // Anticancer Res. 2020. Vol. 40, N 4. P. 1875–1882. doi: 10.21873/anticanres.14141
13. Kose E., Rudin A.V., Kahramangil B., et al. Autofluorescence imaging of parathyroid glands: An assessment of potential indications // Surgery. 2020. Vol. 167, N 1. P. 173–179. doi: 10.1016/j.surg.2019.04.072
14. Wu B., Haigh P.I., Hwang R., et al. Underutilization of parathyroidectomy in elderly patients with primary hyperparathyroidism // J Clin Endocrinol Metab. 2010. Vol. 95, N 9. P. 4324–4330 doi: 10.1210/jc.2009-2819
15. Kovatcheva R.D., Vlahov J.D., Stoinov J.I., et al. High-intensity focused ultrasound (HIFU) treatment in uraemic secondary hyperparathyroidism // Nephrol Dial Transplant. 2012. Vol. 27, N 1. P. 76–80. doi: 10.1093/ndt/gfr590
16. Korkusuz H., Nimsdorf F., Happel C., et al. Percutaneous microwave ablation of benign thyroid nodules. Functional imaging in comparison to nodular volume reduction at a 3-month follow-up // Nuklearmedizin. 2015. Vol. 54, N 1. P. 13–19. doi: 10.3413/Nukmed-0678-14-06
17. Zeng Z., Peng C.Z., Liu J.B., et al. Efficacy of ultrasound-guided radiofrequency ablation of parathyroid hyperplasia: single session vs. two-session for effect on hypocalcemia // Sci Rep. 2020. Vol. 10, N 1. P. 6206. doi: 10.1038/s41598-020-63299-8
18. Casara D., Rubello D., Piotto A., Pelizzo M.R. 99mTc-MIBI radioguided minimally invasive parathyroid surgery planned on the basis of a preoperative combined 99mTc-pertechnetate/99mTc-MIBI and ultrasound imaging protocol // Eur J Nucl Med. 2000. Vol. 27, N 9. P. 1300–1304. doi: 10.1007/s002590000297

19. Huang Z., Lou C. 99mTcO4-/99mTc-MIBI dual-tracer scintigraphy for preoperative localization of parathyroid adenomas // J Int Med Res. 2019. Vol. 47, N 2. P. 836–845. doi: 10.1177/0300060518813742
20. Zhang R., Zhang Z., Huang P., et al. Diagnostic performance of ultrasonography, dual-phase 99mTc-MIBI scintigraphy, early and delayed 99mTc-MIBI SPECT/CT in preoperative parathyroid gland localization in secondary hyperparathyroidism // BMC Med Imaging. 2020. Vol. 20, N 1. P. 91. doi: 10.1186/s12880-020-00490-3
21. Treglia G., Sadeghi R., Schalin-Jäntti C., et al. Detection rate of 99m Tc-MIBI single photon emission computed tomography (SPECT)/CT in preoperative planning for patients with primary hyperparathyroidism: A meta-analysis // Head Neck. 2016. Vol. 38, Suppl 1. P. 2159–2172. doi: 10.1002/hed.24027
22. Huber G.F., Hüllner M., Schmid C., et al. Benefit of 18F-fluorocholine PET imaging in parathyroid surgery // Eur Radiol. 2018. Vol. 28, N 6. P. 2700–2707. doi: 10.1007/s00330-017-5190-4
23. Pacella C.M., Mauri G. History of laser ablation. Image-guided laser ablation. Springer, Cham. 2020. doi: 10.1007/978-3-030-21748-8_1
24. Bown S.G. Phototherapy in tumors // World J Surg. 1983. Vol. 7, N 6. P. 700–709. doi: 10.1007/BF01655209
25. Appelbaum L., Goldberg S.N., Ierace T., Mauri G. US-guided laser treatment of parathyroid adenomas // Int J Hyperthermia. 2020. Vol. 37, N 1. P. 366–372. doi: 10.1080/02656736.2020.1750712
26. Rhim H., Goldberg S.N., Dodd G.D., et al. Essential techniques for successful radio-frequency thermal ablation of malignant hepatic tumors // Radiographics. 2001. Vol. 21. P. 17–35. doi: 10.1148/radiographics.21.suppl_1.g01oc11s17
27. McGahan J.P., Dodd G. Radiofrequency ablation of the liver // American Journal of Roentgenology. 2001. Vol. 176, N 1. P. 3–16. doi 10.2214 / ajr.176.1.1760003
28. Hong K., Georgiades C. Radiofrequency ablation: mechanism of action and devices // J Vasc Interv Radiol. 2010. Vol. 21, Suppl 8. P. 179–186. doi: 10.1016/j.jvir.2010.04.008
29. Zhang M., Tufano R.P., Russell J.O. Ultrasound-Guided radiofrequency ablation versus surgery for low-risk papillary thyroid microcarcinoma: results of over 5 years' follow-up // Thyroid. 2020. Vol. 30, N 3. P. 408–417. doi: 10.1089/thy.2019.0147
30. Schullian P., Johnston E.W., Putzer D., et al. Safety and efficacy of stereotactic radiofrequency ablation for very large (≥8 cm) primary and metastatic liver tumors // Sci Rep. 2020. Vol. 10, N 1. P. 1618. doi: 10.1038/s41598-020-58383-y
31. Marshall H.R., Shakeri S., Hosseiny M., et al. Long-Term survival after percutaneous radiofrequency ablation of pathologically proven renal cell carcinoma in 100 patients // J Vasc Interv Radiol. 2020. Vol. 31, N 1. P. 15–24. doi: 10.1016/j.jvir.2019.09.011
32. Laird A.M., Libutti S.K. Minimally invasive parathyroidectomy versus bilateral neck exploration for primary hyperparathyroidism // Surg Oncol Clin N Am. 2016. Vol. 25, N 1. P. 103–118. doi: 10.1016/j.soc.2015.08.012
33. Ha E.J., Baek J.H., Baek S.M. Minimally invasive treatment for benign parathyroid lesions: treatment efficacy and safety based on nodule characteristics // Korean J Radiol. 2020. Vol. 21, N 12. P. 1383–1392. doi: 10.3348/kjr.2020.0037
34. Сидоров Д.В., Степанов С.О., Гришин Н.А., и др. Микроволновая абляция при лечении злокачественных новообразований печени // Онкология. Журнал им. П.А. Герцена. 2013. Т. 1, № 2. С. 27–31.
35. Lubner M.G., Brace C.L., Hinshaw J.L., Lee F.T. Microwave tumor ablation: mechanism of action, clinical results, and devices // J Vasc Interv Radiol. 2010. Vol. 21, Suppl 8. P. 192–203. doi: 10.1016/j.jvir.2010.04.007
36. Wei Y., Peng L., Li Y., et al. Clinical study on safety and efficacy of microwave ablation for primary hyperparathyroidism // Korean J Radiol. 2020. Vol. 21, N 5. P. 572–581. doi: 10.3348/kjr.2019.0593
37. Schlosser K., Bartsch D.K., Diener M.K., et al. Total parathyroidectomy with routine thymectomy and autotransplantation versus total parathyroidectomy alone for secondary hyperparathyroidism: results of a nonconfirmatory multicenter prospective randomized controlled pilot trial // Annals of Surgery. 2016. Vol. 264, N 5. P. 745–753. doi: 10.1097/SLA.0000000000001875
38. Zhuo L., Zhang L., Peng L.L., et al. Microwave ablation of hyperplastic parathyroid glands is a treatment option for end-stage renal disease patients ineligible for surgical resection // Int J Hyperthermia. 2019. Vol. 36, N 1. P. 29–35. doi: 10.1080/02656736.2018.1528392
39. Copelan A., Hartman J., Chehab M., Venkatesan A.M. High-Intensity focused ultrasound: current status for image-guided therapy // Semin Intervent Radiol. 2015. Vol. 32, N 4. P. 398–415. doi: 10.1055/s-0035-1564793
40. Suleimanov E.A., Filonenko E.V., Moskvicheva L.I., et al. The possibility of hifu therapy at the present stage // Research and Practical Medicine Journal. 2016. Vol. 3, N 3. P. 76–82. doi: 10.17709/2409-2231-2016-3-3-8
41. Limani K., Aoun F., Holz S., et al. Single high intensity focused ultrasound session as a whole gland primary treatment for clinically localized prostate cancer: 10-year outcomes // Prostate Cancer. 2014. Vol. 2014. P. 186782. doi: 10.1155/2014/186782
42. Chung S.R., Baek J.H., Suh C.H., et al. Efficacy and safety of high-intensity focused ultrasound (HIFU) for treating benign thyroid nodules: a systematic review and meta-analysis // Acta Radiologica. 2020. Vol. 61, N 12. P. 1636–1643. doi: 10.1177/0284185120909339
43. Ploussard G. Re: Salvage high-intensity focused ultrasound (HIFU) for locally recurrent prostate cancer after failed radiation therapy: multi-institutional analysis of 418 patients // Eur Urol. 2018. Vol. 73, N 1. P. 140–141. doi: 10.1016/j.eururo.2017.09.031
44. Tsamatropoulos P., Valcavi R. HIFU and RFA ablation for thyroid and parathyroid disease. Advanced thyroid and parathyroid ultrasound. Springer, Cham; 2017. doi: 10.1007/978-3-319-44100-9_36
45. Kovatcheva R., Vlahov J., Stoinov J., et al. US-guided high-intensity focused ultrasound as a promising non-invasive method for treatment of primary hyperparathyroidism // Eur Radiol. 2014. Vol. 24, N 9. P. 2052–2058. doi: 10.1007/s00330-014-3252-4
46. Khwaja A. KDIGO clinical practice guidelines for acute kidney injury // Nephron Clin Pract. 2012. Vol. 120, N 4. P. 179–184. doi: 10.1159/000339789
47. Daugirdas J.T., Depner T.A., Inrig J., et al. KDOQI clinical practice guideline for hemodialysis adequacy: 2015 update // Am J Kidney Dis. 2015. Vol. 66, N 5. P. 884–930. doi: 10.1053/j.ajkd.2015.07.015

AUTHORS' INFO

*** Pavel O. Rumyantsev,** MD, Dr. Sci. (Med.);
address: 8 Malaya Konyushennaya str., Saint Petersburg, 191186, Russia;
ORCID: https://orcid.org/0000-0002-7721-634X;
eLibrary SPIN: 7085-7976; e-mail: pavelrum@gmail.com

Aleksandr A. Bubnov;
ORCID: https://orcid.org/0000-0002-5877-6982;
eLibrary SPIN: 9380-1293; e-mail: bubnov96@mail.ru

Mikhail V. Degtyarev, MD;
ORCID: https://orcid.org/0000-0001-5652-2607;
eLibrary SPIN: 7725-7831; e-mail: germed@mail.ru

Konstantin Y. Slashchuk, MD;
ORCID: https://orcid.org/0000-0002-3220-2438;
eLibrary SPIN:3079-8033; e-mail: slashuk911@gmail.com

Svetlana M. Zakharova, MD, Cand. Sci. (Med.);
ORCID: https://orcid.org/0000-0001-6059-2827;
eLibrary SPIN: 9441-4035; e-mail: smzakharova@mail.ru

Dmitry Yu. Agibalov;
ORCID: https://orcid.org/0000-0003-2995-7140;
eLibrary SPIN: 6938-5804; e-mail: agibalovd@bk.ru

Victor Yu. Timoshenko, Dr. Sci. (Phys-Math), Professor;
ORCID: https://orcid.org/0000-0003-3234-1427;
eLibrary SPIN: 7536-2368; e-mail: vtimoshe@gmail.com

ОБ АВТОРАХ

*** Румянцев Павел Олегович,** д.м.н.;
адрес: Россия, 191186, Санкт-Петербург, ул. Малая Конюшенная, д. 8;
ORCID: https://orcid.org/0000-0002-7721-634X;
eLibrary SPIN: 7085-7976; e-mail: pavelrum@gmail.com

Бубнов Александр Андреевич;
ORCID: https://orcid.org/0000-0002-5877-6982;
eLibrary SPIN: 9380-1293; e-mail: bubnov 96@mail.ru

Дегтярев Михаил Владимирович;
ORCID: https://orcid.org/0000-0001-5652-2607;
eLibrary SPIN: 7725-7831; e-mail: germed@mail.ru

Слащук Константин Юрьевич;
ORCID: https://orcid.org/0000-0002-3220-2438;
eLibrary SPIN:3079-8033; e-mail: slashuk911@gmail.com

Захарова Светлана Михайловна, к.м.н.;
ORCID: https://orcid.org/0000-0001-6059-2827;
eLibrary SPIN: 9441-4035; e-mail: smzakharova@mail.ru

Агибалов Дмитрий Юрьевич;
ORCID: https://orcid.org/0000-0003-2995-7140;
eLibrary SPIN: 6938-5804; e-mail: agibalovd@bk.ru

Тимошенко Виктор Юрьевич, д.ф.-м.н., профессор;
ORCID: https://orcid.org/0000-0003-3234-1427;
eLibrary SPIN: 7536-2368; e-mail: vtimoshe@gmail.com

* Corresponding author / Автор, ответственный за переписку

DOI: https://doi.org/10.17816/DD77959

Радиотераностика приходит на помощь

П.О. Румянцев

Международный медицинский центр «СОГАЗ-Медицина», Санкт-Петербург, Российская Федерация

АННОТАЦИЯ

Ситуация с пандемией COVID-19 не уменьшила интереса к радиотераностике, скорее, наоборот, запрос на визуализацию патологических процессов с помощью кросс-секционных и гибридных томографических исследований (рентеновской и магнитно-резонансной, однофотонной эмиссионной, позитронно-эмиссионной) только усилился. Фактически за последние 15 мес в мире наблюдается экспоненциальный рост инвестиций в новые радиофармацевтические препараты для радиотераностики. По мере выяснения молекулярных механизмов регуляции и исполнения метаболических процессов, расширяется перечень антител и лигандов, меченных «медицинскими» радиоактивными изотопами. Также расширяется спектр диагностических и лечебных радиоактивных изотопов, что в конечном итоге развивает ассортимент и доступность радиотераностики в центрах ядерной медицины во всем мире. Для развития радиотераностики необходимо объединение усилий физиков, радиофармацевтов, химиков, биологов, врачей и математиков. Использование и совершенствование персонализированной дозиметрии для планирования радионуклидной терапии также является приоритетным направлением. Международный фонд Oncidium, например, помогает в информационном плане и обмену опытом, а международное диагностическое исследование NOBLE позволяет повысить доступность и снизить стоимость PSMA-рецепторной сцинтиграфии. В целях интенсификации интеграционного обновления ядерной медицины создана ассоциация развития тераностики.

Ключевые слова: радиотераностика; рак предстательной железы; PSMA.

Как цитировать

Румянцев П.О. Радиотераностика приходит на помощь // *Digital Diagnostics*. 2021. Т. 2, № 3. С. 410–416. DOI: https://doi.org/10.17816/DD77959

Рукопись получена: 13.08.2021 **Рукопись одобрена:** 24.08.2021 **Опубликована:** 23.09.2021

DOI: https://doi.org/10.17816/DD77959

Radiotheranostics is here to help

Pavel O. Rumyantsev

SOGAZ International Medical Center, Saint Petersburg, Russian Federation

ABSTRACT

The COVID-19 pandemic did not diminish interest in radiotheranostics. However, the demand for visualization of pathological processes using cross-sectional and hybrid imaging (CT, MRI, SPECT, and PET) is increased. Over the past 15 months, the world has seen an exponential increase in investment in new radiopharmaceuticals for radiotheranostics. The list of antibodies and ligands labeled with "medical" radioactive isotopes is expanding as the molecular mechanisms of regulation and implementation of metabolic processes become clearer. The range of diagnostic and therapeutic radioactive isotopes is also expanding, ultimately increasing the range and availability of radiotherapy in nuclear medicine centers worldwide. It is necessary to unite the efforts of physicists, radiopharmacists, chemists, biologists, doctors, and mathematicians to develop radio technology. Usage and improvement of personalized dosimetry for planning radionuclide therapy is also a priority. For example, the International Foundation Oncidium helps with information and exchange of experience, while the international diagnostic study NOBLE increases the availability and reduces the cost of PSMA receptor scintigraphy. An association for the development of theranostics was created to intensify the integration renewal of nuclear medicine.

Keywords: radiotheranostics; prostate cancer; PSMA.

To cite this article

Rumyantsev PO. Radiotheranostics is here to help. *Digital Diagnostics.* 2021;2(3):410–416. DOI: https://doi.org/10.17816/DD77959

Received: 13.08.2021 **Accepted:** 24.08.2021 **Published:** 23.09.2021

DOI: https://doi.org/10.17816/DD77959

无线电技术起到了拯救作用

Pavel O. Rumyantsev

SOGAZ International Medical Center, Saint Petersburg, Russian Federation

简评

COVID-19大流行的情况并没有降低人们对无线电恐怖症的兴趣，相反，通过交叉段和混合层析成像技术对病理过程进行成像的请求（伦顿和磁共振，单光子发射，正电子发射）只增加了。事实上，在过去15个月里，世界上用于放射恐怖症的新型放射性药物的投资呈指数级增长。随着新陈代谢过程调节和执行的分子机制的澄清，由“医学”放射性同位素标记的抗体和配体清单正在扩大。诊断和治疗放射性同位素的范围也在不断扩大，最终发展了世界各地核医学中心放射治疗的范围和可用性。 放射恐怖学的发展需要物理学家、放射药剂师、化学家、生物学家、医生和数学家的共同努力。使用和改进个性化剂量测定来规划放射性核素治疗也是一个优先事项。 例如，国际文心 Oncidium帮助提供信息和交流经验，国际诊断研究 NOBLE 有助于提高 PSMA 受体闪烁扫描的可用性并降低成本。 为加强核医学一体化更新，成立了治疗诊断学发展协会。

关键词：放射学； 前列腺癌; PSMA。

引用本文

Rumyantsev PO. 无线电技术起到了拯救作用. *Digital Diagnostics.* 2021;2(3):410–416. DOI: https://doi.org/10.17816/DD77959

收到： 13.08.2021 **接受：** 24.08.2021 **发布日期：** 23.09.2021

INTRODUCTION

Recent studies and nuclear medicine advancements showed the leading role of radiotheranostics in oncology. Whatever the term of this promising area (radiotherapy, theranostics, radiotargeting, radioligand, peptide-receptor, or radionuclide therapy), this is a new area of nuclear medicine, particularly, in the diagnosis and treatment of malignant tumors using radioactive isotopes (Fig. 1).

The situation with the coronavirus disease-2019 pandemic did not diminish the interest in radioteranostics. Contrarily, only the demand for visualization of pathological processes using ultrasound and tomographic studies, such as computed tomography (CT), magnetic resonance imaging (MRI), single-photon emission CT (SPECT), and positron emission tomography (PET), as well as hybrid methods, has increased. The world saw the exponential growth of investments in new radiopharmaceuticals (RPHs) for radioteranostics over the past 15 months. This trend is due to both the availability of funds from promising investors and the realization of the enormous growth market potential of radioactive isotope-labeled molecules for therapy. The growing investments in radiotherapy are based on the advances achieved in this field over the past 10 years. The monetary capital growth estimation in this industry revealed that the nuclear medicine market in 2019 was $4.1 billion and this figure is expected to increase within 5 years to $5.2 billion at an average annual growth rate of 4.7% by 2024[1]. Key players see growing revenues from therapeutics as clearly superior to those from diagnostics. The increased attention to radionuclide technologies in the last 20 years is comparable to the growing interest in cancer immunotherapy in 1980–2000. At that time, the pharmaceutical industry preferred to watch the evolution of technologies through start-ups and small companies, most of which went bankrupt, whereas the rest perfected the technologies and made multibillion-dollar profits.

Currently, the range of radiotherapeutic drugs exceeds 300 items and has long surpassed the list of diagnostic RPHs, which require much fewer financial investments. For the past 50 years, the global RPH industry had an insufficient budget to develop such drugs in government agencies. Only “traditional” pharmaceutical companies had sufficient

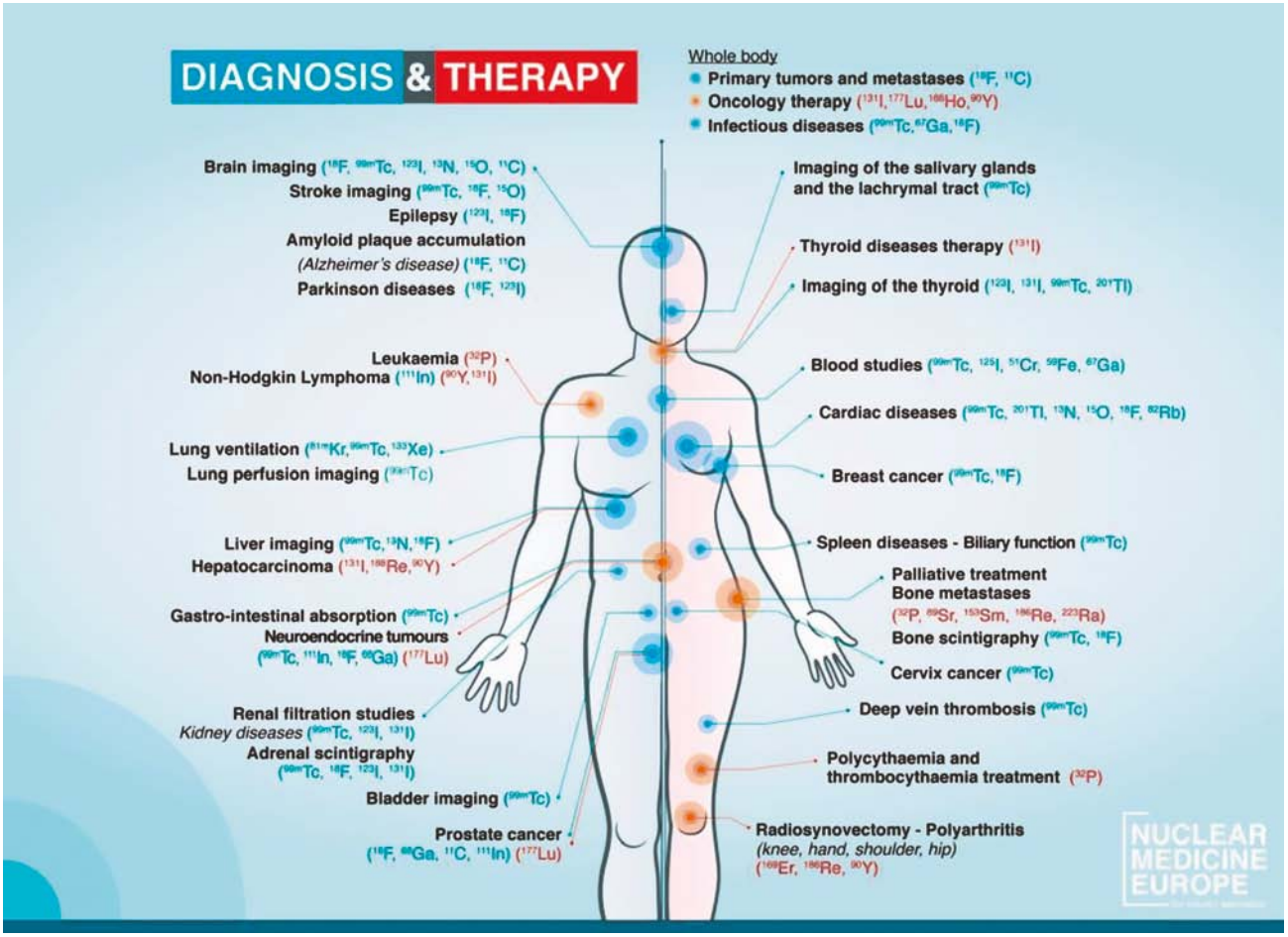

Fig. 1. Radioactive isotopes to diagnose and treat various diseases.

[1] Nuclear Medicine/Radiopharmaceuticals Market by Type (Diagnostic [SPECT—Technetium, PET—F-18], Therapeutic [Beta Emitters—I-131, Alpha Emitters, Brachytherapy—Y-90]), Application (oncology and cardiology), Procedures—Global Forecast to 2026. Available at https://www.marketsandmarkets.com/Market-Reports/radiopharmaceuticals-market-417.html. Accessed on 07/10/2021.

DOI: https://doi.org/10.17816/DD77959

capital and infrastructure to develop and market RPHs. In addition to huge financial resources, they have access to the target audience, i.e., doctors (oncologists, radiologists, endocrinologists, etc.). The pharmaceutical companies, Bayer (Germany) and Novartis (Switzerland), were the first to engage in this area and brought therapeutic RPHs (^{223}Ra-Xofigo and ^{177}Lu-Lutathera, respectively) to the market, which were limited to generic patents, thus have not reached (at least so far) blockbuster levels (annual sales of over $1 billion). Nevertheless, the next generation of therapeutic RPHs, such as glutamate carboxypeptidase II or prostate-specific membrane antigen (PSMA), will be based on proprietary names. The first radioligand, ^{177}Lu-PSMA-617 for prostate cancer (Novartis), is expected to hit the global market next year. In addition to Novartis, which is actively investing in new radiotherapeutic drugs (for example, based on fibroblast activity protein inhibitor for radionuclide therapy of a large number of malignancies or CXCR4, a chemokine receptor-4, which is used in myeloma, lymphoma, aldosterone, esophageal cancer, and glioblastoma), a growing interest is noted in the industry worldwide from iTheranostics (Switzerland), Sofie Biosciences (USA), Aktis Oncology (USA), Astellas (Japan) and Actinium Pharma (USA) collaborations, Jubilant (India), Lantheus and Noria Therapeutics (USA), Bracco Blue Earth Diagnostics (Italy), Scintomics (Germany), Fusion Pharma (Canada), Ipsen (France), and, more recently, EZAG and Pentixapharm consortium (Germany). New names appear annually on the RPH market, such as Abscint (Belgium), Abdera Therapeutics (Canada), Precirix (Belgium), and RayzeBio (US).

All of these companies are very young and emerged at the nexus of nuclear medicine, radiopharmacy, and medical physics. Thus, Telix Pharmaceutical (Australia) develops cutting-edge radiotheranostical agents for prostate cancer (iPSMA, J591), glioblastoma, kidney, bladder, and ovarian cancers by combining ^{177}Lu-labeled peptide-based RPHs and monoclonal antibodies with ^{177}Lu and ^{131}I in its product portfolio.

Current approaches to neuroendocrine tumors and prostate cancer treatment are represented by both radiotargeting therapy in a single-mode, i.e., one RPH during all courses, and the use of "tandem" RHPs by combining the same base molecules with different radiolabels. An example is the sequential use of ^{177}Lu-PSMA-617 and ^{225}Ac-PSMA-617. One of the first companies to specialize in ligand radiolabeling with ^{225}Ac alpha emitter was Fusion Pharmaceuticals (2014). The profile of Precision Molecular Inc. (the US, 2019) is radio targeting therapy for prostate cancer and other malignancies using ^{177}Lu and ^{225}Ac. Since 2020, Point Biopharma (USA) and RayzeBio (with a focus on similar ^{225}Ac-labeled ligands) have actively developed and used radiotheranostical drugs for neuroendocrine tumors and prostate cancer based on ^{177}Lu RPH.

Currently, over 60 radiotheranostical agents that target over 20 malignancies are in various stages of clinical trials; of these, 6 agents are in Phase III. Among the first 27 RPH names (9 for neuroendocrine tumors and 18 for prostate cancer), only a few (the most effective and safe ones) will enter the medical market.

Further development of radiotheranostics, especially in combination with existing anticancer therapy methods, will significantly expand the range of cancers with highly positive treatment responses. In oncology, radiotheranostics is an alternative to surgery (e.g., radioiodine therapy for thyrotoxicosis) or adjuvant treatment (as in thyroid cancer) in conjunction with surgery and hormonal therapy, or with distant radiotherapy, chemotherapy, and targeted drugs in other cases.

Accumulating an evidence-based clinical base will refine the indications for radioactive isotopes in the third, second, and first line of anticancer therapy. The concept of radiotheranostics generates much interest in personalized medicine, in which the patient is treated not according to a general, but to an individual plan, where specific targets and treatment mechanisms are determined using specific radiotheranostical agents (see Table 1). However, this is still a goal, for which a lot of logistical and regulatory issues will have to be resolved, allowing financial investments of pharmaceutical companies and private investors in the promising area of personalized medicine. Moreover, further informational and methodological work should be done with doctors, "non-nuclear" physicists, chemists, and public opinion.

RAPIDLY INCREASING DEVELOPMENT OF RADIOTHERANOSTICS WORLDWIDE

The international non-profit Oncidium[2] Foundation (headquartered in Belgium) was established in 2011 and operates globally to inform the public and professionals about radiotheranostics. The foundation aimed to promote and accelerate the development of radiotheranostics in oncology, making it more accessible to patients with cancer worldwide by updating information about the centers' work. Hopefully, the number of such centers in the Russian Federation will increase.

The corresponding section of the website is continuously updated with information about new RPHs, evidence-based preclinical and clinical trials and practical application, mechanisms of action, efficiency and safety, and combinations with other technologies for cancer diagnosis and treatment. For example, the NOBLE Registry (a project of international collaboration) offers patients with prostate cancer access to SPECT or preferably to SPECT combined with CT (SPECT/CT) and PSMA, regardless of their place of residence and financial situation, particularly, if PET combined with PSMA

[2] Oncidium. Official website: https://www.oncidiumfoundation.org.

Table 1. The concept of radiotheranostics for prostate cancer

Stage	Diagnosis (molecular imaging)		Surgery	Dosimetry	Radionuclide therapy	Follow-up
Aim	Tumor staging, PSMA receptor expression in tumor cells, treatment efficiency monitoring		Intraoperative radionavigation	Radiokinetics, radionuclide therapy planning	Treatment	Tumor recurrence detection and localization
Visualization	SPECT/CT	PET/CT or PET/MRI	Gamma probe	SPECT	SPECT**	SPECT/CT, PET/CT, PET/MRI
RPHs	**^{99m}Tc-HYNIC-PSMA**	^{68}Ga-PSMA-11* ^{18}F-PSMA-1007	**^{99m}Tc-HYNIC-PSMA, ^{99m}Tc-nanocolloid**	^{177}Lu-PSMA (617, I&T, J591)		**^{99m}Tc-HYNIC-PSMA**, ^{68}Ga-PSMA-11*, ^{18}F-PSMA-1007
Additional methods	TRUS, MSCT/MRI, puncturing, OS, and PSA					

Note. * More preferable (theranostic pair with ^{177}Lu-PSMA); ** whole body posttreatment scintigraphy (SPECT for all, SPECT/CT if indicated). SPECT: single-photon emission computed tomography; CT: computed tomography; MRI: magnetic resonance imaging; PET: positron emission tomography; TRUS: transrectal ultrasound; MSCT: multispiral computed tomography; OS: osteoscintigraphy; PSA: prostate-specific antigen.

is unavailable. The simplicity and convenience of SPECT/CT with PSMA (a technetium generator is always at hand) is much higher than PET combined with CT (PET/CT), and the cost is significantly lower, whereas virtual digital registration is possible if SPECT is not performed in hybrid mode using CT. The NOBLE Registry compares SPECT/CT and PET/CT results with PSMA, clarifying accuracy parameters, benefits, limitations, and indications. However, the foundation cannot solve all problems alone, thus 18 nuclear medicine and radiotherapy experts from 11 countries came for assistance, including the Russian Federation representatives, i.e., P.O. Rumyantsev and Ye.V. Kargapoltseva. The Scientific Board of Oncidium Foundation and the NOBLE Registry Steering Committee, consisting of respected leaders of nuclear medicine and I, are honored to be a member. The Scientific Board ensures international communication and radiotheranostic improvements, considering the development of new RPHs and Next-Generation Imaging.

In 2021, the Theranostics Development Association was registered in the Russian Federation[3].

Radiotheranostics provide an opportunity to update approaches to personalized diagnosis, treatment, and rehabilitation of patients with cancer. Therefore, many organizational, methodological, economic, and regulatory issues arise. According to foreign colleagues, the cost of a new-generation radionuclide therapy session per patient ranges between $15,000 and $50,000, excluding the cost for diagnostic examination using SPECT and/or PET, which are necessary for dosimetry-based treatment planning and monitoring.

The toxicity and frequency of radionuclide therapy are much lower than that of chemotherapy or radiation therapy; however, this information is often unknown to doctors who are unfamiliar and inexperienced with this area of medicine. Clinical practice shows that the patient has maximum compliance with a high benefit/convenience ratio of the treatment option.

CONCLUSIONS

Therefore, "nuclear" oncologists greatly enhance the potential of multidisciplinary teams in advanced clinics worldwide. Physicians improve both the treatment outcomes by increasing the radiation dose and the quality of life by minimizing the dose to surrounding tissues in patients with early tumor stages. This is commonly done through regression (not cure), tumor stabilization, or palliative care in advanced stages by a dose reduction for non-tumor tissues. The use and improvement of personalized dosimetry for radionuclide therapy planning are prioritized to ensure the delivery of the optimal dose in tumor tissues and minimize the effects of ionizing radiation on normal tissues for an effective and safe treatment for each patient.

ADDITIONAL INFORMATION

Funding source. The authors declare that there is no external funding for the exploration and analysis work.

Competing interests. The authors declare no obvious and potential conflicts of interest related to the publication of this article.

Author's contribution. The author made a substantial contribution to the conception of the work, acquisition, analysis, interpretation of data for the work, drafting and revising the work, final approval of the version to be published and agree to be accountable for all aspects of the work.

[3] Theranostics Development Association. Official website: http://theranostics.pro.

AUTHORS' INFO

Pavel O. Rumyantsev, MD, Dr. Sci. (Med.);
address: 8 Malaya Konyushennaya str.,
Saint Petersburg, 191186, Russia;
ORCID: https://orcid.org/0000-0002-7721-634X;
eLibrary SPIN: 7085-7976; e-mail: pavelrum@gmail.com

ОБ АВТОРАХ

Румянцев Павел Олегович, д.м.н.;
адрес: Россия, 191186, Санкт-Петербург,
ул. Малая Конюшенная, д. 8;
ORCID: https://orcid.org/0000-0002-7721-634X;
eLibrary SPIN: 7085-7976; e-mail: pavelrum@gmail.com